Interaction of catechol *O*-methyltransferase with gold and silver nanoparticles

A thesis submitted in fulfillment of the requirement for the degree of

DOCTOR OF PHILOSOPHY
of
RHODES UNIVERSITY

by

AMINU USMAN

February 2017

Department of Biochemistry and Microbiology
Rhodes University
Grahamstown 6140, South Africa

Abstract

Catechol *O*-methyltransferase (S-adenosyl-*L*-methionine: catechol *O*-methyltransferase; COMT; EC 2.1.1.6) is a ubiquitous enzyme that catalyses the transfer of a methyl group from the cofactor, *S*-adenosyl-*L*-methionine (SAM) to a hydroxyl group of endogenous and exogenous catechol-containing moieties. The physiological role of this enzyme is the methylation and thereby inactivation of the catechol-containing bio-active and bio-toxic compounds, including catechol-neurotransmitters, catechol-estrogens and catechol-containing drugs. Activity of this enzyme is implicated in the treatment of Parkinson's disease and is associated with other diseases including breast cancer and an array neuropsychological disorders, such as schizophrenia.

This thesis explores the use of gold and silver nanoparticles (NPs) (AuNPs and AgNPs) to inhibit the catalytic activity of mammalian COMT. Because of its accessibility and availability, we initially investigated bovine soluble COMT (BSCOMT) from liver tissue. Bioinformatic analyses and structural modeling revealed high (>90%) sequence similarity between BSCOMT and human soluble COMT (HSCOMT). BSCOMT was partially purified to 7.78 fold, 1.65% yield and had a specific activity of 0.052 U/mg. It had pH and temperature optima of 8.5 and 40°C, respectively. The K_m, V_{max}, K_{cat} and K_{cat}/K_m towards esculetin methylation were respectively 1.475±0.130 μM, 0.0353±0.001 μmol/ml/min, $1.748 \times 10^{-2} \pm 5.0 \times 10^{-4}$ min^{-1} and 1.18×10^{-2} M^{-1}. min^{-1}.

HSCOMT was expressed in *Escherichia coli* BL21(DE3) which showed optimal activity for esculetin methylation at pH and temperature of 7.0 and 30°C, respectively. It was purified to 5.62 fold, 22.6% yield with a specific activity of 3.85 U/mg. HSCOMT kinetic plots, upon

incubation of the reaction mixture at 30°C for 5 min before addition of SAM was hyperbolic with K_m, V_{max}, K_{cat} and K_{cat}/K_m values of 1.79 µM, 0.412 µmol/ml/min, 2.08 min^{-1} and 1.165 M^{-1}. min^{-1}, respectively. AuNPs and AgNPs showed a concentration dependent inhibition of HSCOMT activity upon increasing the 5 min incubation time to 1 h. Interestingly, HSCOMT kinetics, with 1 h incubation at 30°C, showed a sigmoidal curve, as well as increased activity. Incubation of the reaction mixture in the presence of 60 µM AuNPs and/or AgNPs for 1 hreversed the observed sigmoidal to a hyperbolic curve, with kinetic parameters comparable to those of 5 min incubation. SDS-PAGE analyses of HSCOMT after the kinetic experiments showed the enzyme incubated for 5 min as a monomer, while that which was incubated for 1 h migrated substantially as dimer. However, the HSCOMT incubated for 1 h in the presence of 60 µM AuNPs and/or AgNPs migrated as a monomer. This indicated that the extension of the incubation period allowed the dimerization of HSCOMT, which exhibited sigmoidal kinetics and higher activity. The presence of NPs impeded the HSCOMT dimerization which decreased the activity. Varying the concentration of SAM suggested that SAM had an allosteric modulatory effect on HSCOMT.

Absorption spectroscopy indicated adsorption of HSCOMT on the gold and silver NP surfaces and the formation of NPs-HSCOMT corona. Fluorescence spectroscopy showed that the interaction of HSCOMT with both gold and silver NPs was governed by a static quenching mechanism, implying the formation of a non-fluorescent fluorophore–NP complex at the ground state. Further fluorometric analyses indicated that both gold and silver NPs had contact with Trp143; that the interactions were spontaneous and were driven by electrostatic interactions. Fourier transform infrared spectroscopic studies showed the adsorption of HSCOMT of the NPs surfaces to cause relaxation of the enzyme's ß-sheet structures. Molecular docking studies

indicated involvement of largely hydrophilic amino acids, with the interacting distances of less than 3.5Å. These findings signify the potential of nanotechnology in the control of COMT catalytic activity for the management of the COMT-related disorders.

Declaration

I, Aminu Usman, write to state that this thesis is my independent work. It is being submitted for the degree of Doctor of Philosophy at Rhodes University. It has not been submitted for any degree or examination elsewhere.

_____

Signed on the 27th February 2017

Dedication

To the memory of my late father, to my ailing mother, to my beloved wife and to my lovely children.

Aknowledgements

- All praises, gratitudes and glories be to Allah (T) who made me and enabled me.
- To my mentor and supervisor, Dr. Brenden S. Wilhelmi, your mentorship and passion for training are inspiring. Thank you for your professional support and guidance, for your patience, encouragements, moral and financial support during my PhD research. Sir, I remain grateful.
- To my co-supervisor, Professor Chris G. Whiteley, I thank you for your invaluable suggestions, encouragements, scholarly and constructive criticisms. Sir, your financial supports are gratefully acknowledged.
- To my beloved mother, wife and children. Thank you for your understanding, patience and encouragements. I thank you my dear wife, Samira, for standing by me during one of the most challenging time of my life.
- To Dr Kevin Lobb, Chemistry Department, Rhodes University, thank you for the selfless and untiring assistance with molecular docking.
- Magaji Barde and family, I thank you for your kind friendship.
- To my colleagues, my Lab mates and friends of Labs 412 and 256 (2013-2017). Thank you for your warm and kind company during the hard times. Thanks for your words of encouragements.
- Umaru Yar'Ádua University, Katsina and Tertiary Education Trust Fund (TETFund) are gratefully acknowledged for granting me study fellowship to pursue this PhD.
- To Rhodes University for the provision of an enabling environment and to MRC for funding the project.

Table of Contents

List of Figures

List of Tables

List of Equations

List of abbreviations and symbols

$\times g$	times gravity
ΔG	Gibbs free energy
3-OMD	3 *O*-methyldopa
Å	Angstroms
AADC	aromatic amino acid decarboxylase
Ag	silver
$AgNO_3$	silver nitrate
AgNPs	silver nanoparticles
Au	gold
AuNPs	gold nanoparticles
BBB	blood-brain barrier
BCOMT	bovine catechol *O*-methyltransferase
BSA	bovine serum albumin
cDNA	complementary DNA
COD	crystallography open database
COMT	catechol *O*-methyltransferase
COMT	catechol *O*-methyltransferase gene
$COMT^{HH}$	high activity *COMT* allele
$COMT^{LH}$	intermediate activity *COMT* allele
$COMT^{LL}$	low activity *COMT* allele
DBS	deep brain stimulation
DEAE	diethylaminoethyl
DMSO	dimethyl sulfoxide
DNC	3,5-dinitrocatechol
DSV4.0 4.0	Discovery Studio Visualiser
EC	enzyme commission number
EDTA	ethylenediaminetetraacetic acid
F	fluorescence in presence of quencher
F_o	fluorescence in absence of quencher
FPLC	fast protein liquid chromatography
FTIR	Fourier transform infrared
h	Hill coefficient
HCl	hydrochloric acid
HSCOMT	human soluble catechol *O*-methyltransferase
HSP	host cell proteins
IMAC	immobilized metal affinity chromatography
IR	infrared
$K_{0.5}$	substrate concentration for allosteric half-saturation
K_a	association constant
kb	kilobases
K_{cat}	turnover number
K_{cat}/K_m	catalytic efficiency
K_d	dissociation constant
kDa	kilodaltons

K_m	substrate concentration for half-saturation
K_{sv}	Stern-Volmer quenching constant
LB	Luria-Bertani
MB-COMT	membrane-bound catechol *O*-methyltransferase
Mg^{2+}	magnesium ion
$MgCl_2$	magnesium chloride
n	number of binding sites of ligand on protein
NCBI	national center for biotechnology information
NP	nanoparticle
NTA	nitrilotriacetic acid
^oC	degree Celsius
PD	Parkinson's disease
PDB	protein data bank
PVP	polyvinylpyrrolidone
Q	quencher
R^2	correlation coefficient
RFLP	restriction fragment length polymorphism
ROS	reactive oxygen species
rpm	revolution per minute
SAH	s-adenosyl-*L*-homocysteine
SAM	s-adenosyl-*L*-methionine
SCOMT	soluble catechol *O*-methyltransferase
SD	standard deviation
SDS-PAGE	sodium dodecyl sulfate polyacrylamide gel electrophoresis
SEC	size exclusion chromatography
S_N2	nucleophilic substitution reaction
SNCA	synuclein, alpha gene
SNP	single nucleotide polymorphism
SNpc	substantia nigra pars compacta
ß	beta
TEM	transmission electron microscopy
Tris	hydroxymethyl aminomethane
U	unit
UV	ulraviolet
UV-vis	ultraviolet -visible
V_{max}	maximum enzyme reaction velocity at specified condition
w/v	Weight per volume
α	alpha
ΔH	change in enthalpy
ΔS	change in entropy
θ	number of tryptophan exposed on protein
π	pie

Amino acids abbreviations

Ala	alanine
Arg	arginine
Asn	asparagines
Asp	aspartate
Cys	cysteine
Gln	glutamine
Glu	glutamate
His	histidine
Leu	leucine
Lys	lysine
Met	methionine
Phe	phenylalanine
Pro	proline
Ser	serine
Trp	tryptophan
Tyr	tyrosine
Val	valine

Chapter one

Review of Literature

1.1 Introduction

In this thesis, research is undertaken on the medically significant enzyme, catechol *O*-methyltransferase (COMT; EC 2.1.1.6), because of its relevance in Parkinson's disease (PD). It is involved in the metabolism of levodopa, which has important implications for the treatment of the disease. In this study the enzyme is characterized and the effects of gold and silver nanoparticles on its activity investigated.

1.2 Parkinson's disease: a background

Neurodegeneration is a blanket name for disease conditions characterised by a gradual loss of structure and function of neurons, thereby debilitating the biological function of the central nervous system (Przedborski *et al.,* 2003). PD is the second most common neurodegenerative disorder, after Alzheimer's disease. The disease was first described by James Parkinson in 1817, in his article, "*An essay on the shaking palsy"* (Parkinson, 1817). He described its features as an ''involuntary tremulous motion, with lessened muscular power, in parts not in action and even when supported; with a propensity to bend the trunk forwards, and to pass from a walking to a running pace: the senses and intellect being uninjured". PD mainly affects neurons in the substantia nigra pars compacta (SNpc), a structure in the brain region that controls movement, addiction and reward (Figure 1.1) (Morello and Partanen, 2015). PD-related loss of dopaminergic neurons has a unique pattern, different from that caused by normal aging (Fearnley and Lees, 1991). In PD, cell loss is intense at ventrolateral and caudal portions of the SNpc, while in normal aging the dorsomedial part of SNpc is affected (Fearnley and Lees, 1991;

Morello and Partanen, 2015). PD is, therefore, a disorder of motor function characterized by cardinal motor symptoms, including bradykinesia, rigidity, resting tremor, and postural disorders (Massano and Bhatia, 2012).

Figure 1.1: Brain region showing the position of substantia nigra pars compacta (SNpc), SNpc of healthy brain and diminished dopaminergic neurons of SNpc in Parkinson's disease (Adapted from MedlinePlus, 2015).

1.2.1 Risk factors of PD

Despite the intensive research on the pathology and etiology of PD, the causes of the disease remain elusive. Little is known about the pathogenesis of the disease as it is a complex disorder with variable contributions of a multitude of factors including age, genetic constitution, environment and gender (Friedman *et al.*, 2016).

Age influences the clinical progression of PD and is one of the most important risk factors for sporadic PD. The possible role of aging in the pathogenesis of PD is suggested by the disease occurrence in middle age and increasing prevalence at older age (Moon and Peak, 2015). Although aging is no longer considered the exclusive cause of the disease (Diederich, *et al.*, 2003), old-age could be a contributing factor to the phenotypic expression of PD symptoms. It remains the most important risk factor for PD since the disease is more prevalent in the

population of 65 years and older (Blin *et al.,* 1991; Levy *et al.*, 2002; de Lau and Breteler, 2006; Dawson *et al.,* 2010).

Although most known cases of PD are idiopathic, molecular genetics analyses reveal that more than 500 different DNA variants are associated with five disease genes linked to familial PD (Nuytemans *et al.,* 2010). Family-linked Parkinsonisms include young onset, onset with dystonia and the early occurrence of dementia (Corti *et al.,* 2011). However, just 5–10% of PD patients have a mutation in one of the genes known to cause autosomal dominant or recessive types of the disease (Corti *et al.,* 2011).

Mitochondria are exposed to a highly oxidative environment, and reactive oxygen species (ROS) are produced in the process of oxidative metabolism (Henchcliffe and Beal, 2008). Mitochondrial dysfunctions linked to human exposure to environmental contaminants are recognized as significant contributing factors for the development of PD (Moon and Peak, 2015). Features related to rural environments, including drinking well-water and exposure to pesticides, are reported risk factors for PD (Priyadarshi *et al.,* 2001; Dick *et al.,* 2007). Environmental pollutants from industrial and mining activities, including organic wastes, organo-halogens, heavy metals and solvents also contribute markedly to the environmental risk factors of the disease (Caudle *et al.,* 2012; Kwakye *et al.,* 2015).

More men than women have been identified with PD, and some gender differences have been reported in the disease (Ivy *et al.,* 2010). For example, circulating testosterone has been reported to enhance dopamine depletion by methamphetamine in males, but not females, and promote neurodegeneration and PD in particular (Gao and Dluzen, 2001; Lewis and Dluzen, 2008; Gillies *et al.,* 2014).

1.2.2 Epidemiology and socioeconomic burden of PD

PD is prevalent in aged people, affecting more than 1.5% of the world population over 65 years of age (Dawson *et al.,* 2010). Although mutations in the *Parkin* gene area also cause early-onset autosomal recessive familial PD, and isolated juvenile-onset PD at or before the age of 20 years (Lücking, *et al.,* 2000), patients with old-age PD onset have greater motor impairment than patients with early PD onset (Diederich *et al.,* 2003), and only 5-10% of the PD patients are below 40 years (Samii *et al.,* 2004). The incidence of the disease therefore increases with age and consequently, since there is an anticipated increase in life expectancy, PD is expected to impose an increased burden on humanity (de Lau and Breteler, 2006).

In comparison to the USA and Europe, reported prevalence of PD in Sub-Saharan Africa is low due to the relative youthfulness of the population, rareness of published reports, and cultural view of neurological disorders as part of normal ageing (Akinyemi, 2012). By and large, the prevalence of Parkinsonism and PD has been reported in Africa since 1970s (Osuntokun, 1971). There is a demographic transition in African nations, with an increase in life expectancy, and therefore its population is becoming older (Nair, 2014). As a result, there is an anticipation of a surge of age-related conditions such as PD (Kahn, *et al.,* 2006; Lekoubou *et al.,* 2014; Nair, 2014). Within the last five years reports have indicated a high prevalence of PD in South Africa (van der Merwe, *et al.,* 2012) and Nigeria (Akinyemi 2012, Femi, *et al.,* 2012) in both the aged and juvenile sectors, attributable to genetic and/or environmental risk factors (van der Merwe, *et al.,* 2012).

The burden of PD is a crucial health issue, causing major economic and social trammels impacting the quality of life of affected communities, families and individuals (Dodel *et al.,*

1998; Keränen, *et al.,* 2003). Care for patients with PD is mainly provided by family. The care-givers not only provide bodily and emotional supports for the Parkinson's patients but also accord them the necessary economic requirements for medications and to prevent early nursing home placement (Schrag, *et al.,* 2006).

1.2.3 Pathogenesis of PD

Even though the cause and pathogenesis of selective demise of dopaminergic neurons in PD remains unclear, converging reports suggest evidence for vital roles of mitochondrial dysfunction (Winklhofer and Haass, 2010; Moon and Peak, 2015) and the levels of α-synuclein expression (Recasens and Dehay, 2014) in the pathogenesis of the disease.

The indication for the role of mitochondrial dysfunction in the pathogenesis of PD comes primarily from two sources. The *PINK2*, *PINK1* and *PINK7* genes encoding for the E3 ubiquitin ligase parkin, mitochondrial kinase and the protein DJ-1, respectively, are not only known to correlate with the prevalence of familial PD but are also involved in mitochondrial functions (Cookson, 2012). The E3 ubiquitin ligase parkin and mitochondrial kinase are central for the maintenance of mitochondrial turnover (Winklhofer and Haass, 2010; Charan and LaVoie, 2015), while DJ-1 is involved in oxidative stress responses (Antony *et al.,* 2013). Secondly, defects in the mitochondrial complex I functions in the electron transport chain have long been associated with the pathogenesis of PD. The defects have been observed in some animal models of PD (Meredith and Rademacher, 2011) and also in the tissues of people with PD (Keeney *et al.,* 2006; Subramaniam and Chesselet, 2013).

One of the important genes linked to sporadic PD is *SNCA*, which encodes for α-synuclein, a protein with undefined physiological function (Stefanis, 2012). PD is characterized by the

pathological accumulation of intraneuronal protein, the Lewy bodies, which are abnormal aggregates of α-synuclein (Olanow and Brundin, 2013). The presence of Lewy bodies is the histopathological hallmark of PD (Wakabayashi *et al.,* 2007; Wakabayashi *et al.,* 2013).

Dopamine is the primary neurotransmitter that controls the brain reward system (Blum *et al.,* 2014). Although PD is a condition arising from multiple etiologies that originate from a variety of interactions, the loss of dopaminergic (dopamine containing) neurons of the SNpc region (Figure 1.1) of the brain is essential for the diagnostic Parkinsonian features (Morello and Partanen, 2015). The factors leading to the loss of dopaminergic neurons in the disease are the subjects of continuing debate and experimental studies (Sulzer, 2007; Blum *et al.,* 2014). Replacement of dopamine in SNpc region, which is deficient in endogenous dopamine as a consequence of the neurodegenerative process induced by PD, remains the most effective strategy for managing the disease symptoms, prolonging life expectancy and improving the quality of life of patients (Sarkar *et al.,* 2016).

1.2.4 Treatments of PD

Parkinson dedicated a chapter in his essay to "considerations respecting the means of cure" (Parkinson, 1817). This is indicative that the history of PD treatment goes with that of the disease. He prescribed venesection on the neck, to allow blood flow from the neck, and cause a "sufficient quantity" of pus discharge (Parkinson, 1817). This practice was aimed at relieving pressure on the brain and spinal cord, and thus the medulla, which he considered as the basis of neurological dysfunction, from inflammatory pressure. This in turn alleviated PD symptoms.

Since there are as yet no available medications to cure the inherent neurodegenerative process in PD, surgical and pharmacologically-based remedies are presently in use as symptomatic therapies to improve the life quality of PD patients (Barker *et al.*, 2016).

Surgical treatment options for PD have been in practice for more than 50 years. Deep brain stimulation (DBS), the currently preferred surgical option for treatment of PD, was first used in 1997, replacing thalamotomy to treat the characteristic tremor of the disease. (Benabid, *et al.*, 2009). DBS involves implantation of electrodes at the target brain region for delivery of continuous electrical impulse to block the brain's anomalous activities that cause the symptoms of PD. The firmly entrenched electrodes are connected to an internalized programmable stimulator (Benabid, 2003). The surgical procedure is hindered by the old age of the majority of patients, and therefore is feasible for only a few PD patients (not more than 1%) (Mehanna and Lai, 2013). The ideal candidates for this surgery are young, non-demented patients having no psychopathology and severe refractory motor fluctuations. The effect of the surgical brain stimulation is comparable to that seen with the maximum levodopa response with respect to relief of the cardinal motor symptoms (Lees, 2002; Mehanna and Lai, 2013). Levodopa, a precursor of dopamine which crosses the blood-brain barrier (BBB), replaces dopamine levels in the striatum of the SNpc and subsequently alleviates PD clinical motor symptoms. Administration of this drug remains the basic pharmacological therapy for PD (Siddiqi *et al.*, 2016).

1.2.5 Levodopa: a pivotal substance for PD pharmacological therapy

In 1957, the existence of dopamine as a precursor of norepinephrine in the mammalian brain was reported (Mongatu, 1957). In the same year, Arvid Carlsson demonstrated that dopamine was not

just a precursor of norepinephrine but also a neurotransmitter in the brain, playing a vital role in motor function (Yeragani *et al.,* 2010; Lees *et al.,* 2015). He also showed that levodopa restores reserpine-depleted dopamine in animals; and consequently reverses reserpine-induced immobility (Lees *et al.,* 2015). Carlsson's findings led to the discovery of dopamine deficiency in the striatum of post-mortem brain of PD patients (Ehringer and Hornykiewicz, 1998). This deficiency was distinctive only for PD, as other disorders of basal ganglia, such as Huntington's disease were not associated with a significant change in striatal dopamine levels (Hornykiewicz, 2010). A treatment trial was started by Hornykiewicz with intravenous levodopa, to restore depleted dopamine in PD patients. This trial resulted in a remarkable result: a remedy for the key feature of PD: akinesia (Birkmayer and Hornykiewicz 1961), and thus the beginning of levodopa therapy.

Since the introduction of levodopa therapy in 1960s, its effectiveness has generally been accepted (Salata and Tolosa, 2013; Siddiqi *et al.,* 2016) and it remains the centre of pharmacological symptomatic medication of PD. Levodopa offers more relief of symptoms than any other single agent used for the treatment of PD. Although levodopa, the "gold standard" treatment of PD, improves the function and quality of life, morbidity, and mortality, and therefore decreases individual and societal costs, its application has some crucial drawbacks. It is quickly metabolized in the periphery and has a short plasma half-life (about 1.5 h). The metabolism of levodopa in the periphery results in fluctuations, including wearing-off of its effect and inconsistent symptomatic relief in addition to the development of dyskinesias, both increasing with the advancement of the disease (Nutt, 2008; Dhall and Kreitzman, 2016). Levodopa monotherapy is frequently compromised by dose-limiting nausea caused by the peripheral conversion of levodopa to dopamine by the aromatic amino acid decarboxylase

(AADC) (Davis, 1998). Co-administration of AADC-inhibitors was therefore devised to prevent peripheral metabolism by AADC and subsequently increase delivery of levodopa to the brain (Hsu *et al.,* 2015).

1.3 Catechol *O*-methyltransferase (COMT; EC 2.1.1.6) inhibition in the treatment of PD

1.3.1 Rationale for the COMT inhibition

After blockage of the peripheral decarboxylation of levodopa by AADC-inhibiton, *O*-methylation by the peripheral (soluble) catechol *O*-methyltransferase (SCOMT) to 3 *O*-methyldopa (3-OMD) becomes the major route for levodopa degradation in the periphery (Davis, 1998; Kaakkola, 2000). It has been suggested that 3-OMD may decrease brain uptake of levodopa by competing for active transport across the BBB (Nyholm *et al.,* 2012), thereby demonstrating an additional importance of COMT as a target for therapeutic strategies. Indeed, based on the approach of peripheral COMT inhibition, various COMT inhibitors were introduced into clinical applications to increase the brain availability of levodopa in PD treatment (Figure 1.2) (Kiss and Soares-da-Silva, 2014).

1.3.2 COMT: Gene, structure and reaction mechanism

COMT is magnesium dependent and catalyses the *O*-methylation of catecholamines and other catechols using S-adenosyl-*L*-methionine (SAM) as the methyl donor (Axelrod and Tomchick, 1958). The substrates for this enzyme are a wide variety of endogenous and exogenous catechols, including catecholamines, catecholestrogens, ascorbic acid, dietary phytochemicals and catechol-containing drugs (Zhu *et al.,* 2000; Bonifácio *et al.,* 2007). The physiological importance of COMT is the methylation and subsequent deactivation of bio-active and biotoxic catechol-containing compounds.

In the 1990s, the attention of researchers was drawn to COMT when the potent and selective second-generation COMT inhibitors were developed and soon after, the COMT gene and 3D structure were characterized and COMT polypeptide cDNAs were cloned (Mannisto and Kaakkola, 1990; Mannisto *et al.*, 1992).

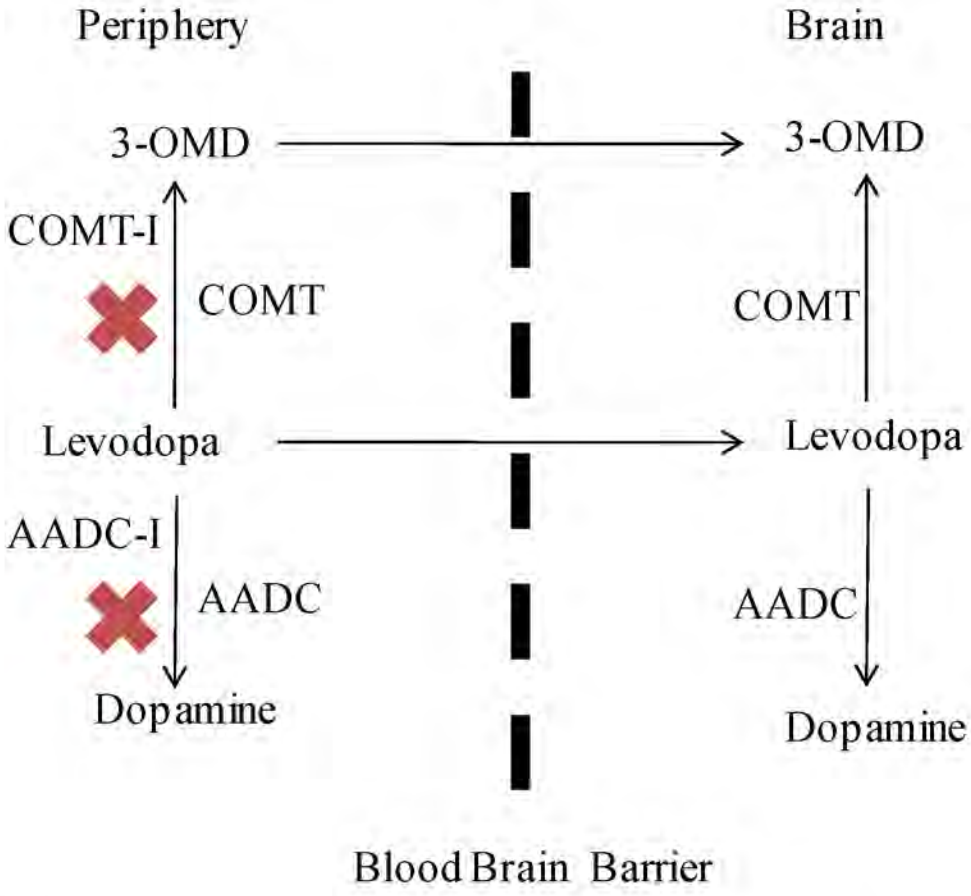

Figure1.2: Inhibition of both COMT and AADC in the periphery allowing more levodopa to cross the BBB. Further, inhibition of COMT activity restrains the synthesis of 3 -OMD which competes with levodopa for the BBB transporter system (Adapted from Goncalves *et al.*, 2012).

1.3.3 COMT: two proteins, one gene

Studies from the sub-cellular fractionation identified two forms of the COMT enzyme in mammals, the membrane-bound (MB-COMT) and the cytoplasmic soluble (SCOMT) (Kaakkola *et al.,* 1987). Chemical cross-linking and purification results indicated that SCOMT is a monomeric enzyme (Lundström *et al.,* 1995). Cloning of the human COMT allowed expression and biochemical characterizations of the recombinant MB-COMT protein. These studies revealed that, in comparison with human SCOMT (HSCOMT), which contains 221 amino acid residues with molecular mass of about 26 kDa, the human MB-COMT had an N-terminal extension of fifty hydrophobic amino acid residues and a molecular mass of 32 kDa (Ulmanen and Lundström, 1991; Lundström *et al.,* 1991; Bertocci *et al.,* 1991). The extension contains a signal-anchor region, facilitating the anchoring of the MB-COMT protein onto cellular membranes (Lundström *et al.,* 1991; Ulmanen and Lundström, 1991).

DNA analyses indicated that human, rat, canine and monkey cells have one gene for both SCOMT and MB-COMT (Lundström *et al.,* 1991). The exon-intron organization of human *COMT* gene was characterized by comparing the sequences of the known cDNA clones and genomic regions, and by polymerase chain reaction analysis (Lundström *et al.,* 1991; Bertocci *et al.,* 1991). The overall structure of the human *COMT* gene is very similar to that of rat (Salminen, *et al.,* 1990), indicative of the similarity in mammalian COMT enzymes. Cellular hybrid techniques showed that the human *COMT* gene is localized on chromosome 22, band *q11.2* which contains six exons, with the first two being noncoding (Mannisto and Kaakkola, 1999). The cellular expression of the *COMT* gene is controlled by two different promoters, both located in exon 3 (Lundström *et al.,* 1991). The distal 59 promoter (P2) regulates the synthesis of 1.5-kb mRNA which codes for MB-COMT and SCOMT through the leaky scanning mechanism

of translation initiation (Mannisto and Kaakkola, 1999). The expression of the shorter transcript of 1.3-kb is regulated by the P1 promoter, which is located between SCOMT and MB-COMT ATG start codons, and in part overlaps the MB-COMT coding sequence (Figure 1.3). MB-COMT AUG translation initiation codon is not included in these transcripts, and therefore codes only for SCOMT polypeptide (Mannisto and Kaakkola, 1999).

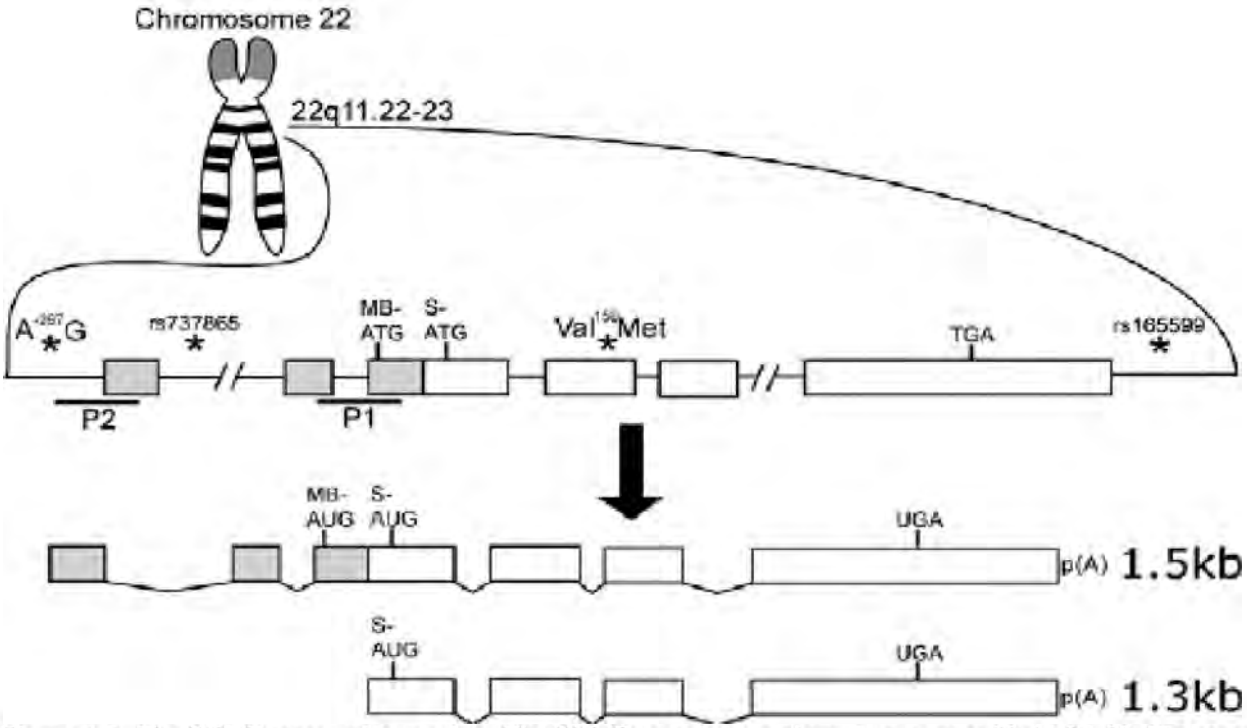

Figure 1.3: The COMT gene and transcripts. The COMT gene is located on chromosome 22q11.22–23. The gene consists of six exons (sequences in gray are unique to the 1.5-kb transcript) and has two promoters, P2 and P1, responsible, respectively, for controlling expression of the 1.5-kb and 1.3-kb transcripts (Tunbridge *et al.*, 2006).

COMT is an intracellular ubiquitous enzyme in mammals (Mannisto and Kaakkola, 1999). The long transcript is particularly abundant in human brain, kidneys, adrenals, and lungs (Bonifácio *et al.*, 2007). The short transcript, however, has higher levels in the liver, mammary glands kidneys (Tenhunen *et al.*, 1994) and smaller amounts in the brain (Tenhunen and Ulmanen,

1993). However, there is no direct correlation between COMT transcript and protein levels (Bonifácio *et al.,* 2007). In most human tissues, the levels of SCOMT exceed that of MB-COMT, except in the brain, where it represents about 30% of the total COMT (Tenhunen *et al.,* 1994). A higher membrane-bound to soluble ratio has also been reported in human adrenals and pheochromocytomas (Eisenhofer *et al.,* 1998; Ellingson *et al.,* 1999).

1.3.4 COMT genetic polymorphism

In humans, COMT catalytic activity is associated with a functional single nucleotide polymorphism (SNP). According to segregation analysis of family studies this polymorphism is caused by autosomal codominant alleles and is linked with three- to four-fold differences in COMT activity among homozygous subjects (Weinshilboum and Raymond, 1977; Mannisto and Kaakkola, 1999). A substitution between G →A at codon 108/158 (start codon for SCOMT/MB-COMT), leads to a valine-to-methionine substitution with Val-108/158 variant having higher activity and thermostability than the Met-108/158 variant. This genetic polymorphism therefore results in a trimodal COMT enzymatic activity of high ($COMT^{HH}$), intermediate ($COMT^{LH}$), and low ($COMT^{LL}$) allele (Weinshilboum and Raymond, 1977).

The association of this polymorphism with PD has been extensively studied, but generally no association occurs between this polymorphism and PD (Mannisto and Kaakkola, 1999; Hoda *et al.,* 1996; Jiménez-Jiménez *et al.,* 2014). However, in a study on Japanese individuals with PD, the $COMT^{HH}$ showed higher frequency in PD patients than in controls (Yoritaka *et al.,* 1997).

There are, however, some neuropsychological disorders wherein some connections have been reported. Lachman *et al.,* (1998) reported a connection between low COMT activity allele with aggressive and highly violent impulsive schizophrenia. The low activity COMT allele also has a

correlation with an obsessive-compulsive disorder in which the affected individuals are implicated with anxiety complications (Karayiorgou *et al.,* 1997). A velo-cardio-facial syndrome, where the chromosome *22q.11* (harbouring the COMT gene) is deleted in some individuals is a congenital disorder associated with low activity COMT allele (Lachman *et al.,* 1996). The low activity allele is reported to have a positive correlation with an increased risk of breast cancer (Huang *et al.,* 1999; Dawling *et al.,* 2001), abdominal obesity and high blood pressure (Annerbrink *et al.,* 2008) and an array of other neuropsychological disorders including late-onset alcoholism type 1 (Tiihonen *et al.,* 1999), depression (Mannisto and Kaakkola 1999), bipolar disorder (Shifman *et al.,* 2004), increased pain sensation (Zubieta *et al.,* 2003; Loggia *et al.,* 2011), Irritable Bowel Syndrome (Karling *et al.,* 2011), fibromyalgia (Cohen *et al.,* 2009) and panic disorder (Woo *et al.,* 2002; Woo *et al.,* 2004; Domschke *et al*., 2007).

The high activity allele gene is reported as having positive correlations with the genetic susceptibility to anorexia nervosa (Frisch, *et al*., 2001), attention-deficit hyperactivity disorder (Eisenberg, *et al.,* 1999), increased appetite in children (Galvão *et al.,* 2010) and increased vulnerability to drugs and general substance abuse (Vandenbergh*et al.,* 1997). Recently, the high activity allele gene is reported to impact on language performance and processing ability in children (6 to 10 years) (Sugiura, *et al.,* 2016).

Several other *COMT* gene polymorphisms have been reported but none of them have any physiological significance (Shield *et al.,* 2004; Bonifácio *et al.,* 2007).

1.3.5 Structure of COMT enzyme protein

The three-dimensional structures of the recombinant HSCOMT in complex with SAM co-substrate, the magnesium ion (Mg^{2+}) and the competitive inhibitor 3,5-dinitrocatechol (DNC)

(Rutherford *et al.,* 2008b) as well as with SAM, Mg^{2+} and nebicapone (BIA) (1-(3,4-dihydroxy-5-nitrophenyl)-3-(N-3-trifluormethylphenyl)-piperazine-1-propanonedihydrochloride) (Bonifácio *et al.,* 2002) have been resolved.

The structure of HSCOMT is a one-domain α/ß protein (Bonifácio *et al.,* 2002; Rutherford *et al.,* 2008). It is composed of a seven-stranded ß-sheets core (3↑2↑1↑4↑5↑7↓6↑) flanked by a set of α-helices (Figure 1.4). This is the characteristic structure of the SAM-dependent methyltransferase family, differing only in the presence of an extended loop between ß-strands 6 and 7 forming part of the catechol-binding site (Martin and McMillan, 2002). The helix 6 is a π-helix, while helix 7 is a 3_{10} structure. These structures in helices 6 and 7 are due to the presence of proline residues, Pro124 and Pro149, respectively, which disrupt the helices. One tyrosine residue (Tyr68) falls within the disallowed region of the Ramachandran plot (Ramachandran *et al.,* 1963). This residue is located in the SAM-binding domain, where it adopts an unfavourable conformation that allows SAM binding. This disallowed geometry occurs in human COMT structures and in all published structures of rat COMT (Bonifácio *et al.,* 2007). The human HSCOMT enzyme is structurally similar to rat SCOMT (Bonifácio *et al.,* 2002; Rutherford *et al.,* 2008b) and the modelled structure of bovine SCOMT (Figure 2.3) further emphasizing the functional and kinetic similarities between these proteins in mammals.

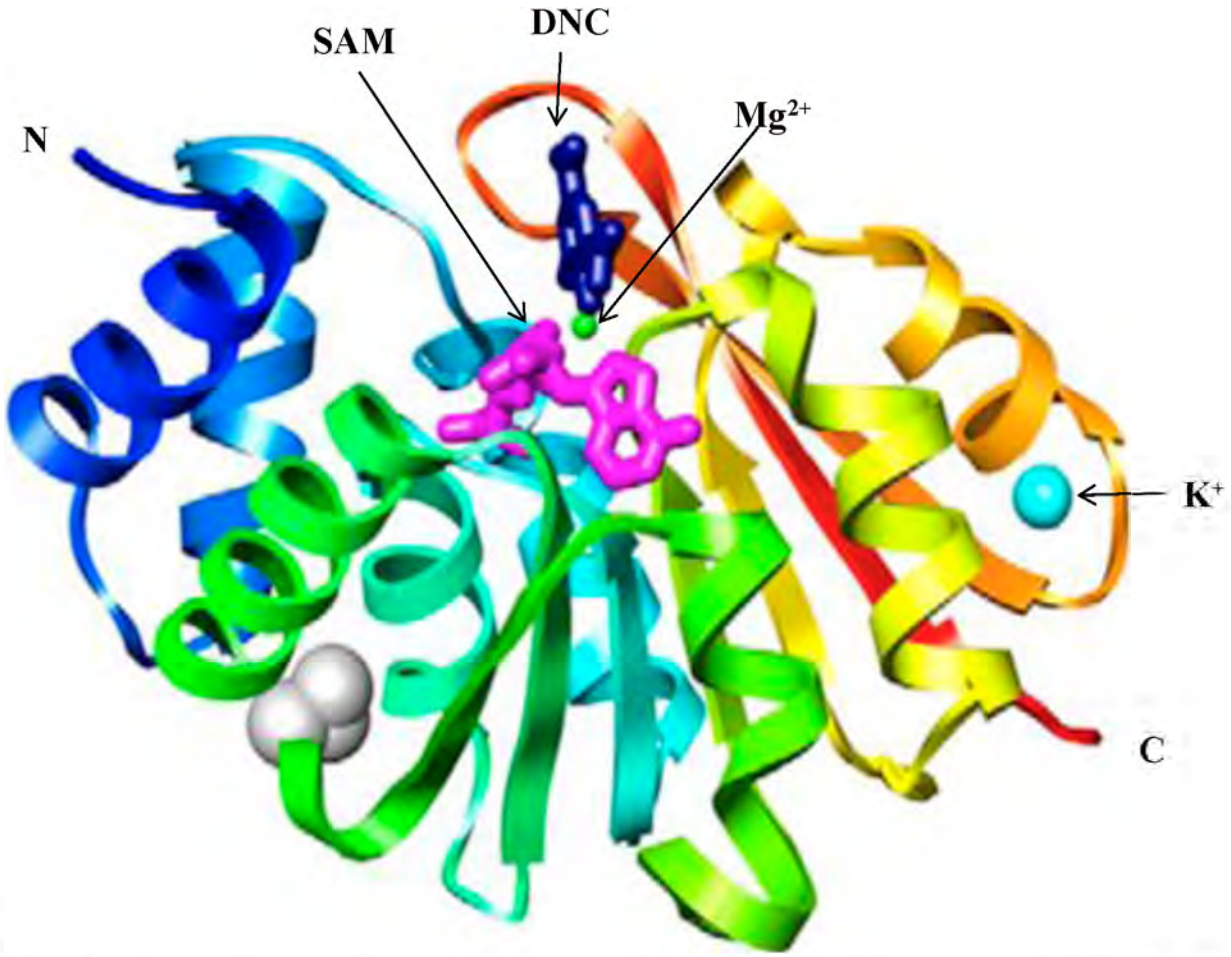

Figure 1.4: The ribbon diagram of the crystal structure for HSCOMT. The structures coloured from blue (N-terminus) to red (C-terminus) are shown. The HSCOMT was co-crystallized with SAM (magenta), DNC (dark blue), Mg^{2+} (green) and K^+ (cyan). The K^+ is from the protein environment (Rutherford *et al.*, 2008b).

1.3.6 Catalytic mechanism of COMT

SAM-dependent methyltransferases are enzymes catalysing the transfer of methyl groups from SAM to oxygen, nitrogen, or sulfur nucleophiles of different molecules (Kurogi *et al.*, 2012). These enzymes methylate DNA (Siedlecki and Zielenkiewicz, 2006), RNA (Blanco and Frye, 2014), proteins (Sawan and Herceg, 2010), and other exogenous and endogenous molecules such as catechols (Axelrod and Tomchick, 1958).

COMT, a Mg^{2+}-dependent enzyme, catalyzes the transfer of the methyl group from SAM to a hydroxyl group on a catecholic substrate. Earlier kinetic studies with the partially purified enzyme suggested different catalytic mechanisms, including the random equilibrium and ping–pong mechanisms (Coward, *et al.,* 1973). Later kinetic studies (Lotta *et al.,* 1995), X-ray crystal structures (Bonifácio *et al.,* 2002; Rutherford *et al.,* 2008b) and *in silico* investigations (Kuhn and Kollman, 2000; Ma *et al.,* 2013) revealed a sequential mechanism. The sequential mechanism operates via a nucleophilic substitution where the rate determining step involves two components (S_N2). The methyl donor, SAM, binds to the active site of COMT first, followed by a Mg^{2+} and the catechol substrate. Deprotonation of the catechol is a prerequisite for methylation. It is proposed that the side chain NH_2 of Lys144 acts as the base to abstract the proton from the catechol (Zheng and Bruice, 1997). The divalent Mg^{2+} is octahedrally coordinated with Asp141, Asp169, Asn170, one hydroxyl group from a water molecule and the remaining two free coordination sites are occupied by the two catechol hydroxyl groups of the substrate (Fig 1.5). The Mg^{2+} is therefore responsible for securing the substrate and/or inhibitor molecules at the catalytic position. Glu199 and Lys144 residues form additional hydrogen bonds with two catechol hydroxyls, with one of the hydroxyls positioned in proximity to the activated methyl group of the co-substrate, SAM. The "gatekeeper" residues, Trp38, Trp143, Pro174, and Leu198, flank the hydrophobic entrance of the catalytic pocket, help to keep the planar catechol ring in the correct orientation. It is noteworthy that the Mg^{2+} also lowers the pK_a of the catechol hydroxyls, making them more easily ionized. The methyl group transfer is the rate-determining step of the reaction, with an S_N2-like transition state, where the methyl moiety is located symmetrically and tightly between the leaving group and the nucleophile. After the catalytic reaction, the products dissociate in reverse order (Bonifácio *et al.,* 2007).

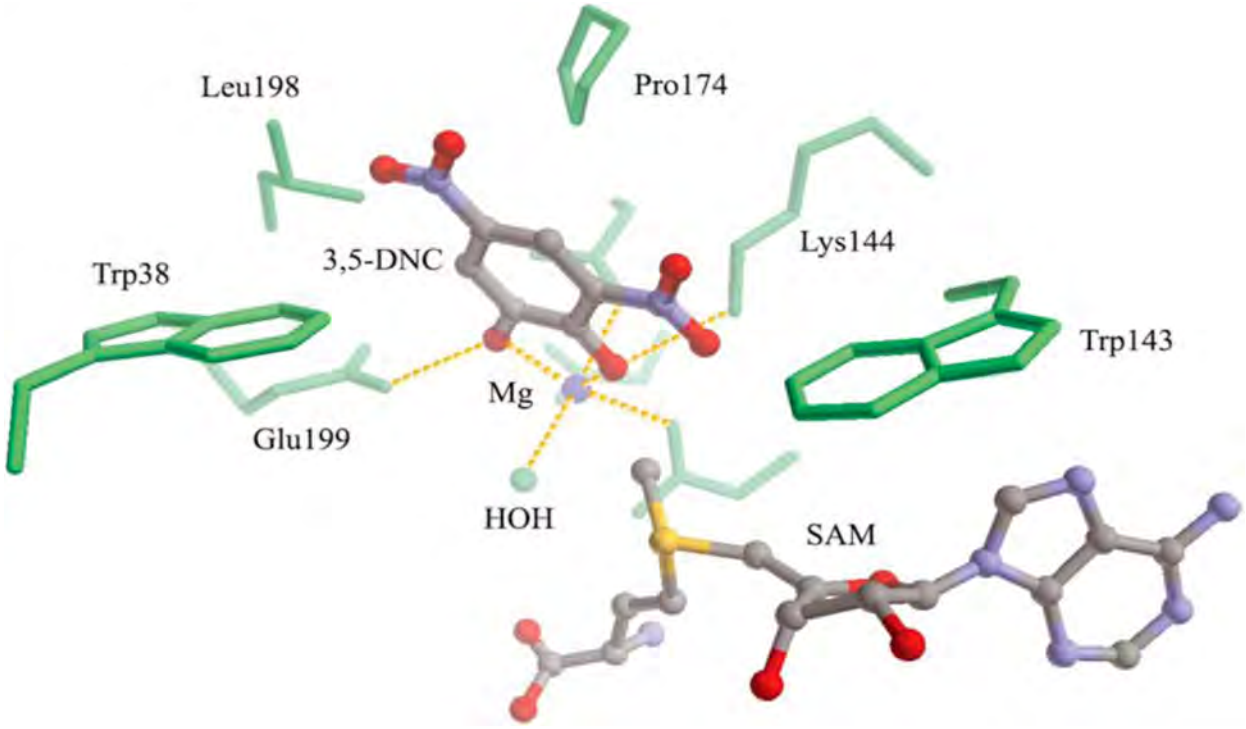

Figure 1.5: The Michaelis catalytic structure of COMT complexed with SAM and DNC. The coordination bonds to the Mg^{2+} and hydrogen bonds to Lys144 and Glu199 are illustrated in gold (Bonifácio *et al.*, 2007).

The catalytic *O*-methylation of catechols by COMT is regioselective (Masri *et al.*, 1964), favouring *meta O*-methylated products *in vivo* (Axelrod, 1966) and *para O*-methylated products *in vitro* (Kiss and Soares-da-Silva, 2014). Investigations on the catalytic properties of the monomeric and dimeric HSCOMT indicated that the enzyme monomer favours *para O*-methylation while the dimer prefers *meta O*-methylation (Law *et al.*, 2016), suggesting that the COMT dimer is the physiologically relevant protein *in vivo*.

Multi-substrates with sequential reaction mechanism, for COMT kinetics, have more often been explained by the rate-substrate concentration relationship, the classical hyperbola, in conformity with the Michaelis-Menten model of kinetics (Veser, 1987; Bonifácio, *et al.*, 2002; Lotta *et al.*, 1995). However, a few studies reported sigmoidal kinetics of COMT, including methylation of

epinephrine at a specific reaction condition (Ball *et al.,* 1972) and the methylation of two out of four catechol estrogens reported by Dawling *et al.,* (2001), signifying cooperativity in the mechanism (Ferrel, 2009).

The general structure-based drug design of the nitrocatechol-based COMT inhibitors (section 1.3.7) is based on the closed enzyme conformation, with a representative Michaelis complex of the crystal structure of COMT monomer (Figures 1.4 and 1.5) (Bonifácio *et al.,* 2002; Rutherford *et al.,* 2008b). However, a HSCOMT homodimer, formed by an intramolecular disulfide bond between Cys188 and 199 residues, also catalyzes *O*-methylation of catechols (Cotton *et al.,* 2004). There are variations between the HSCOMT monomer and dimer in regioselectivity towards different catechol substrates (Law *et al.,* 2016), indicating that the aforesaid prescribed catalytic/inhibition mechanism is not sacrosanct. The ordered sequential mechanism, with SAM binding first to COMT followed by the $Mg^{2+}$and finally catechol substrate (Lotta *et al.,* 1995; Kuhn and Kollman, 2000; Bonifácio *et al.,* 2002; Rutherford *et al.,* 2008b; Ma *et al.,* 2013), is an indication that the apo form, the semi-holo form with SAM bound (but not Mg^{2+}) and the holo form with both SAM and Mg^{2+} bound are all obligatory intermediates in the reaction mechanism. Similarly, the large size of SAM, which is entirely enclosed within COMT (Figures 1.4 and 1.5), and the obligatory exchange of the reaction product S-Adenosyl-*L*-homocysteine (SAH) with SAM for the subsequent catalysis (Law *et al.,* 2016), is indicative of substantial conformational changes during COMT catalysis.

Tsuji *et al.,* (2009) reported the first conformational flexibility of (rat) COMT presented by the apo structure, which demonstrated different α2/α3 and ß6/ß7 loop regions in comparison with the SAM and catechol-bound structure. In comparison with other nitrocatechol-bound structures, Tsuji *et al.,* (2009) reported some differences between 4-phenyl-7,8-dihydroxycoumarin

(4PCM)-COMT and the other previously reported structures. The phenyl ring of the 4PCM was unable to make relevant contacts with the protein due to unusual conformational restriction by the side chains of Trp38 and Pro174. From a study of rat SCOMT in complex with 3,4-dihydroxy-2-nitrobenzophenone (BIA 8-176), the enzyme formed a dimeric crystal structure (PDB: 2CL5), and the phenyl group of the BIA 8-176 made a hydrophobic contact with adjacent protein residue (Palma *et al.,* 2006).

Ehler *et al.,* (2014), reported the catalytically relevant apo (PDB: 4PYI), semi-holo (PDB: 4PYL) and holo (PDB: 4PYN) structural form of HSCOMT. They further showed the formation of HSCOMT dimer (PDB: 4PYJ) and higher oligomer (PDB: 4PYK) caused by the single and the rarely double domain swap. They also demonstrated the possibility for the apo state of COMT to adopt several conformations owing to an absence of conformational restrictions on the active-site loops.

Domain swaps also occur in HSCOMT (Ehler *et al.,* 2014; Law *et al.,* 2016). The domain swap involves exchange between three hinge regions, α2/α3, ß5/ß9 and ß6/ß7. These regions also change their conformations during ligand binding (Ehler *et al.,* 2014). According to Law *et al.,* (2016), the domain swapping causes ß7 strands to exchange between the two enzyme monomers and results in the formation of the enzyme dimer which maintains its overall Rossman fold tertiary structure. However, Glu199 and Tyr200 lie on the ß6/ß7 interconnecting loop, which is pulled out of the active site as a result of the domain swapping, and consequently leads to the loss of the Glu199–substrate interaction (PDB: 5FHR).

1.3.7 COMT inhibitors

In the 1960s several molecules were identified to inhibit COMT catalytic methylation activity *in vitro*. These were the first generation COMT inhibitors which included derivatives of pyrogallol and catechols such as gallic acid, caffeic acid, U-0521, 2-hydroxyoestrogens and some flavonoids. Other non-catecholic molecules such as tropolones and ascorbic acid also inhibited COMT (Crout, 1961) but these were highly toxic, short acting, and had unfavourable pharmacokinetics, poor selectivity and/or poor bioavailability, and therefore low efficacy *in vivo* (Mannisto and Kaakkola, 1990; Bonifácio *et al.,* 2007; Jatana *et al.,* 2013).

The second generation COMT inhibitors with appreciable *in vivo* efficacy were developed in the late 1980s and early 1990s. These inhibitors either act peripherally or both in the periphery and in the brain (Mannisto and Kaakkola, 1990; Mannisto *et al.,* 1992). Due to high COMT activities in the liver, intestine and kidney (Lancaster *et al.,* 1973; Nissinen *et al.,* 1988) and consequent *O*-methylation of levodopa at the periphery thereby decreasing the amounts to cross the BBB, peripheral COMT inhibitors are of greater interest than those acting in the brain (Mannisto and Kaakkola, 1999).

Nitrocatechol-containing structures exert reversible inhibition of COMT and represent the second generation COMT inhibitors. This category is designed based on di-substituted catechols with a nitro group at the ortho position to hydroxyl group of the catechol moiety. These include DNC, tolcapone, entacapone, nitecapone and nebicapone (Figure 1.6) (Bäckström *et al.,* 1989; Lotta *et al.,* 1995; Mannisto and Kaakkola, 1999; Jatana *et al.,* 2013). These compounds are rapidly absorbed from the gastrointestinal tract after oral administration in humans, with maximum drug concentrations in the plasma being attained in about 0.5–2 h post-ingestion

(Schultz *et al.*, 1991; Keränen *et al.*, 1994; Jorga *et al.*, 1998; Loureiro, *et al.*, 2006). These nitrocatechols possess the same binding motif as the catechol substrates in addition to the presence of a strong electron-withdrawing nitro function which blocks their reactivity towards *O*-methylation. These compounds inhibit COMT activity with variable potency (Bäckström *et al.*, 1989; Ma *et al.*, 2013).The basic structure of these compounds is DNC where the molecule occupies the substrate binding site, in a competitive mode and the 3-nitro group has favourable van der Waals interactions with Trp143, while the benzene ring forms $\pi \rightarrow \pi$ interactions with Trp38 (Figure 1.5) (Ma *et al.*, 2013).

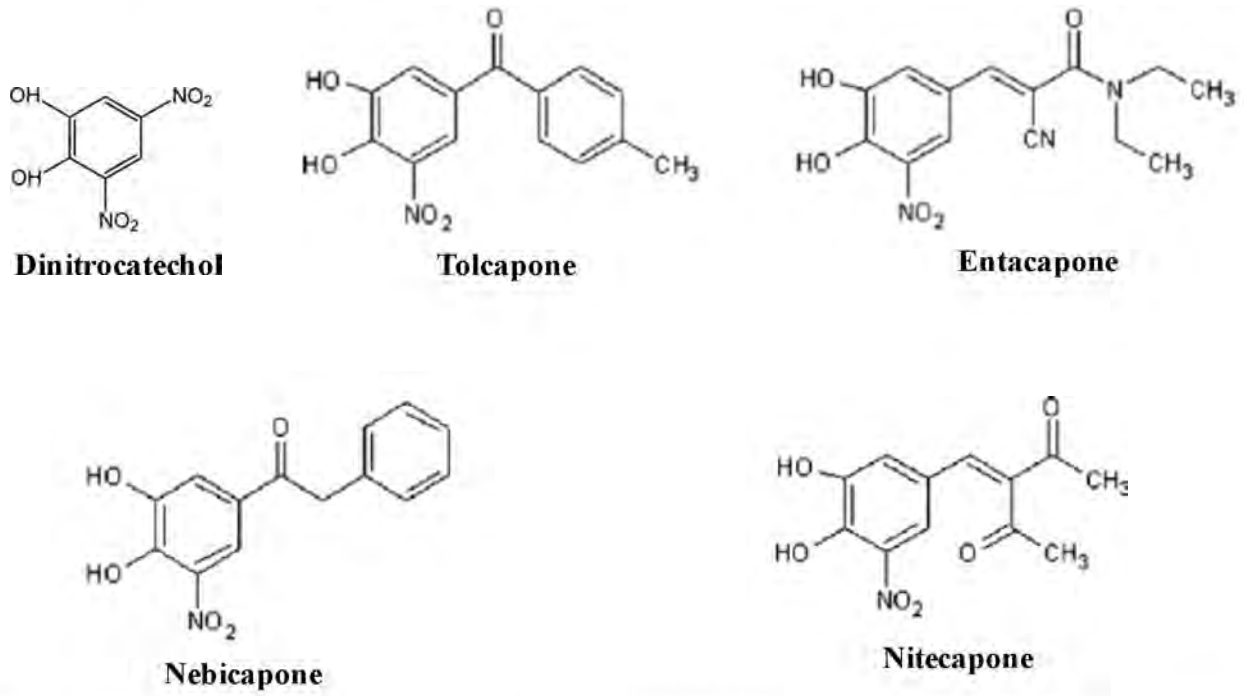

Figure 1.6: Chemical structures of some second generation COMT inhibitors (Adapted from Bonifácio *et al.*, 2007).

Two nitrocatechol-containing compounds, the brain-penetrating tolcapone, and peripherally acting entecapone, are the major inhibitors of COMT presently available in the drug market (Ma *et al.*, 2013; Detrait *et al.*, 2016). They are used as adjuncts to levodopa therapy in the management of PD and other neuropsychological disorders (Mannisto and Kaakkola, 1990; Ma

et al., 2013; Detrait *et al.,* 2016). Both tolcapone and entacapone decreased fluctuations in plasma levodopa levels, lowering patients' daily levodopa requirements (Waters, 2000; Ma *et al.,* 2013). However, each of these drugs has problems either in pharmacokinetics, clinical efficacy or in toxicity. Both drugs inhibit the bile salt export protein and cause dose-dependent mitochondrial dysfunction, leading to decreased adenosine triphosphate synthesis and increased heat production (Haasio *et al.,* 2002; Nissinen *et al.,* 2007; Nadanaciva *et al.,* 2012), while liver injury has been associated with tolcapone use (Nissinen *et al.,* 2007). Other adverse effects with entacapone treatments include dyskinesias, urine discoloration, hypotension, dizziness, nausea, and constipation (Waters, 2000).

The occurrence of catalytically relevant HCOMT conformations which differ from the DNC-based COMT structure is indicative that COMT is a malleable enzyme, and therefore a complex drug target. The difficult nature of COMT, the adverse toxicity of the currently available COMT inhibitors and the demographic transition of the world population towards old age are clarion calls for the search for new and robust strategies for the modification of COMT catalytic activity. One of the strategies may be through the application of metallic nanotechnology, since these nanomaterials interact with, and modify the catalytic activity of several enzymes (Adeyemi and Whiteley, 2013; Adeyemi and Whiteley, 2014; Yao *et al.,* 2015).

1.4 Nanotechnology

During his classic lecture titled "There is plenty of room at the bottom", presented at the American Physical Society meeting at Caltech in 1959 (published in 1961), the Nobel Prize winner (in Physics 1965), Richard Phillips Feynman said "the principles of physics, as far as I can see, do not speak against the possibility of manoeuvring things atom by atom" (Feynman,

1961). At that time, Feynman's words were considered as a pure science fiction, but nowadays are believe to be the basis for the concept of nanotechnology (Drexler, 2004).

1.4.1 Nanoparticles, nanotechnology and nanomedicine

The prefix "nano," is adapted from the Greek word "nanos," signifying "dwarf," and is becoming increasingly common in scientific literature referring to one billionth (10^{-9}) when used as a prefix. A nanometer (nm) is therefore one billionth of a meter, which is equivalent to the length of three atoms side by side (Tahan, 2007). Nanoparticles (NPs) are solid colloidal particles ranging in size from 1 to 100 nm that may differ from the bulk materials due to their sizes (Krukemeyer, 2015; McNamara and Tofail, 2016).

Nanotechnology on the other hand, is an emerging field of science involving the synthesis, development, characterization and applications of matter of sizes ranging between 1 and 100 nm (Krukemeyer, 2015). It is therefore a technology developed at the atomic, molecular, and/or macromolecular levels. As defined by size, nanotechnology is a multidisciplinary field of science which embraces chemistry, biochemistry, molecular biology, medicine, physics, electronics, semiconductors, information technology, microfabrication and molecular engineering (Saini *et al.,* 2010).

Nanomedicine is a broad application of nanotechnology for biomedical purposes; exploitation of the nanoscale materials for the development of novel therapeutic and diagnostic agents, which culminate in purposeful contact of the materials with human or animal bodies (Freitas, 2005).

1.4.2 Reactivity of nanoparticles (NPs)

Interactions of bulk materials with their environment are determined by the atomic and electronic structure as well as the general chemistry of the materials' surfaces. However, the influence of surface chemistry on the bulk of the material is generally considered to be small in comparison to that of NPs (Biener *et al.,* 2009). Such unique properties of NPs that support their beneficial characteristics relative to bulk materials include electrical, catalytic, magnetic, mechanical, thermal and/or imaging features (Gatoo *et al.,* 2014).

The "smallness" of the NPs accords them a large surface area to volume ratio, which is the driving factor for the increased reactivity of the materials surfaces with their contiguous milieu, including biomolecules (Powers *et al.,* 2006; Jiang *et al.,* 2009). These properties and reactivity make the NPs a relevant topic in pharmaceutical and biomedical applications.

1.4.3 Nanomedicine: medicinal application of metallic NPs

Historically, metals have been used, in a variety of forms, as therapeutics against many diseases, notably by the *Ayurvedic* system of medicine in India and ancient Chinese medicine (Huaizhi and Yuantao, 2000; Richards *et al.,* 2002). Vessels of gold (Au) and silver (Ag) have been used to preserve and disinfect food by the Persians, the Greeks, the Romans and the Egyptians for thousands of years (Fricker, 1996; Alexander, 2009).

There is a rising interest in the applications of different metallic nanosystems for different biomedical applications such as targeted drug delivery, hyperthermia, photoablation therapy, bioimaging, vaccines, biosensors, and also for the purpose of modifying biological functions of proteins (Saptarshi *et al.,* 2013; Edmundson *et al.,* 2014; Yao *et al.,* 2015; McNamara and Tofail, 2016).

Interaction of NPs with proteins is believed to be the basis of the NPs bio-reactivity which culminates in the formation of a NP-protein corona (Saptarshi *et al.,* 2013). The NP surface can induce conformational changes on the adsorbed protein structure, which may affect the biological function of the adsorbed protein (Ballet *et al.,* 2010; Saptarshi *et al.,* 2013). Although difficult to evidence directly, the induced conformational changes have important consequences, since the partial unfolding of protein domains could expose hitherto hidden amino acid residues (Figure 1.7) (Saptarshi *et al.,* 2013; Ballet *et al.,* 2010). For example, lysozyme adsorbed onto the surface of gold NPs is reported to lose 10% of its secondary structure and to show a marked decrease in enzymatic activity (Gagner *et al.,* 2011).

Recently metallic NPs have been reported to modify the catalytic activities of various enzymes *in vivo*, through exerting a non-competitive inhibition on the catalytic activity of arginine kinase from *Trypanosoma brucei* (Adeyemi and Whiteley, 2013; Adeyemi and Whiteley, 2014), thiazolekinase and triosephosphate isomerase from *Plasmodium falciparum* (Yao *et al.,* 2015; De Moor *et al.,* 2015).

1.4.4 Safety implications of protein adsorption onto NP surfaces

Considering the small size and the consequent reactivity of NPs, it is likely that they can not only encounter different types of cellular biomolecules but also pass across biological membranes. NP uptake into lysosomes (Lesniak *et al.,* 2012), intracellular vacuoles (Yehia *et al.,* 2007) and/or the cytoplasm (Davda and Labhasetwar, 2002) occurs by endocytosis, phagocytosis and/or macropinocytosis (Saptarshi *et al.,* 2013). Cytotoxicity and immune-modulation are, therefore, the major safety concerns of NP bio-applications (Jiao *et al.,* 2014).

NPs interact with the immune system (protein) and modulate its function (Figure 1.7D), leading to immunosuppression or immunostimulation that might be respectively, harmful or beneficial. The NP-induced immune modulation is complex and multi-factorial, relating to particle composition, size, surface chemistry, plasma protein binding, and exposure route (Jiao *et al.,* 2014).

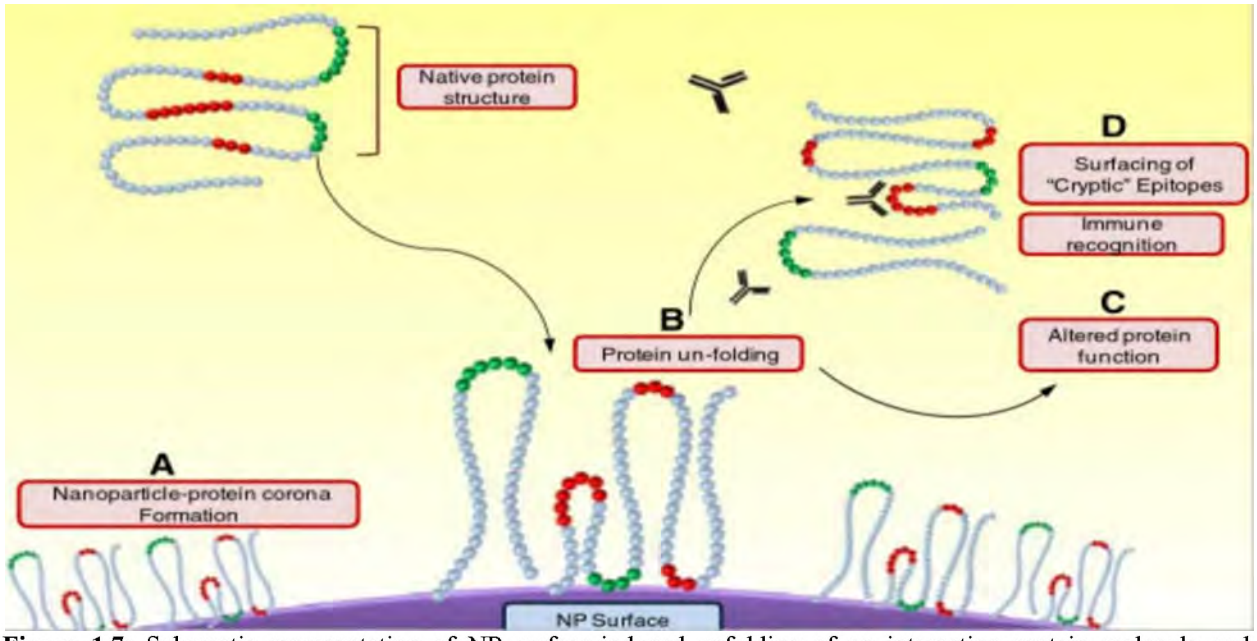

Figure 1.7: Schematic representation of NP surface-induced unfolding of an interacting protein molecule and consequences. (A) Protein molecules adsorb on to the NP surface, to form a complex termed the NP-protein corona. (B) NP surface may induce some conformational changes to the native structure of the adsorbed protein, causing it to unfold. The conformational changes may either (C) alter the function of the native protein or even lead to (D) exposure of "cryptic" epitopes which could result in immunological recognition of the complex (Saptarshi *et al.,* 2013 with permission from Professor Lopata).

Although metallic NPs have been extensively investigated for toxicity, there is still a lack of precise knowledge about their toxicity because of inconsistencies and conflicting reports on the cytotoxicity assessments (Yen *et al.,* 2009; Lanone *et al.,* 2009; Johnston *et al.,* 2010; Bahadar *et al.,* 2016; Hau *et al.,* 2016; Składanowski *et al.,* 2016). Certain factors may lead to these inconsistent findings. The presence or absence (and also type) of coating agent is one of the important factors determining the nature of the interactions between the NPs and biomolecules

(Nishimori *et al.,* 2009; Gnanadhas *et al.,* 2013). On the other hand, contradictory results for size-dependent toxicity studies are subject to further research, for example, on the influence of different administration routes (Yildirimer *et al.,* 2011). By and large, toxicological hazards of NPs and their constituents are vital considerations in NPs bio-applications, because it is generally accepted that exposure to ultrafine particles poses health risks to humans. Because of their size and ability to across biological barriers, NPs have properties that could result in increased toxicity compared to bulk materials.

1.5 Conclusion

Levadopa, a precursor of dopamine that crosses the BBB, remains the most effective medication for the management of PD. However, the use of this drug is constrained by its metabolism, catalysed by AAD in the periphery, into dopamine, which does not cross the barrier. To enhance its delivery to the brain, levodopa is co-administered with AAD inhibitors. Under this condition, levodopa is deactivated by COMT into 3-OMD in the periphery.

In mammals, this enzyme exists in two isoforms, the SCOMT and MB-COMT, with higher activity of the former in the periphery and the latter in the brain. The biological activity of this enzyme is subject to variations, caused by a single nucleotide polymorphism and is implicated in many disease conditions. Two COMT inhibitors are currently on the market. Entacapone, which does not cross the BBB and acts mainly in the periphery, and tolcapone, which crosses the BBB, and inhibits COMT both in the periphery and the brain. Clinical applications of these drugs are restricted by their adverse effects, including liver toxicity and mitochondrial dysfunction.

The universal approach for the design of COMT inhibitors, including entacapone and tolcapone, is based on the closed structural Michaelis-conformation of the protein monomer complexed

with SAM, Mg^{2+}, and the catechol substrate/inhibitor. The identification of another enzymatically relevant conformation different from the "established" Michaelis conformation (Tsuji *et al.,* 2009), and the occurrence of functional homodimer (Cotton *et al.,* 2004) indicate the existence of alternative conformations and mechanism for COMT catalysis. Furthermore, two groups of researchers, Ehler *et al.,* (2014) and Law *et al.,* (2016), reported the occurrence of domains swap, a structural phenomenon for the control of biological activities of protein, in HSCOMT. The domain swap according to Ehler *et al.,* (2014), involves three hinged regions that are also involved in the catalytic activity of the enzyme. Consequent to the domain swap is the formation of a catalytically functional dimer and higher oligomers of COMT, indicating the occurrence of biologically relevant oligomers of this enzyme.

The alternative catalytic conformation of the HSCOMT monomer and the occurrence of catalytically relevant oligomers indicate the occurrence of multiple catalytic mechanisms for COMT, rendering the enzyme a difficult drug target. Proteins, adsorbed onto the surfaces of NPs, influence their secondary structure and biological function (Saptarshi *et al.,* 2013; Yao *et al.,* 2015). These are the motifs that prompted the effort to challenge the catalytic activity of COMT with gold and/or silver NPs, which could interact with the enzyme non-specifically (Saptarshi *et al.,* 2013) and perhaps modify its catalytic activity.

1.6 Hypothesis

Gold and/or silver NPs inhibit the enzymatic activity of SCOMT.

1.7 Aim and objectives

1.7.1 Aim

To study the interaction of gold and/or silver NPs with mammalian SCOMT

1.7.2 Objectives

- Obtain the amino acid sequences for various mammalian SCOMTs and perform the bioinformatic analyses of the sequences to identify their similarities
- Model the secondary structure of bovine SCOMT (BSCOMT) for further analyses and identification of the similarities
- Purify BSCOMT from bovine liver using differential centrifugation, ammonium sulfate fractionation, size exclusion chromatography and ion exchange chromatography
- Optimize a COMT enzymatic assay
- Characterize the BSCOMT by assessing its pH and temperature optima, and its kinetic parameters
- Obtain the coding sequence for HSCOMT and synthesise the gene, transform *E. coli* JM109 with pET -22-(b+) vector harbouring the HSCOMT gene, propagate and extract the gene and perform Restriction Fragment Length Polymorphism (RFLP) and DNA sequencing to confirm the correct insertion of HSCOMT gene
- Transform *E. coli* BL 21 (DE3) cells with pET-22b(+) harbouring the HSCOMT gene for the subsequent over-expression of HSCOMT enzyme

- Purify the HSCOMT enzyme by ultracentrifugation, nickel affinity chromatography and size exclusion (desalting) chromatography
- Characterize the recombinant HSCOMT by assessing pH and temperature optima and its kinetic parameters
- Synthesize and characterize gold and silver NPs using UV/VIS spectroscopy and TEM, and also assess their size distribution and stability
- Interact HSCOMT with both gold and silver NPs and assess changes in the enzyme's kinetic pattern and/or parameters
- Perform spectroscopic and *in silico* studies to deduce the possible reasons for differences and the effects of the NPs

Chapter two

Bioinformatic identification and analysis, partial purification and characterization of Bovine catechol *O*-methyltransferase

2.1 Introduction

The use of animals, especially mammals, as models of humans in scientific investigations is an ancient practice in medicine and biological research. The physiological and anatomical similarities between humans and other mammals have prompted researchers to investigate mechanisms and assess novel therapies in animal models, as surrogate humans, before applying the scientific findings to humans (Barré-Sinoussi and Montagutelli, 2015).

Catechol *O*-methyltransferase has been identified in various organisms: plants and animals, eukaryotes and prokaryotes alike. Because of its accessibility and availability, bovine soluble catechol *O*-methyltransferase (BSCOMT) will be used as a model for the human soluble catechol *O*-methyltransferase (HSCOMT). However, since not all results obtained on animal models can be directly translated to humans (Barré-Sinoussi and Montagutelli, 2015), it is pertinent to compare the two enzyme proteins.

Bioinformatic analyses of primary structures and predictions of secondary structures are methods for the determination of properties and functions of proteins by accurately assigning a structure and function to a protein of unknown structure (Rost, 2001). Recent advances in structural genomics present an increasing number of protein sequences with indefinite structures in databases such as the UniProt (The UniProt Consortium, 2016) and the Protein Data Bank (PDB) (Westbrook *et al.,* 2003), and bioinformatic tools are used in predicting and analyzing their functions and structures.

The study of proteins and their functions is key to understanding the biochemical processes of health and diseases (Gonzalez and Kann, 2012). In-depth studies on enzyme catalysis, kinetics of the catalysis and efficacy of modulators that inhibit or enhance the catalysis are convincing if such studies are carried out with an enzyme of high purity. It is pertinent, therefore, to isolate an enzyme of interest from a complex biological mixture containing proteins, nucleic acids and other biomolecules, for clear understanding and elucidation of its biological characteristics and functions (Berg *et al.,* 2002).

Protein purification involves multi-stage experiments and procedures, aimed at isolating the target protein. The purification of a protein is possible due to the variations in the chemical and physical properties among proteins and other biomolecules. The choice of procedures is complex, as it depends on many parameters, including the source and biological nature, target amount and purity, as well as whether biological activity of the protein of interest is required. Again, selection of purification strategies depends on whether the protein or similar protein has been previously purified (Cutler, 2004), since established isolation procedures provide an insight in preparing a strategy for the isolation. Multiple purification steps are usually necessary to purify a protein (Reymond and Sicard, 2006). Optimum yield of enzyme and highest possible specific enzymatic activity (minimization of total protein) are the objectives of enzyme purification. These require techniques for separating the protein as well as for detecting its presence. Sodium dodecyl sulfate polyacrylamide gel electrophoresis (SDS-PAGE) and consistent enzyme activity assay are used to evaluate a purification process.

Mammalian catechol *O*-methyltransferase (COMT) is commonly purified from mammalian liver (Park, 1986). However, the enzyme has also been purified from other tissues, such as kidney (Darmenton *et al.,* 1976), placenta (Tilgmann and Kalkkinen, 1991), brain (White and Wu, 1975)

and heart (Borchardt and Cheng 1978). Similar purification stratagem has been reported by many researchers; the purification process involves homogenization, differential centrifugation, ammonium sulfate fractionation, gel filtration and ion-exchange chromatography (Axelrod and Tomchick, 1958; Ball *et al.,* 1971; White and Wu, 1975; Darmenton *et al.,* 1976; Tilgmann and Kalkkinen, 1990; Tilgmann and Kalkkinen, 1991; Piedrafita *et al.,* 1992). Similar properties have been reported for mammalian COMT, irrespective of the tissues and organism of origin (Borchardt and Cheng, 1978).

The aims of this chapter are to identify amino acid sequences of soluble catechol *O*-methyltransferases (SCOMT) of bovine, human and other mammals from UniProt for bioinformatic comparisons, and to purify and characterize the enzyme from bovine liver.

2.2 Materials and Methods

2.2.1 Materials

All chemicals, reagents and equipment used in this section are outlined in appendix I.

2.2.2 Methods

2.2.2.1 Mammalian SCOMT amino acid sequence, alignment and *in silico* prediction of the structure of BSCOMT

Amino acid sequences of SCOMT from six mammals, viz. bovine, human, rat, mouse, horse and dog were obtained from UniProt (Table 2.1) (The UniProt Consortium, 2016). Multiple alignment of amino acid sequences was conducted with ClustalW (Thompson *et al.,* 1994), conserved motifs and domains were identified using Multiple EM for Motif Elicitation (MEME-

suite) (Baileyand Elkan, 1994) while secondary structure of BSCOMT was predicted by Protein Homology/analogy Recognition Engine v. 2.0 (Phyre2) (Kelley and Sternberg, 2009).

Table 2.1: Accession codes for soluble catechol *O*-methyltransferase (SCOMT) of bovine, human, rat, mouse, horse and dog accessed from UniProt.

ORGANISM OF ORIGIN	ACCESSION CODE
Bovine	A7MBI7 (COMT_BOVIN)
Human	B8XPJ7 (B8XPJ7_HUMAN)
Mouse	P22734 (COMT_RAT)
Rat	O88587 (COMT_MOUSE)
Horse	Q5H879 (COMT_HORSE)
Dog	Q69FG4 (Q69FG4_CANLF)

2.2.2.2 Purification of BSCOMT

Unless otherwise stated, all purification steps were carried out on ice. One milliliter sample of each purification stage was taken and stored at -20°C for protein concentration determination, SDS-PAGE analyses, and enzyme activity assays to facilitate construction of a purification table.

2.2.2.2.1 Homogenization

Bovine liver (40 g) was homogenized in 160 ml (1:4 w/v) ice cold 0.1 M KCl, 5 mM $MgCl_2$, 0.1 mM dithiothreitol, with a household kitchen mixer (Braun Multiquick, Minipimer, Poland) for 2 × 45 sec.

2.2.2.2.2 Differential centrifugation

The homogenate was centrifuged (14 000 × *g*, 30 min; 100 000 × g, 60 min). After discarding the pellets, the supernatant fractions were adjusted to pH 5.2 with ice-cold 1 M acetic acid and stirred for 15 min before undergoing further centrifugation (14 000 × g, 10 min).

2.2.2.2.3 Ammonium sulfate fractionation

The supernate was adjusted to pH 6.8 with sodium phosphate buffer (0.5 M, pH 7.5) followed by the addition of 32.3 g ammonium sulphate to 190 ml of the resultant volume (0.17 g/ml) (in 15 min) with stirring (to 30% saturation). The mixture was stirred for an additional 45 min and the precipitate discarded after centrifugation at 14, 000 × *g* for 10 min. To the resultant supernatant fraction (150 ml), additional 0.22 g/ml ammonium sulfate (33.0 g) was added (to 65% saturation) over a stirring period of 15 min and the mixture stirred for a further 45 min. This solution was allowed to stand for 60 min and the precipitate collected by centrifugation at 14 000 × *g* for 20 min and dissolved in 6 ml of 10 mM Tris-HCl buffer pH 7.4, 20 mM mercaptoethanol 20% glycerol (storage buffer).

2.2.2.2.4 Size Exclusion Chromatography

Size exclusion chromatography was performed on a Sephadex G-100 column, which had been equilibrated with the storage buffer, at a flow rate of 0.4 ml per min. Four millilitres of the extract were loaded onto the column. Fractions of 1 ml were collected and those with the highest COMT activity were pooled.

2.2.2.2.5 Ion Exchange Chromatography

Ion-exchange chromatography was performed on a diethylaminoethyl cellulose (DEAE-cellulose) column equilibrated with the storage buffer overnight. Five millilitres of the pooled fractions with highest COMT activity from the size exclusion column were loaded onto the column. The enzyme was eluted with an increasing gradient of the buffer ionic strength (0 to 500 mM $NaCl_2$) in 1 ml fractions at a flow rate of 0.4 ml per min. The fractions with highest COMT activity were pooled and stored at -20C in 40 µl aliquots.

2.2.2.3 Determination of protein concentration

Protein concentration was routinely assayed by the Bradford method (Bradford 1976), in triplicate using a 96-well microplate, with bovine serum albumin as standard. Protein (5 µl) was added to a well, followed by Bradford reagent (245 µl). The mixture was incubated at 22°C for 10 min and absorbance of the solution measured at 595 nm.

2.2.2.4 COMT Activity Assay

Enzymatic activity of COMT was assayed based on the reports of enzymatic methylation of esculetin to a fluorescent compound, scopoletin, with S-(5'-adenosyl)-*L*-methionine (SAM) as a methyl donor (Müller-Enoch *et al.,* 1976; Kurkela *et al.*, 2004). The assay was performed using a black clear bottom 96-well microtitre plate (Greiner CELLSTAR®). For the assay, the final reaction concentrations of the BSCOMT preparation, the substrate esculetin, and the co-factor SAM, were respectively 10 µg/200 µl, 4 µM and 60 µM in a total of 200 µl reaction mixture. Four-fold concentrations each of the final assay concentration of the enzyme preparation, esculetin and SAM were prepared in the enzyme activity buffer (100 mM phosphate, 5 mM $MgCl_2$, 20 mM *L*-cysteine, pH 7.4). The substrate, esculetin was dissolved in dimethyl sulfoxide

(DMSO) and then diluted with the reaction buffer to a final DMSO concentration of 2% (v/v) (8% in four-fold concentration). Fifty microliters each of the four-fold reaction concentrations of enzyme preparation and esculetin were added to 50 µl of the reaction buffer and incubated at 37°C for 5 min, before addition of 50 µl of the four-fold concentration of SAM to initiate the catalytic reaction. Change in fluorescence was followed for 20 min with a Synergy Gen5 Multi-Mode Reader at the excitation and emission wavelengths of 355 nm and 460 nm, respectively. The change in fluorescence caused by the enzymatic methylation of esculetin to scopoletin was used as the index of COMT activity. Controls without esculetin, SAM and/or the enzyme preparation were routinely included.

2.2.2.5 Sodium dodecyl sulfate-polyacrylamide gel electrophoresis

Sodium dodecyl sulfate-polyacrylamide gel electrophoresis (SDS-PAGE) was performed with 4% and 12% acrylamide in stacking and resolving gels, respectively, in a Tris-glycine buffer system using the protocol described by Laemmli (1970). Samples were mixed in a 1:1 ratio with loading dye (50 µl TD + 200 µl TS) (appendix II), heated at 95°C for 5 min on a BIO-RAD dry heating block and loaded onto the gel after cooling to room temperature. For every SDS-PAGE gel run, 5 µl of molecular weight marker of size range 15-180 kDa (PageRuler™ Prestained Protein Ladder (Thermo Scientific)) was included alongside the samples. Electrophoresis was carried out using the BioRad Mini-PROTEAN® Tetra Cell and a BioRadPowerPac™ power supply at 120 constant volts for 90 min. SDS-PAGE gels were stained and destained using a modified Fairbanks method (Fairbanks *et al.,* 1971) to enable visualization of the proteins. This method entails staining the gels with Coomassie Brilliant Blue R250 overnight on a BioRad UltraRocker rocking platform at 50 rpm and destaining by a series of heating and cooling cycles

in solutions of decreasing concentrations of Coomassie Brilliant Blue R250 (Fairbanks solutions B, C, and D) (appendix II) (Fairbanks *et al.,* 1971).

2.2.2.6 Characterization of BSCOMT

After its partial purification, the pH optimum for BSCOMT activity was determined as described in section 2.2.2.4 at a pH range of 5 to 10, at 37°C. A cocktail of buffer salts (appendix II) covering a pH range between 4 and 10 was used to conduct pH studies. For temperature optimization, the assay was performed at optimum pH (8.5; section 2.3.3) with a temperature range of 20°C to 65°C. Kinetic parameters (K_m and V_{max}) of the enzyme were determined by running the enzyme assays at pH and temperature optima with a range of esculetin concentrations (0 to 8μM). The concentration range of esculetin was attained by monitoring the trend in enzyme activity at various substrate concentrations.

2.3 Results and Discussion

2.3.1 Multiple sequence alignment and prediction of the structure of BSCOMT

The purpose of the sequence alignment was to identify sequence similarities between different mammalian SCOMT, from which their structural and catalytic similarities can be inferred. From the multiple sequence alignment, there is high (>90%) sequence similarity among the amino acid sequences of SCOMT of bovine, human, rat, mouse, horse and dog. Bovine soluble catechol *O*-methyltransferase (SCOMT) has 78% sequence identity with human SCOMT and 80% sequence identity with rat SCOMT, whereas it has 81% sequence identity each with mouse SCOMT, horse SCOMT and dog SCOMT. As expected, amino acid residues reported as important for catalytic activity are all conserved in the aligned sequences (Figure 2.1) (Rutherford *et al.,* 2008b; Tsao *et al.,* 2011).

Figure 2.1: Multiple sequence alignments of SCOMT from human, bovine, rat, mouse, horse and dog accessed at UniProt. Multiple sequence alignment was carried out using ClustalW to determine conserved amino acids among SCOMT sequences of the organisms. Asterisk (*) indicates the position of fully conserved amino acid residues. A colon (:) shows conservation of amino acids with strong similarity properties, while a period (.) indicates conservation between groups of weakly similar properties. Amino acid residues reported to be important for SAM-binding (▮) and catechol-binding (▼) are conserved in all the sequences. All the five sequences contain a CXXS motif reported to be associated with cysteine redox signalling.

Cotton *et al.*, (2004) reported conservation of CGYS motif in SCOMT protein sequences of human, zebra fish, frog, rat, mouse and pig. From the alignment, this motif is also conserved in BSCOMT. The CGYS motif is in conformity with CXXS motif reported to be associated with cysteine redox signalling (Fomenko andGladyshev, 2002; Klomsiri *et al.*, 2011; Paulsen and Carroll, 2013), which was reported in HSCOMT and may be linked to the enzyme's inactivation by oxidation (Cotton *et al.*, 2004).

MEME-suite, a collection of software tools for discovering and characterizing motifs and domains in DNA or protein sequences (Bailey *et al.*, 2009) was used to analyze conserved motifs and domains between the sequences. The result in Figure 2.2 shows conserved motifs in all the protein sequences. The analysis reveals very low E-values for all the motif sequences, indicating that the results are statistically significant (Bailey *et al.*, 2009). The observed sequence similarity and identity, conserved motifs and domains indicate the resemblance in structures and catalytic mechanisms among these enzyme proteins.

Figure 2.2: Depiction of motifs and domain discovered using MEME-Suite in the SCOMT protein sequences of bovine, human, rat, mouse, horse and dog. E-values are displayed on the right.

Structural prediction of BSCOMT was performed using (Phyre2) (Kelley and Sternberg, 2009). The program allows submission of amino acid sequence, which uses profile-to-profile matching algorithms to automatically predict the three-dimensional structure of the queried sequence based

on (similar) proteins of known function and structure. For BSCOMT sequence, the program uses rat SCOMT as a template (Figure 2.3) (Kelley and Sternberg, 2009).

The prediction reveals the submitted amino acid sequence to be a SAM-dependent methyltransferase (COMT-like family) protein. The predicted structure of BSCOMT is also similar to the crystal structure of HSCOMT reported by Rutherford *et al.*, (2008b). Both structures have a seven stranded β-sheet squeezed between set of α-helices (Figure 2.3), a characteristic structural feature of SAM-dependent methyltransferases (Martin and McMillan, 2002).

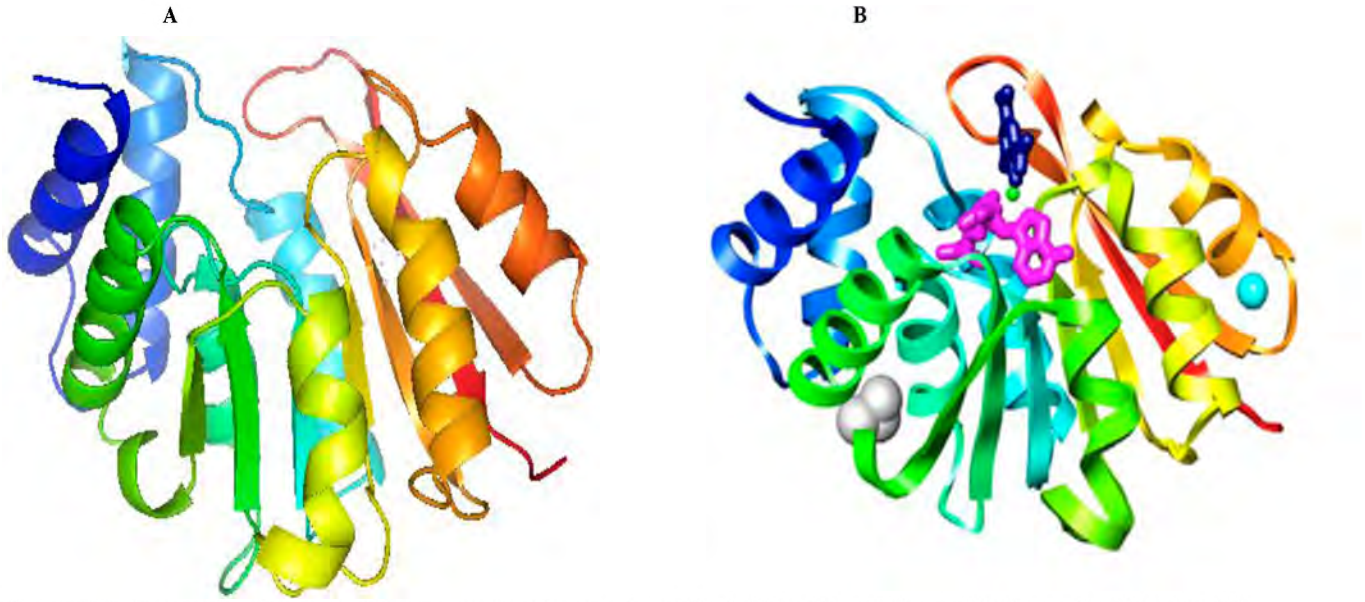

Figure 2.3: Comparison between 3D structures of bovine (modelled) (A) and experimentally determined human (B) SCOMT structures. Proteins coloured from blue (N-terminus) to red (C-terminus) are shown in stereo. The human COMT was co-crystallized with SAM (magenta), DNC (dark blue), Mg^{2+} (green) and K^{+} (cyan). The K^{+} is from the protein environment (Figure 2.3B was taken from Rutherford *et al.*, 2008b). Both structures are made of seven ß-sheets sandwiched between set of α-helices. This is a characteristic feature of SAM-dependent methyltransferases (Martin and McMillan, 2002).

Although amino acid residues that bind the common cofactor, SAM, are poorly conserved in SAM-dependent methyltransferases (Martin and McMillan 2002), these residues are conserved in BSCOMT and HSCOMT. The domains and motifs conservation, structural similarity and high

sequence identity, between BSCOMT and HSCOMT must reflect similar reaction mechanisms, and hence, their catalytic activities would be influenced in the same way and by the same modulators (inhibitor or activator).

2.3.2 Partial purification of BSCOMT

Purification of BSCOMT was carried out in five stages, as described in section 2.2.2.2. The results of the enzyme activities obtained at each stage of the purification are summarized in Table 2.2. The enzyme was purified to 7.78 fold with specific activity of 0.052U/mg. The partially purified BSCOMT was stable for more than seven days at 4°C and more than a month at -20°C.

Table 2.2: Partial purification table of BSCOMT

Step	Volume (ml)	Total protein (mg)	Total activity (U)	Specific activity (U/mg)	Purification fold	Yield (%)
Crude Homogenate	500	1038	6.89	0.006	1	100
Supernatant	240	224	5	0.022	3.36	72.5
Gel Filtration (Sephadex G-100)	4	4.24	0.19	0.046	6.85	2.8
Ion Exchange (DEAE-cellulose)	5	2.2	0.11	0.052	7.78	1.65

The purity of BSCOMT was checked by SDS-PAGE. Figure 2.4 shows the purification SDS-PAGE image of samples collected along the purification stages of BSCOMT. The figure is commensurate with the purification table since the purity of the enzyme protein appears to increase along the purification stages. The molecular weight of BSCOMT, estimated from the SDS-PAGE gel according to the method reported by Shapiro *et al.*,(1967), was 24.5 kDa, which

agrees with the theoretical value of 24.792 kDa calculated using an online bioinformatics resource portal, ExPASy (http://web.expasy.org/compute_pi/) (Artimo, *et al.*, 2012). Although there is an increase of COMT enzymatic activity as indicated in the purification table (Table 2.2), SDS-PAGE analysis indicated protein impurities in the enzyme (Figure 2.4).

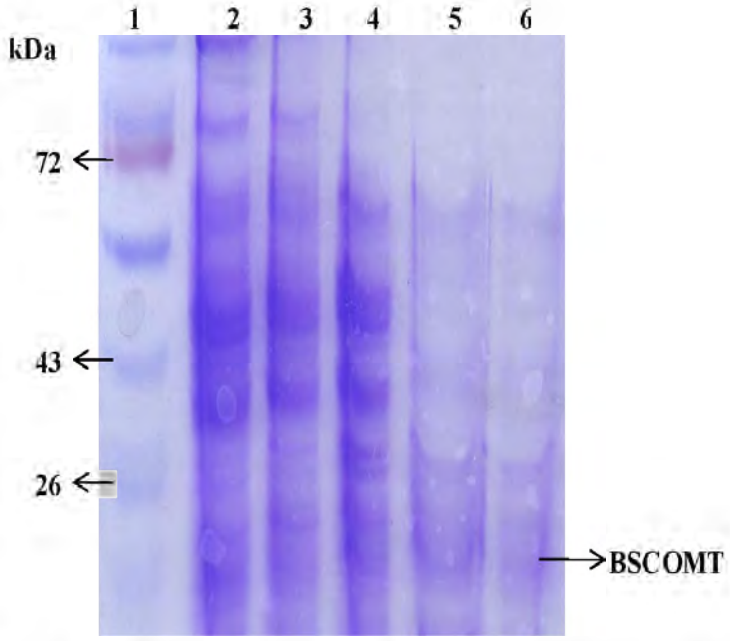

Figure 2.4: SDS-PAGE gel image showing purification profile of BSCOMT. Lane 1 is the protein ladder; lane 2 is the crude homogenate; lane 3 is the supernatant, lane 4 is the ammonium sulfate fractionation, lane 5 is the gel filtration (Sephadex G-100) and lane 6 is ion-exchange (DEAE-cellulose).

2.3.3 Characterization of BSCOMT

The pH and temperature for the optimum catalytic methylation of esculetin by BSCOMT were determined as described in section 2.2.2.6. The observed pH and temperature optima of BSCOMT enzymatic methylation of esculetin were 8.5 and 40°C, respectively (Figures 2.5 and 2.6). The observed pH optimum (of 8.5, Figure 2.5), for BSCOMT activity is not the same as that reported for the bovine's body physiological pH (Fallon, 1962). There is appreciable BSCOMT activity (of at least 54%) at a pH range of 7.0 to 9.0, and this activity drops to 25% at

6.5 and to less than 10% at 6.0 (Figure 2.5). The observed temperature optimum (40°C, Figure 2.6) is in agreement with that reported for bovine's body physiological temperature of 39°C (Fallon, 1962). The BSCOMT catalytic activity is substantial between 25°C (65%) and 55°C (82%). The enzymatic activity is 51% at 20°C and drops to less than 25% at 65°C (Figure 2.6).

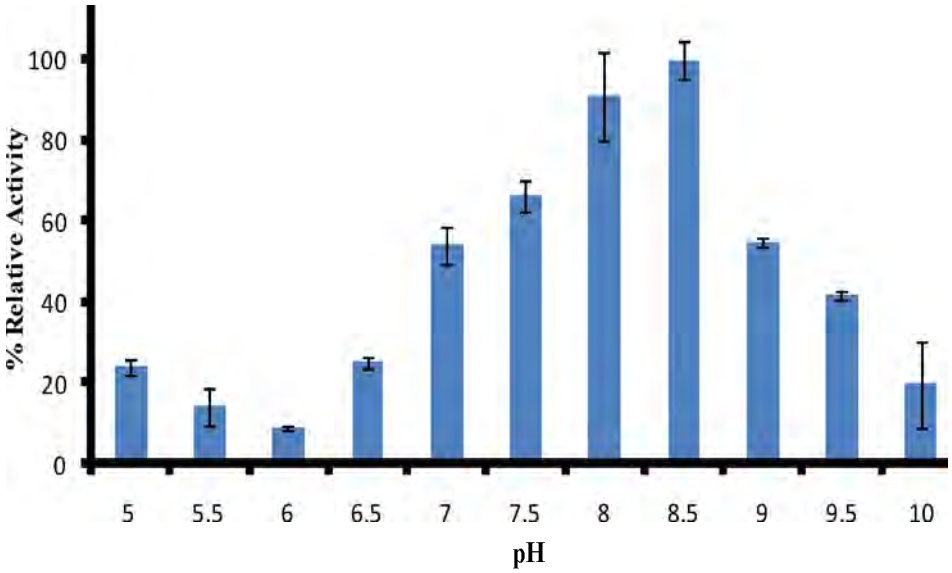

Figure 2.5: pH profile of BSCOMT observed at 37°C. Values represent the mean (n = 3, ± SD).

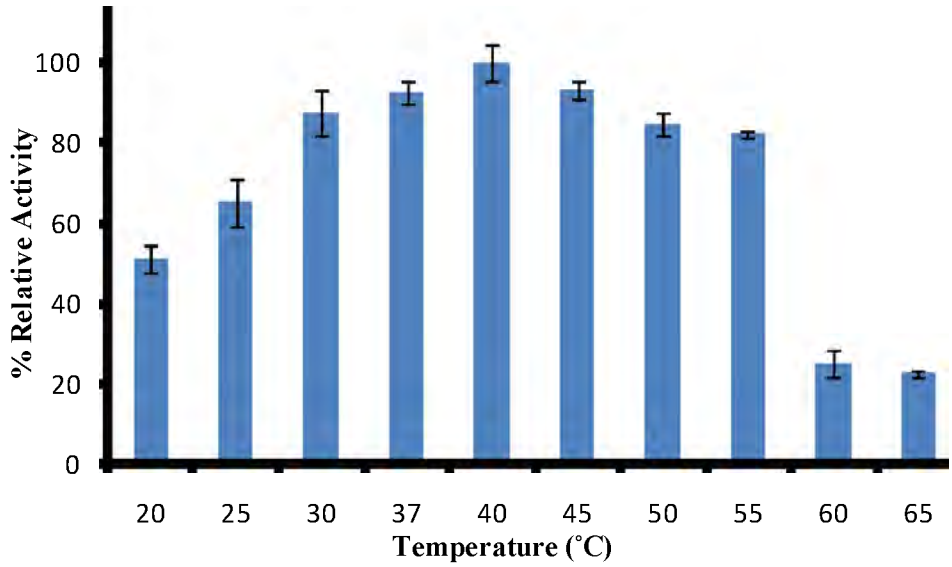

Figure 2.6: Temperature profile of BSCOMT observed at pH 8.5. Values represent the mean (n = 3, ± SD).

2.3.4 Kinetic study

To investigate the kinetic profile of BSCOMT, its enzymatic activity was assayed with increasing concentration (0 to 8 μM) of esculetin, at pH and temperature optima and conditions of the other reaction components described in section 2.2.2.6. The plot for the rate of BSCOMT catalyzed methylation of esculetin as a function of the esculetin concentration presents a hyperbolic curve (Figure 2.7), suggesting the kinetics to be of Michaelis-Menten pattern (Michaelis and Menten, 1913). Hanes–Woolf linearization of the hyperbolic Michaelis-Menten curve position the independent variables, the substrate concentrations ([S]), on both sides of the equation, and hence on both axes of the plot. It does not, therefore, exaggerate the data obtained at low or high [S], which allows more accurate estimation of both K_m and V_{max} (Ritchie and Prvan, 1996). Because of its advantages, the Hanes–Woolf plot was used to linearize the hyperbolic plot and the graph is shown in Figure 2.8. The kinetic parameters calculated using GraphPad Prism 5 and Hanes–Woolf plot are shown in Table 2.3.

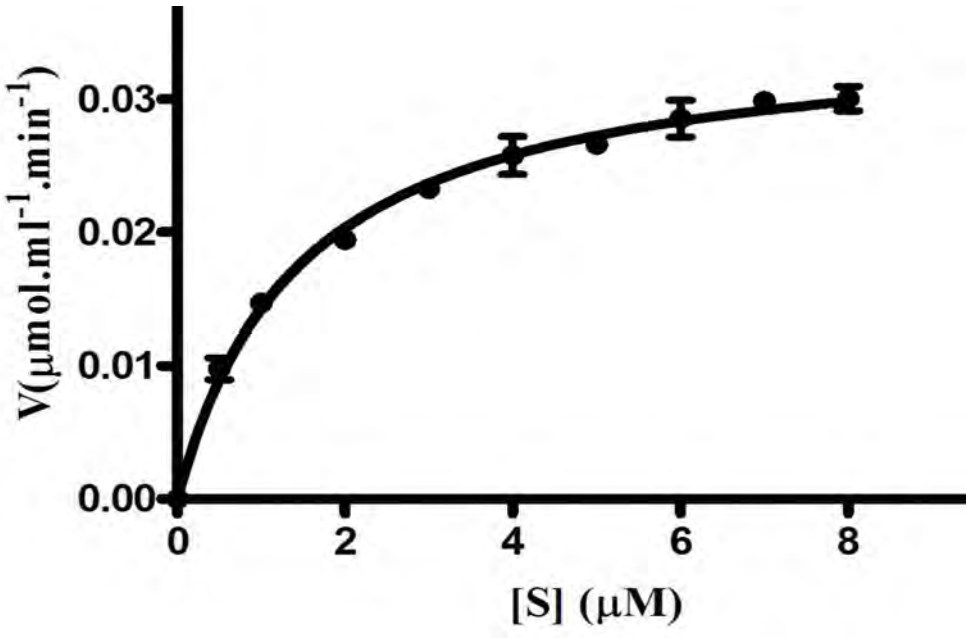

Figure 2.7: Michaelis-Menten graph of HSCOMT activity on esculetin. Results were obtained from 3 data sets. Values represent the mean (n = 3, ± SD).

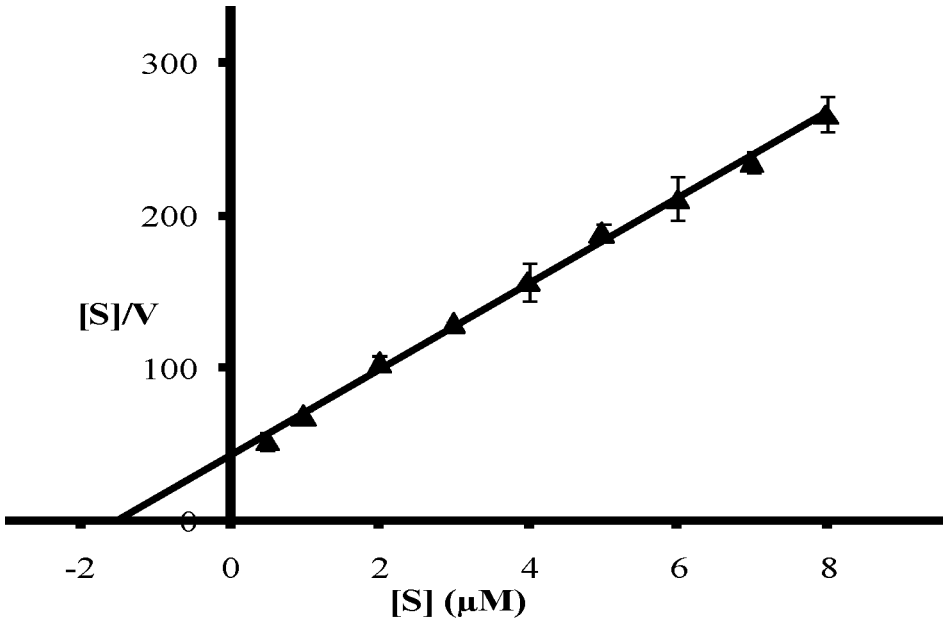

Figure 2.8: The Hanes-Woolf plot of the kinetic study data represented in the Michaelis-Menten curve in Figure 2.7 K_m and V_{max} were calculated using the linear equation y = 28.15x + 42.35. R^2 value = 0.997. Values represent the mean (n = 3, ± SD).

Table 2.3: Kinetic parameters of BSCOMT from both hyperbolic and Hanes-Woolf linear plots.

Plot	Variables			
	K_m(μM)	V_{max} (μmol.ml^{-1}.min^{-1})	K_{cat}(min^{-1})	K_{cat}/K_m (M^{-1}. min^{-1})
Hyperbolic (non-linear)	1.475±0.130	0.0353±0.001	1.748 x 10^{-2}±5.0 × 10^{-4}	1.18 × 10^{-2}
Hanes–Woolf (linear)	1.504	0.0355	1.757 × 10^{-2}	1.17 × 10^{-2}

A wide range of K_m values for SCOMT catalytic activity has been reported by different researchers (Mannisto and Kaakkola, 1999). These values depend on the enzyme source, substrates and reactions conditions (White and Wu, 1975; Tilgmann and Kalkkinen, 1991; Dawling *et al.,* 2001). In the present study, the K_m values from the hyperbolic and linear plots are 1.475±0.130 and 1.504 μM, respectively, whilst V_{max} values from the hyperbolic and linear plots are, respectively 0.0353±0.001 and 0.0355 μmol/ml/min. The enzyme turnover index (K_{cat}) and

the measure of the enzyme efficiency (K_{cat}/K_m) are $1.748 \times 10^{-2} \pm 5.0 \times 10^{-4}$ min^{-1} and 1.18×10^{-2} $M^{-1}.min^{-1}$, respectively. Dhar and Rosazza, (2000) reported the K_m of 500±21.5 mM for esculetin using COMT isolated from *Streptomyces griseus*, while report of Veser (1987) showed K_m of 6.2 µM for esculetin using COMT from *Candida tropicalis*. COMT has been reported as rather a slow enzyme (Vidgren *et al.,* 1994). To the best of my knowledge, bovine COMT has not been characterized, and therefore its kinetic parameters are not reported in the literature. Also to my knowledge, the kinetic parameters of mammalian COMT, using esculetin as substrate, have not been reported in the literature.

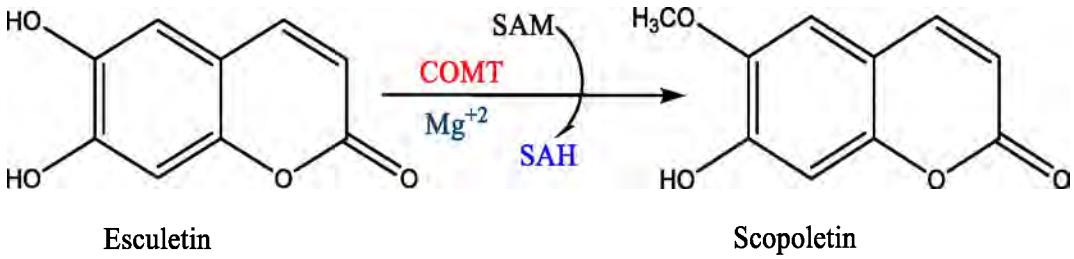

Figure 2.9: The schematic representation showing the catalytic methylation of escultin to the fluorescent compound, esculetin by COMT, with concurrent conversion of SAM to SAH in the presence of Mg^{+2}.

2.4 Conclusion

This chapter aimed at three objectives. Firstly, the use of bioinformatic tools and WebPages to access amino acid sequence of BSCOMT and to compare the sequence with human and other mammalian homologues. From the comparison, BSCOMT has more than 90% sequence similarity with SCOMT from human, rat, mouse, horse and dog. The predicted structure of BSCOMT also, has a high similarity with experimentally determined crystal structure of HSCOMT in addition to several conserved motifs and domains in all the analyzed sequences.

The observed similarity indicates common catalytic mechanisms and functions among these proteins. These enzymes can, therefore, have common modulator(s) influencing their catalytic activities in similar pattern, and hence it is with a high level of certainty that BSCOMT can be used as a model for HSCOMT. Secondly, development of an assay; a consistent COMT assay was optimised based on the report of the catalytic methylation of esculetin to a fluorescence compound, scopoletin. Lastly, this section also aimed to purify and characterize BSCOMT. The strategy here was based on reported procedures for the purification of SCOMT from other mammals, involving homogenization, differential centrifugation, ammonium sulfate fractionation, gel filtration and ion exchange chromatography. The partially purified enzyme had specific activity of 0.052 U/mg and pH and temperature optima of 8.5 and 40°C respectively. K_m, V_{max}, K_{cat} and K_{cat}/K_m of the partially purified enzyme were 1.475±0.130 μM, 0.0353±0.001 μmol/ml/min, $1.748 \times 10^{-2} \pm 5.0 \times 10^{-4}$ min^{-1} and 1.18×10^{-2} $M^{-1}.min^{-1}$, respectively. There was an increase in specific COMT enzymatic activity along the purification stages, but SDS-PAGE gel analysis of the samples showed some proteins impurities. The impurities may interfere with the downstream experiments. An adage of biochemistry is: "Never waste pure thoughts on an impure protein". Therefore, a decision was made to continue the research using a recombinant HSCOMT.

Chapter three

Recombinant expression, purification and characterization of human soluble catechol *O*-methyltransferase

3.1 Introduction

Expression of protein is a process by which protein is synthesized in living systems. Advances in gene cloning and genetic engineering have enabled recombinant expression and subsequent isolation of heterologous proteins for research, industrial, agricultural and medical applications (Ashwini *et al.,* 2016).

3.1.1 Expression systems of recombinant proteins

Different recombinant expression systems, including bacteria, yeast, insect and mammalian cells have been reported and used in the production of recombinant proteins (Rai and Padh, 2001). The choice of a suitable system for protein expression is multi-factorial. The factors include characteristic host cell growth, levels of protein expression, post-translational modifications, host cell toxicity, intracellular-extracellular expression capabilities, and the biological nature and activity of the desired protein (Makrides, 1996).

3.1.2 Bacterial Expression System

Escherichi coli expression is the most frequently used system among the bacterial expression systems (Chen, 2012). There are well-known advantages of *E. coli* as a host organism for recombinant protein expression. It has fast growth kinetics, with about 20 min doubling time at optimum conditions (Sezonov *et al.,* 2007), fast and easy transformation (Pope and Kent, 1996), it grows in cheap and simple media (Sezonov *et al.,* 2007) and can express a protein of interest

up to 50% of the total cellular protein (Francis and Page, 2010). Strategies often employed to achieve high expression of an exogenous gene coding for the target protein include optimizations of bacterial cell growth, codon frequency in cDNA to reflect the codon use of the host cells and culture conditions for specific protein expression (McNulty *et al.,* 2003; Baeshen *et al.,* 2015). Again, configuring the specific gene regulatory factors such as promoter and distal regulatory elements, including inducer, silencer or locus control regions, is a prerequisite for efficient gene transcription and subsequent translation of the recombinant protein genes in any host organism (Hannig and Makrides, 1998).

Amidst different protein expression methods exploited in *E. coli*, those linked to the *lac* operon are most commonly employed. Although this expression has been achieved through auto-induction using glucose, glycerol and lactose (Studier *et al.* 2005; Jacob and Monod, 1961), it is frequently achieved by the inclusion of non-metabolisable *lac* inducer, isopropyl β-D-1-thiogalactopyranoside (IPTG). In the process, the IPTG mimics a lactose metabolite, allolactose, which elicits the transcription of the *lac* operon. It binds the *lac* repressor to subsequently release the operator to allow DNA transcription and thus protein expression (Donovan *et al.,* 1996). However, the formation of insoluble inclusion bodies, lack of post-translational modification machinery and inability to secrete proteins extracellularly are among the factors hindering the application of the *E. coli* expression system (Hannig and Makrides, 1998).

3.1.3 Recombinant expression of mammalian COMT

Various expression systems have been employed to express recombinant mammalian COMT for functional, structural, and pharmacological studies. The systems employed for mammalian COMT recombinant expression include bacterial (*Brevibacillus choshinensis*) (Pedro *et al.,* 2011;

Santos *et al.,* 2013), yeast (Pedro *et al.,* 2015) and mammalian (Tilgmann *et al.,* 1992) cells. However, the majority of the reported recombinant expression of mammalian COMT are based on the *E. coli* expression system (Lundström *et al.,* 1991; Lundström *et al.,* 1992; Lotta *et al.,* 1995; Bonifácio, *et al.,*2001; Dawling *et al.,* 2001; Bonifácio, *et al.,* 2002; Taskinen *et al.,* 2003; Cotton *et al.,* 2004; Passarinha *et al* 2006; Passarinha *et al* 2008; Rutherford *et al.,* 2008a; Rutherford *et al.,* 2008b; Passarinha *et al.,* 2009; Ho *et al.,* 2013; Santo *et al.,* 2014).

pET vectors are the most commonly used expression vectors for protein expression in *E. coli*. Protein expression in these vectors is under the influence of T7 promoter, which effects the production of T7 RNA polymerase. This in turn facilitates the transcription of coding sequences and the consequent expression of the target protein (Studier, 1991).

3.1.4 Purification of recombinant proteins

While conventional protein purification strategies are laborious, fusion tags are often expressed with recombinant proteins to improve solubility and allow for affinity purification (Costa *et al.,* 2014). An example of such a tag is 6 histidine residues (His-tag) on either the C-terminal or the N-terminal of the expressed protein. The tag facilitates recombinant protein purification using immobilized metal affinity chromatography (IMAC). In this process, separation of the recombinant protein is based on the interaction of histidine with ions of the transition metals which are immobilized on a matrix (such as silica beads) via a chelating ligand, such as nitrilotriacetic acid (NTA) (Hochuli *et al.,* 1988). Metal ions with a substantial affinity for histidine that enable protein purification include Ni^{2+} (Bornhorst and Falke, 2000). Histidine is the amino acid with the strongest affinity for metal ions. Electron donor groups on the histidine and imidazole ring freely form coordination bonds with the transition metals. Proteins bearing

sequence(s) of consecutive histidine amino acids are therefore retained on the IMAC column matrices. After washing the matrix material, the protein containing the polyhistidine portion can be easily eluted by either the addition of imidazole to replace the histidine or adjusting the pH of the column buffer to protonate the histidine residues and thus disrupt the histidine-metal coordination bonds (Bornhorst and Falke, 2000).

Protein eluted from an IMAC column usually contains a high concentration of imidazole and may contain some contaminating proteins. Further purification is, therefore, pertinent to remove these contaminants which could affect the protein of interest and/or subsequent experiments. Additional purification can be achieved by dialysis or molecular sieve chromatography. The latter is also termed size exclusion chromatography (SEC), desalting or gel filtration chromatography. It is based on the difference in pore sizes between the column beads and the protein molecules of interest (Hong *et al.,* 2012). The size of a molecule determines whether it can penetrate the pores; molecules that are totally excluded elute from the column first, in the void volume (V_O). This is the volume outside the support particles (the interstitial space). Molecules that pass into the pores have access to an additional space, the internal pore volume (V_I). Such molecules emerge at the total column volume (V_T), which is also the elution volume of the molecules small enough to be distributed both inside and outside the pores (Irvine, 1997).

3.1.5 Enzyme kinetics

Catalytic mechanisms of enzymes' action are intricate, and hence a thorough and accurate characterization of activities and assay conditions is essential (Heinrich *et al.,* 2002). Enzyme kinetics involves the study of the velocity of enzyme-catalyzed reactions and factors which influence the velocity (Bisswanger, 2008). Physiological factors influencing enzyme reaction

velocity include enzyme concentration, pH, temperature, the ionic strength of the reaction mixture, and the presence of modulator (activator or inhibitor) (Bisswanger, 2014). The Michaelis-Menten model, characterized by a hyperbolic curve of the plot between the reaction velocity (v) and the substrate concentration [S], accounts for the kinetic patterns of most studied enzyme-catalysed reactions (Berg *et al.,* 2002a).

Characterization of an enzyme requires knowledge of kinetic behaviour, temperature and pH for optimum catalytic activity as well as temperature stability of the enzyme. These allow logical choices of consistent assay conditions. Additionally, enzyme characterization provides insight on the catalytic behaviours that can be used in detecting changes in an enzyme's activities when assay conditions are altered. It can also give an insight into the enzyme mechanism.

Determination of optimum temperature for enzymatic catalysis can be achieved by assaying the enzyme activity under the same reaction conditions over a range of temperatures. Thermostability, however, is determined by incubating the enzyme at a specific temperature for a specific period and subsequently performing an activity assay to check whether such incubation affects the enzyme activity. In the same way, optimum pH for enzymatic activity is determined by assaying the activity under the same reaction conditions over a pH range.

Kinetic parameters are the experimentally determine reaction velocity attained when the substrate concentration is at saturation (V_{max}) and enzyme's affinity for a particular substrate (K_m) at specified assay conditions. This is achieved by performing enzyme assays at varying substrate concentrations and plotting reaction velocity (v) against substrate concentration [S]. This relation is defined by the well-known Michaelis-Menten equation (Equation 3.1) (Michaelis and Menten 1913).

Equation 3.1 $$v = \frac{V_{max}[S]}{K_m + [S]}$$

Definitive determination of experimental V_{max} and K_m values from the plot of v against [S] is an intricate task since V_{max} can only be approached and not reached and K_m is dependent on V_{max}. However, accurate V_{max} can be determined by the linearization of the "equation 3.1" (Berg *et al.*, 2002b).

The Hanes–Woolf plot is a graphical representation of enzyme kinetics based on a rearrangement of the Michaelis–Menten equation, in which the ratio of the initial substrate concentration [S] to the reaction velocity (v) is plotted against [S] (Hanes, 1932). It is represented by equation 3.2.

Equation 3.2 $$\frac{[S]}{v} = \frac{[S]}{V_{max}} + \frac{K_m}{V_{max}}$$

Where the slope is $1/V_{max}$, the y-intercept is K_m/V_{max} and x-intercept denotes $-K_m$ (in the second quadrant).

Since the independent variable [S] appears on both sides of the equation, and hence on both axes of the plot, this approach does not overemphasize the data obtained at low or high [S] and thus allows accurate estimation of both K_m and V_{max} (Ritchie and Prvan, 1996).

This chapter is aimed at the gene identification, synthesis and over-expression of the HSCOMT in *E. coli* BL21(DE3) cells using the pET -22-(b+) expression vector with IPTG induction, and the purification and characterization of the enzyme. Purification strategies employed are centrifugation, IMAC and desalting. After each purification step, COMT activity assays and SDS-PAGE were used to check the presence of enzymatically active HCOMT, and to evaluate its purity. After obtaining the purified HSCOMT, the characterization was performed using an

optimized COMT activity assay. The characterization includes the determination of pH and temperature optima, the kinetics constants (V_{max}, K_m and k_{cat}) and temperature stability of the enzyme.

3.2 Materials and methods

3.2.1 Materials

All chemicals, reagents and equipment used in this section are outlined in appendix I.

3.2.2 Methods

3.2.2.1 Artificial synthesis of HSCOMT gene

The HSCOMT amino acid sequence was taken from the National Center for Biotechnology Information (NCBI) (accession code: NP_009294.1). The sequence was translated back to its corresponding nucleotide sequence using the reverse translation tool from the ExPASy Bioinformatics Resource Portal website (http://www.bioinformatics.org/sms2/rev_trans.html) (Artimo *et al.*, 2012) and subsequently optimized for *E. coli* expression (Puigbò *et al.*, 2007). The optimized gene was synthesized by GenScript (GenScript USA Inc.) and received in lyophilised pET-22b(+) vector. The plasmid was reconstituted in 40 µl milli-Q water and chemically competent *E. coli* JM109 cells were transformed with the plasmid for propagation.

3.2.2.2 Preparation of chemically competent cells

Competent bacterial cells of *E. coli* (BL21(DE3) and JM109) were generated according to the method reported by Tu *et al.* (2005). In brief, a 100 µl glycerol stock of *E. coli* cells harbouring no foreign plasmids was thawed at room temperature and 10 µl of the thawed stock inoculated

into 40 ml super optimal broth (SOB) media (appendix II) and grown at 37ºC on a shaker at 150 rpm until an OD_{600} ~0.35 was reached. After 1 h incubation at 37ºC, this culture was placed on a shaker, at the same temperature, at 200 rpm for 1 h. The cells were placed on ice for 10 min and then centrifuged (2 500 × *g*; 4 min; 4ºC). The cells were resuspended in 20 ml of sterile ice cold TB buffer (10 mM HEPES, 15 mM $CaCl_2$, 250 mM KCl and 55 mM $MnCl_2$, pH 6.7), and incubated on ice for 25 min. After another centrifugation (2 500 × *g*; 2 min; 4ºC), the pellet was resuspended in 4 ml of sterile ice cold TB buffer. Sterile glycerol was added to a final concentration of 20%, and the cells were aliquoted (100 µl) into ice cold microcentrifuge tubes (1.5 ml) and snap frozen in liquid nitrogen and kept at -80 °C.

3.2.2.3 Protocol for *E. coli* transformation

A heat shock transformation method reported by Froger and Hall (2007), with modifications, was used. Briefly, competent *E. coli* cells were transformed by adding 2 µl of reconstituted plasmid to 100 µl of competent cells (prepared as stated in section 3.2.2.2), tapped to mix and kept on ice for 30 min. The mixture was heat shocked by incubation at 42°C for 45 sec, then 2 min on ice. To the transformation mixture, 250 µl of pre-heated (37°C) super optimal broth with catabolite repression (SOC) media (SOB media supplemented with 20mM glucose) was added and incubated at 37°C for 30 min with shaking (150 rpm). The positive transformants were selected on Luria–Bertani (LB) agar plates containing ampicillin (100 µg/ml), incubated overnight at 37°C. Single colonies were inoculated into 5 ml LB broth containing ampicillin (100 µg/ml) to maintain the selection pressure, and then grown overnight at 37°C.

3.2.2.4 Plasmid extraction

Plasmid-bearing HSCOMT was extracted from the overnight grown culture using the BioFlux BioSpin Plasmid Extraction Kit according to the manufacturer's instruction (Bioer Technology Co., Ltd). The cell pellet was collected by centrifugation in 1.5 ml Eppendorf tubes using an Eppendorf MiniSpin Plus microcentrifuge. The pellet was resuspended in resuspension buffer, lysed by the addition of lysis buffer, neutralized with neutralizing buffer and spun down to separate the DNA-containing supernate from cell debris. The DNA contained in the supernatant fraction was washed and eluted in 50 µl elution buffer, using the kit's spin column. The resuspension, lysis, neutralizing and elution buffers were provided in the extraction kit.

3.2.2.5 HSCOMT gene insert screening

Restriction fragment length polymorphism (RFLP) and DNA sequencing were used to ascertain the correct insertion of HSCOMT into the pET-22b(+) plasmid. For the RFLP insert verification, the plasmid construct was digested using *Nde*I and *Xho*I in a 20 µl digestion reaction, which was made of 4 µl of 106 µg/µl *HSCOMT*-plasmid DNA, 2 µl *Nde*I, 2 µl *Xho*I (10 U/µl restriction enzymes), 2 µl of reaction buffer (33 mM Tris-acetate, 10 mM magnesium acetate, 66 mM potassium acetate, 0.1 mg/ml BSA, pH 7.9) and 10 µl of milli-Q water. Single digestions were performed by substituting either of the restriction enzymes with milli-Q water; the reaction buffer with 50 mM Tris-HCl, 10 mM $MgCl_2$, 100 mM NaCl, 0.1 mg/ml BSA, pH 7.5 for *Nde*I digestion and 10 mM Tris-HCl, 10 mM $MgCl_2$, 100 mM KCl, 0.1 mg/ml BSA, pH 8.5 for *Xho*I digestion. The reaction mixture was incubated at 37°C overnight. The mixture was separated by agarose gel electrophoresis and viewed under UV-light (ChemiDoc XRS Gel Documentation system, Bio-Rad, USA) (section 3.2.2.6).

For sequence verification, the plasmid was sequenced (Inqaba Biotech™) to confirm the HSCOMT nucleotide sequence. Electropherograms received from Inqaba Biotech™ were analyzed using Geospiza's FinchTV version 1.4.0. Reverse complementation and sequence alignments were performed using BioEdit version 7.3.1.0.

3.2.2.6 Agarose gel electrophoresis

Agarose gels were made by dissolving agarose powder (0.8% w/v) in 1X TAE buffer (0.04 M Tris-HCl, 1 mM EDTA, 0.021 mM glacial acetic acid, pH 8.0) with 0.6 µg/ml ethidium bromide. DNA was separated by running the gel at 100 V for 1 h and visualized under UV source (300 nm) (ChemiDoc XRS Gel Documentation system, Bio-Rad, USA). Estimations of DNA fragment sizes were made with reference to electrophoretic mobility of the GeneRuler DNA Ladder Mix™(Thermo Scientific, SM0334), covering a range of 10 000 to 100 base pairs .

3.2.2.7 Over-expression of HSCOMT

Prior to large-scale over-expression of HSCOMT, an induction study was carried out to confirm the expression of the HCOMT and to determine optimum incubation conditions for the expression. For the induction study, a negative control of BL21(DE3) cells transformed with empty pET-22b(+) was grown alongside the one harbouring the HSCOMT gene. The cell-growing protocol involved transformation of 100 µl of competent BL21(DE3) cells with 2 µl of the plasmid. Positive transformants were selected using ampicillin (100 µg/ml) on LB agar plates incubated overnight at 37°C. Single colonies were picked using a sterile toothpick and inoculated into a 5 ml test tube with 2 ml of LB media containing ampicillin (100 µg/ml), to maintain the selection pressure. These tubes were placed on a Labcon shaker at 150 rpm, and the cells grown at 37°C for 8 h. One milliliter samples of each of these cultures was poured into 1.5 ml

microcentrifuge tubes, centrifuged (12 000 × *g*; 2 min) and the pellet used as an uninduced control. Another 10 µl of each of the cultures was sub-cultured into 50 ml LB media (containing 100 µg/ml ampicillin) in a 250 ml conical flask and incubated at 37°C with shaking at 150 rpm. When the cultures reached an absorbance of 0.7 at 600 nm, IPTG was added to a final concentration of 0.7 mM. Expression of the HSCOMT gene was monitored hourly by withdrawal of 1 ml of the expression culture. Samples were collected at 0, 1, 2, 3, and 4 h intervals. These were centrifuged (12 000 × *g*, 4 min), the supernatant discarded and the pellet stored at -20°C for SDS-PAGE analysis.

The frozen cell pellets of the induction study samples were thawed, resuspended in 100 µl (100 mM Tris-HCl buffer, 5 mM $MgCl_2$, pH 7.5) and subjected to six rounds of sonication at 100 mA each for 10 sec (Sonics and materials Inc. USA). The protein concentration of these samples was determined (section 2.2.2.3) and used for SDS-PAGE (section 2.2.2.5) induction analyses. After this study, the over-expression was proportionally up-scaled to 1.8 l to express sufficient HSCOMT for downstream experiments.

3.2.2.8 Purification of His-tagged HSCOMT

Unless otherwise stated, all of the following purification steps were carried out on ice or at 4°C. One millilitre sample of each purification stage was taken and stored at -20°C for protein concentration determination, SDS-PAGE analyses, and enzyme activity assays to facilitate the construction of a purification table.

3.2.2.8.1 Cell harvest and lysis

After 4 h of expression (section3.2.2.7), *E. coli* BL12(D3) cells containing the intracellular his-tagged HSCOMT were harvested by three rounds of centrifugation (6 000 × *g*; 15 min) and washing (100 mM Tris-HCl buffer, 5 mM $MgCl_2$, pH 7.5). The resultant pellet was resuspended (5% w/v) in the enzyme's storage buffer (100 mM Tris-HCl buffer, 5 mM $MgCl_2$, 5 mM ß–mercaptoethanol, 0.1 mM dithiothreitol pH 7.5). The cell suspension was lysed by adding 1 mg/ml lysozyme and incubated with shaking (Labcon) (70 rpm) at 37°C for 1 h. The lysed culture was stored at -80°C overnight to aid cell disruption.

Samples were thawed on ice and centrifuged (15000 × *g*; 30 min) using an Avanti J. E. centrifuge (Coulter Beckman, USA) to remove unlysed cells and debris. To separate the soluble fractions, the supernatant was subjected to ultra-centrifugation (100 000 × *g*; 60 min) using an Optima L-90K ultracentrifuge (Coulter Beckman, USA) and the resultant supernate was used for IMAC.

3.2.2.8.2. Immobilized metal affinity chromatography (IMAC)

For the IMAC, the buffers (appendix II) were prepared and filtered using a syringe-driven 33 mm diameter sterile filter with a 0.22 µm pore size (hydrophilic PVDF membrane) (Merck SA, Pty) and degassed under vacuum. The IMCA experiment was done using the ÄKTA fast protein liquid chromatography (FPLC) (GE Healthcare, UK) system. A flow rate of 1 ml per min was set and the column was pre-equilibrated in accordance with the manufacturer's recommendations. In brief, the column was washed with 10 column volumes (50 ml) distilled, degassed water and equilibrated with 10 column volumes binding buffer (appendix II). The cleared protein was loaded onto a Superloop™ 150 ml (GE Healthcare) sample loop attached to a HisTrap FF

column (5 ml, GE Healthcare) connected to an ÄKTA FPLC. Unbound proteins were eluted with 10 column volumes of wash buffer. His-tagged bound HSCOMT was then eluted, in 5 ml fractions, using 100 ml elution volume with a linear gradient (0–100%, 0–400 mM) imidazole concentration. Fractions of interest were selected according to their UV absorbance peaks (280 nm). A sample of each fraction was taken for protein quantification, SDS-PAGE analyses and COMT activity assay.

3.2.2.8.3 Desalting

IMAC fractions matching UV absorbance peaks (280 nm) and verified by SDS-PAGE analyses were pooled and concentrated to 5 ml using Vivaspin columns MWCO 10000 (Sartorius Stedim Biotech) according to the manufacturer's instructions. The resultant 5 ml concentrated sample was divided into two, and each of the portions loaded onto Sephadex G-25 PD-10 desalting column (GE Healthcare) equilibrated with 25 ml storage buffer (100 mM Tris-HCl buffer, 5 mM $MgCl_2$, 5 mM ß–mercaptoethanol, 0.1 mM dithiothreitol pH 7.5). HSCOMT was eluted with storage buffer in 10 x 1.0 ml fractions.

3.2.2.9 Western blot

A western blot was employed to confirm that the expressed and purified protein was a his-tagged HSCOMT. The western blot analysis was performed according to the protocol described by Towbin *et al.,* (1979). The separated proteins on the SDS-PAGE were transferred onto nitrocellulose membranes for 50 min at 0.4 A using Western transfer buffer (13 mM Tris-HCl 100 mM glycine 20% (v/v) ethanol), and transferred proteins were confirmed by Ponceau staining (0.5% (w/v) Ponceau S, 1% (v/v) glacial acetic acid). Nitrocellulose membranes with transferred proteins were blocked with 1% BLOTTO non-fat dry milk (Sant Cruz Biotechnology)

in Tris-buffered saline (TBS; 50 mM Tris, pH 7.5, 150 mM NaCl) for 1 h and incubated with His-probe (Rabbit polyclonal; Santa Cruz Biotechnology (sc-8040)), diluted 1:1 000 in 1% BLOTTO at 4°C for 90 min. After four cycles of rinsing in TBS-Tween® (TBST) (50 mM Tris, pH 7.5, 150 mM NaCl, 1% (v/v) Tween®-20) for 15 min, the membranes were incubated with anti-Rabbit IgG conjugated to horseradish peroxidase (HRP) (AbCAM, ab6802) at 1:5 000 dilutions in 1% BLOTTO for 45 min with shaking (Stuart roller mixer 40 rpm) at 22°C. The membrane was again rinsed four times with TBST for 15 minutes each, replacing the TBST at each rinse. His-tagged specific protein bands were detected using an enhanced chemiluminescence (ECL) (ChemiDoc™, Bio-Rad, USA).

3.2.2.10 Determination of protein concentration

Protein concentration was routinely assayed by the Bradford method (Bradford 1976) as outlined in section 2.2.2.3.

3.2.2.11 COMT activity assay

HSCOMT enzymatic activity was assayed according the procedure explained in section 2.2.2.4, with 1 µg HSCOMT in the reaction mixture instead of 10 µg of partially purified BSCOMT.

3.2.2.12 Optimization of S-(5'-adenosyl)-*L*-methionine (SAM) concentration

Concentration of S-(5'-adenosyl)-*L*-methionine (SAM) for the optimum HSCOMT activity was optimized by running the assay at fixed concentrations of the enzyme (10 µg/ml) and the substrate esculetin (20 µM). The range of SAM concentration was determined by monitoring the trends in HSCOMT enzymatic activity at various SAM concentrations.

3.2.2.13 Characterization of recombinant His-tagged HSCOMT

After purification, pH for the optimum enzymatic activity of recombinant HSCOMT was determined using the enzyme activity assay described in section 3.2.2.1.1 at a pH range of 4.5 to 8.5 at 37°C. A cocktail of buffer salts covering the pH range was used (appendix II). For temperature optimization, the assay was performed at optimum pH (7.0) in a temperature range of 20 to 65°C. The kinetic parameters (K_m and V_{max}) were determined from enzyme activity assays at the pH and temperature optima. The range of esculetin concentrations was determined by monitoring the trends in HSCOMT enzymatic activity at various esculetin concentrations.

3.2.2.14 Thermal stability

The stability of the HSCOMT at the temperature of its optimum activity (30°C) was studied over a period of 2 h. Prior to the stability study, serial dilutions followed by enzyme assays were performed to obtain the enzyme concentration giving optimum activity. A BioRad Dry Bath heating block was set at 30°C for 30 min prior to experimental start time. The enzyme samples incubated at this temperature were used for the assays as described in section 3.2.2.11, at times 5, 15, 30, 45, 60, 75, 90, 105 and 120 min. Control assays without SAM were run alongside these experiments. The percentage relative HSCOMT activity was calculated using the highest activity at a given time as the 100% activity.

3.3 Results and discussion

3.3.1 Artificial synthesis of HSCOMT gene

The amino acid sequence of HSCOMT was retrieved from NCBI and back translated to the corresponding nucleotide sequence, optimized for *E. coli* expression before being synthesized by

GenScript. The catechol, SAM, and Mg^{+2} binding domains of the HSCOMT polypeptide are not located at its C-terminal (Schluckebier *et al.,* 1995). Several articles have reported the expression of enzymatically active C-terminal tagged mammalian COMT (Cotton *et al.,* 2004; Passarinha *et al.,*2006; Passarinha *et al.,*2008; Passarinha *et al.,* 2009; Ho *et al.,*2013; Santo *et al.,* 2014). These sources justified the choice to employ C-terminal His-tagging. *Xho*I and *Nde*I restriction sequences were considered for DNA digestion due to their absence in the optimized expression nucleotide sequence of the HSCOMT gene (section 3.2.2.1). The HSCOMT gene was received from GenScriptin in the pET-22(b+) lyophilized plasmid.

The restriction digestion was done using the chosen restriction enzymes (section 3.2.2.5) and separated by agarose gel electrophoresis (section 3.2.2.6). For the circular (undigested) plasmid, multiple bands were detected due to the possible occurrence of multiple forms of the circular plasmid (Aaij and Borst, 1972). A single band of about 6 033 bp, corresponding to the size of "pET-22b(+) + His-tagged HSCOMT", was observed in the linear plasmid digested with only *Xho*I or *Nde*I restriction enzymes. The double digestion (*Xho*I and *Nde*I) lane showed a band corresponding to approximately 660 bp and another at around 5 500 bp, confirming the insertion of HSCOMT gene in pET-22b(+) (Figure 3.1).

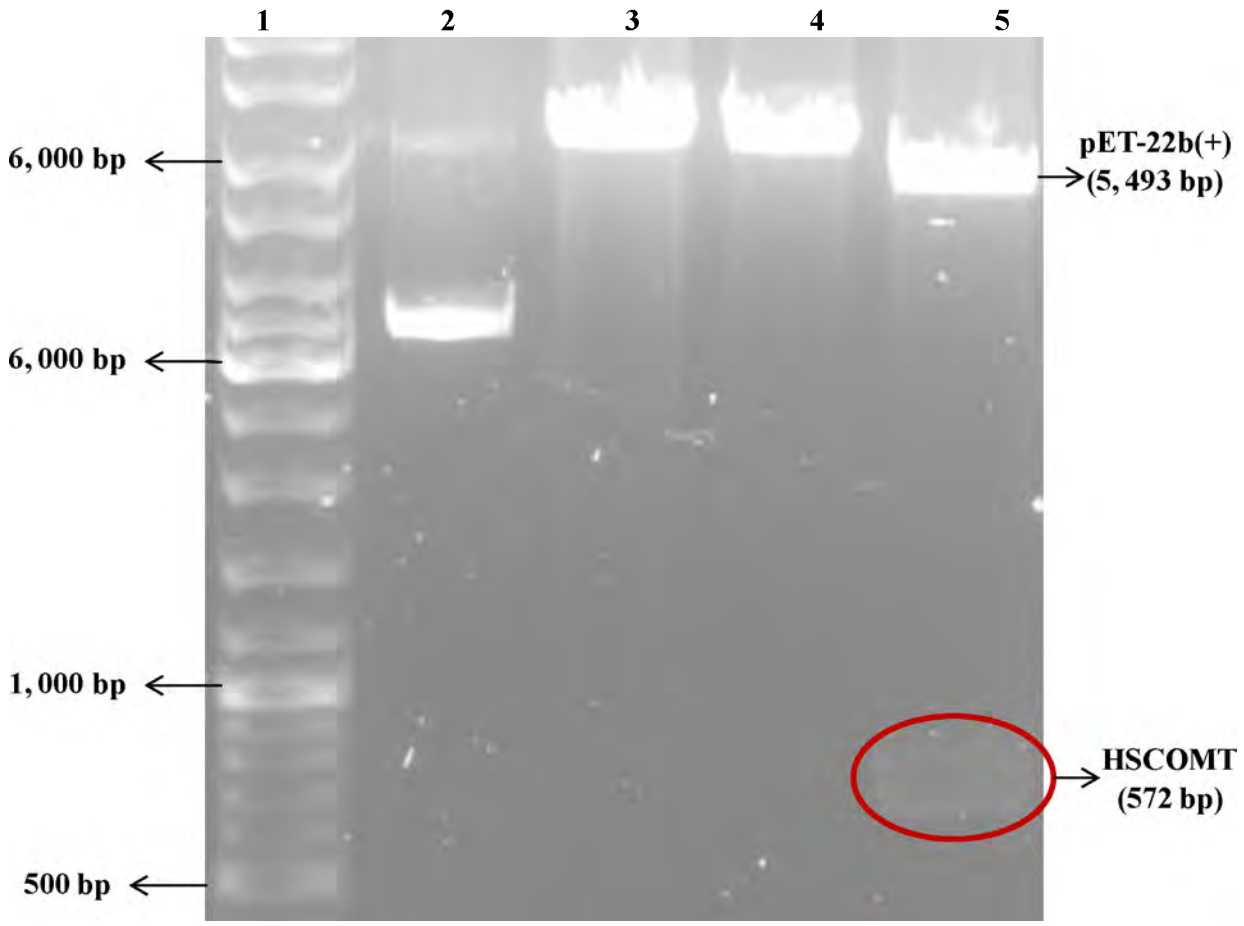

Figure 3.1: An agarose gel electrophoresis image showing results of the restriction digestions of pET-22b(+) housing HSCOMT. Lane 1: gene ladder, lane 2: undigested (circular plasmid), lane 3: *Nde*I digested, lane 4::*Xho*I digested, lane 5: double (*Nde*I and *Xho*I) digested.

An aliquot of the four samples of extracted plasmid (section 3.2.2.4) were sequenced by Inqaba Biotech™. Electropherograms of the sequencing results received from Inqaba Biotech™ were analyzed using Geospiza's Finch TV version 1.4.0., while sequence alignments with the reference sequence (optimized HSCOMT gene sequence for *E. coli* expression; section 3.2.2.1) were performed using BioEdit version 7.3.1.0. The alignment of the insert showed 100% identity (672/672) to the reference gene, confirming the correct insertion of the appropriate gene (HSCOMT) in the plasmid DNA (Figure 3.2).

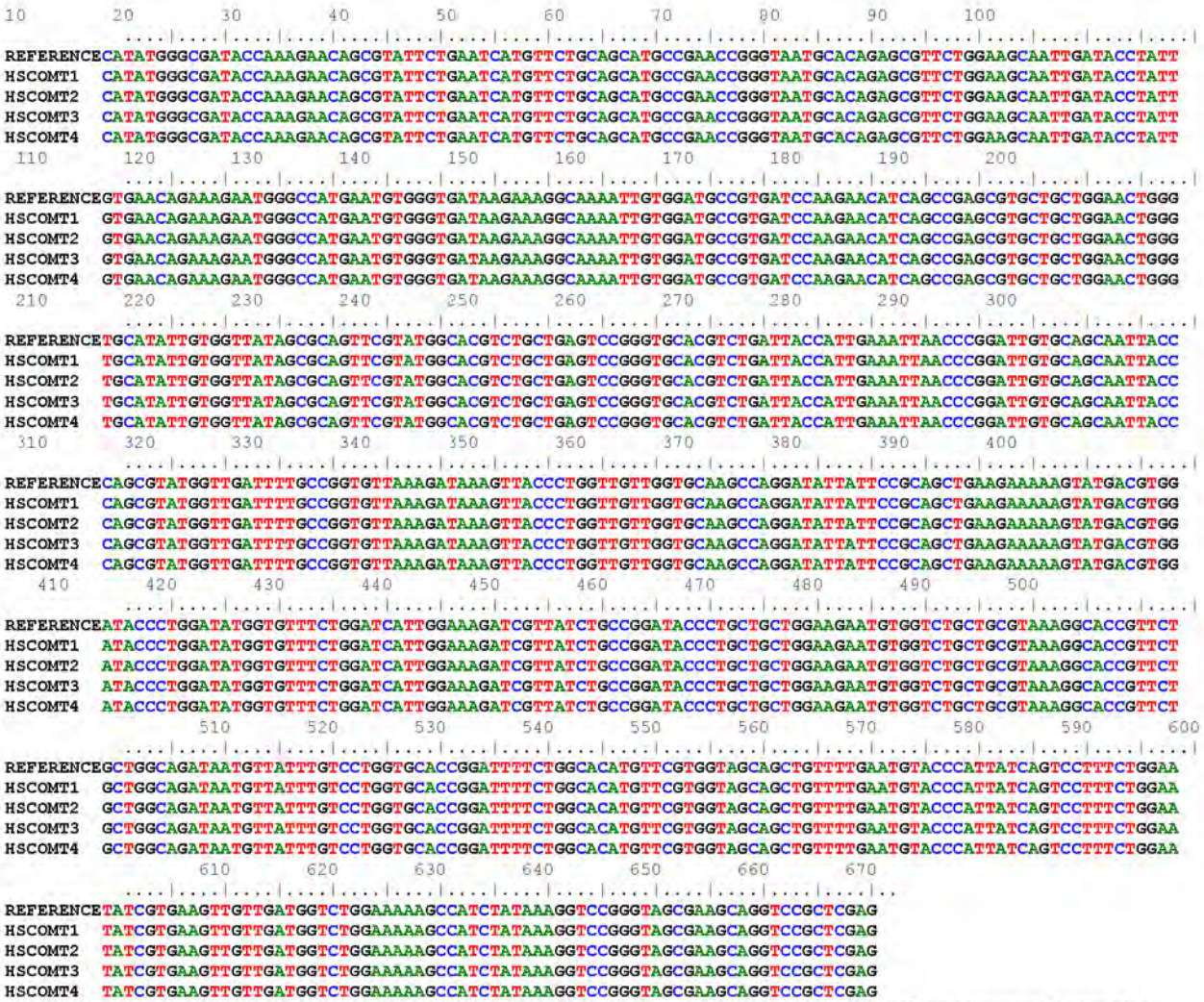

Figure 3.2: Alignments of reference HSCOMT (optimized for *E. coli* expression) with four sequenced samples.

3.3.2 Over-expression of His-tagged HSCOMT

Due to the advantages of *E. coli* and pET vectors systems (section 3.1.2) and their consequent dominance in recombinant protein expression processes, these were chosen and used for the over-expression of His-tagged HSCOMT. Chemically competent *E. coli* BL21(DE3) cells and pET-22b(+) plasmid were used for over-expressing his-tagged HSCOMT.

The chemically competent *E. coli* BL21(DE3) cells were transformed with the pET-22b(+) plasmid harbouring HSCOMT gene. The enzyme protein was expressed under the influence of

T7 promoter upon IPTG induction. Results of the induction study, analyzed and confirmed by SDS-PAGE and western blotting respectively, clearly indicate the over-expression of His-tagged HSCOMT as confirmed by the notable protein bands at ~25 kDa (Figure 3.3). High expression levels of his-tagged HSCOMT, as evident from the Figure, is in conformity with the report that upon induction, *E. coli* protein expression mechanism can synthesize high levels of the target protein (Francis and Page, 2010). The controls, namely *E. coli* cells harbouring empty (no HSCOMT gene insert) plasmid and uninduced (without IPGT induction) cultures, lack the obvious bands corresponding to the size of HSCOMT (Figure 3.3A), suggesting the non-expression of the enzyme. However, a band corresponding to the enzyme's molecular size is seen in the uninduced lane of the western blot image (Figure 3.3B). Due to the high specificity of antibodies that govern the principles of western blot technique, a possible trivial protein that might be expressed in the "uninduced" cells due to inducer exclusion effect (Studier, 2014), could be detected by western blot.

Oligomer formation by HSCOMT has been reported (Cotton *et al.,* 2004; Ehler *et al.,* 2014). The enzyme has been reported to substantially migrate as a dimer, at a concentration of ~1.2 mg/ml and above, even under reduced denaturing conditions of SDS-PAGE, with evident bands representing the dimer (Cotton *et al.,* 2004). Figure 3.3 indicates the dimerization of HSCOMT due to appearance of a band corresponding to twice the size of the monomer. It is noteworthy that Cotton and co-workers (2004) reported COMT catalytic methylation of catechols in both monomer and dimer form of the enzyme and believed the observed dimerization was due to the formation of intermolecular disulfide bonds between cysteines 188 and 191.

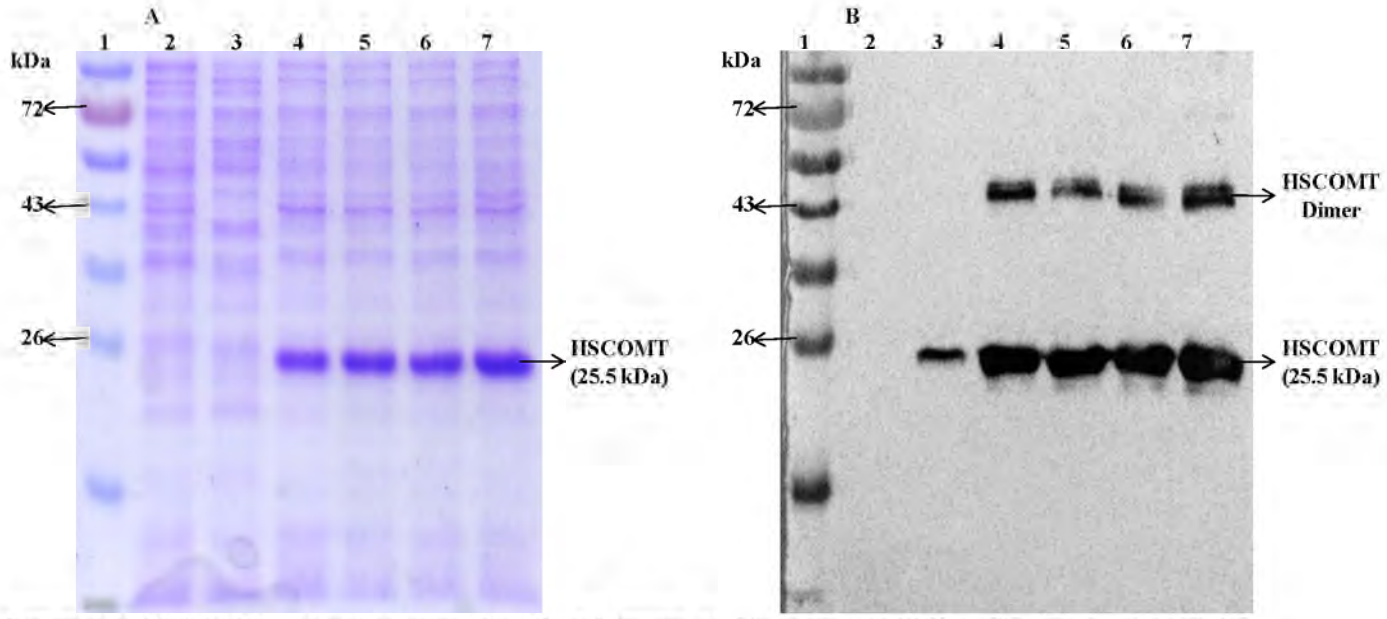

Figure 3.3: SDS-PAGE (A) and western blot (B) gel images of His-tagged HCSOMT of samples collected for COMT induction study. Lane 1: protein ladder, lane 2: empty plasmid, lane 3: uninduced, lanes 4 to7: 1 to 4 h of the induction.

3.3.3 Purification of recombinant HSCOMT

3.3.3.1 Cell harvest and lysis

Biomass was harvested by centrifugation after 4 h of IPTG-induce expression. The resultant cell pellet was washed thrice prior to enzymatic lysing, and finally frozen at -80°C (section 3.2.2.8.1). The freezing (freeze-thaw) was intended to complement the cell lysis by lysozyme because both of the lysis methods compromise each of the bacterial occlusions that retain the target recombinant protein in the cells. Enzymatic, freeze-thaw and other conventional cell lysis methods (such as the French pressure cell press and sonication) result in the total lysis of all cells, and hence may lead to the presence of other proteins and biomolecules as contaminants of the target protein (Structural Genomics Consortium *et al.*, 2008). Removal of these contaminants and isolation of the protein of interest therefore requires thorough purification procedures such as IMAC, which was used in this study.

3.3.3.2HSCOMT immobilized metal affinity chromatography (IMAC)

IMAC employs the specificity and high affinity of polyhistidine amino acid-tagged proteins to immobilized metal ions such as Ni^{2+} in aqueous solutions (Block *et al.,* 2009; Cheung *et al.,* 2012). This allows the separation of the tagged protein from other bacterial biomass with high purity (Hengen, 1995). The polyhistidine amino acid residues (typically not fewer than six) commonly used in IMAC could also be specifically identified by the antibody. IMAC was performed according to the procedure described in section 3.2.2.8.2. The his-tagged HSCOMT IMAC elusion profile and the corresponding SDS-PAGE image are shown in Figure 3.4.

The observed bands at ~25 kDa, as expected for HSCOMT, Figure 3.4 (B) is indicative that the peak in Figure 3.4 (A) was because of his-tagged HSCOMT elution. HSCOMT was eluted between 20% and 50% concentrations of the elution buffer (Figure 3.4 A). Increasing concentrations of imidazole during elution of the HSCOMT pinpoints the presence of high concentration of the former in the later. Again, the IMAC column could bind to other endogenous bacterial proteins, the host cell proteins (HSP), bearing multi-histidine amino acid residues, and therefore could be eluted as contaminants with the target protein (Structural Genomics Consortium *et al.,* 2008). It is, therefore, pertinent to remove the imidazole, the possible protein contaminants and concurrently transfer the enzyme into a buffer which supports the enzyme's prolonged catalytic stability (Cotton *et al.,* 2004).

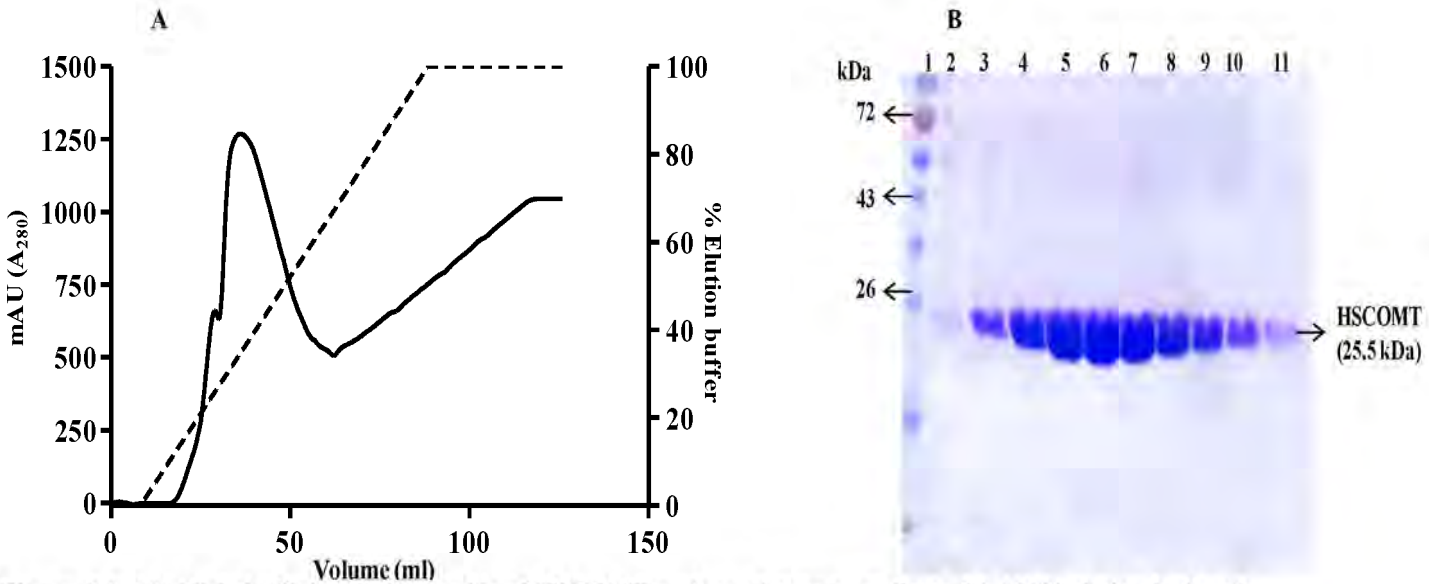

Figure 3.4: (A) Nickel affinity elution profile of HSCOMT performed over a gradient of 0-100% elution buffer (0 to 400 mM imidazole). The broken line represents the gradient of the elution buffer and the continuous line is the elution outline of HSCOMT. (B) SDS-PAGE image of the corresponding elution profile. Fractions (5 ml) were collected; lane 1 is the protein marker and lanes 2 to 11 are consecutively, fractions 3 to 12.

3.3.3.3 HSCOMT desalting

Usually, the aim of desalting is the removal of unwanted contaminants and the protein transfer to a buffer that promotes its higher stability. To enhance the purification of HSCOMT, to remove imidazole and to transfer the enzyme into the storage buffer (100 mMTris-HCl buffer, 5 mM $MgCl_2$, 5 mM ß–mercaptoethanol, 0.1 mM dithiothreitol pH 7.5), desalting was performed after IMAC, as described in section 3.2.2.8.3. The elution profile and the corresponding SDS-PAGE analyses of the desalting process are shown in Figures 3.5A and 3.5B, respectively.

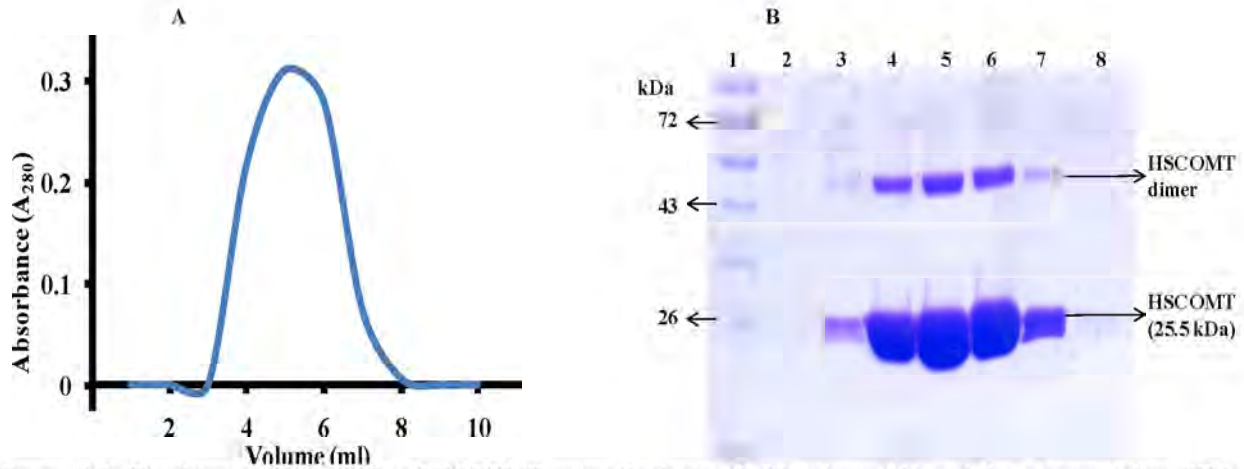

Figure 3.5: Desalting elution profile of HSCOMT using Sephadex G-25 column (A) and the corresponding SDS-PAGE gel image (B). 1 is a protein ladder while 2 to 8 represents the serial number of collected fractions. Fractions that showed higher HSCOMT concentrations from the peak and SDS-PAGE gel were pooled.

In Figure 3.5, the band at ~25 kDa indicates that the observed peak in the desalting elution profile was due to HSCOMT, which was confirmed by COMT enzymatic activity assay. The SDS-PAGE image of the desalting indicated that the his-tagged HSCOMT is pure. Increased prominence of the band corresponding to the size of HSCOMT dimer was observed in the post–desalting fractions (Figure 3.5). The increase in the enzyme dimerization corresponds to the increase in the concentration and purity of the enzyme, as pure HSCOMT dimerizes at higher concentrations (Figure 3.5) (Cotton *et al.*, 2004). Oligomerization of homogenous proteins, even under reduced SDS-PAGE conditions, has been reported to be caused by the intermolecular disulfide cross-linkage (Kumar *et al.*, 1993; Kumar *et al.*, 1994; Cotton *et al.*, 2004). A faint band at ~75 kDa was visible using enhanced Fairbank's SDS-PAGE destaining, which allows visualizing as little as 25 ng of protein (Fairbanks *et al,* 1971). The band maybe a trimer of HSCOMT since it is not detectable in the control lane (empty plasmid) in a western blot image of the HSCOMT purification gel (Figure 3.6B).

3.3.3.4 His-tagged HSCOMT purification assessment

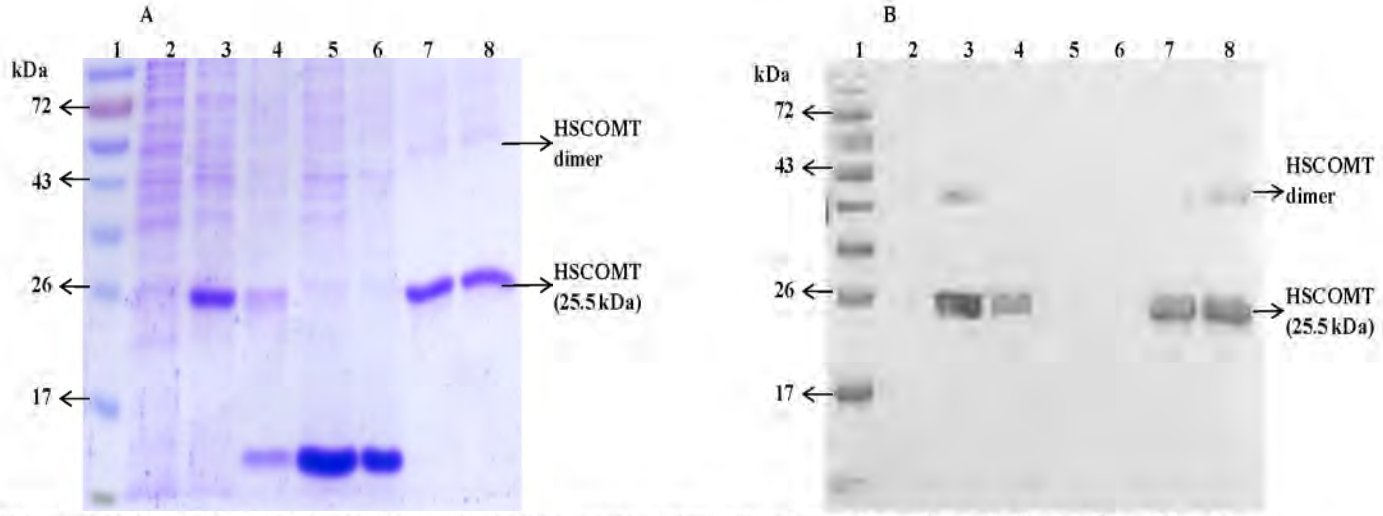

Figure 3.6: (A) SDS-PAGE and (B) corresponding western blot gels of samples collected after each purification stage showing the protein ladder (1), grown *E. coli* cells harbouring empty (no HSCOMT gene) plasmid (2), crude lysate sample (3), cleared lysate sample (4), IMAC flow-through sample (5), IMAC Wash sample (6), IMAC eluate sample (7) and size exclusion elute sample (8).

COMT catalytic methylation activity, SDS-PAGE analyses and Bradford protein quantification assays were performed at each purification stage. Quantification of protein concentrations allowed loading of an equal amount of protein on SDS-PAGE and activity assay wells for the evaluation of HSCOMT purity and catalytic activity, respectively. Western blot was employed to confirm the presence of his-tagged HSCOMT in the purification stages indicated by SDS-PAGE gel (section 3.2.2.9). Figure 3.6 shows the results of both the SDS-PAGE and resultant western blot gels of the purification trend.

From the SDS-PAGE purification progress gel (Figure 3.6A), the HSCOMT purity increased across the purification stages, which was confirmed by the enzyme's purification table (Table 3.1). The majority of host cell protein (HSP) contaminants were eliminated after IMAC, supporting the appropriateness of the IMAC in recombinant protein purification. The presence of bands at ~12 kDa each in the cleared lysate flow-through and wash indicates a presence of

peptide fragments in these samples. The presence of the low molecular weight peptides is possibly because of an intrinsic non-specific proteolytic activity of lysozyme culminating in proteolytic artefacts associated with the lysis of bacterial cells by lysozyme (Oliver and Stadman, 1983). This non-specific degradation of protein by lysozyme may not be restricted to HSP; rather, it might include the protein of interest, thereby impacting on the eventual yield of the target protein.

A protein quantification assay of the samples collected in all the purification steps was concurrently performed and the same amount of protein (in all the samples) was used for COMT activity assay. Results from this experiment showed an increase in COMT-specific activity across the purification ladder. The results were used in constructing the HSCOMT purification table (Table 3.1).

Table 3.1 Purification table of recombinant HSCOMT

Fraction	Volume (ml)	Protein concentration (mg/ml)	Total protein (mg)	Total activity (U)	Specific activity (U/mg)	Purification fold	% Yield
Crude lysate	162	3.87	626.94	429.1	0.68	1	100
Soluble fraction	118	2.14	252.52	398.23	1.58	2.3	92.81
IMAC	40	0.71	28.40	103.63	3.65	5.33	24.15
Desalting	7.2	3.5	25.20	96.96	3.85	5.62	22.6

Table 3.1 represents the purification of HSCOMT expressed in a volume of 1.8 l. The total protein obtained after the purification was 25.2 mg, with a purification fold of 5.62. The yield is comparable to 15 mg/l reported by Cotton *et al.*, (2004). The purified HSCOMT was stored in 20 µl aliquots at -20ºC.The HSCOMT catalytic activity was stable at -20ºC for over three months and for up to seven days at 4ºC.

3.3.3.5 Western blot

Monoclonal antibodies specifically binding to polyhistidine allow the detection of his-tagged recombinant proteins using western blot procedures (section 3.2.2.9) (Debeljak *et al.,* 2006). The western blot was carried out using the anti-polyhistidine antibodies to specifically detect and confirm that the expressed protein is his-tagged HSCOMT. Prominent bands corresponding to the sizes of monomer (~25 kDa) and dimer (~50 kDa) (at high concentrations) of HSCOMT appeared in both western blot figures (Figures 3.3B and 3.6B), indicating HSCOMT dimerization. This agrees with the reported HSCOMT dimerization (Cotton *et al.,* 2004; Law *et al.,* 2016). Furthermore, a faint band at ~75 kDa matching the HSCOMT trimer was also seen. The HSCOMT dimer and trimer occur at high protein concentrations due to intermolecular disulfide bond and domain swap (Cotton *et al.,* 2004; Law *et al.,* 2016). It is noteworthy that the monomer and dimer of HCOMT are reported to be catalytically active (Cotton *et al.,* 2004; Law *et al.,* 2016), with some variations in regioselectivity towards different catechol substrates (Law *et al.,* 2016). The western blot detection of his-tagged HSCOMT, lack of COMT enzymatic activities in assay controls (blank activity assay lacking SAM and HSCOMT or presence 3,5-dinitrocatechol COMT inhibition) are confirmatory indications that the catalytic methylation activity observed in the samples is due to his-tagged HSCOMT enzyme.

3.3.4 Characterization of HSCOMT

3.3.4.1 Optimization of S-(5'-adenosyl)-*L*-methionine (SAM) concentration

Figure 3.7 shows the result for the optimization study for the concentration requirement of S-(5'-adenosyl)-*L*-methionine (SAM) in HSCOMT catalytic methylation of esculetin. From the figure, HSCOMT (10 μg/ml) rate of catalysis, at 20 μM esculetin, was linear up to the SAM

concentration of 10 µM. The rate begins to level off at SAM concentration of 40 to 60 µM. To ensure that SAM is not a rate limiting factor in HSCOMT activity assays, 60 µM SAM was considered as the concentration for subsequent HSCOMT activity assays, with concentrations of the enzyme and esculetin less than 10 µg/ml and 20 µM, respectively.

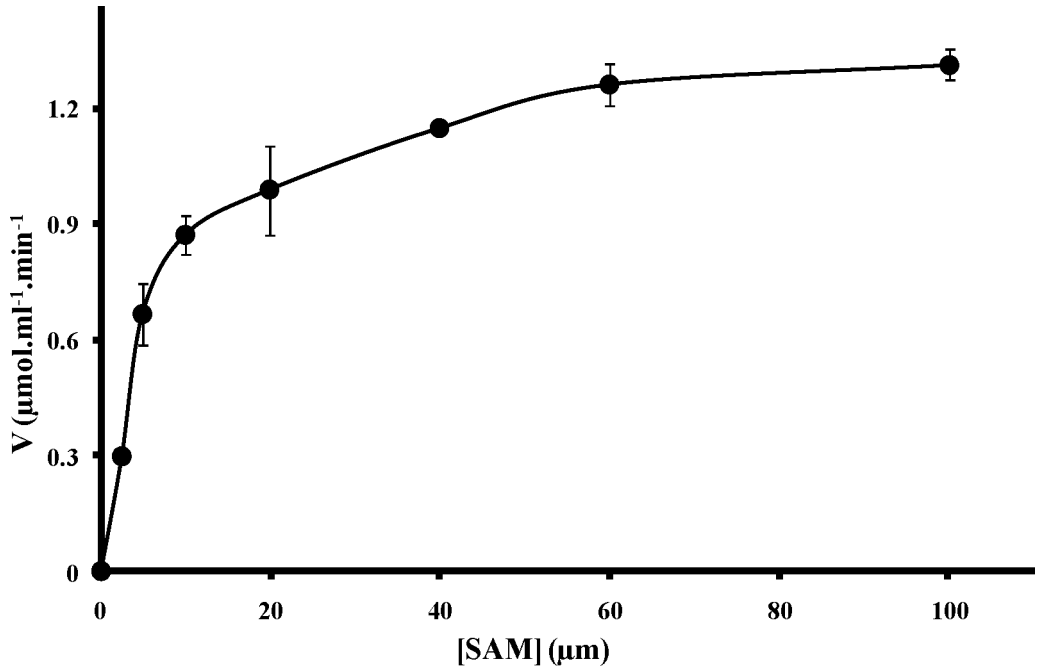

Figure 3.7: SAM concentration optimization study. HSCOMT activity was performed at fixed esculetin and enzyme concentrations of 20 µM and 10 µg/ml, respectively. Values represent the mean (n = 3, ± SD).

3.3.4.2 pH and temperature profiles of HSCOMT

The biological functions of proteins depend on their three-dimensional structures. In the majority of proteins, and hence enzymes, biological functions are viable at definite structural conformations. These structural conformations are dependent on the surrounding pH and temperature. The surrounding pH influences the ionization state of substrates and also that of each contributing amino acids in the enzyme protein sequence. The ionization state, in turn, influences the protein structure and substrate binding, which dictate the catalytic activity of

enzymes. Hydrogen bonds governing the secondary structure of the protein are dependent on the immediate temperatures, as higher temperature decreases the strength of hydrogen bonds. It is therefore worthwhile to determine the pH and temperature values that favour optimum biological function of the enzyme. The HSCOMT activity was assayed over a pH range of 4.5 to 8.5 at 37°C using a cocktail of buffer salts (appendix II), while temperature optimization was performed at the optimum pH (7.0) as described in section 3.2.2.13. For both studies, the activity reaction mixture without methyl donor SAM was incubated at specified conditions for 5 min before its (SAM) addition to initiate the reaction. The results obtained for the pH and temperature optimization of HSCOMT catalytic activity are presented in Figures 3.8 and 3.9 respectively.

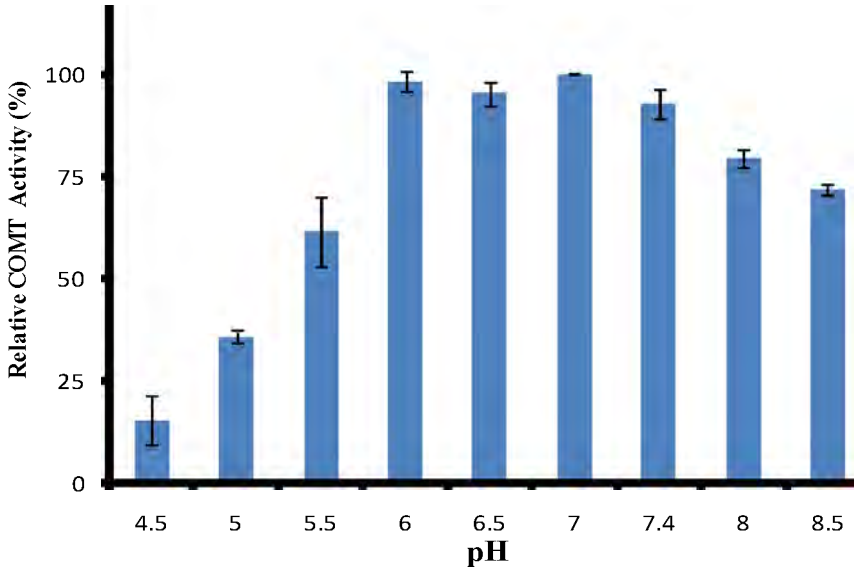

Figure 3.8: pH profiles of HSCOMT activity at 37°C over a period of 30 min. Results were obtained from 3 data sets. Values represent the mean (n = 3, ± SD).

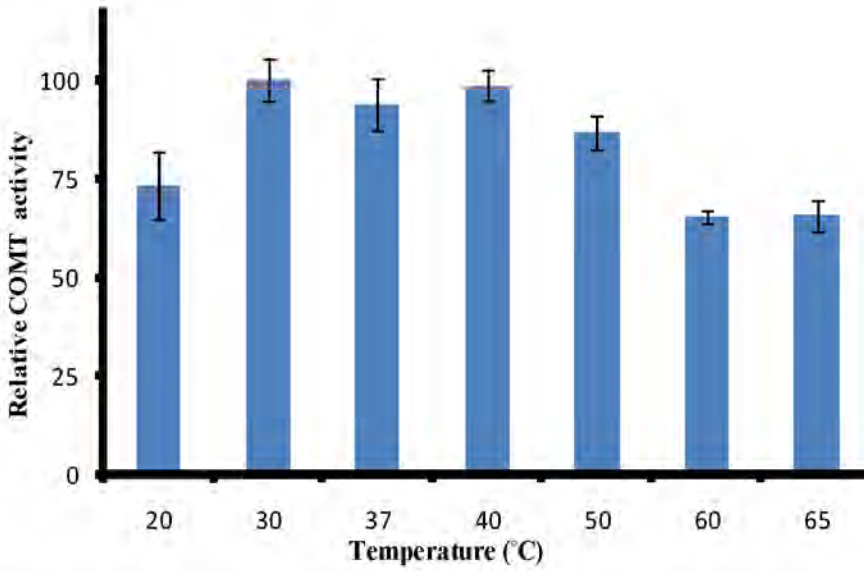

Figure 3.9: Temperature profile of HSCOMT activity observed at pH 7 over a period of 30 min. Results were obtained from 3 data sets. Values represent the mean (n = 3, ± SD).

Percentage activity at various pH and temperature values was calculated in relation to the highest activity (for each pH and temperature set of experiments). The observed pH and temperature for HSCOMT catalytic methylation of esculetin to scopoletin were 7.0 and 30°C, respectively.

A broad range of pH (6.5 to 10.5) has been reported for COMT optimum catalytic methylation of various catechol substrates (Ball *et al.*, 1972; Gulliver and Tipton, 1978; Nohta *et al.*, 1984; Alazizi *et al.*, 2011). The observed pH profile in the present study is within the reported range, and the enzyme showed substantial stability between pH range of 6.0 to 8.5.

Replacement of valine with methionine at position 108 of HCOMT is associated with variation in COMT catalytic activity and thermal stability (Bertocci *et al.*, 1991; Lachman *et al.*, 1996). The methionine-108 variant is about four times more thermolabile than the valine-108 variant. The latter retains its full catalytic activity at physiological temperatures for more than 30 min (Lotta *et al.*, 1995), while Ball *et al.*, (1972) reported 42°C as the temperature of its optimum

catalytic activity. For the current study, the valine-108 variant showed a catalytic activity of more than 60% in range of 20 to 65°C (Figure 3.9). Because HSCOMT is a human protein, it was anticipated that optimum activity would be at 37°C. Although HSCOMT showed catalytic activity of 91% at 37°C, the manifestation of the HSCOMT catalytic activity at higher and lower temperatures than human physiological temperature (Ball *et al.*, 1972) could be based on the different catecholic substrates and reaction conditions exhibiting different catalytic patterns (Dawling *et al.*, 2001).

3.3.4.3 Thermal stability of HSCOMT

Thermal stability of HSCOMT was performed according to the procedure described in section 3.2.2.14. The stability was investigated at the temperature optimum (30°C), and Figure 3.10 shows the thermal stability profile of the enzyme at this temperature.

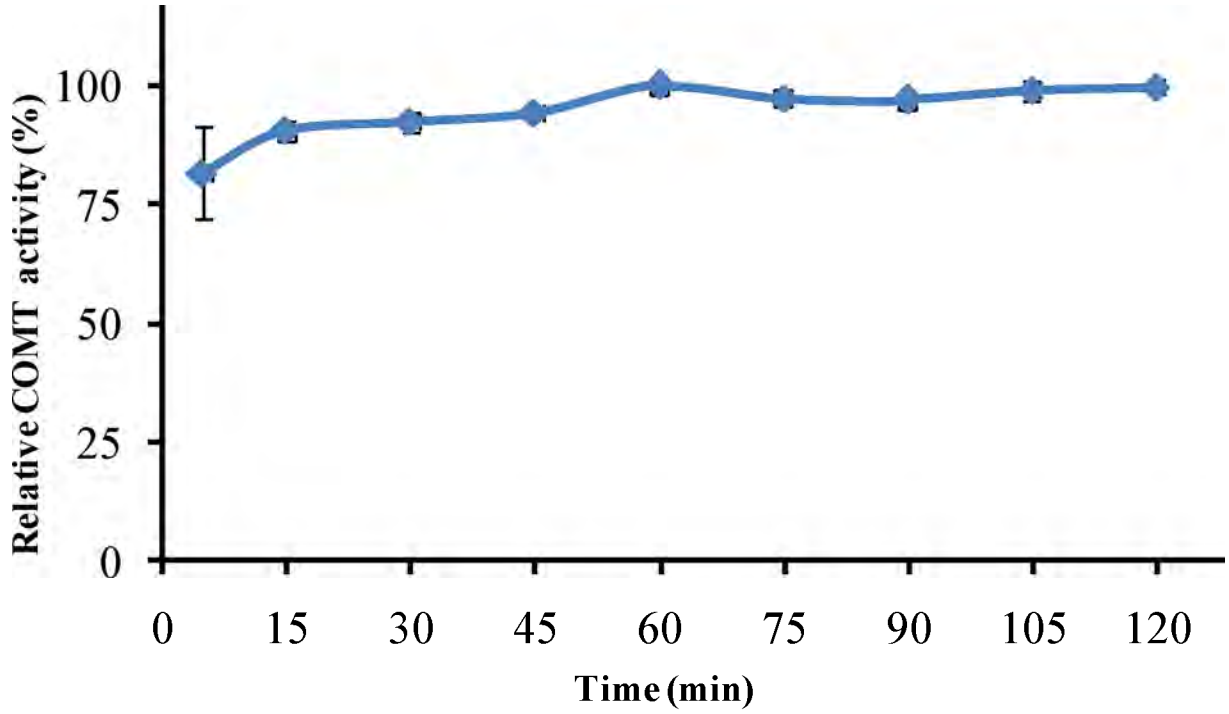

Figure 3.10: Temperature stability profile of HSCOMT activity observed at pH 7 at a time range of 5 to 120 min at 30°C. Values represent the mean (n = 3, ± SD).

Since all the enzyme assays involve an incubation period of least 5 min, this time is considered the minimum incubation time for the stability study. Interestingly, HSCOMT activity at 30°C increases from 81% (t = 5 min) to 100% (t = 60 min), and was stable for up to 120 min.

3.3.4.4 Kinetic studies

Kinetics studies were performed as described in section 3.2.2.13. The study, using HSCOMT activity assay procedure described in section 3.2.2.11, resulted in a conventional hyperbolic curve described by Michaelis-Menten kinetics (Figure 3.11). Each set of experiments was performed in triplicate and the calculation and analysis of kinetic parameters, K_m and V_{max}, were performed using the GraphPad Prism 5 software. Hanes–Woolf linearization of the hyperbolic Michaelis-Menten curve position the independent variable ([S]) to appear on both sides of the equation, and hence on both axes of the plot. This approach, therefore, does not overplay the data obtained at low or high [S], thus allowing an accurate estimation of both K_m and V_{max} (Ritchie and Prvan, 1996). Because of its advantages, the choice in this study is the Hanes–Woolf plot, and the graph is shown in Figure 3.12. The kinetic parameters calculated using GraphPad Prism 5 and Hanes–Woolf plot are shown (Table 3.2).

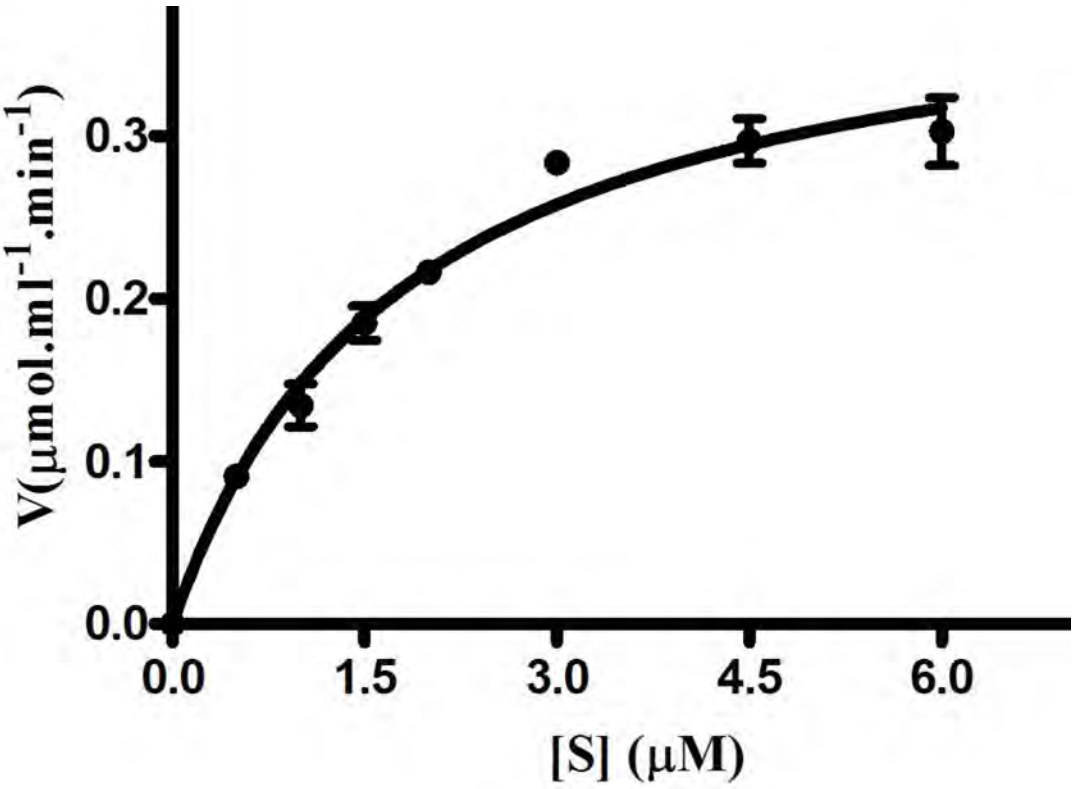

Figure 3.11: The Michaelis-Menten curve of HSCOMT activity with varying concentrations of esculetin. Values represent the mean (n = 3, ± SD).

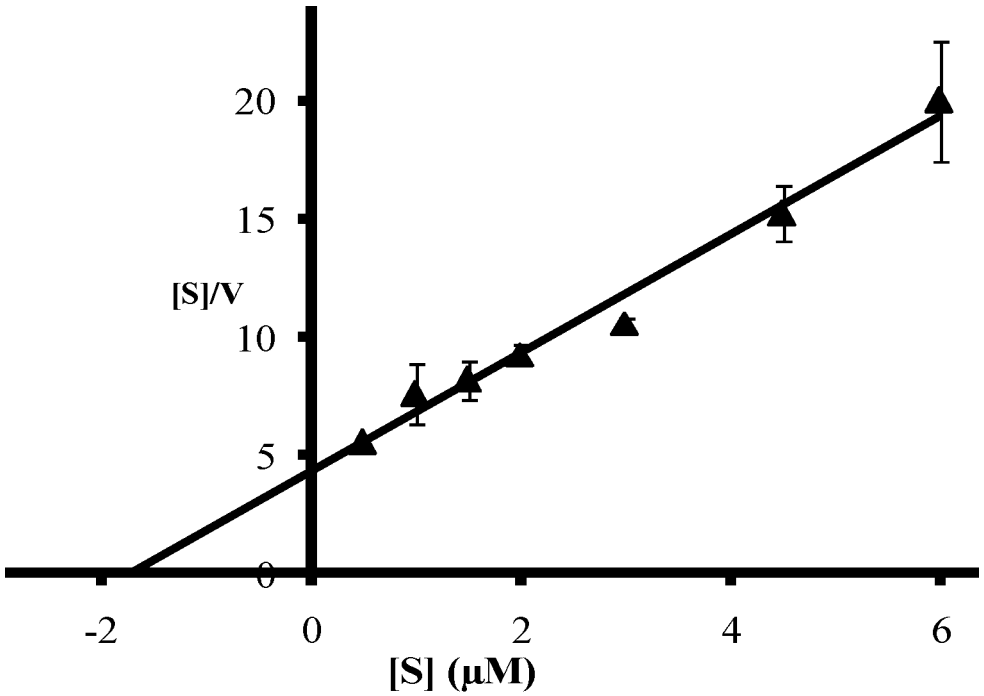

Figure 3.12: The Hanes-Woolf linearization of the kinetic study data represented in the Michaelis-Menten curve in Figure 3.11. Linear equation y = 2.502x + 4.292; R^2= 0.982.Values represent the mean (n = 3, ± SD).

Table 3.2: Kinetic parameters of HSCOMT from both hyperbolic and Hanes-Woolf linear plots.

Plot	Variables			
	K_m (μM)	V_{max} (μmol.ml^{-1}.min^{-1})	K_{cat} (min^{-1})	K_{cat}/K_m (M^{-1}. min^{-1})
Hyperbolic (non-linear)	1.788±0.246	0.412±0.022	2.082±0.111	1.165
Hanes-Woolf (linear)	1.715	0.4000	2.020	1.178

Michaelis-Menten plots have been reported for the majority of COMT kinetic studies. The HSCOMT index of the affinity for the substrate, esculetin (K_m) and catalytic number (V_{max}) are 1.788±0.246μM and 0.412±0.022 μmol/ml/min, respectively. The turnover index (K_{cat}) and the measure of the enzyme efficiency (K_{cat}/K_m) are 2.082±0.111 min^{-1} and1.165 M^{-1}.min-^{1}, respectively. The K_m value of HSCOMT is comparable to that of partially purified BSCOMT (section 2.3.4), while V_{max}, K_{cat} and K_{cat}/K_m are higher than those of BSCOMT, possibly due to higher purity of HSCOMT. Generally, COMT affinity index (K_m) and catalytic number (V_{max}) are dependent on enzyme source and catechol substrate (Cotton *et al.,* 2004; Lotta *et al.,* 1995; Mannisto and Kaakkola, 1999). It is noteworthy that none of the reported kinetics was generated using HSCOMT catalytic methylation of esculetin. K_m and V_{max} values reported for COMT catalysis differ with different enzyme sources, substrate and reaction conditions (Mannisto and Kaakkola, 1999).

Some enzymes, such as COMT, show broad specificity, acting on various substances that are structurally related to their physiological substrate. These enzymes present different kinetic parameters with different substrates and reaction conditions by adjusting to changes in substrates and reaction conditions, and mould the mechanisms of catalysis to conform to the existing

substrates and reaction conditions (Ulusu, 2015). Kinetic mechanisms of these enzymes, according to Ulusu (2015), evolved with substrate variability and reaction conditions.

3.4 Conclusion

The key objectives of this section were to identify and procure the gene of HSCOMT enzyme protein; to express, purify and catalytically characterize the recombinant enzyme protein. Virtual cloning of the gene using pET-22b(+) vector suggested the feasibility and appropriateness of the gene insertion into the expression vector. After the artificial gene synthesis, restriction fragment length polymorphism (RFLP) and DNA sequencing (Figures 3.1 and 3.2) confirmed that the insert was the correct size and nucleotide sequence for HSCOMT.

The his-tagged enzyme was subsequently expressed in *E. coli* BL21(DE3) upon IPTG induction. The increase in protein concentration, at the position that corresponds to the size of HSCOMT, with induction time and subsequent specific (western blot) identification of the his-tagged HSCOMT verified the expression of the enzyme. The expressed enzyme was purified by ultracentrifugation, IMAC and desalting. The enzyme was purified to 5.62 fold with 22.6% yield and a specific activity of 3.85 U/mg. The purified enzyme showed higher catalytic methylation of esculetin at pH 7.0 and 30^{o}C. Kinetic parameters were determined and the enzyme exhibited a hyperbolic curve defined by the Michaelis-Menten equation. Analysis of the kinetic curve gave a K_m value of 1.79 (1.715 for Hanes-Woolf) μM and a V_{max} value of 0.412 (0.4000 for Hanes-Woolf) μmol/ml/min. The K_{cat} and K_{cat}/K_m are 2.08 (2.020 for Hanes-Woolf) $min^{-1}$and 1.165 (1.178 for Hanes-Woolf) $M^{-1}.min^{-1}$, respectively. While the K_m is comparable to that of BSCOMT, the V_{max}, K_{cat} and K_{cat}/K_m are higher in HSCOMT.

In summary, enzymatically active HSCOMT was adequately expressed, purified and characterized. This enzyme is therefore suitable for subsequent usage to observe whether nanoparticles influence its catalytic activity at the determined optimum conditions.

Chapter four

Synthesis and characterization of gold and silver nanoparticles

4.1 Introduction

Deliberate use of nanoparticles (NPs) is gaining relevance in various domains of technology. The practice of designing, synthesis, manipulating and subsequent application of NPs is referred to as nanotechnology. Nanomedicine involves intentional exposure of nanomaterials to the human body (Freitas, 2005). Therefore, controlled synthesis and clear insight of the properties of the materials are required for customized use.

Top-down and bottom-up are the two general methods for the synthesis of metallic NPs (Toshima and Yonezawa, 1998). The top-down NPs preparation approach entails scaling down the bulk materials to the nanometer dimensions, while the bottom-up method involves assembly of nanostructures by physicochemical processes from basic units, that is, growth of nanomaterials from small building blocks, that is to say, atom by atom, molecule by molecule or cluster by cluster (Hu and Shaw, 1999).

Bottom-up, otherwise called self-assembly, is the common and preferred approach for nanofabrication (Ozin *et al.*, 2009). Chemical and biological syntheses of NPs rely on this self-organizing method (Thakkar, *et al.,* 2010) thereby exploiting the physicochemical properties of "the building blocks" to induce their self-assembly into nanomaterials (Cunningham and Bürgi, 2013). The method has the advantages of synthesizing nanomaterials with narrow size distributions and a wide range of the particles preparation approaches (Betke and Kickelbick, 2014). However, the top-down method, comprising of physical techniques, usually requires

expensive equipment and high energy milling which make this technique cumbersome and environmentally unfavourable (Umer *et al.*, 2012).

The formation of metallic NPs in an aqueous solution is generally associated with characteristic colour changes, which depend on the particles' optical properties governed by their size and shape (Liz-Marzán, 2004). These optical properties are due to the Surface Plasmon Resonance (SPR) of the particles' surfaces, which arises from the interplay of excited electromagnetic surfaces and electron density oscillations as a function of the particles' physical environment (Khlebtsov and Dykman, 2010; Ma *et al.*, 2015). The electron oscillations on the particle surface induce a charge separation with respect to the ionic lattice, forming a dipole oscillation in the direction of the electromagnetic field. The SPR educes a strong light absorption at UV-vis region that can be measured spectrophotometrically as a "stereotype character" of the NPs. The SPR absorption wavelength and intensity depend on such factors as particle size, shape, structure, metal type and the dielectric constant of the particles' environment which affect the electron charge density on the particle surface (Huang and El-Sayed, 2010).

The characteristic colours and plasmonic absorptions do not reveal the precise shape and size of metallic NPs; therefore further characterization of the particles to unravel such properties is worthwhile. Transmission electron microscopy (TEM) involves the application of high-energy (60-3 000 keV) electrons through a sample to reveal the sample's image, diffraction patterns and spectroscopic information. This technique has gained extensive applications because of its exceptional capacity to resolve structural and chemical behaviour down to atomic dimensions. TEM has therefore, been employed for studying the morphology, size and size distribution of nanostructured materials (Smith, 2007), since the technique can provide interpretable particle imaging at a resolution of 0.05 nm (Erni *et al.*, 2009).

The aim of this section is to synthesize gold and silver NPs and to characterize them using absorption spectroscopy and TEM.

4.2 Materials and methods

4.2.1 Materials

All the chemicals, reagents and equipment used in this section are in appendix I.

4.2.2 Methods

4.2.2.1 Synthesis of NPs

Gold NPs were synthesized by a citrate reduction method (McFarland, *et al.,* 2004). To a stirred (800 rpm) boiling solution of aqueous tetrachloroauric acid (1.0 mM, 20 ml) was added trisodium citrate (1%, 2 ml) until the solution turned a brilliant red colour, indicating the reduction of gold ions into AuNPs (Toma *et al.,* 2010; Erni *et al.,* 2009).

Silver NPs were synthesized using a microwave-assisted method (Pal *et al.,* 2008). A mixture of an ethanolic solution of polyvinylpyrrolidone (PVP) (1%, w/v, 10 ml) and $AgNO_3$ (0.1 M, 0.2 ml) was microwaved (LG; 720 W; 2, 450 MHz) for 7 sec. The initially colourless solution turned to pale yellow, indicating the formation of AgNPs (Pal *et al.*, 2008; Khan *et al.,* 2011).

4.2.2.2 Characterization of NPs

Plasmonic absorptions of the gold and silver NPs were recorded using a BioTek Synergy MX (BioTek®) microplate reader. The wave scans were performed in triplicate between 300 and 700 nm using a 96 well micro plate. Wave scans of trisodium citrate and ethanolic PVP solutions

corresponding to their concentrations in the gold and silver NPs, respectively, were recorded as controls.

A Transmission Electron Microscope (TEM) (Zeiss Libra 120; keV coupled to an Olympus Soft Imaging Solutions digital camera) was used to measure the morphology and size of the particles. A drop of the NPs solution was placed on a carbon-coated copper grid (Agar Scientific) and allowed to settle for 30 sec. Excess was removed using blotting paper and the grid was air-dried for 24 h prior to TEM viewing. Size distributions of the NPs were determined by counting the NPs in the TEM images using the ImageJ version1.42 software (Rasband, W. S; National Institutes of Health, Bethesda, Maryland, USA).

4.3 Results and discussions

4.3.1 Synthesis of NPs

Gold ions were reduced to AuNPs by sodium citrate, indicated by a reddish brown colour. The colour change is attributed to the oscillation of the free electrons caused by an interacting electromagnetic field, which is absent in the bulk material and individual atoms (Huang and El-Sayed, 2010) (Figure 4.1).

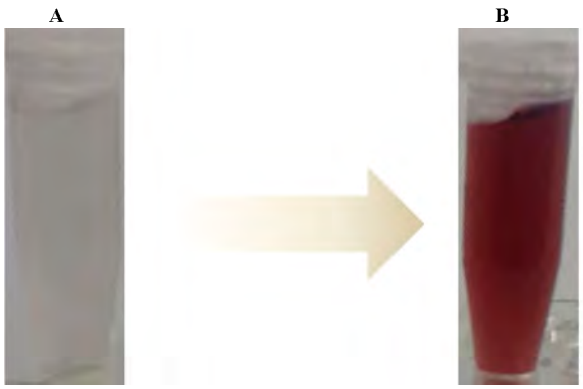

Figure 4.1: Synthesis of AuNPs by citrate reduction. (A) Aqueous tetrachloroauric acid (1.0 mM) and (B) reddish-brown colour indicating the formation of AuNPs after the addition of trisodium citrate (2 ml; 1%).

For AgNPs, the colourless mixture of ethanolic PVP (1% w/v) and $AgNO_3$ (0.002M) turned to pale yellow after 7 sec of microwaving, indicating the formation of AgNPs (Pal *et al.*, 2008; Khan *et al.*, 2011). Storage of the synthesized AgNPs in the dark at 23°C for 48 h gave a deep yellow colour (Figure 4.2). This deep yellow colour development of AgNPs has been reported by Šileikaitė *et al.*, (2009) to be caused by the particles' maturation from the initial non-reduced metal ion seeds in the solution and their growth to NPs.

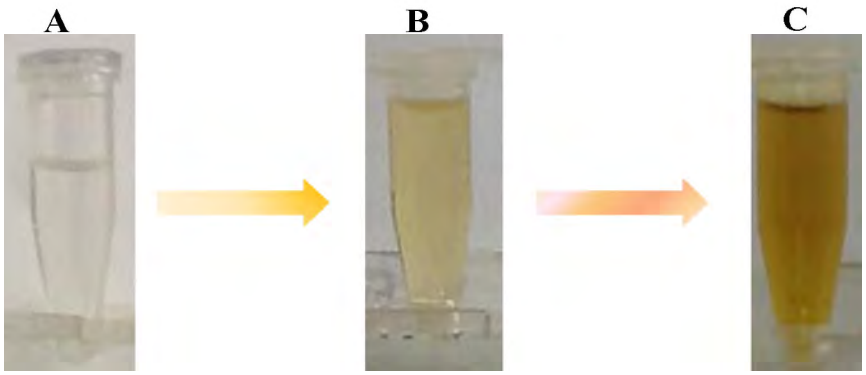

Figure 4.2: Microwave assisted synthesis of AgNPs showing (A) solution before microwaving, (B) characteristic pale yellow colour indicating the synthesis of AgNPs immediately after microwaving and (C) 48 hours later showing intense yellow colour formation.

4.3.2 Characterization of NPs

4.3.2.1 Plasmonic absorption of gold and silver NPs

Absorption spectroscopy is a renowned technique for characterizing the formation of gold and silver NPs due to their plasmonic nature (Gangula *et al.*, 2011). The absorption band of the synthesized AuNPs exhibited SPR at 520 nm (Figure 4.3), a characteristic absorption spectrum of AuNPs (Huang and El-Sayed, 2010). AuNPs have been reported to be stable in the dark at 4°C for more than a month (Balasubramanian, *et al.*, 2010). Increased plasmon absorption and a slight red-shift from 520 nm to 523nm (Figure 4.3) were observed when AuNPs were stored in

the dark at 4°C for 48 h. Increased plasmonic absorption of the particles after 48 h storage could be caused by maturation of seeded gold ions to NPs. Two weeks storage in the dark at 4°C resulted in a further increase in the red-shift, and a decrease in plasmonic absorption of the particles, suggesting the aggregation and consequent formation of larger particles. The red-shift of AuNPs is reported to be caused by the delocalization of the conduction electrons on the particles' surfaces, leading to aggregation and an increase in sizes and decrease in numbers of particles (Fatin *et al.*, 2013).

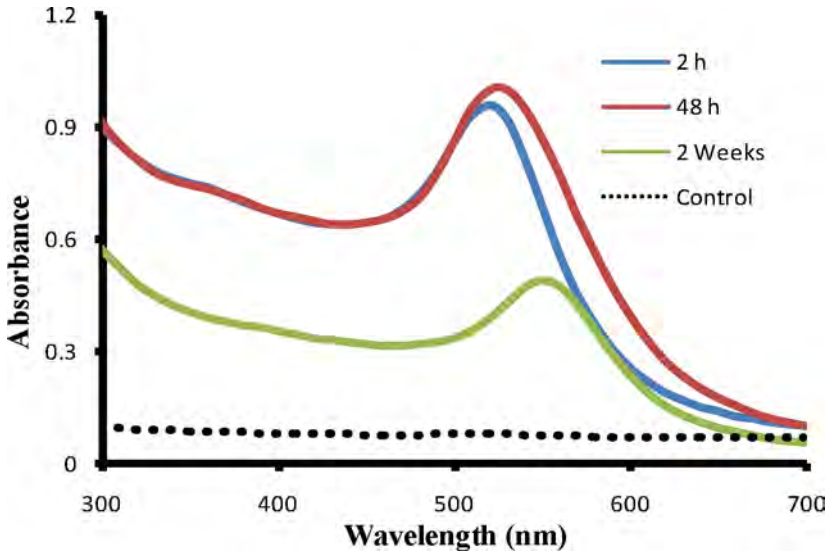

Figure 4.3: Absorption spectrum of AuNPs samples taken at different times of storage in the dark at 4°C after synthesis, as indicated on the graphs. The discontinuous line is the absorption of trisodium citrate.

The absorption spectrum of the AgNPs exhibited an absorption peak at 417 nm (Figure 4.4), and is similar to those reported in the literature (Pal *et al.*, 2008; Hsu and Wu, 2010; Patil *et al.*, 2011). PVP-stabilized AgNPs have been reported to be stable in the dark at room temperature for up to two months (Ibarra-Hurtado *et al.*, 2014). Storage of the synthesized AgNPs in the dark at 23°C for 2 h caused increased colour intensity, an indication of continuous formation of AgNPs (Pal *et*

al., 2008). Storage for 48 h under these conditions caused a blue-shift (from 417 nm to 400 nm) and increase of the plasmonic absorption. Extending the storage time to a fortnight caused only a slight blue-shift (from 400 nm to 398 nm) and decrease of the pasmonic absorption (Figure 4.4), indicating that the AgNPs were stable during this time.

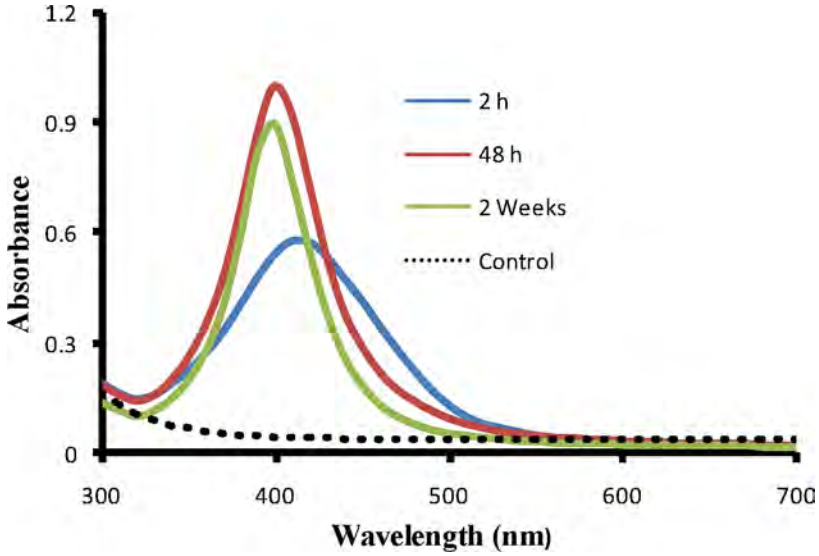

Figure 4.4: The plasmonic absorption spectrum of AgNPs samples taken at different times of storage in the dark at 23°C after synthesis. The discontinuous line is the absorption of ethanolic PVP solution.

4.3.2.2 Transmission electron microscopy (TEM)

The shape, size and distribution of the synthesized gold and silver NPs were visualized by TEM and counted using ImageJ version 1.42. TEM images and size distribution graphs are shown in Figures 4.5 and 4.6.

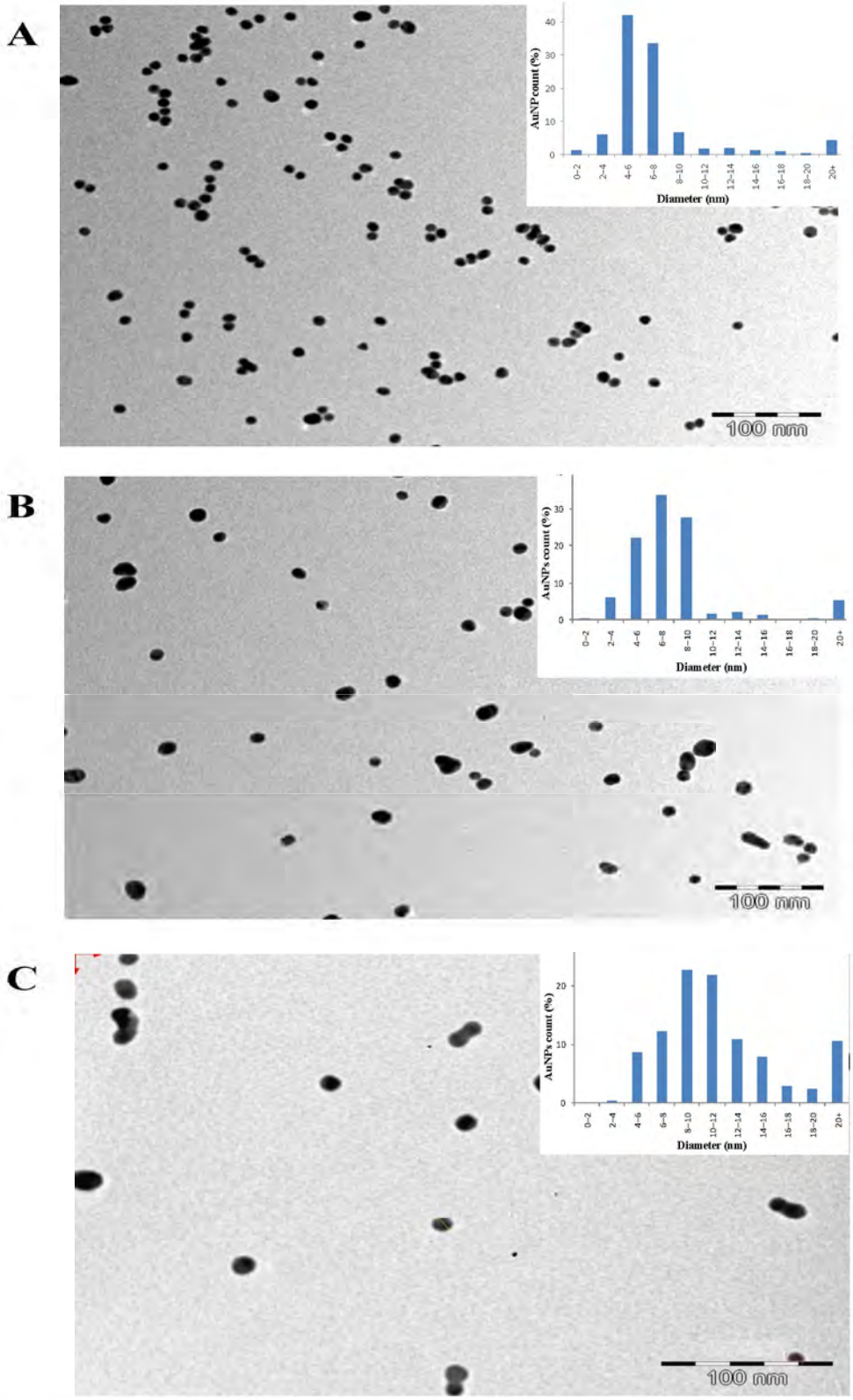

Figure 4.5: TEM images of AuNPs stored in the dark at 4°C after synthesis for (A) 2 h (B) 48 h and (C) 2 weeks. The corresponding insets are the size distribution graphs shown adjacent to each TEM image. Scale bars are shown.

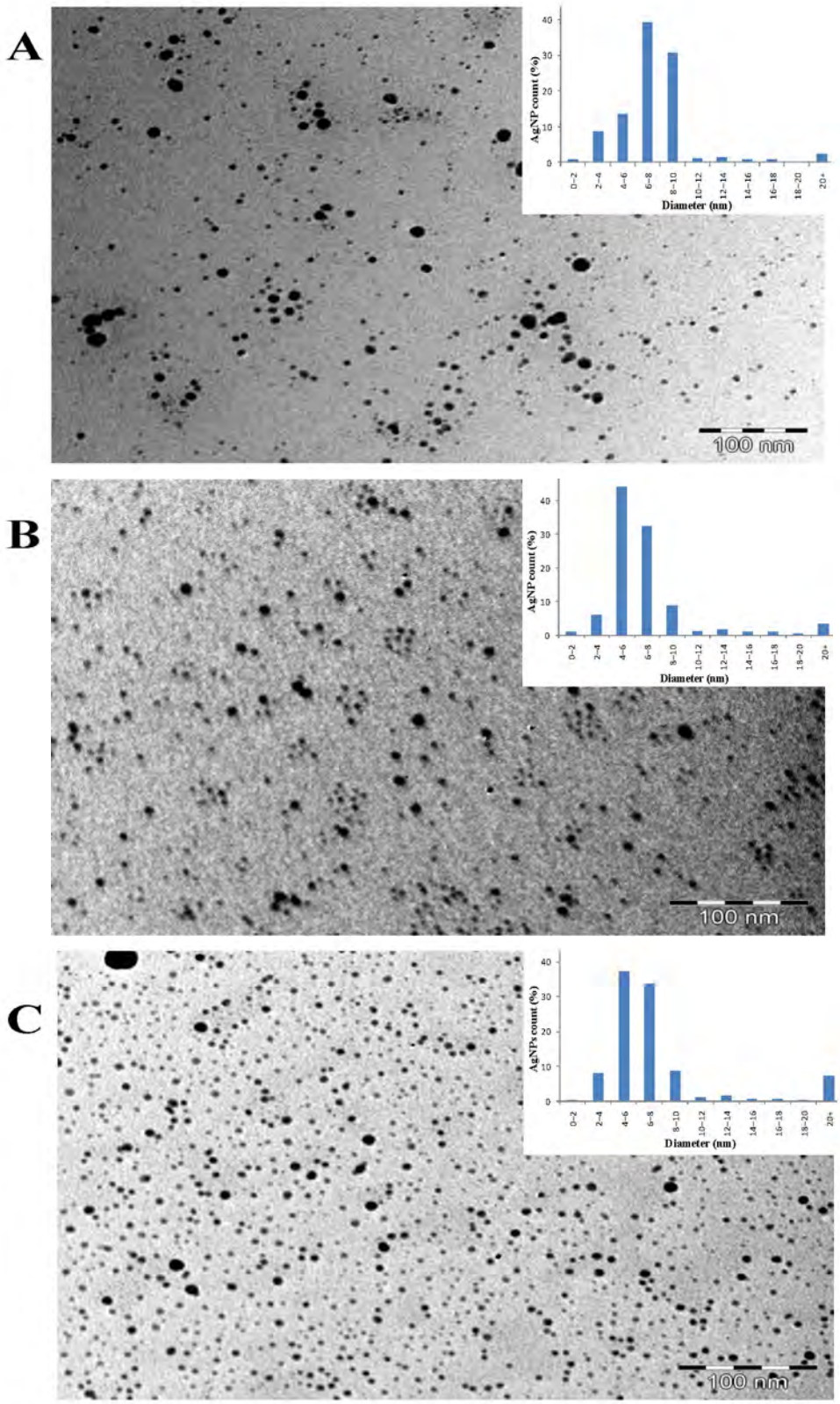

Figure 4.6: TEM images of AgNPs stored in the dark at 23°C, after synthesis for (A) 2 h (B) 48h and (C) 2 weeks. The corresponding insets are the size distribution graphs shown adjacent to each TEM image. Scale bars are shown.

The AuNPs synthesized were spherical and the size distribution showed a good range of monodispersion (Figure 4.5), with a majority in the 4-8 nm diameter range. Red-shift of the plasmon absorption of the particles from 520 nm to 523 nm occurred during storage in the dark at 4°C for 48 h depicted in figure 4.4. The red shift complements the increase in sizes (from 4-8 nm range to 4-10 nm range) of the particles, as shown by the size distribution (Figure 4.5). TEM image and size distribution of AuNPs kept in the dark at 4°C for two weeks showed larger and fewer particles, indicating the gradual aggregation over time. This is indicated by the appearance of more particles with the size of 20+ nm in the size distribution graph of the sample stored for two weeks.

The sizes and the monodispersions of AgNPs kept in the dark at 23°C from 48 h to two weeks are similar (Figure 4.6), with general diameter range of 2-10 nm, signifying the stability of the particles within this period and condition.

4.4 Conclusion

Gold and silver NPs were synthesized using chemical reduction methods; AuNPs by citrate reduction and AgNPs by microwave-assisted synthesis with ethanol and PVP as reducing and stabilizing agents respectively. Both gold and silver NPs have a characteristic spherical shape and good degree of monodispersion, with most of the particles with diameter of $\leq$ 10 nm.

AuNPs were stable in the dark at 4°C for up to 48 h, but storage in these conditions for two weeks resulted in decreased plasmonic absorption and a considerable red-shift. TEM image and size distribution graphs indicated that the decreased absorption and the red-shift are caused by aggregation of particles. The aggregation, in turn, is reported to be caused by the delocalization of the conduction electrons on the particles' surfaces, causing their aggregation and resulting in

larger particles (Fatin *et al.*, 2013). On the other hand, AgNPs were stable in the dark at 23°C with consistency in morphology and size distributions after a fortnight.

Synthesized AuNPs were therefore stored in the dark at 4°C and used for the enzyme interaction experiments within 48 h of synthesis. AgNPs, in contrast, are stored in the dark at 23°C and used within two week of the particles' synthesis, for the downstream experiments.

Chapter five

Interaction of gold and silver NPs with HSCOMT

5.1 Introduction

Proteins bind to the surfaces of nanomaterials when mixed in a physiological environment (Aggarwal *et al.,* 2009). The binding of nanoparticles influences the structures, folding and biological activities of the protein (Fei and Perrett, 2009; Saptarshi *et al.,* 2013).

Interactions of nanomaterials with enzymes have been reported to disturb the allosteric mechanisms of some allosteric enzymes (Jiang *et al.,* 2010; Netto *et al.,* 2016), and sometimes induces allostery to non-allosteric enzymes (El-Sayed *et al.,* 2016). This is possibly caused by the perturbation of the protein structure, affecting the functional folding, and thus modification of the activity and mechanisms of the enzymes (Saptarshi *et al.,* 2013). Gold and silver nanoparticles (NPs) have been reported to influence the biological activities of several enzymes *in vitro* (Adeyemi and Whiteley, 2013; Adeyemi and Whiteley, 2014; Yao *et al.,* 2015).

Like most *O*-methyltransferases, HSCOMT is a monomeric protein (Martin and McMillan, 2002; Rutherford *et al.,* 2008b). Oligomers of HSCOMT are caused by intermolecular disulfide bonds between cysteine amino acid residues in the protein molecule (Cotton *et al.,* 2004). The intermolecular disulfide bonds, via cysteine residues, serve as redox-sensing switches for the regulation of protein functions (Nagahara, 2011). Domain swapping is a mechanism for the formation of homo dimeric or higher oligomeric proteins from their monomers, which involves the exchange of folding motifs between two copies of the same polypeptide (Bennett *et al.,* 1995). This phenomenon not only plays a role in monomeric to oligomeric transition, but also provides a mechanism to achieve modulations, including allostery, in protein biological

functions (Bennett *et al.,* 1995; Park *et al.,* 2010; Zhang *et al.,* 2016). Domain swapping with characteristic energy requirements causes significant movements at different positions of human and rat SCOMT, resulting in both single and double domain-swapped HSCOMT oligomers (Ehler *et al.,* 2014; Law *et al.,* 2016). Three hinge regions of HSCOMT, α2/α3, ß5/ß9 and ß6/ß7, which are involved in the domain swaps, also change their conformations during substrate binding (Figure 5.1) (Ehler *et al.,* 2014), indicating their significance in both catalysis and structural domain swap.

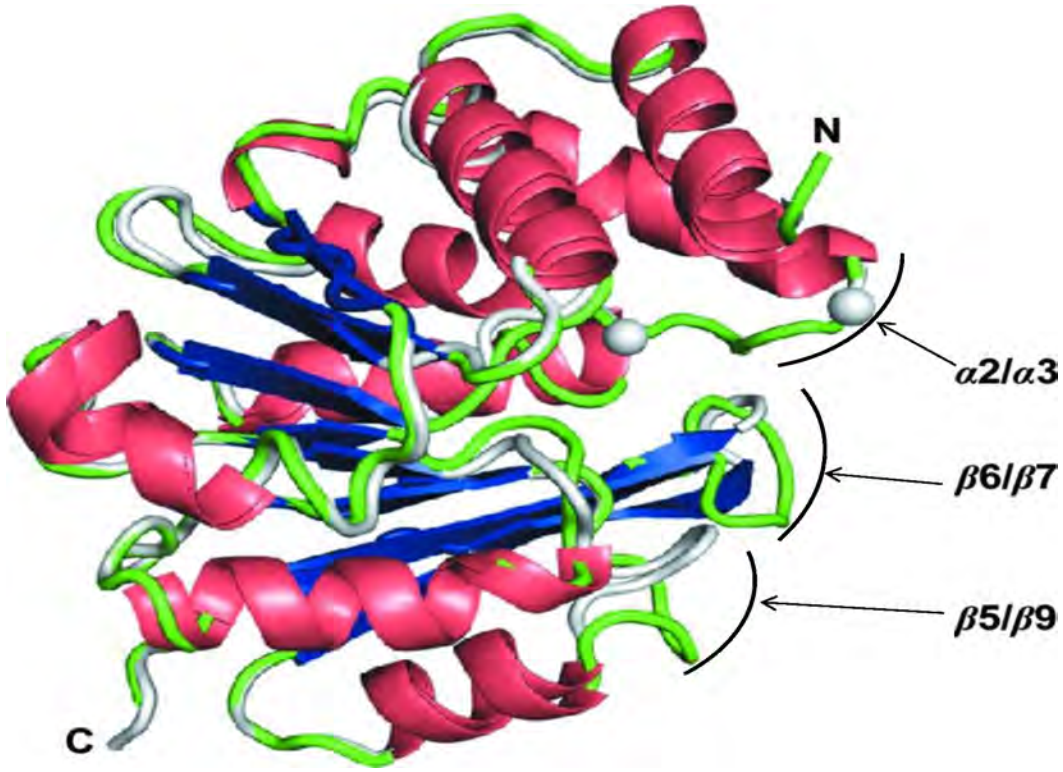

Figure 5.1: Human (grey) and mouse (green) apo COMT crystal structures. The ribbon diagrams show a central seven-stranded ß-sheet flanked by α-helices. The three loop regions that are important for catalysis and for domain swapping are labelled α2/α3, ß5/ß9 and ß6/ß7 (adapted from Ehler *et al.,* 2014).

The catalytic *O*-methylation of catechols by COMT is regioselective (Masri*et al.,* 1964), favouring *meta O*-methylated products *in vivo* (Axelrod, 1966) and *para O*-methylated products *in vitro* (Kiss and Soares-da-Silva, 2014). Investigations on the catalytic properties of the

monomeric and dimeric HSCOMT have indicated that the enzyme monomer favours *para O*-methylation, while the dimer prefers *meta O*-methylation (Law *et al.*, 2016). It is plausible, therefore, to assume that the physiologically relevant form of COMT *in vivo* is the dimer.

The aim of this section is to investigate the effect of gold and silver NPs on the catalytic methylation of esculetin by HSCOMT and to evaluate the effect(s) of the particles on kinetic mechanisms/parameters of the methylation.

5.2 Materials and methods

5.2.1 Materials

All chemicals and reagents used in this section are listed in appendix I.

5.2.2 Methods

5.2.2.1 Influence of gold and/or silver NPs on HSCOMT activity

Time dependence has been reported for the adsorption of proteins to nanomaterials surfaces, with optimum adsorption time varying from ~5 to 60 min, depending on the protein's affinity for the material's surface, and the interaction medium (Rahman, *et al.*, 2013). To allow adsorption of HSCOMT on the NPs surfaces, the enzyme was incubated with a range of 0-100 µM of both gold and silver NPs for 1 h, at the COMT activity reaction conditions outlined in sections 2.2.2.4 and 3.2.2.11 at the HSCOMT pH and temperature optima of 7.0 and 30°C, respectively.

For these experiments, 5 µg/ml (~0.2 µM) HSCOMT was used for all the reactions. The NPs working solutions were four-fold concentrations of the various test concentrations prepared by diluting the stock NPs solutions with the enzyme activity buffer (100 mM phosphate, 5 mM $MgCl_2$, 20 mM *L*-cysteine, pH 7.0). Four-fold concentrations each of the final concentrations of

the HSCOMT (5 µg/ml), substrate esculetin (4 µM) and co-factor *S*-(5'-adenosyl)-*L*-methionine (SAM) (60 µM) were also prepared using the reaction buffer. The substrate esculetin was dissolved in dimethyl sulfoxide (DMSO) and then diluted with the reaction buffer to a final DMSO concentration of 2% (v/v) (8% in four-fold concentration). Fifty microliters each of the four-fold concentrations of the test NPs, HSCOMT and esculetin were mixed and incubated at 30°C for 5 min, and finally, 50 µl of the four-fold concentration of SAM was added to initiate the HSCOMT catalytic reaction. These experiments were repeated with 1 h incubation. Control assays were done with all the reaction components but with no NP (50 µl reaction buffer was added in place of the NP). Also, NP control assays were performed, using trisodium citrate and tetrachloroauric acid (for AuNPs) and ethanolic PVP and silver nitrate (for AgNPs) solutions in equivalent dilutions to that of the 100 µM NPs samples, instead of the gold and silver NPs, respectively. Full negative controls of the HSCOMT activity assay protocol, lacking the HSCOMT, SAM and/or esculetin were routinely included. All the experiments were performed in triplicate.

5.2.2.2 HSCOMT kinetics in the presence of gold and/or silver NPs

For the kinetic study in the presence of NPs, appropriate NP concentration, which had a significant effect on enzyme activity yet still allowed the enzyme reaction to proceed for kinetic studies to be performed, was determined. Since gold and silver NPs at a concentration of 60 µM decrease the HSCOMT activity to 70% and 73%, respectively (section 5.3.1), this concentration of NPs was selected to investigate the effects of NPs on the enzyme's kinetics. Furthermore, to allow adsorption of the enzyme onto the particles' surfaces (Rahman, *et al.*, 2013); the assay components were incubated with the NPs at 30°C for 1 h before the addition of SAM to initiate the reaction. Control kinetic assays involved replicating the kinetic experiment (with 1 h

incubation at 30°C before addition of SAM to initiate the reaction) without the NPs. All experiments were performed in triplicate. Analysis of results and calculation of kinetic parameters were performed using the GraphPad Prism 5 software. The Hanes–Woolf plot (Hanes, 1932), having the advantage of positioning the independent variable [S], on both axes, and consequently a more accurate estimation of both K_m and V_{max} (Ritchie and Prvan, 1996), was used for linearisation of the hyperbolic Michaelis-Menten curves. After the kinetic study experiments, the HSCOMT enzyme protein was analyzed by SDS-PAGE (section 2.2.2.5). The kinetic assay with incubation of the reaction components at 30°C for 1 h before addition of SAM to initiate the reaction was repeated with concentration ranges of SAM (6 to 300 μM) and $MgCl_2$ (1 to 10 mM).

5.3 Results and discussion

5.3.1 Influence of gold and/or silver NPs on HSCOMT activity

After characterization of HSCOMT, the effects of gold and silver NPs on the catalytic activity of this enzyme were investigated according to the procedure described in section 5.2.2.1.

Figure 5.2 shows HSCOMT activity with varying concentrations of AuNPs. There was no noticeable effect on HSCOMT enzymatic activity by AuNPs (up to 100 μM) and sodium citrate/gold ions solution at a concentration equivalent to 100 μM AuNP samples, in the HSCOMT performed with 5 min incubation at 30°C before addition of SAM to initiate the reaction.

Figure 5.3 shows the effect of AuNPs on the enzymatic activity of HSCOMT for the assay performed with 1 h incubation at 30°C of the reaction mixture prior to the addition of SAM. The figure shows that AuNPs up to 20 μM have no obvious effect on the activity; 40 μM AuNPs

decreased the HSCOMT catalytic activity to 79%, as compared to the control (0 μM AuNPs), 60 μM of AuNPs decreased the activity to 70%, 80 μM to 40% and 100 μM of the AuNPs decreased the activity to 25%. The control HSCOMT assay containing equivalent concentration of trisodium citrate and tetrachloroauric acid solution in 100 μM AuNPs produced 103% of the enzyme catalytic activity (compared to 0 μM NPs assay), indicating that these solutions did not affect the HSCOMT activity, and suggesting that the decrease in HCOMT activity was due to the presence of the AuNPs.

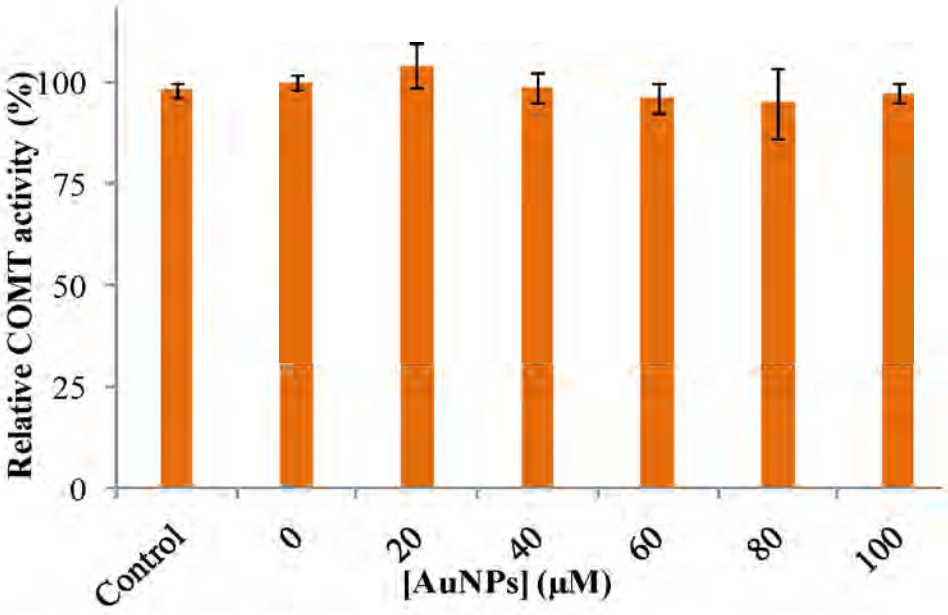

Figure 5.2: Bar graph showing relative HSCOMT activity in the absence and presence of different concentrations of AuNPs (with 5 min incubation at 30°C before addition of SAM to initiate the reaction). The control is the HSCOMT assay in the presence of the equivalent concentration of trisodium citrate and tetrachloroauric acidsolution in 100 μM AuNPs, while "0" represents the HSCOMT activity without AuNPs and was used as 100% reference standard for calculating the relative % activity. Values represent the mean (n = 3, ± SD).

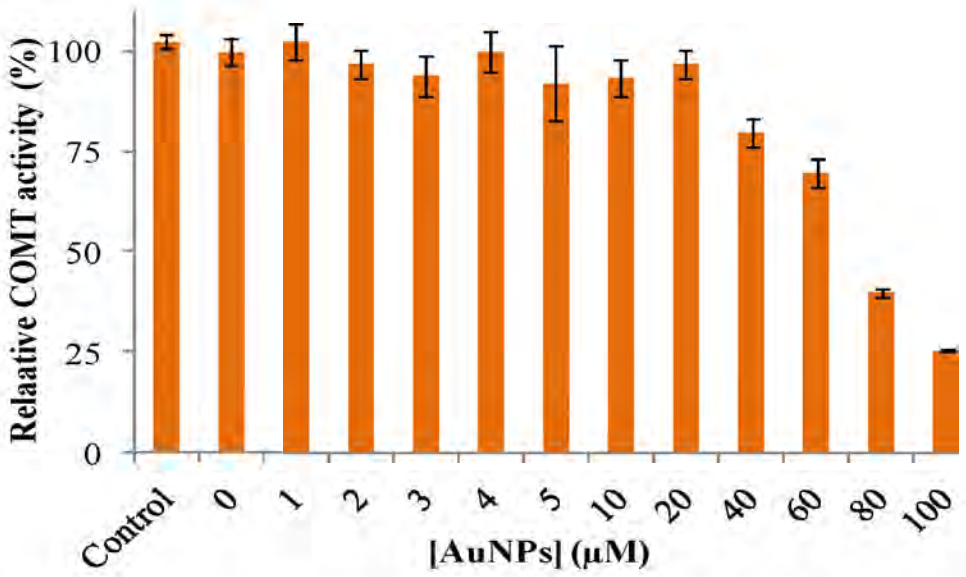

Figure 5.3: Bar graph showing relative HSCOMT activity incubated with different concentrations of AuNPs (0 to 100 µM) at 30°C for 1 h before addition of SAM to initiate the reaction. The control is the HSCOMT assay in the presence of equivalent concentration of trisodium citrate and tetrachloroauric acidsolution in 100 µM AuNPs, while "0" represents the HSCOMT activity without AuNPs and was used as 100% reference standard for calculating the relative % activity. Values represent the mean (n = 3, ± SD).

Similarly, experiments performed to determine the effects of AgNPs concentration on HSCOMT activity (without 1 h incubation) indicated no evident effect on HSCOMT enzymatic activity by AgNPs (up to 100 µM) (Figure 5.4). Ethanolic PVP and silver nitrate solution at a concentration equivalent to 100 µMAuNP samples did not affect the enzyme activity, although high ethanol concentration (50 to 1 000 mM) has been reported to increase the enzymatic activity of HSCOMT (Männistö and Kaakkola, 1999).

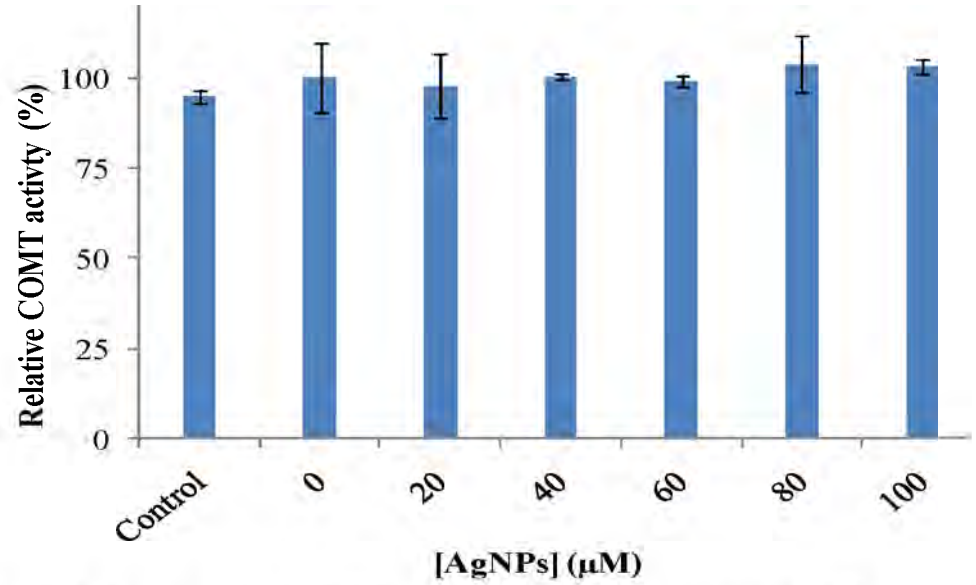

Figure 5.4: Bar graph showing relative HSCOMT activity in the absence and presence of different concentrations of AgNPs (with 5 min incubation at 30°C before addition of SAM to initiate the reaction). The control is the HSCOMT assay in the presence of equivalent concentration of ethanolic PVP andsilver nitrate solution in 100 µM AgNPs while "0" represents the HSCOMT activity without AgNPs and was used as 100% reference standard for calculating the relative % activity. Values represent the mean (n = 3, ± SD).

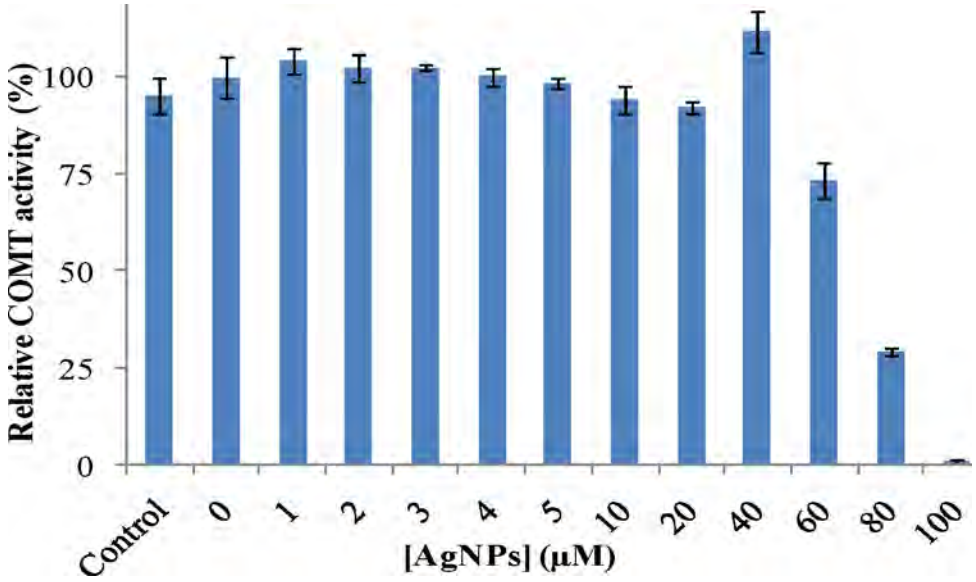

Figure 5.5: Bar graph showing relative HSCOMT activity incubated with different concentrations of AgNPs (0 to 100 µM) at 30°Cfor 1 h before addition of SAM to initiate the reaction. The control is the HSCOMT assay in the presence of equivalent concentration of ethanolic PVP and silver nitrate solutions in 100 µM AgNPs, while "0" represents the HSCOMT activity without AgNPs and was used as 100% reference standard for calculating the relative % activity. Values represent the mean (n = 3, ± SD).

Figure 5.5 shows the effect of the different concentrations of AgNPs on HSCOMT activity after 1 h incubation at 30°C of the reaction components. The figure indicates that AgNPs up to 40 μM have no considerable effect on HSCOMT activity. HSCOMT enzymatic activity decreased to 73%, 29% and 1% in the presence of 60 μM, 80 μM and 100 μM AgNPs, respectively. HSCOMT assay containing equivalent concentrations of ethanolic PVP and silver nitrate solutions in 100 μM AgNPs produced 95% of the enzyme catalytic activity (as compared to 0 μM NPs assay), signifying that these solutions had limited effect on the HSCOMT enzymatic activity at these concentrations, an indication that the decrease in HCOMT activity is because of the presence of the AgNPs.

5.3.2 HSCOMT kinetics in the presence of gold and silver NPs

Kinetic studies were performed according to the procedure described in section 5.2.2.2. Figure 5.6 shows the kinetic profile of HSCOMT in the absence (control) and presence of gold and/or silver NPs.

HSCOMT exhibited a sigmoidal kinetic curve, with Hill coefficient of 1.89±0.17, upon incubating the kinetic assay components at 30°C for 1 h before the addition of SAM to initiate the reaction (Figure 5.6), which suggests co-operativity during the catalysis. However, the enzyme exhibited hyperbolic kinetic curves when these experiments (with the 1 h incubation) were performed in the presence of 60 μM of gold and/or silver NPs (Figure 5.6). We may recall that the enzyme exhibited a hyperbolic kinetic curve during kinetic experiments with the incubation of 5 min at 30°C, before the addition of SAM (section 3.3.4.4). HSCOMT has been reported to exhibit a hyperbolic or a sigmoidal kinetic curve depending on the catecholic substrate (Dawling *et al.,* 2001) and reaction conditions (Ball *et al.,* 1972).

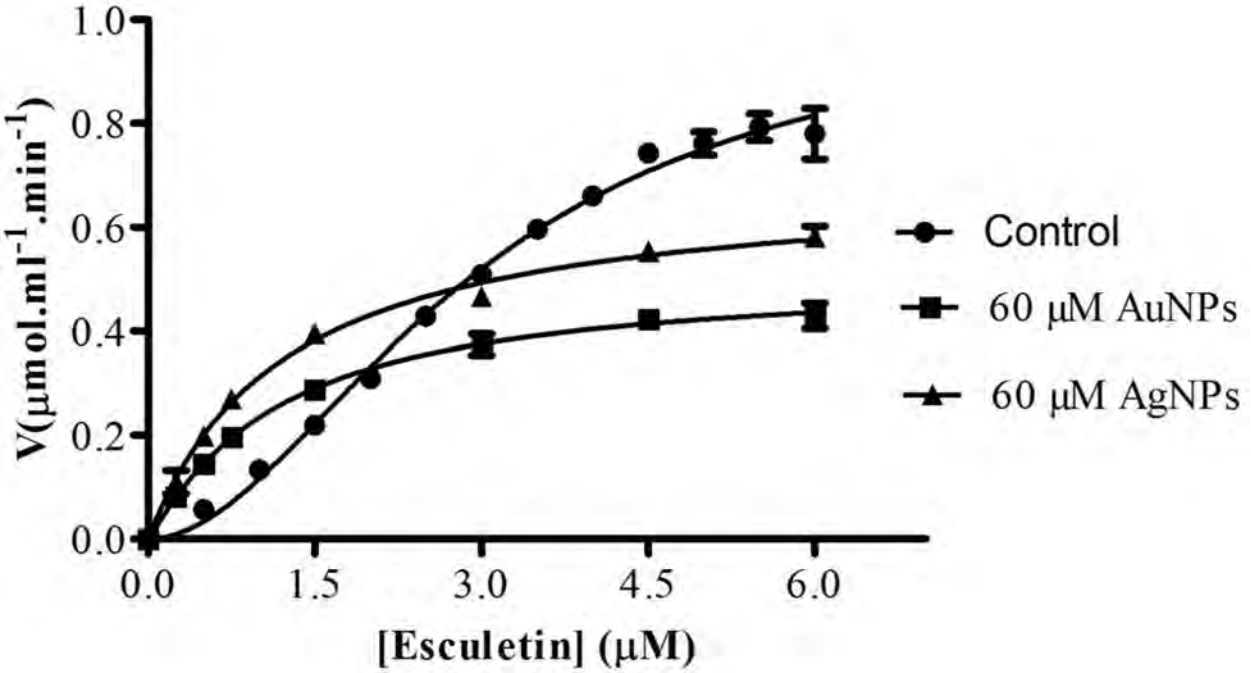

Figure 5.6: Kinetic plots of HSCOMT in the absence of NPs (control (●)) and presence of 60 μM each of gold (■) and silver NPs (▲). Kinetic assays were performed by incubating all the reaction components at 30°C for 1 h before addition of SAM to initiate the reaction. The results were analysed using GraphPad Prism 5 software. The plot for the control kinetic was best fitted for sigmoidal while those that performed in the presence of 60 μM of gold and silver NP were best fitted for hyperbolic curves. Values represent the mean (n = 3, ± SD).

Linear plots (Hanes-Woolf) of the HSCOMT hyperbolic kinetics in the presence of 60 μM gold and/or silver NPs are presented in figure 5.7. Lines of best fit were drawn and the line equations were used to calculate K_m and V_{max}. The kinetic parameters of sigmoidal, hyperbolic and linear plots are presented in table 5.1.

We may also recall that the K_m, V_{max}, K_{cat}, and K_{cat}/K_m of HSCOMT kinetic study with 5 min incubation before the addition of SAM to initiate the reaction were 1.778±0.246 μM, 0.412±0.022 $\mu mol.ml^{-1}.min^{-1}$, 2.082±0.111 $min^{-1}$and $1.165M^{-1}.min^{-1}$, respectively (Table 3.2, section 3.3.4.4).

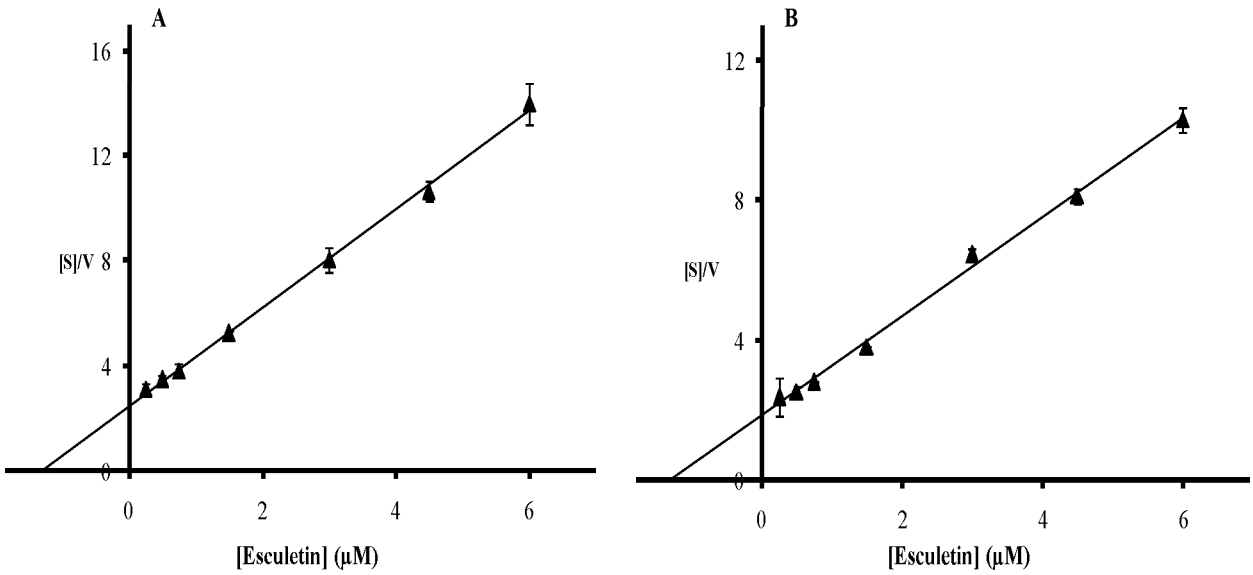

Figure 5.7: The Hanes-Woolf linear plots of the Michaelis-Menten curves for the kinetic studies of HSCOMT (with 1 h incubation) in the presence of 60 µM AuNPs (A) with a linear equation of y = 1.881x + 2.456; R^2 = 0.998 and 60 µM AgNPs (B) with a linear equation of y = 1.417x + 1.848; R^2 = 0.996. Values represent the mean (n = 3, ± SD).

Table 5.1: Kinetic parameters of HSCOMT incubated at 30°C for 1 h, in the absence and presence of AuNPs and/or AgNPs.

Reaction	Plot	Variables				
		$K_{0.5}$ or K_m (µM) [#]	V_{max} (µmol.ml^{-1}.min^{-1})	K_{cat} (min^{-1})	K_{cat}/K_m (M^{-1}. min^{-1})	Hill coefficient
Control (no NPs)	Sigmoidal (non-linear)	2.973±0.261	1.031	5.211±0.364	1.753	1.89±0.17
60 µM AuNPs	Hyperbolic (non-linear)	1.300±0.075	0.534±0.011	2.699±0.056	2.080	H*
	Hanes-Woolf (linear)	1.305	0.532	2.687	2.058	H*
60 µM AgNPs	Hyperbolic (non-linear)	1.227±0.070	0.700±0.013	3.538±0.066	2.883	H*
	Hanes-Woolf (linear)	1.61116	0.872	4.407	2.74	H*

[#] $K_{0.5}$ for the sigmoidal kinetic and K_m for the hyperbolic kinetics.

[*] Data best fit for hyperbolic kinetic.

From Table 5.1, it can be seen that the extension of the incubation time from 5 min to 1 h caused an increase in the K_m ($K_{0.5}$) from 1.778±0.246 to 2.973 ±0.261µM and maximum velocity (V_{max})

from 0.412±0.22 to 1.031±0.072 μmol.ml^{-1}.min^{-1}, respectively. These results suggest that the incubation caused not only a change in the kinetic model, but also a decrease in the enzyme's affinity for the substrate esculetin and an increase in the enzyme catalytic activity, respectively. The HSCOMT turnover number (K_{cat}) and the measure of catalytic efficiency (K_{cat}/K_m) were also increased from 2.082±0.111 to 5.211±0.364 min^{-1} and from 1.165 to 1.753 M^{-1}.min^{-1}, respectively, due to the 1 h incubation.

The kinetic parameters of HSCOMT performed with co-incubation of the enzyme with gold and/or silver NPs are presented in table 5.1. In comparison with the control (the sigmoidal plot), co-incubation of HSCOMT with 60 μM AuNPs at 30°C for 1 h caused a decrease in K_m (increase in HSCOMT affinity for esculetin), from 2.973±0.261 to 1.300±0.075 μM, a decrease in maximum velocity (V_{max}) from 1.031±0.072 to 0.534±0.011μmol.ml^{-1}.min^{-1}, a decrease in the enzyme turnover (K_{cat}) from 5.211±0.364 to 2.699±0.056 min^{-1} and an increase in catalytic efficiency (K_{cat}/K_m) from 1.753 to 2.080 M^{-1}.min^{-1}. Similarly, co-incubation of HSCOMT with 60 μM AgNPs at 30°C for 1 h caused decrease in K_m, from 2.973±0.261 to 1.227±0.070 μM, a decrease in V_{max} from 1.031±0.072 to 0.700±0.013 μmol.ml^{-1}.min^{-1}, a decrease in K_{cat} from 5.211±0.364 to 3.538±0.066 min^{-1} and an increase in K_{cat}/K_m from 1.753to 2.883M^{-1}. min^{-1}. These kinetic parameters from the assays performed in the presence 60 μM of gold and/or silver NPs (with 1 h incubation) are comparable to those from the kinetic assay with 5 min incubation in the absence of the NPs with 5 min incubation (Table 3.2).

These intriguing observations prompted the SDS-PAGE analyses of the HSCOMT after the kinetic studies. Figure 5.8 shows the gel images of the analyses.

It is apparent from Figure 5.8 that, as expected of HSCOMT, it exists as a monomer (at 5 µg/ml concentration) after the kinetic assay that involves 5 min incubation (Figure 5.8A, lane 2). Extending the incubation period to 1 h caused the formation of a band equivalent to twice the size of HSCOMT, suggesting that during the extended incubation time dimerization of the enzyme protein had occurred (Figure 5.8A, lane 3).

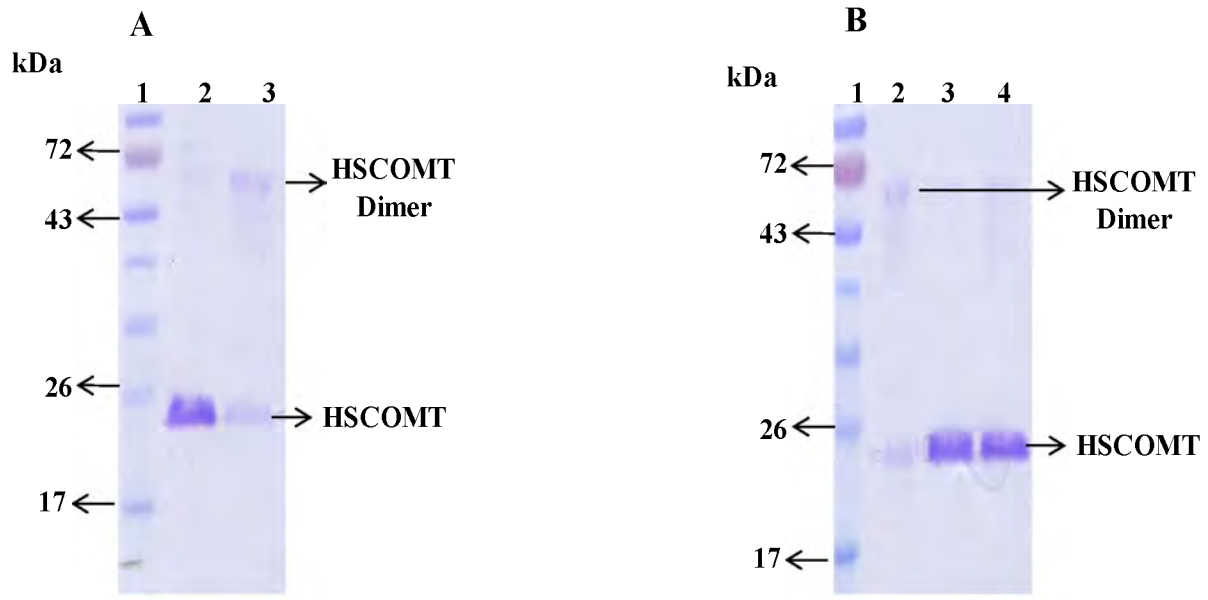

Figure 5.8: Gel images of HSCOMT analyzed by SDS-PAGE after the kinetic studies. For image (A); lane 1 is the protein ladder, lane 2 is the HSCOMT after the kinetic assay with 5 min incubation time and lane 3 shows the HSCOMT after the kinetic assay with 1 h incubation at 30°C before addition of SAM. Image (B) show the protein ladder (lane 1), HSCOMT after the kinetic assay with 1 h incubation at 30°C (without NPs) (lane 2), HSCOMT after the kinetic assay in the presence of 60 µM AuNPs with 1 h incubation at 30°C (lane 3) and HSCOMT after the kinetic assay in the presence of 60 µM AgNPs with 1 h incubation at 30°C (lane 4).

The change in kinetic pattern, the variations in the kinetic parameters and the dimerization of the enzyme protein signify that the enzyme may exist in two active conformations; monomer and dimer, with different reactivity properties. It is also possible that the incubation of HSCOMT at 30°C for up to 1 h favours the dimer conformation, with the latter having higher turnover number and catalytic efficiency but lower affinity for the substrate, esculetin, than the former. The phenomenon of the enzyme's existence in monomer and homo oligomer conformations, with

each having different reactivity and kinetic parameters towards the same substrate, has been reported to occur in some enzymes (Jaffe, 2010; Jaffe and Lawrence, 2012), which include phosphoenolpyruvate carboxylase from *Crassula* (Wu and Wedding, 1985), *D*-amino acid oxidase (Shiga and Shiga, 1971), ribonuclease A (Park and Raines, 2000), citrate synthase from *Escherichia coli* (Tong and Duckworth, 1975) and HIV-1 Integrase (Faure *et al.*, 2005; Guiot *et al.*, 2006).

Co-incubation (at 30°C for 1 h) of the HSCOMT kinetic assay mixture with 60 μM gold and/or silver NPs changed the sigmoidal kinetic (observed in the 1 h incubation) to hyperbolic (Figure 5.6) and prevented the incubation-favoured dimerization (Figure 5.8). Similarly, the co-incubation with NP for 1 h yielded HSCOMT kinetic parameters comparable to those with 5 min incubation without the NP (Tables 5.1 and 3.2). Gold and/or silver NPs could therefore effect the decrease in the HSCOMT catalytic methylation of esculetin by preventing the dimerization of the enzyme.

To assess whether the increased catalytic activity exhibited by HSCOMT is caused exclusively by the monomer-dimer structural/activity variation and kinetic hysteresis, or whether it is linked to co-operativity during the catalysis, the kinetic assay procedure, with 1 h incubation at 30°C prior to the addition of SAM to initiate the reaction, was repeated using a range of SAM (6 to 300 μM) and $MgCl_2$ (1 to 10 mM) concentrations. Figure 5.9 shows the kinetic plots of HSCOMT with different concentrations of SAM, and Figure 5.10 shows the plots with different concentrations of $MgCl_2$. Table 5.2 shows the index values of the HSCOMT affinity for the substrate (esculetin) ($K_{0.5}$), and also the index values of the HSCOMT catalytic co-operativity (Hill coefficient) at the aforementioned concentrations of SAM and $MgCl_2$.

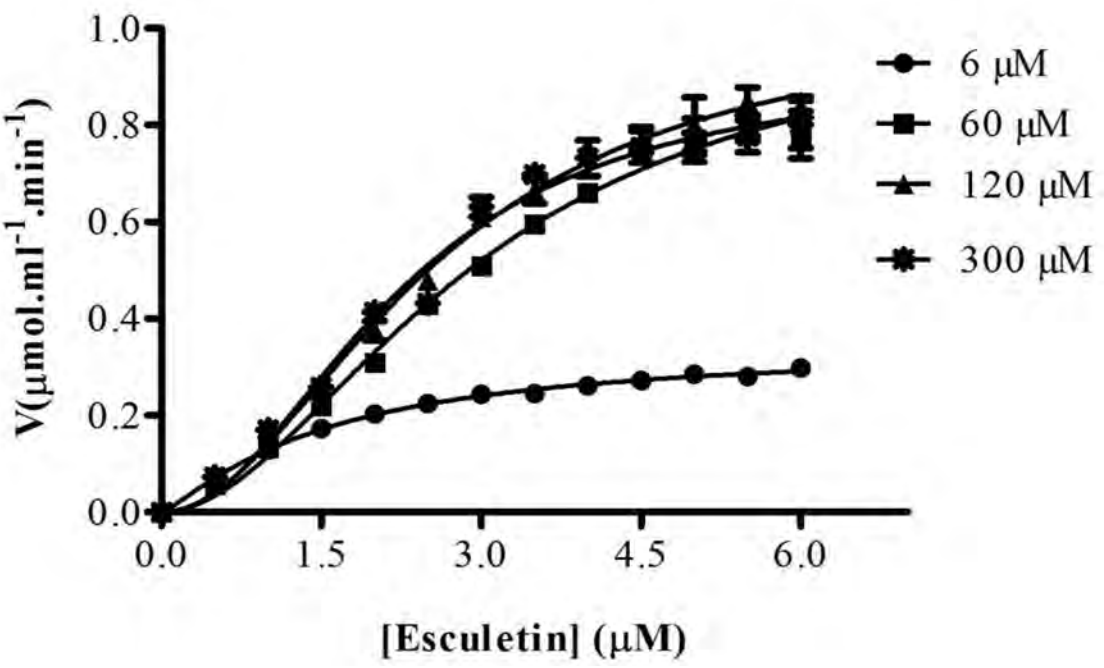

Figure 5.9: Plots of HSCOMT kinetic graphs in the absence of NPs with varying concentrations of SAM (indicated by the legends). Kinetic assays were performed by incubating all the reaction components at 30°C for 1 h before addition of SAM to initiate the reaction. The results were analyzed using GraphPad Prism 5 software. Values represent the mean (n = 3, ± SD).

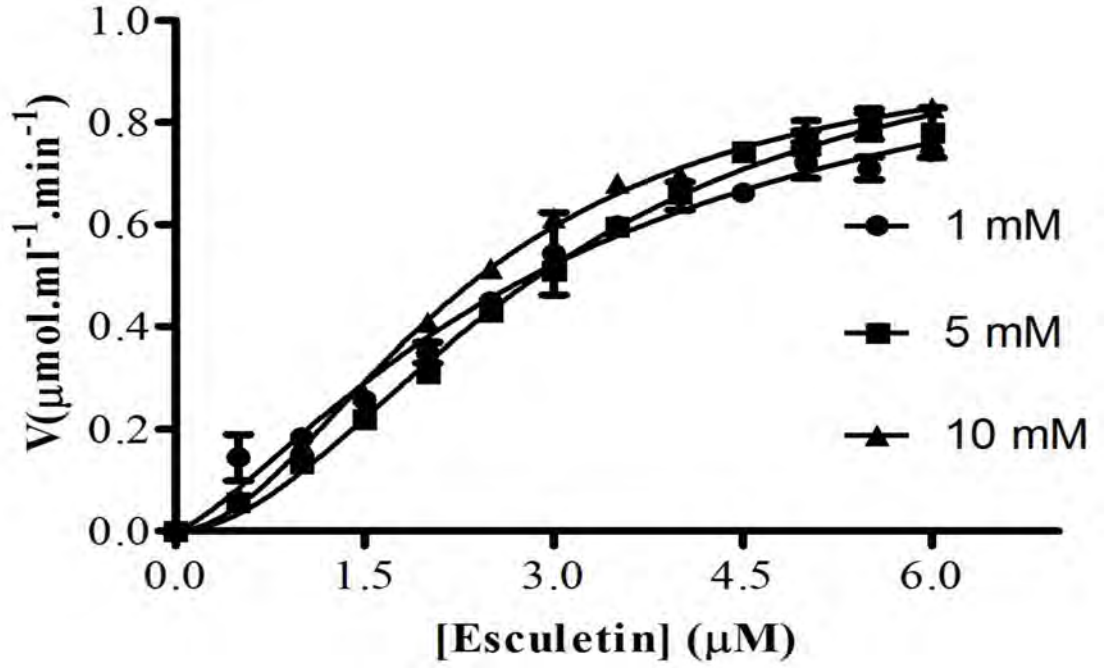

Figure 5.10: Plots of HSCOMT kinetic graphs in the absence of NPs and with varying concentrations of $MgCl_2$ (indicated by the legends). Kinetic assays were performed by incubating all the reaction components at 30°C for 1 h before addition of SAM to initiate the reaction. The results were analyzed using GraphPad Prism 5 software. Values represent the mean (n = 3, ± SD).

Table 5.2: The HSCOMT co-operativity index values (Hill coefficient) and affinity index values ($K_{0.5}$) of kinetic assays performed at different concentrations of SAM and $MgCl_2$. The kinetic assays were performed by incubating the assay components at 30°C for 1 h, before addition of SAM to initiate the reaction.

	Variables		
	Concentration	**Hill coefficient**	**$K_{0.5}$(μM)**
SAM	6 μM	1.11±0.08	1.532±0.109
	60 μM	1.89±0.17	2.973±0.261
	90 μM	1.95±0.16	2.570±0.176
	300 μM	2.05±0.29	2.256±0.176
$MgCl_2$	1 mM	1.34±0.21	3.178±0.816
	5 mM	1.89±0.17	2.973±0.261
	10 mM	1.89±0.11	2.34±0.111

In Figure 5.9, the plots of the HSCOMT kinetics performed with 60, 120 and 300 μM of SAM exhibited sigmoidal curves, whereas the kinetics performed with 6 μM of the co-substrate exhibited a hyperbolic curve. From Table 5.2, the analyses (GraphPad Prism 5 software) of the HSCOMT kinetic data, preformed with 60, 120 and 300 μM of SAM revealed a Hill coefficient (the measure of co-operativity) of greater than 1 (h>1), while for the kinetic assay with 6 μM SAM, the Hill coefficient is equivalent to 1 (h≈1) (Table 5.2). The generation of h>1 in the kinetic experiments with ≥60 μM SAM concentrations indicates co-operativity during the catalysis at these concentrations. The observed hyperbolic curve and Hill coefficient equivalent to 1 in the kinetic experiment with SAM concentration of 6 μM suggests that there is little or no modulatory effect of SAM on HSCOMT activity at this concentration.

In Table 5.2, the Hill coefficient and $K_{0.5}$ increased with increasing SAM concentration, indicating a decrease in the enzyme's affinity for the substrate, and an increase in co-operativity with increase in SAM concentration, respectively. The decrease in affinity with the increase in

SAM concentration indicates co-operative modulation of HSCOMT activity by SAM (Liu *et al.,* 2008). The Hill coefficient value does not increase with increase in $MgCl_2$ concentration from 1 to 10 mM, suggesting that $MgCl_2$ has no co-operative modulatory effect on HSCOMT. Attempts to increase the $MgCl_2$ concentration beyond 10 mM caused precipitation of the reaction mixture.

Feedback inhibition, an allosteric cooperative control mechanism in which accumulated end products of an enzymatic catalysis inhibit the catalytic activity of the enzyme (Cárdenas, 2015), has been reported in ratSCOMT (Zhu *et al.,* 1994). S-Adenosyl-*L*-homocysteine, a product of HSCOMT enzymatic activity, demonstrates a strong competitive feedback inhibition mechanism with respect SAM, and a mixed inhibition with respect to the catechol substrate (Zhu *et al.,* 1994). HSCOMT showed allostery for methylation of two catechol estrogens, 4-hydroxyestrone and 4-hydroxyestradiol, out of eighteen catechol estrogens reported by Dawling *et al.,* (2001), while Ball *et al.,* (1972) reported this enzyme to exhibit allostery under certain assay conditions, indicating that allostery in HSCOMT has preferences in catecholic substrate and assay conditions.

Although no direct evidence in our research, occurrence of domain swapping in HSCOMT has been reported by Ehler *et al.,* (2014) and Law *et al.,* (2016) with the subsequent formation of different homo-oligomers. In our study, the enzyme exists in different functional conformations that differ in reactivity toward the same substrate. These observations suggest that the enzyme is possibly a morpheein protein. Morpheein proteins interconvert between monomeric and homo-oligomeric forms under physiological conditions and can exist as equilibria of monomer and oligomers (Jaffe, 2005). Domain swapping and variations in reactivity and kinetic parameters are the common features of these proteins (Lawrence and Jaffe, 2008; Gronenborn, 2009; Liu and Eisenberg, 2002; Jaffe, 2016). The reported occurrence of domain swapping and the existence of

HSCOMT as a dimer and homo-oligomer, with different activity and kinetic parameters, are the characteristic features of morpheein protein.

5.4 Conclusion

The activity assay of HSCOMT in the presence of gold and silver NPs (up to 100 μM) showed no apparent effect on the enzyme's catalytic methylation of esculetin with 5 min incubation at 30°C. Upon extending the incubation time to 1 h, both gold and/or silver NPs caused a concentration dependent decrease in HSCOMT activity. The extension of the incubation time caused the deviation of the enzyme's kinetic curve from hyperbolic (chapter three) to sigmoidal, signifying co-operativity in the catalytic mechanism of the 1 h incubated enzyme. The extension of the incubation time also caused an increase in HSCOMT activity, turnover number and a decrease in the enzyme affinity towards the substrate, esculetin. Co-incubation of the reaction mixture with 60 μM of gold and/or silver NPs, during the kinetic assays which involved 1 h incubation at 30°C, caused reversal of the sigmoidal kinetic plot to hyperbolic. The co-incubation of the reaction mixture with 60 μM of gold and/or silver NPs also caused reversal of the kinetic parameters to those comparable with the parameters obtained with 5 min incubation; that is to say, a decrease in maximum velocity (V_{max}) and increase in the enzyme affinity towards esculetin (decrease in K_m).

These observations prompted the SDS-PAGE analyses of the HSCOMT after the kinetic assays. The SDS-PAGE analysis of HSCOMT after kinetic assays at 1 h incubation at 30°C revealed the formation of a HSCOMT dimer. SDS-PAGE analyses of the HSCOMT used for the kinetic study in the presence of the NPs (with the 1 h incubation) showed the protein as monomer, suggesting the NPs may prevent the dimerization of the enzyme. These observations are indicative that,

upon 1 h incubation at 30°C, HSCOMT exists in monomer and dimer conformations that differ in kinetic properties. Further kinetic assays with varying concentrations of SAM indicated that the dimer form of HSCOMT exhibited co-operativity with SAM exerting a modulatory effect on the enzyme.

In conclusion, extension of the incubation time at 30°C from 5 min to 1 h allowed formation of a HSCOMT dimer at lower concentration than the dissociation constant of the dimer. Unlike the monomer HSCOMT, which had a hyperbolic kinetic plot, the dimer enzyme exhibited a sigmoidal kinetic curve, signifying co-operativity during the catalysis. Again, the dimer and monomer showed variance in their kinetic parameters. The presence of 60 μM gold and/or silver NPs during the 1 h incubation not only impeded the dimerization, but reversed the sigmoidal kinetic to hyperbolic, implying that the NPs might affect the enzyme activity by hindering the formation of the dimer. HSCOMT kinetic assays (with 1 h incubation at 30°C) with varying concentrations of SAM indicated the latter to exert a modulatory effect on the enzyme.

Chapter six

Interaction of gold and silver NPs with HSCOMT: towards understanding the mechanism

6.1 Introduction

The change in enzymatic activity upon binding of the enzyme protein to the surfaces of nanoparticles (NPs) is an indicator of conformational change or binding close to the active site of an enzyme (Yang *et al.,* 2013). Investigation of NPs–enzyme interactions is therefore important for the evaluation of both the particles' biocompatibility and nano-safety. Analytical methods and strategies are necessary for understanding the possible mechanisms of the interaction. Even though there are no "gold standard" techniques to determine, with precision, the mechanism of NPs–protein interactions (Docter *et al.,* 2015; Šutković and Jašarević, 2016), there are methods to examine some mechanism-related information such as corona formation, effect on the protein's structural conformation, binding positions, binding constant and computational simulation approaches to complement the laboratory experiments. Various approaches have been employed for the investigation of the NPs-protein interactions (Li *et al.,* 2010; Mariam *et al.,* 2011; Saptarshi *et al.,* 2013; Pramanik *et al.,* 2013).

6.1.1 Absorbance spectroscopy

The binding of protein onto NP surfaces causes changes in the plasmonic spectra of the NPs, and these changes are used for evaluation of the binding (Delfino and Cannistraro, 2009; Li *et al.,* 2010; Wanga and Ni, 2014). The spectral shift and broadening of the plasmonic absorption of the NP–protein corona depend on the particles' size, local dielectric environments, aggregations as well as the concentration of the protein (Kathiravan *et al.,* 2009; Ma *et al.,* 2015). For instance, red shift and widening of the peak in the plasmonic absorption spectra of AuNPs-protein

(Delfino and Cannistraro, 2009) and AgNPs-protein (Wanga and Ni, 2014) in solution have been reported to depend on the concentration of the protein bound on the particles' surface. Although plasmonic absorption, using UV-vis spectroscopy, can be used to analyze NP–protein bindings, the absorption spectra may show different characters for different NPs (Li *et al.*, 2010). The method also does not usually reveal structural effects on the protein. It is therefore essential to use other analytic methods in conjunction with absorbance spectroscopy.

6.1.2 Spectrofluorimetric analyses

Proteins are polymers of amino acids and contain fluorophore amino acid residues including tryptophan, (Trp) tyrosine (Tyr) and phenylalanine (Phe) (Lakowicz, 2006). These amino acids absorb and fluoresce in the ultraviolet (UV) range (250–400 nm). The intrinsic fluorescence of proteins emanating from the fluorophore amino acid residues reveals information about the structure, folding and binding position(s) attributable to protein-ligand interactions (Munishkina and Fink, 2007). The changes in the fluorescence emission are indications of protein conformational transitions, subunit association/dissociation, denaturation or substrate/ligand binding (Lakowicz, 2006). Decrease in the intensity of the protein fluorescence emission is termed "protein fluorescence quenching" and a "quencher" refers to any ligand such as gold and silver NPs which interact with the amino acid fluorophore (e.g. Trp residues on HSCOMT) and decreases the fluorescence of the protein (Eftink and Ghiron, 1981). The Stern–Volmer equation (equation 6.1), named after Otto Stern and Max Volmer (Stern and Volmer, 1919), defines the kinetics for fluorescent proteins. The parameters determined include the Stern-Volmer quenching constant (K_{sv}), which quantifies the efficiency and sensitivity of the quenching process, and therefore provides information on the ligand's accessibility to the fluorophore. Another parameter (θ), signifies the fraction of fluorophores (e.g. Trp residues) near to or on the surface

of the enzyme and is calculated from the modified Stern–Volmer equation (equation 6.2) (Lehrer, 1971; Eftink and Ghiron, 1981; Adeyemi and Whiteley, 2014). The binding constant (K_a) and the number of binding sites (n) of ligand (such as gold and silver NPs) can be determined by the logarithmic derivative of the Stern–Volmer equation (equation 6.3) (Azimi *et al.*, 2011).

Equation 6.1 $$\frac{F_o}{F} = 1 + K_{sv}[Q]$$

Equation 6.2 $$\frac{F_o}{F_o - F} = \frac{F_o}{\Delta F} = \frac{1}{\theta K_a[Q]} + \frac{1}{\theta}$$

Equation 6.3 $$\frac{(F_o - F)}{F} = logKa + nlog[Q]$$

Where F_0 and F are, respectively, the fluorescence intensities in the absence and presence of the quencher (Q), [Q] is the concentration of the quencher (e.g. gold and silver NPs), K_{sv} is the Stern-Volmer quenching constant, ΔF is the change in fluorescence of the fluorophore (HSCOMT), θ is the number of the exposed fluorophores, n is the number of binding sites available for the binding of the quencher (Au or Ag NPs) on the purified protein (HSCOMT) and (K_a) is the association constant of the interaction. The dissociation constant (K_d), which is the reciprocal of the association constant (K_a), can also be estimated from the equations.

Two mechanisms usually define the protein fluorescence quenching process; dynamic and static mechanisms (Eftink and Ghiron, 1981; Samworth *et al.*, 1988; Lakowicz, 2006). These mechanisms are distinguishable by the Stern-Volmer quenching constant (K_{sv}) determined at different temperatures. Higher temperature results in faster diffusion and larger amount of collisional quenching and leads to the dissociation of weakly bound complexes. The quenching

constant, therefore, increases with an increase in temperature for dynamic quenching, and decreases with an increase in temperature for static quenching (Samworth *et al.,* 1988; Chen *et al.,* 2010; Lakowicz, 2006).

Fluorescence spectroscopy of a protein allows the elucidation of the thermodynamics for the protein-ligand interaction, and therefore determination of the thermodynamic parameters (Lakowicz, 2006; Padayachee and Whiteley, 2011; Padayachee and Whiteley, 2013a; Padayachee and Whiteley, 2013b; Adeyemi and Whiteley, 2014; Shing *et al.,* 2014). The equilibrium constant is dependent on the binding free energy, which is also termed the Gibbs free energy (ΔG). The thermodynamic parameters can be calculated from the Gibbs thermodynamic equation (equations 6.4) and the Van't Hoff equation (equation 6.5) (de Ruiter and Oostenbrink, 2011; Du, *et al.,* 2016).

Equation 6.4 $$\Delta G = -RT\, In K_{sv} = \Delta H - T\Delta S$$

Equation 6.5 $$In\left(\frac{K_{sv2}}{K_{sv1}}\right) = \frac{\Delta H}{R}\left(\frac{1}{T_1} - \frac{1}{T_2}\right)$$

Where ΔG is change in Gibbs free energy, R is the gas constant (8.314 $J.mol^{-1}.K^{-1}$), T is the temperature (in Kelvin), K_{sv} is the binding constant, ΔH is the enthalpy change, and ΔS is the entropy change.

6.1.3 Fourier transform infrared (FTIR) spectroscopy

The vibrational spectra of proteins contain important details of their structure (Hamm *et al.,* 1998). Fourier transform infrared (FTIR) spectroscopy measures molecular vibrations and provides information regarding the molecular structure and structural interactions (Haris, 1999). The technique is recognised as an important tool for examining the secondary structure of

proteins and peptides in water-based solution, deuterated forms and dried states (Kong and Yu, 2007). Peptide bonds, the structural repeating units of proteins, exhibit nine characteristic infrared (IR) bands termed amide A, B and I to VII (Arrondo *et al.,* 1993). The secondary structures of proteins are analyzed based on the absorption of the amide bands. The amide I band between ~1600 and 1700 cm^{-1} primarily results from the C=O stretching vibration and is directly linked to the protein backbone conformation. Amide II is associated with the N-H bending vibration and C-N stretching vibration, while amides III and IV are complex bands originating from a mixture of coordinate displacements. Amides V, VI and VII are associated with out-of-plane motions. The amide A and B bands (~3500 $cm^{-1}$and ~3100 cm^{-1}, respectively) originate from a Fermi resonance between the first overtone of amide II and the N-H stretching vibration (Jabs, 2015). Amidst the amides, amide I band is the major band of a protein's vibrational spectrum that gives the signature of the secondary structure of the protein and is frequently used to study protein conformation (Arrondo *et al.,* 1993; Li *et al.,* 2010). The amide I band consists of overlapping component bands, representing α-helices, ß-sheets, turns and random structures (Kong and Yu, 2007). The peaks with maxima at ~1650 cm^{-1} are reported to arise from α-helices, ~1690 cm^{-1} from ß-turn, and ~1630 to ~1635 cm^{-1} from ß-sheets and aggregated strands (Jackson and Mantsch, 1995; Fabian and Mäntele, 2002). The overall shape of the amide I band can therefore be used to gain insight on the perturbation of protein secondary structure upon its adsorption onto the NPs surfaces. Differences in protein secondary structures (ß-sheet, ß-turn, α-helices and random coil) result in different vibrational frequency bands and consequently affect the vibrational bands. For these reasons, FTIR spectroscopy has been used, by various researchers, to monitor the structures of NP-bound proteins (Xiao *et al.,* 2008; Podila *et al.,* 2012; Treuel *et al.,* 2014; Zhang *et al.,* 2016).

6.1.4 Computational analysis: Molecular docking

Computational analysis gauges the nature and strength of protein-ligand interaction by providing insights on the binding factors, mode and energies. The method, therefore, can connect results from different techniques that involve diverse conditions and different approaches. Molecular docking methods explore the ligand conformations adopted within the binding sites of protein for the estimation of the ligand-receptor binding free energy through the evaluation of the critical phenomena involved in the protein-ligand recognition process (Ferreira *et al.,* 2015). The approach predicts the conformation of ligand within the target binding site of protein (Meng *et al.,* 2011). Docking is achieved by the sampling conformations of the ligand, setting an AutoGrid in the target protein; the AutoGrid generates an electrostatic potential grid map, a desolvation map and ranking of the conformations using a scoring function. Sampling algorithms predict the binding mode, while the scoring function ranks the highest among all generated conformations (Meng *et al.,* 2011).

AutoGrid is used to estimate the energy of interaction between the rigid part of the receptor and a probe atom located at the grid lattice. For AutoDock simulation, the dissociation constant (K_d) is related to the free energy of binding (ΔG) according to equation 6.6 (Morris *et al.,* 2009).

Equation 6.6 $$\Delta G = -RTInK_d$$

Where R is the gas constant (8.314 J.mol^{-1}.K^{-1}), T = 298K.

Molecular docking studies have been reported to reveal the mechanisms of the interactions between nanomaterials and proteins (Chibber and Ahmad, 2016; Whiteley *et al.,* 2016).

The aim of this chapter is to employ spectroscopic techniques and molecular docking simulation to gain insight on the mechanism of interaction of HSCOMT with gold and silver NPs.

6.2 Materials and methods

6.2.1 Materials

All chemicals, reagents and equipment used in this section are outlined in appendix I.

6.2.2 Methods

6.2.2.1 Synthesis and characterization of gold and silver nanoparticle synthesis

As described in Chapter four (sections 4.2.2.1 and 4.2.2.2).

6.2.2.2 Determination of protein concentration

As described in chapter three (section 3.2.2.10).

6.2.2.3 Absorbance spectroscopy

HSCOMT of 0, 5, 10, 20, 40 and 80 µg/ml was incubated (30°C, 1 h, in the dark) with either gold or silver NPs (250 µM) in a final volume of 1 ml in 1.5 ml reaction tubes. The colour of the NPs changes, and their plasmonic absorbance spectra (between 400 to 900 nm for AuNPs and 300 to 800 nm for AgNPs), as well as that for 80 µg/ml HSCOMT, were recorded using a 96-well BioTek Synergy MX (BioTek®) microplate reader.

6.2.2.4 Spectrofluorimetric analyses

Emission spectra of HSCOMT in the presence and absence of the NPs were measured using a PowerWave microplate spectrofluorimeter (BioTek Synergy MX, BioTek®) (equipped with

Gen5 software) operated at 2.5 nm bandwidth. The excitation wavelength was set at 295 nm and the emission was recorded between 350 and 750nm, in a buffer containing 100 mM Tris, 5 mM $MgCl_2$, 200 mM NaCl, pH 7.5. Five micrograms of HSCOMT was mixed with 0, 10, 20, 30, 40, 50 and 60 µM of either gold or silver NPs, in a final reaction volume of 200 µl; and incubated for 1 h with tin foil protection from ambient light. The incubations were performed at four temperatures: 25°C (298 K) 30°C (303 K), 35°C (308K) and 40°C (313K) before recording the fluorescence in a clear-bottomed black 96-well plate (Greiner Bio-one, Frickenhausen, Germany). The experiments were conducted in triplicate and results represented the mean (± SD).

6.2.2.5 Fourier transform infrared (FTIR) spectroscopy

FTIR was employed to study the interaction between gold and silver NPs with HSCOMT. The reaction mixture, in 1.5 ml reaction tubes, contained 0.5 mg HSCOMT in 60 µM NPs, in a final volume of 1 ml. These solutions (and HSCOMT without NPs) were covered with tin foil, incubated (30°C, 1 h) then frozen at –80°C. After freezing, the tin foil was punched with small holes and samples lyophilized using a Labconco FreeZone 6Plus freeze dryer (Vacutec, Johannesburg, South Africa) at 0.01 mBar, at –70°C. The spectra of the lyophilized samples were obtained using FTIR/ATR spectrometer Spectrum100 (PerkinElmer, Shelton, CT) in the frequency range of 4 000 to 500 cm^{-1} (2 cm^{-1} resolution) with air as background. Spectra were displayed in the transmittance mode and baseline corrected using PerkinElmer Spectrum software (Version 6.0.2.0025, PerkinElmer, Shelton, CT–USA).

6.2.2.6 Computational simulation: Molecular docking

The X-ray diffraction crystal structure of HSCOMT at 1.98 Å resolution bound to S-adenosyl-*L*-methionine (SAM) and 3,5-dinitrocatechol (DNC) was obtained from the RCSB Protein Data Bank (PDB code: 3BWM) (Rutherford *et al.*, 2008b). The molecular docking procedures for both gold and silver NPs were performed by a rigid-docking approach using the LigandFit protocol on Discovery Studio Visualiser 4.0 (DSV4.0). The crystal structures of gold and silver were obtained from crystallography open database (COD) (Grazulis *et al.*, 2012). The gold crystal structure (COD ID No. 9013045) was deposited by Suh *et al.*, (1988) and silver crystal structure (COD ID No. 1509145) by Novgorodovo *et al.*, (1979).

Gold and silver atoms were not listed in the default AutoDockparameter (AD4 files) library, therefore, these parameters were respectively added and new parameter files were created where gold and silver atoms were included along with the other required parameters (radius= 5.0 Å, volume = 523.6 Å). While running the grid and energy calculations (AutoGrid4), the new parameter libraries for gold and silver were used instead of the default AutoDock parameter library. The NPs surfaces were modified by changing the coordinates in the extended PDB (PDBQT) files. The flat surfaces were constructed using MATLAB7.10.0 and NOTEPAD++. The molecules were optimized by MGLTools 1.5.4 by adding Marsilli-Gasteiger partial charges on each constituent atom (Khan *et al.*, 2014).

The HSCOMT crystal structure (3BWM) was prepared for docking using the Discovery Studio software and the co-crystallized ligands (SAM and DNC) in the crystal structure were removed. The crystallographic water molecules were eliminated from the 3D coordinate file; non-polar hydrogens (C-H) were merged leaving only polar hydrogen atoms on the protein. Gasteiger

partial charges were calculated to ensure the atoms were in conformity with AutoDock tools (ADT) atoms type requirements. Extended PDB files (PDBQT files) were generated to coordinate files containing partial atomic charges. These PDBQT files were created from PDB files using ADT. Grid box with dimension of 49.026 Å, 51.0687 Å and 51.0687 Å was constructed in the SAM pocket of 3BWM. Autogrid was used to pre-calculate the grid maps of the interaction energies of the NPs (with the protein). Docking was then performed using the Lamarckian Generic Algorism (LGA), using 100 population size. GA runs used to perform the docking was 10 and the docking procedure was completed in 5 h. The post-docking assessment was followed by extracting the lowest energy bound conformation and aligning the NPs with the 3BWM crystal structure and DSV4.0 was used to evaluate and record the docking mode.

6.3 Results and discussions

6.3.1 Absorbance spectroscopy

The colour and plasmon band of gold and silver NPs are sensitive to the interaction with protein and this criterion has been employed to monitor the interaction of NPs with proteins (Tom*et al.*, 2007; Canaveras *et al.*, 2012; Banerjee and Das, 2013).

The colour of 250 µM AuNP and the normalized plasmonic absorption spectra (400 to 900 nm) with increasing concentrations (0 to 80 µg/ml) of adsorbed HSCOMT are shown (Figures 6.1 and 6.2 respectively). From Figure 6.1, a colour change from reddish-brown to light purple is seen due to the adsorption of HSCOMT to AuNP. As the concentration of HSCOMT increases, so the light purple colour darkens, indicating a UV-Vis spectroscopic quantitative measure for this HSCOMT-AuNP interaction (Ho *et al.*, 2015).

The plasmonic peak of AuNPs exhibited HSCOMT concentration-dependent red shift and broadening (Figure 6.2), which indicates a direct conjugation of HSCOMT to AuNPs (Rahman *et al.*, 2013).

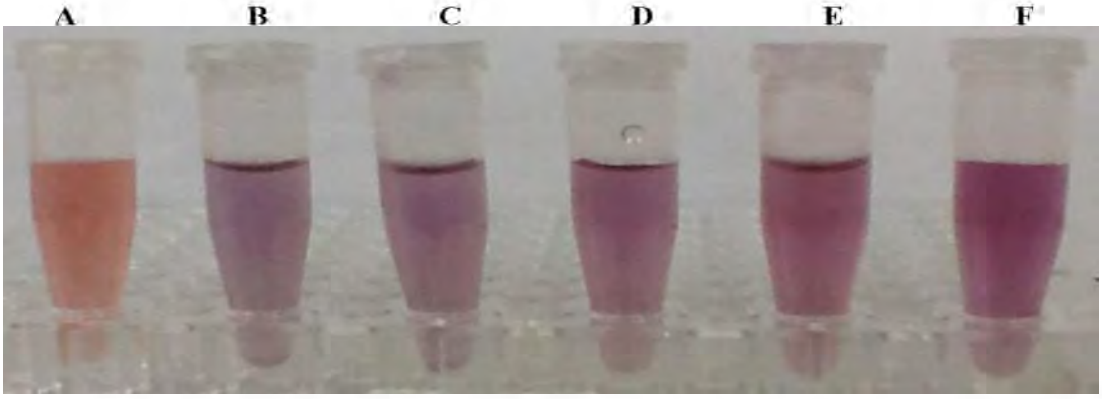

Figure 6.1: Image for 1 ml of 250 µM AuNPs incubated (in the dark at 30°C for 1 h) with HSCOMT. The concentration of the enzyme was 0 µg/ml (A), 5 µg/ml (B), 10 µg/ml (C), 20 µg/ml (D), 40 µg/ml (E) and 80 µg/ml (F).

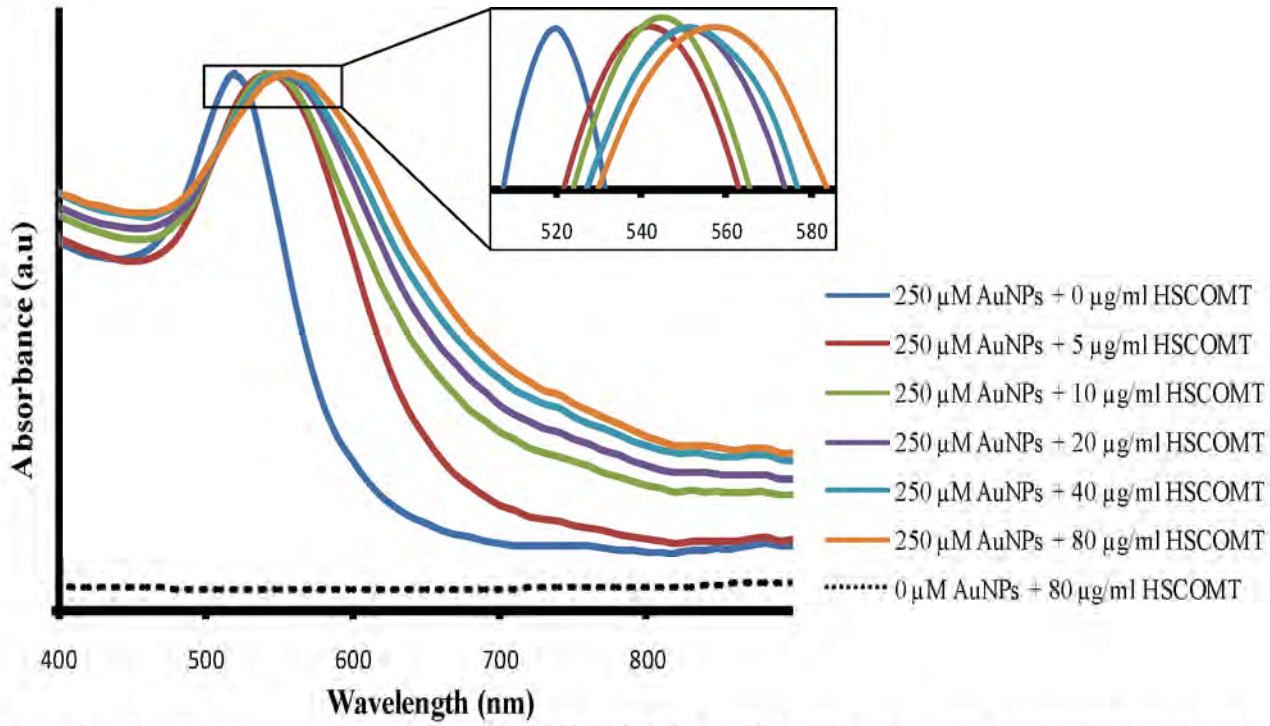

Figure 6.2: Normalized absorption spectra of 250 µM AuNPs from 400 to 900 nm, incubated in the dark for 1 h at 30°C, in the absence and presence of increasing concentrations of HSCOMT. Inset are the enlarged plasmon peaks, emphasizing the broadening and bathochromic red shift of the peaks. The increase in HSCOMT concentration correlates with red shift and increase in the peak broadening, indicating formation of AuNP-HSCOMT corona. The discontinuous curve is the absorption spectrum of 80 µg/ml HSCOMT between 400 and 900 nm.

The colour of 250 µM AgNPs and the normalized plasmonic absorption spectra (300 to 800 nm) with increasing concentrations (0 to 80 µg/ml) of adsorbed HSCOMT are shown in Figures 6.3 and 6.4, respectively. From Figure 6.3, a colour change from light to dark-yellow is seen due to the adsorption of HSCOMT to AgNP, indicating a UV-vis spectroscopic quantitative measure for this AgNPs-HSCOMT interaction (Ho *et al.,* 2015).

The plasmonic peak of AgNPs exhibited HSCOMTconcentration-dependent red shift and broadening (Figure 6.2), which indicates a direct conjugation of HSCOMT to AgNPs (Rahman, *et al.,* 2013). Furthermore this shift, and broadening of the plasmonic band of the AgNPs–protein corona, depends on the particles' size and the concentration of the adsorbed protein (Kathiravan *et al.,* 2009; Ma *et al.,* 2015) and reflects the formation of AgNP-HSCOMT corona (Tom *et al.,* 2007; Banerjee and Das, 2013).

Incubating 250 µM AgNPs with 80 µg/ml HSCOMT for 1 h at 30°C decreases the plasmonic peak of the NPs. This can be attributed to the saturation of the protein binding positions, since citrate-stabilized NPs adsorb more protein on their surfaces than polyvinylpyrrolidone-coated NPs (Treuel *et al.,* 2010).

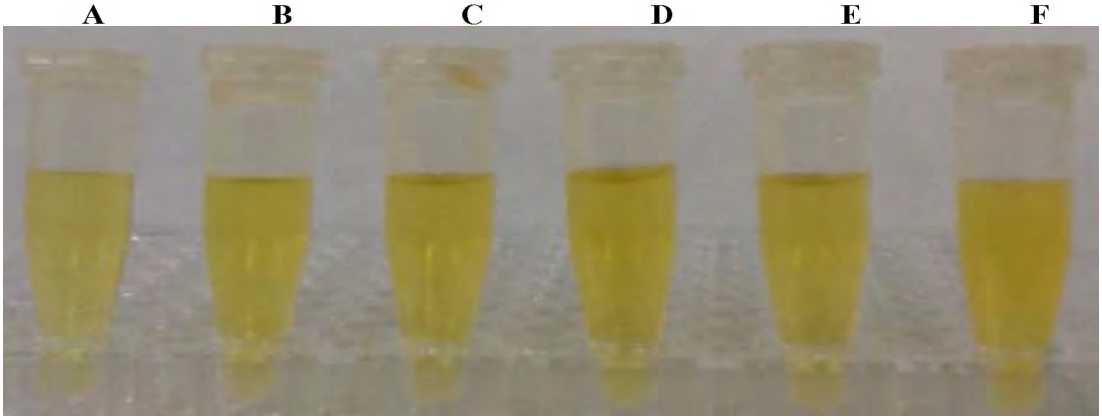

Figure 6.3: Image for 1 ml of 250 µM AgNPs incubated (in the dark at 30°C for 1 h) with HSCOMT. The concentration of the enzyme was 0 µg/ml (A), 5 µg/ml (B), 10 µg/ml (C), 20 µg/ml (D), 40 µg/ml (E) and 80 µg/ml (F).

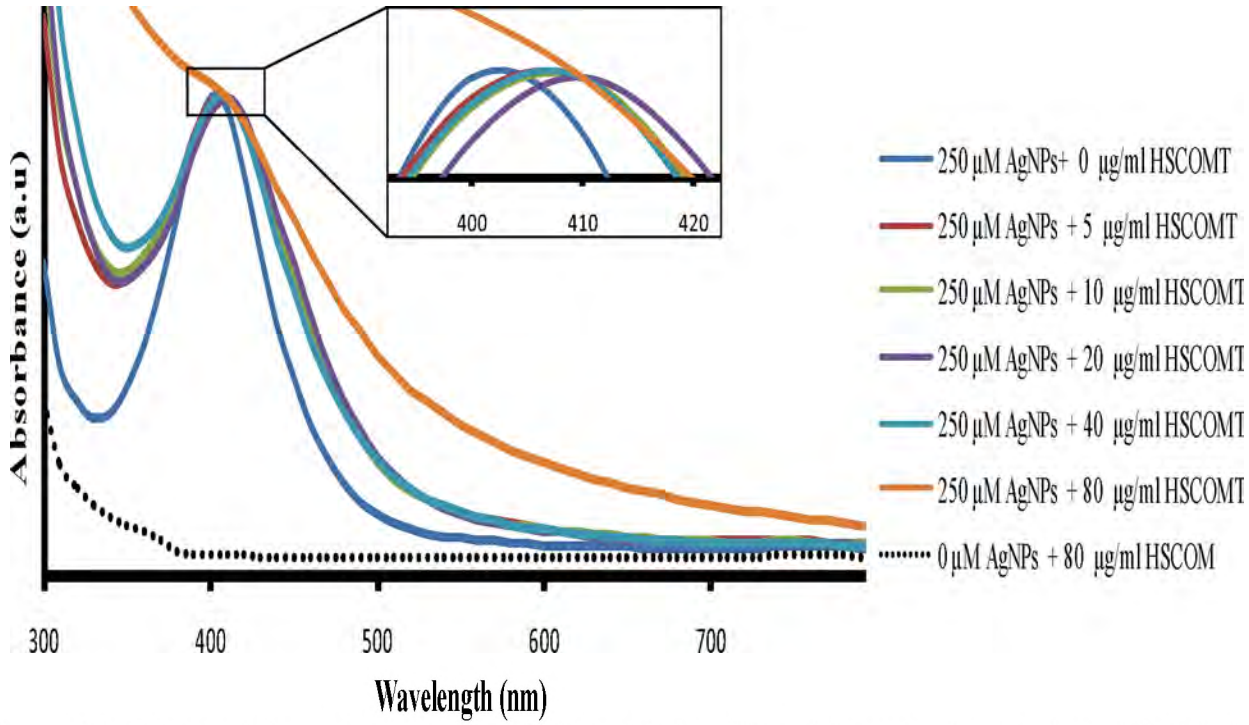

Figure 6.4: Normalized absorption spectra of 250 µM AgNPs from 300 to 800 nm, incubated in the dark for 1 h at 30°C, in the absence and presence of increasing concentrations of HSCOMT. Inset are the enlarged plasmon peaks, emphasizing the broadening and bathochromic red shift of the peaks. The increase in HSCOMT concentration correlates with red shift and increase in the peak broadening, indicating formation of AgNP-HSCOMT corona. The discontinuous curve is the absorption spectrum of 80 µg/ml HSCOMT at 300 to 800 nm.

For both gold and silver NPs, the HSCOMT concentration-dependent colour change, plasmonic peak shift and broadening are indicative of the adsorption of the enzyme onto the particles' surface and resultant formation of the NP-HSCOMT corona.

6.3.2 Spectrofluorimetric analyses

The quenching of HSCOMT fluorescence by gold and silver NPs was analyzed by Stern-Volmer plot and thermodynamic parameters of the quenching were analyzed by Van't Hoff plot.

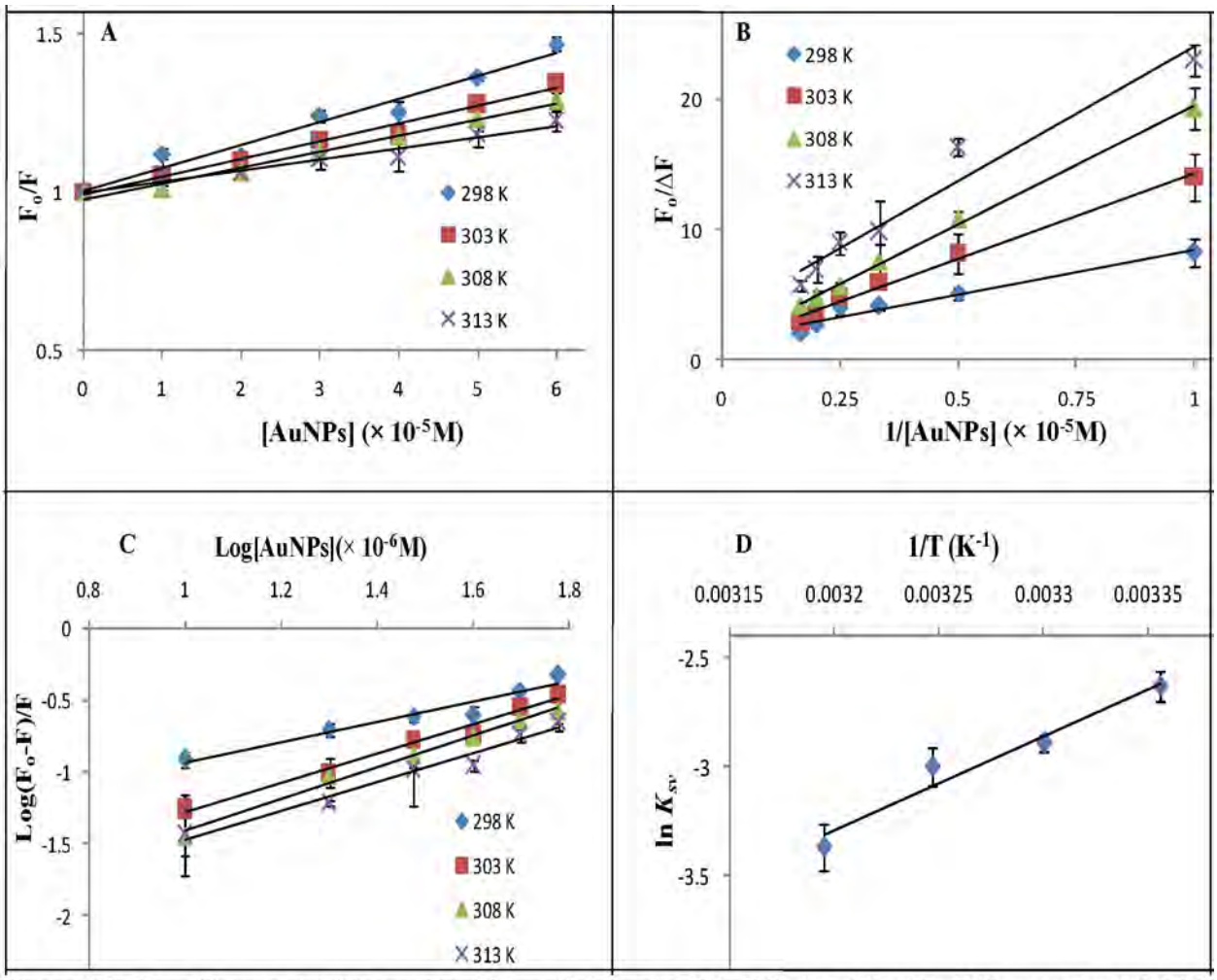

Figure 6.5: Stern–Volmer plot (A), modified Stern–Volmer plot (B), Hill plot of log $(F_o\text{-}F)/F$ versus log [AuNPs] (C) and Van't Hoff plot (D) for fluorescence quenching of 5 µg HSCOMT (5 µl) in 100 mM Tris, 5 mM $MgCl_2$, 200 mM NaCl, pH 7.5 buffer, treated with AuNPs (0-60 µM) in a final volume of 200 µl at different temperatures (298, 303, 308 and 313 K). The λ_{ex} was 295 nm and the λ_{em} was 350 to 750 nm.

Table 6.1: Values for the fluorescent parameters at different temperatures (K); K_{sv}, θ, K_a, K_d, n and thermodynamic parameters ΔH, ΔS and ΔG for the interaction of AuNPs with HSCOMT various temperatures.

Temperature	K_{sv} (µM)	θ	K_a (µM^{-1})	K_d (µM)	n	ΔG (kJ.mol^{-1}.K^{-1})
298	7.2×10^{-2}	0.602	2.45×10^{-1}	4.08	0.70	-78.89
303	5.6×10^{-2}	0.612	1.25×10^{-1}	7.99	1.0	-79.60
308	5.0×10^{-2}	0.764	7.20×10^{-2}	14.39	1.1	-80.32
313	3.5×10^{-2}	0.791	6.13×10^{-2}	15.76	1.1	-81.04

*$\Delta H = -3.62 \times 10^4$(J.mol^{-1}.K^{-1}).

**$\Delta S = 1.43 \times 10^2$ (J.mol^{-1}.K^{-1}).

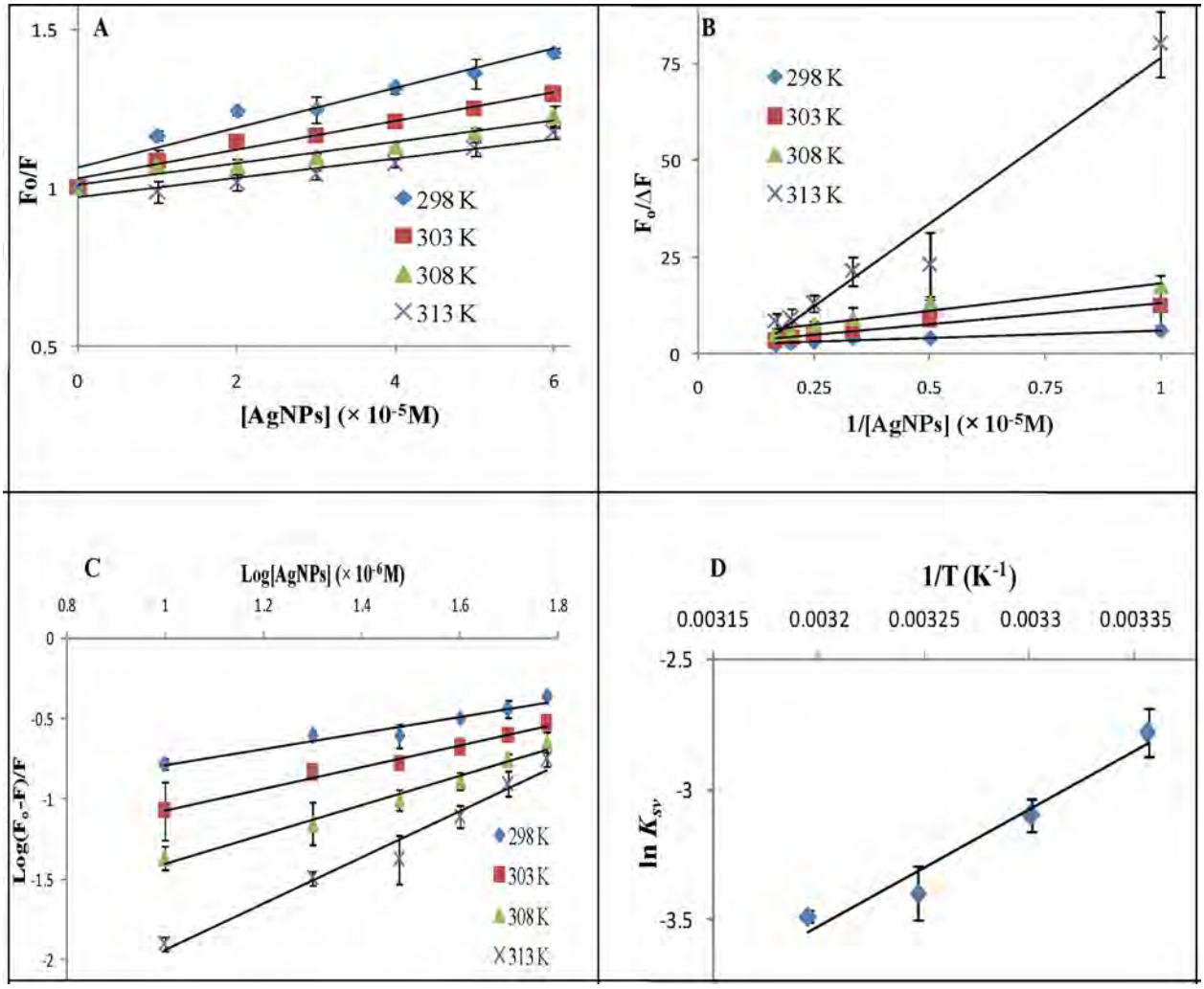

Figure 6.6: Stern–Volmer plot (A), modified Stern–Volmer plot (B), Hill plot of log (F_o-F)/F versus log [AgNPs] (C) and Van't Hoff plot (D) for fluorescence quenching of 5 µg HSCOMT (5 µl) in 100 mM Tris, 5 mM $MgCl_2$, 200 mM NaCl, pH 7.5 buffer, treated with AgNPs (0-60 µM) in a final volume of 200 µl at different temperatures (298, 303, 308 and 313 K). The λ_{ex} was 295 nm and the λ_{em} was 350 to 750 nm.

Table 6.2: Values for the fluorescent parameters at different temperatures (K); K_{sv}, θ, K_a, K_d, n and thermodynamic parameters ΔH, ΔS and ΔG for the interaction of AgNPs with HSCOMT at various temperatures.

Temperature (K)	K_{sv} (µM)	θ	K_a (µM^{-1})	K_d (µM)	n	ΔG (kJ.mol^{-1}.K^{-1})
298	6.2×10^{-2}	0.561	4.35×10^{-1}	2.30	0.51	-82.25
303	4.5×10^{-2}	0.583	1.58×10^{-1}	6.32	0.67	-83.00
308	3.3×10^{-2}	0.595	1.15×10^{-1}	8.70	0.91	-83.75
313	3.0×10^{-2}	0.601	2.33×10^{-2}	42.83	1.41	-84.50

*ΔH = -3.76×10^4(J.mol^{-1}.K^{-1})
**ΔS = 1.50×10^2(J.mol^{-1}.K^{-1})

Of the two tryptophan residues found in HSCOMT (Trp143 and Trp38) only Trp143 is exposed and accounts for the fluorescence of HSCOMT that is available for quenching. This amino acid interacts closely with the adenosine ring of S-adenosyl-*L*-methionine (SAM) (Rutherford *et al.*, 2008a). It is also part of the so-called "gatekeeper" residues (Trp38, Trp143, Pro174 and Leu198) of HSCOMT, which flank the hydrophobic entrance of the catalytic pocket, that keeps the planar catechol ring in the correct orientation during catalysis (Bonifacio *et al.*, 2007). These gatekeeper residues are also responsible for the preferential *O*-methylation of catechol substrates as well as the regioselection of the methylation of several substrates (Lautala *et al.*, 2001; Lotta *et al.*, 1995).

The excitation wavelength at 295 nm selectively excites the tryptophan residues in the HSCOMT (McGuinness *et al.*, 2005), thus the observed fluorescence was emitted by tryptophan. The Stern–Volmer plots obtained by using experimentally determined values of F_o and F are linear (Figures 6.5A and 6.6A). The plots indicated that the observed tryptophanyl emission of HSCOMT is accessible to, and quenched by, gold and silver NPs; and the decrease in fluorescence is because of the quenching of internal fluors (amino acids) within the HSCOMT and not external quenching caused by the interplay of other fluors in the solution. This is interpreted by the "y-intercept" of the linear plots being equivalent to 1 (Padayachee and Whiteley, 2013b).

The Stern-Volmer quenching constant (K_{sv}) for the quenching of HSCOMT fluorescence by AuNPs at 298, 303, 308 and 313 K are respectively 7.2, 5.6, 5.0 and 3.5×10^{-2} μM (Table 6.1); and the K_{sv} for the quenching of HSCOMT fluorescence by AgNPs are respectively, 6.2, 4.5, 3.3 and 3.0×10^{-2} μM (Table 6.2). The K_{sv} values decrease with the increase in temperature for static quenching, while they increase with increase in temperature for dynamic (collisional) quenching

(Padayachee and Whiteley, 2013b). The results (Tables 6.1 and 6.2) show that the K_{sv} values decrease with increase in HSCOMT fluorescence quenching temperature for both gold and silver NPs, demonstrating that the quenching of HSCOMT fluorescence by both gold and silver NPs is controlled by a static mechanism, indicating the formation of a non-fluorescent NP–fluorophore complex at the ground state (Al-Kady *et al.,* 2011; Adeyemi and Whiteley, 2014). Similar experimental results were also observed in our research group (Adeyemi and Whiteley, 2014) and other researchers (Garabagiu, 2011; Mariam *et al.,* 2011; Dasgupta *et al.,* 2016) for the analysis of interaction between gold and silver nanoparticles with proteins using the Stern-Volmer relation. By and large, AuNPs exhibited higher quenching abilities (Table 6.1) than AgNPs (Table 6.2), indicating that the former quenched more tryptophanyl fluorescence of HSCOMT than the latter. This correlated with the lower enzymatic activity of HSCOMT when incubated with 60 µM AuNPs than when incubated with 60 µM AgNPs (Chapter 5).

The data derived from the Stern-Volmer analysis of the quenching were further evaluated using the modified Stern-Volmer equation (Equation 6.2) (Lehrer, 1971). The plots of the equation allowed calculation of the number of fluorophores accessible to quenching (θ) by the NPs and the association constant (K_a) as well as its reciprocal, the dissociation constant (K_d) (binding affinities) of the binding of HSCOMT to the NPs.

From the equation, reciprocal of the ordinate intercept denotes the fraction of solvent-accessible tryptophan residues (θ). Figures 6.5B and 6.6B show the plot of the equation with respect to the quenching of HSCOMT fluorescence by gold and silver NPs, respectively. The quenching effect of both gold and silver NPs was associated with the exposure of a single Trp residue ($\theta \approx 1$) (Tables 6.1; 6.2). The value of the parameter, $\theta \approx 1$, at all four temperatures indicates the formation NP–SCOMT complex at the ground state (Kahana *et al.,* 1992), a classical feature of

static quenching mechanism. The quenching of HSCOMT fluorescence by gold and/or silver NPs therefore involves the interaction with Trp 143, since this amino acid is the only exposed Trp residue (Rutherford *et al.,* 2008a), and the quenching involves the formation of a complex at the ground state (static), and the observed number of the exposed fluor (Trp) in the present study is 1.

The association constant (K_a) and its reciprocal, the dissociation constant (K_d), which is the measure of HSCOMT binding affinity to gold and silver NPs at the four temperatures, were also extrapolated from the plots of equation 6.2 (Tables 6.1 and 6.2). As shown in Tables 6.1 and 6.2, the K_d values increase with temperature for both gold and silver NPs, and since K_d is inversely related to the binding affinity (Eaton *et al.,* 1995), the binding affinities of HCOMT to the gold and silver NPs therefore decrease with increase in temperature, which is a classical feature of an exothermic interaction (Weber and Campbell, 2011). This indicates that the interaction of HSCOMT with the surfaces of the NPs is energetically favourable. At the three temperatures 298, 303 and 308 K, AuNPs have lower binding affinities (K_d = 4.08, 7.99 and 14.39 μM, respectively) than the AgNPs (K_d = 2.30, 6.32 and 8.70 μM, respectively), signifying that the AgNPs are more tightly associated with HSCOMT at these temperatures. The high affinity of AgNPs at these temperatures could be explained by the surface stabilization of AgNPs by polyvinylpyrrolidone (PVP) since PVP-coated gold and silver NPs have higher binding affinities to proteins than citrate-coated particles (Ahlberg *et al.,* 2014). However, at 313 K, the binding affinity of AuNPs is higher than that of AgNPs, with K_d values of 15.79 μM and 42.83 μM respectively. This is probably because of the temperature relaxation of PVP-coated NPs is caused by steric repulsion imparted by the large PVP polymer (Rawat *et al.,* 2014).

The logarithmic derivative of the Stern-Volmer equation (equation 6.3) was used to calculate the number of available binding site(s) (n) of the NPs on the HSCOMT. Both gold and silver NPs are associated at a single binding site ($n \approx 1$) with the purified HSCOMT at 298, 303, 308, and 313 K (Tables 6.1 and 6.2); indicating that the increase in temperature does not lead to the exposure of more Trp residues for quenching, lending further support for a static quenching mechanism, and thus formation of a HSCOMT-NP complex at ground state.

The thermodynamic parameters; change in enthalpy (ΔH), change in entropy (ΔS) and free energy change (ΔG) for the interaction of the gold and silver NPs with HSCOMT were determined from the Van't Hoff plot (Figures 6.5D and 6.6D), and the values of the parameters are presented in Tables 6.1and 6.2.

The negative ΔH value and positive ΔS value for the interaction of both the gold and silver NPs with the purified HSCOMT (Tables 6.1and 6.2.) imply that the interactions between gold and silver NPs with the purified HSCOMT are largely driven by electrostatic interactions (Ross and Subramanian, 1981). Similarly, the negative ΔG values for the interactions (Tables 6.1and 6.2.) indicate that the interactions of gold and silver NPs with HSCOMT are spontaneous (exothermic) and thermodynamically favourable. These results agree with the observed decrease in binding affinity with increase in temperature for the interactions of both gold and silver NPs with HSCOMT implying an exothermic interaction (Weber and Campbell, 2011). There are high free energies for the interaction of AuNPs with HSCOMT at 298, 303, 308, and 313 K, which respectively correspond to -79.89, -79.60, -80.30 and -81.04 $kJ.mol^{-1}.K^{-1}$ (Table 6.1); and even higher free energies for the interaction of AgNPs with HSCOMT at 298, 303, 308, and 313 K, corresponding to -82.25, -83.00, -83.75 and -84.50 $kJ.mol^{-1}.K^{-1}$ (Table 6.2). This could be due to the high energy on the NPs surfaces (with respect to surface area to volume ratio) in relation to

the protein's physiological environment (Monopoli, *et al.*, 2011). These findings indicate both the release of high amounts of heat and high entropy change during the binding of both gold and silver NPs with HSCOMT (Chakraborti *et al.*, 2012).

Trp143 is adjacent to Lys144 (Rutherford *et al.*, 2008b) and Lys144 is part of ß5/ß9 loop which partakes in domain swapping for HSCOMT dimerization (Law *et al.*, 2014). Consequently the interaction of gold and/or silver NPs with Trp143 must change the microenvironment and therefore impede the dimerisation.

6.3.3 Fourier transform infrared (FTIR) spectroscopic analysis

To investigate whether the interaction with gold/silver NPs changes the conformation of HSCOMT, FTIR measurements were performed in the absence and presence of the NPs according to the procedure described in section 6.2.2.5.

The FTIR spectra of HSCOMT in the presence and absence of AuNPs and AgNPs are shown in Figure 6.7 and Figure 6.8, respectively. The FTIR spectrum of HSCOMT exhibited a strong peak for amide I band (1600–1700 cm^{-1}), which is sensitive to changes of protein conformation (Figures 6.7 and 6.8). This band originates from an overlapping component of bands from α-helices, ß-sheets, turns and random coil structures (Kong and Yu, 2007). The peaks with maxima at ~1650 cm^{-1}arise from α-helices and ~ 1630 to ~1635 cm^{-1} from ß-sheet structures (Jackson and Mantsch, 1995; Fabian and Mäntele, 2002).

The adsorption of the pure HSCOMT onto both gold and silver NPs caused a vibrational shift of the amide I band at 1635 cm^{-1}; for HSCOMT adsorption onto AuNPs, the ß-sheets peak at 1635 cm^{-1} shifted to 1638 cm^{-1} (Figure 6.7) and for HSCOMT adsorbed onto AgNPs, the ß-sheets peak at 1635 cm^{-1}shifted to 1646 cm^{-1}(Figure 6.8), indicating that the HSCOMT absorption onto

both gold and silver NPs caused relaxation of ß-sheet structures within the enzyme. Interestingly, a greater shift (from 1635 cm^{-1} to 1646 cm^{-1}) was observed from the HSCOMT adsorbed on AgNPs than the HSCOMT adsorbed on AuNPs (from 1635 cm^{-1} to 1638 cm^{-1}), which correlated with the higher binding affinity of the HSCOMT with AgNPs than with AuNPs (section 6.3.2).

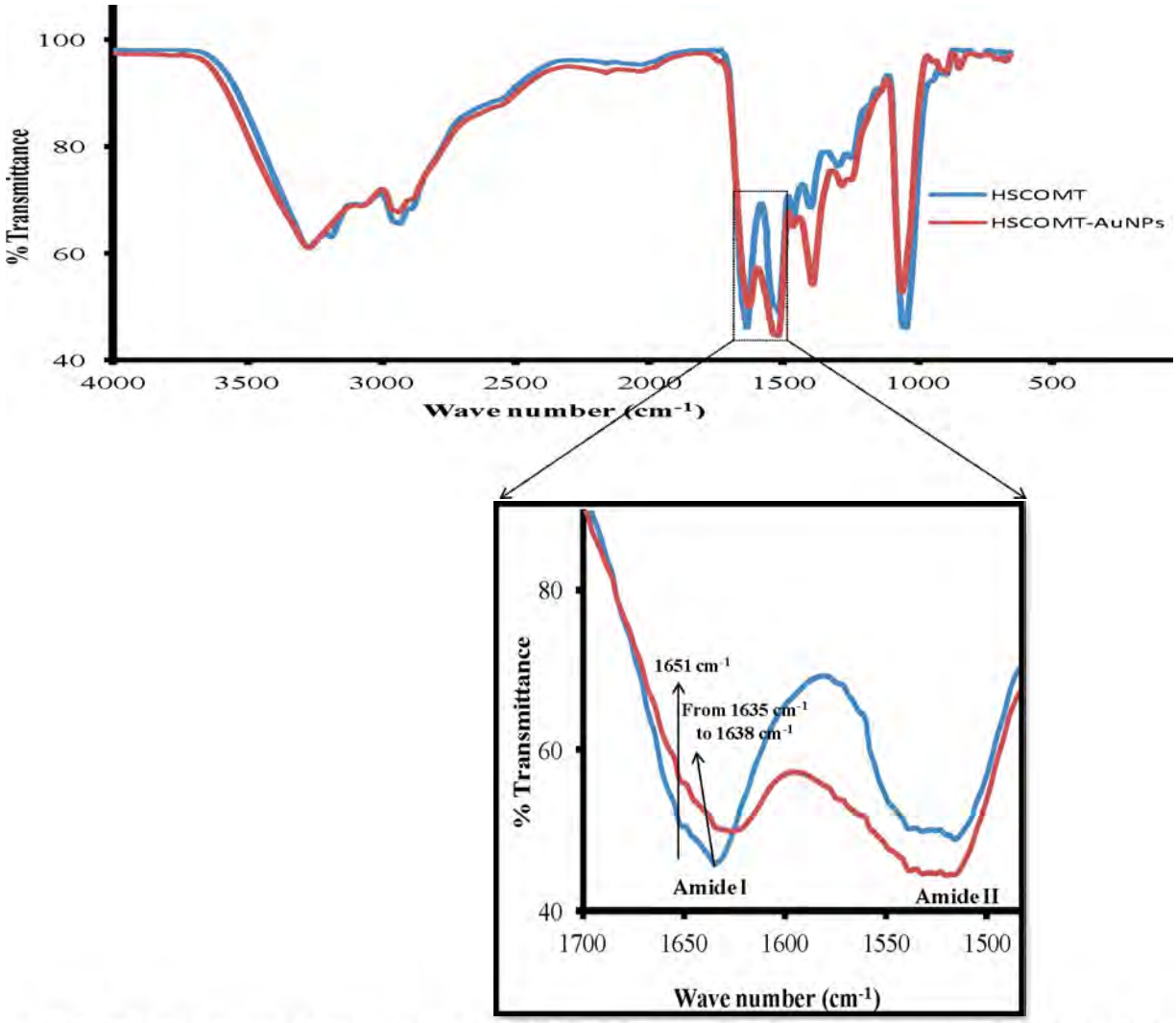

Figure 6.7: The FTIR spectra of the lyophilised HSCOMT (0.5 mg) in the absence and presence of 60 µM AuNPs. Inset are the enlarged amides I and II bands, showing a shift of amide I region at 1635 cm^{-1} (to 1638 cm^{-1}), indicating relaxation of ß-sheet structures.

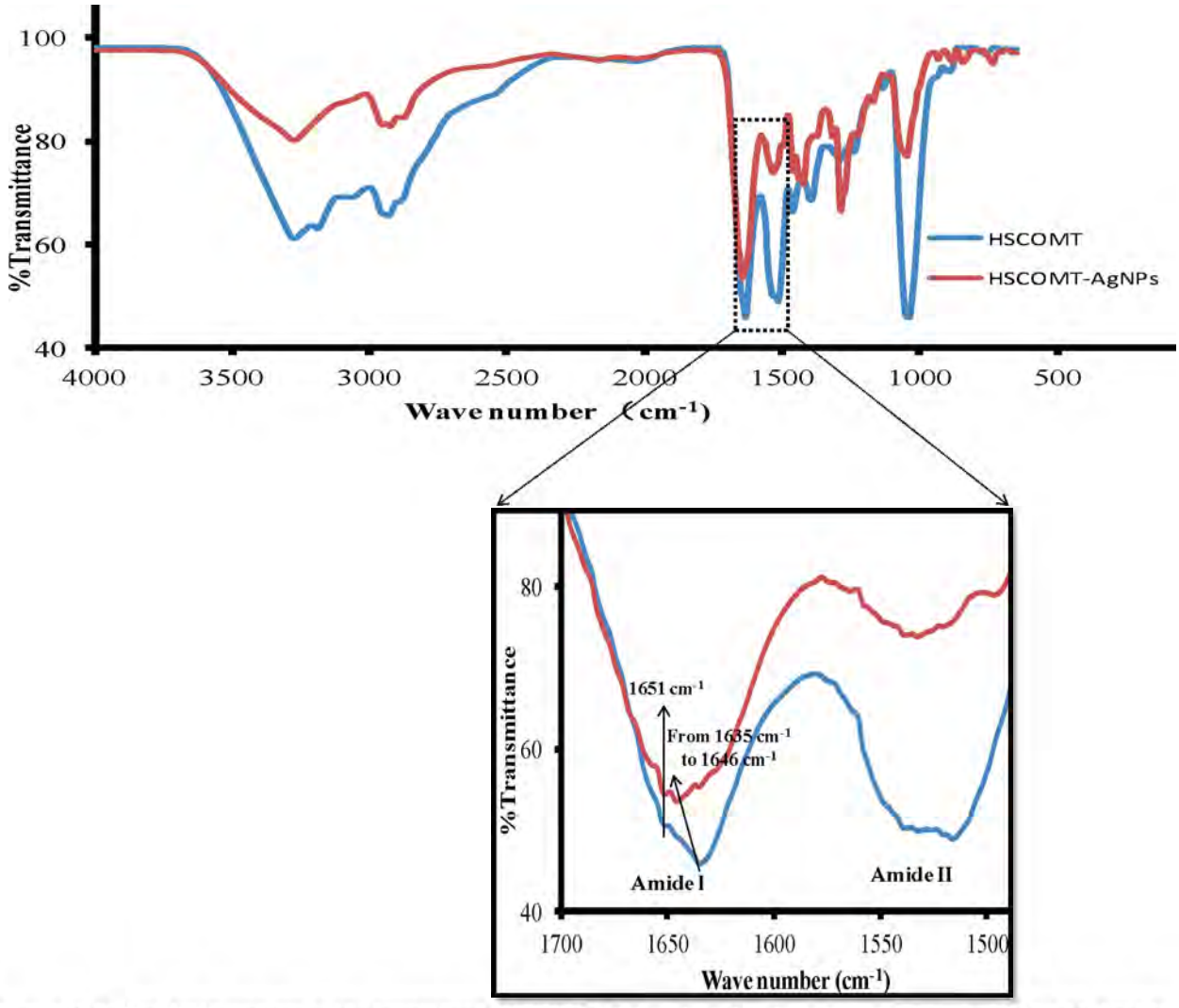

Figure 6.8: The FTIR spectra of the lyophilised HSCOMT (0.5 mg) in the absence and presence of 60 µM AgNPs. Inset are the enlarged amides I and II bands, showing a shift of amide I region at 1635 cm^{-1} (to 1646 cm^{-1}), indicating relaxation of ß-sheet structures.

The structure of HCOMT comprises of seven-stranded ß-sheet core (3↑2↑1↑4↑5↑7↓6↑) sandwiched between sets of α-helices, the characteristic structure of the SAM-dependent methyltransferases (Rutherford *et al.*, 2008b). The overall decrease in transmittance in both gold and silver NPS adsorbed on HSCOMT could be attributed to the overall relaxation of the protein conformational structure caused by its adsorption on the NPs surfaces as a function of changes in

out-of-plane motions in the enzyme's structure (Figures 6.7 and 6.8) (Fabian and Mäntele, 2002; Jabs, 2015).

However, for both AuNPs and AgNPs with HSCOMT, there is no observable shift in the peak at 1651 cm^{-1}which originates from α-helices, suggesting that the adsorptions do not cause relaxation of α-helix structures of the enzyme.

In HSCOMT, domain swapping occurs at α2/α3, ß5/ß9 and/or ß6/ß7 and leads to the formation of the dimer (Ehler *et al.,* 2014). Relaxation of ß-sheet structures of this enzyme caused by interaction with gold and/or silver NPs could therefore obstruct the dimerization. Cysteine residues 188 and 199 are involved in the formation of an intermolecular disulfide bond, which is also related to the dimerization of HSCOMT (Cotton *et al.,* 2004). The latter (Cysteine 199) is a resident of ß6 in the protein structure (Rutherford *et al.,* 2008b). Relaxation of this ß6 will restrict participation of this amino acid in the formation of the disulfide bond.

6.3.4 Computational simulation: molecular docking

Because there is no "stand-alone" technique to determine the mechanism of NPs-protein interaction, the molecular docking study was attempted to gain more insight on the interaction between HSCOMT with gold/silver NPs.

The geometrical fitting and orientation of protein onto the NPs surfaces depend on the particle curvature (size), and protein structure and size (Khan *et al.,* 2014). The docking study showed that HSCOMT recognizes 10 nm (diameter) gold and silver NPs as flat surfaces (Figures 6.9 and 6.10).

The recognition of 10 nm particles size as a "flat surface" by HSCOMT is expected in consideration of the enzyme's molecular size of 24.6 kDa (Figures 6.9A and 6.10A) (Khan *et al.*,2014). The "crawling like structures" of different proteins on the surfaces of NPs have been reported (Brancolini *et al.*, 2012; Chaudhary *et al.*, 2014; Khan *et al.*, 2014).

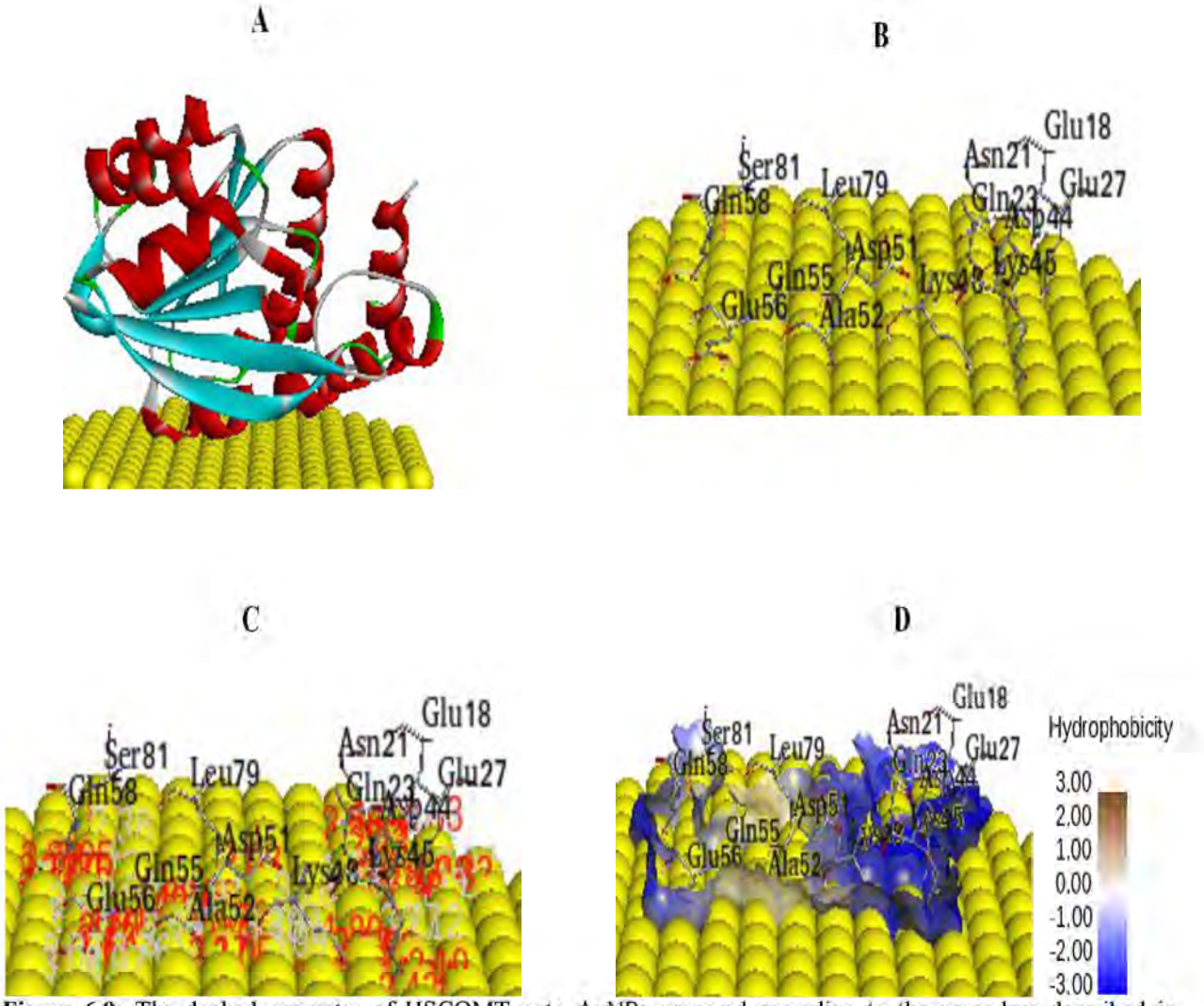

Figure 6.9: The docked geometry of HSCOMT onto AuNPs prepared according to the procedure described in section 6.2.2.6. The image shows the crawling like structure of HSCOMT on the AuNPs surface (A), the amino acid residues involved for the interaction (B), the distances of the "involved" amino acids to the NPs surface (C) and the hydrophobicity of the binding region (D).

The footprint of HSCOMT on the surface of AuNPs shows that the enzyme uses fourteen amino acid residues, predominantly from helical structures, to fit onto the particle's surface (Figure 6.9A). Four different binding domains were observed in this orientation. The upper domain, which consists of the binding of Glu18 (no assigned secondary structure), Gln18, Gln23 and Glu27 (α-helix 2); the upper middle domain, which includes the binding of Asp44, Lys45, Lys48, Asp51, Ala52, Gln55, Glu56 (α-helix3) and Gln58 (no assigned secondary structure); the lower middle domain which involves Leu79 (Turn 4) and the lower domain with the attachment Ser81 (no assigned secondary structure) and Asp121 (α-helix7) (Rutherford *et al.,* 2008b).

Ser19 is adjacent to Gln120 in HSCOMT secondary structure, where both residues form hydrogen bonds with SAM, and therefore are crucial for the enzyme's catalysis (Bonifácio *et al.,* 2002; Rutherford *et al.,* 2008b). The interaction of AuNPs with Glu18 and Asp121, which are neighbours to and in the same loop as Ser19 and Glu120, respectively, could affect the SAM binding during catalysis. The "turn" (structure) plays a vital role in protein folding by bringing structural components together and enables interactions between different structural components (Venkatachalam, 1968). The binding of Leu79 (Turn 4) could interfere with the optimum native folding of HSCOMT. His142 and Trp143, which reside in α-helix 7, are two crucial amino acids involved in the catalysis of HSCOMT (Rutherford *et al.,* 2008b). Binding of Asp121, another resident of α-helix 7 could alter the helical structural conformation, which could in turn affect the enzyme catalytic activity. By and large, the overall interaction of AuNPs with HSCOMT changes the structural and catalytic microenvironment, and therefore, could impact on the HSCOMT dimerization and catalytic mechanism.

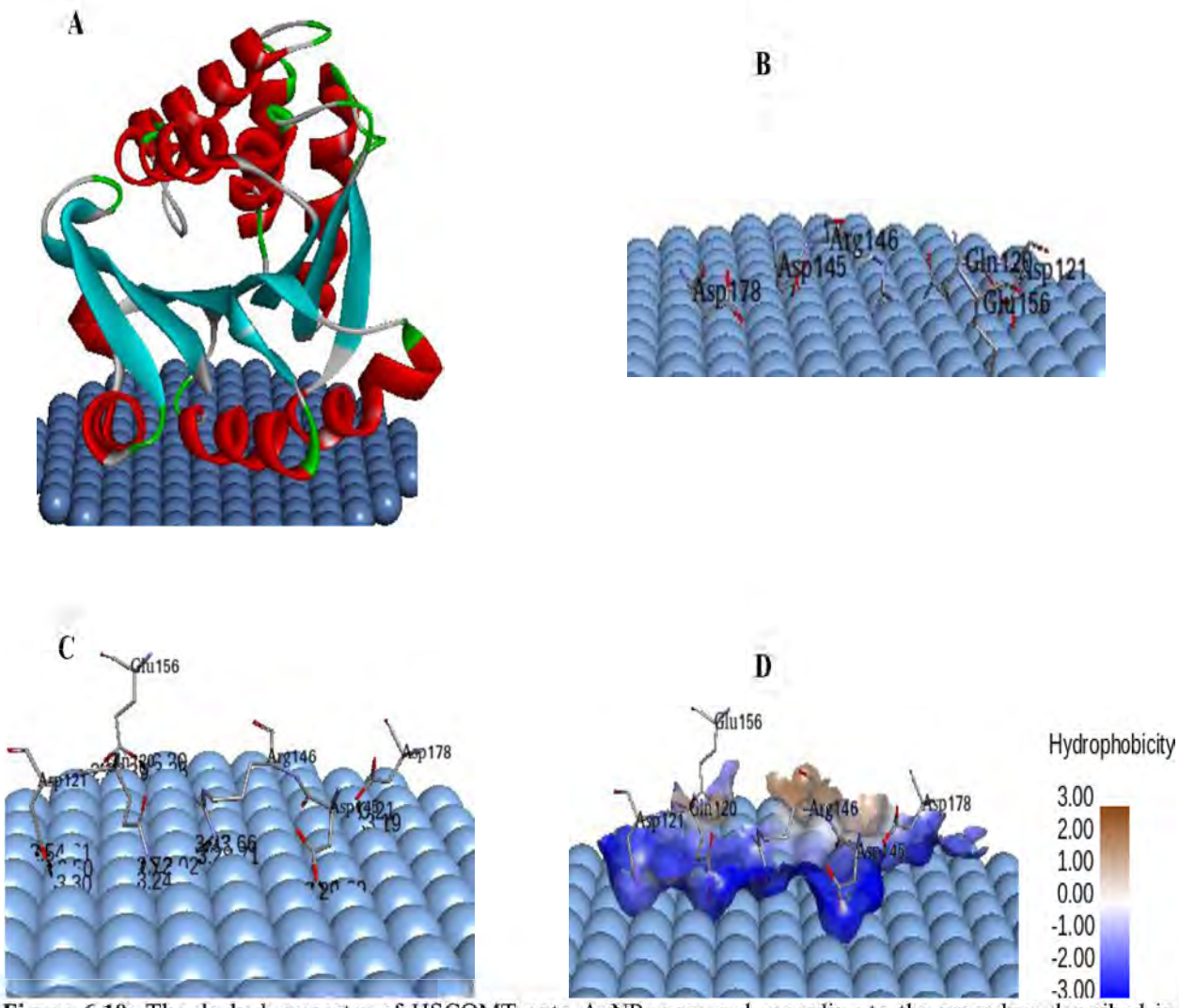

Figure 6.10: The docked geometry of HSCOMT onto AgNPs prepared according to the procedure described in section 6.2.2.6. The image shows the crawling like structureof HSCOMT on the AgNPs surface (A), the amino acid residues involved for the interaction (B), the distances of the "involved" amino acids to the NPs surface (C) and the hydrophobicity of the binding region (D).

The interaction of HSCOMT with AgNPs is facilitated by binding six amino acid residues, from predominantly helical structures, onto the particle's surface (Figure 6.10A). Four binding regions are involved in this interaction. The first region consists of the binding of Gln120 and Asp121 (α-helix 7); the second region involves the binding of Asp145 and Arg146 (3_{10} helix, helix 10); the third region is the binding of Glu156 (α-helix 11) and the fourth region is the binding of Asp178 (α-helix 13) (Rutherford *et al.*, 2008b).

The Gln120 (α-helix 7) is located in the SAM pocket, where the adenine ring of the SAM forms hydrogen bonds with the side-chain oxygen atoms of Ser119 and Gln120 (Rutherford *et al.,* 2008b; Bonifácio *et al.,* 2002). The binding of this amino acid residue on the surface of AgNPs could most probably affect the SAM binding, and thus the HSCOMT catalytic activity. Similarly, since Gln120 and Asp 121 reside in the same structural region (α-helix 7) with the catalytic amino acid residues, His142 and Trp143, their binding to AgNPs will consequently influence the microenvironment and biological activity of the catalytic amino acid residues. In the PDB deposited crystal structure of HSCOMT, Rutherford and co-workers (2008b) reported Asp145, Arg146 and Glu156, among other amino acid residues, to be associated with Mg^{2+} positioning in HSCOMT. The binding of these amino acid residues on the AgNPs surface would therefore interfere with the Mg^{2+} positioning, and subsequently the HSCOMT enzymatic activity.

Figure 6.9C and Table 6.3 show the binding distances between AuNPs and participating amino acid residues for the AuNPs-HSCOMT interaction; while Figure 6.10C and Table 6.4 show the binding distances between AgNPs and participating amino acid residues for the AgNPs-HSCOMT interaction. All the binding distances between the participating amino acids and the AuNPs surface in HSCOMT-AuNPs binding are less than 2.5 Å, while the distances between the participating amino acids and the AgNPs surface in HSCOMT-AgNPs binding are less than 3.5 Å. The short distance ($\leq$ 6.0Å) suggests a very strong association between the gold/silver NPs surfaces and the amino acid residues (Gao and Skolnick, 2012).

The HSCOMT domains that interact with both gold and silver NPs surfaces are mainly hydrophilic (Figures 6.9D and 6.10D). Of fourteen participating amino acid residues in AuNPs-HSCOMT interaction, only Ala52 and Leu79 are hydrophobic, while Glu18, Gln23, Glu27,

Asp44, Lys45, Lys48, Asp51, Gln55, Glu56, Gln58, Ser81 and Asp121 are hydrophilic. All the six amino acid residues in HSCOMT that bind to AgNPs surface, Gln120, Asp121, Asp145, Arg146, Glu156 and Asp178, are also hydrophilic. This indicates that the interaction domains of HSCOMT with both gold and silver NPs surfaces are solvent-exposed hydrophilic regions, further supporting the formantion of NP-HSCOMT complex at the ground state (section 6.3.2).

Table 6.3: The binding distances between AuNP surface and HSCOMT participating amino acid residues for the AuNPs-HSCOMT interaction

Amino acid residue	Binding distance (Å)
Glu18	1.31
Gln23	1.42
Glu27	2.23
Asp44	1.86
Lys45	1.22
Lys48	1.86
Asp51	2.04
Ala52	2.05
Gln55	1.36
Glu56	1.64
Gln58	1.49
Leu79	2.08
Ser81	2.38
Asp121	1.75

Table 6.4: The binding distances between AgNP surface and HSCOMT participating amino acid residues for the AgNPs-HSCOMT interaction

Amino acid residue	Interaction distance (Å)
Gln120	2.72
Asp121	2.50
Asp145	2.29
Arg146	2.66
Glu156	2.82
Asp178	3.19

Table 6.5 shows the binding energies (ΔG) (kcal.mol^{-1}) for the interaction of HSCOMT and gold/silver NPs and the Inhibition constant (K_i) for the AgNPs-HSCOMT interaction estimated from the molecular docking study.

From Table 6.5, the estimated free energy for the interaction between HSCOMT and AuNPs is positive, indicating that this interaction is endothermic and non-spontaneous. The interaction between HSCOMT and AgNPs is negative, indicating that this interaction is exothermic and spontaneous (Moradi *et al.*, 2015).

Table 6.5: The binding energies (ΔG) (kcal.mol^{-1}) for the interaction of HSCOMT and gold/silver NPs and the inhibition constant (K_i) for AgNPs-HSCOMT interaction estimated from the molecular docking study.

	Estimated free energy of binding (ΔG) (kcal.mol^{-1})	**Estimated inhibition constant (K_i)**
AuNPs	3.09×10^3	–
AgNPs	-3.74	1.82 mM

Ala52 and Leu79 are non-polar (hydrophobic) amino acid residues and are buried within the HSCOMT structure. The involvement of these hydrophobic amino acid residues is probably responsible for the energy requirement (to expose them for the interaction), and hence, non-spontaneity of the interaction between HSCOMT and AuNPs. Conversely, the interaction between HCOMT and AgNPs involves only polar amino acids; hence no energy requirement to expose any residue, therefore, the interaction is spontaneous and the estimated free energy of the interaction is negative. From the docking study, the inhibition constant (K_i), for the thermodynamically favourable interaction between HSCOMT with AgNPs was 1.82 mM. It is noteworthy that Autodock tools do not estimate inhibition constant for the simulation of thermodynamically unfavourable interactions because it is perceived to be unfavourable.

The functional groups from the capping, stabilizing, and/or dispersing agents on the surfaces of the NPs affect the particles' interaction with biomolecules and, in particular, play an important role in the formation of NPs-protein corona (Gnanadhas *et al.,* 2013). The uncoated and surfactant-free NPs derived from a laser ablation process exhibit increased changes in entropy compared with citrate and PVP-coated NPs (Podila *et al.,* 2012). In the present study, citrate (for AuNP) and PVP (for AgNP) were not included for the molecular docking of HSCOMT with the NPs since this may reflect the variations between the interaction study of molecular docking and the experimentally observed interaction from fluorescence and infrared spectroscopy.

6.4 Conclusion

Spectroscopic techniques provide insight on the binding and mechanisms of interactions of gold/silver NPs with HSCOMT.

The visual gold/silver NPs colour changes, observed upon incubation of the NPs with increasing concentration of HSCOMT, are indicative of the changes of the plasmonic properties of the NPs caused by the HSCOMT adsorption. Absorbance spectroscopy analyses reveal HSCOMT concentration-dependent red shift and broadening of both gold and silver NPs plasmonic absorption peaks, indicating the adsorption of HSCOMT on the surface of gold and silver NPs, and the formation of both AuNPs-HSCOMT and AgNPs-HSCOMT coronas.

Fluorescence quenching analyses indicated that both gold and silver NPs quenched HSCOMT fluorescence via a static quenching mechanism. This was evident from the decrease in the Stern-Volmer quenching constant (K_{sv}) with increase in the interaction temperatures for both gold and silver NPs interaction with HSCOMT. The fraction of exposed Trp residues (fluorophore), (θ), during quenching, was equivalent to one ($\theta \approx 1$) for the quenching of HSCOMT by both gold and silver NPs, suggesting that both NPs had access to a single fluorophore during the quenching. The number of binding site(s) (n) was also equivalent to one ($n \approx 1$) for both gold and silver NPs interactions with HSCOMT, signifying that both NPs made contact with one fluorophore for the quenching process. Further fluorometric analyses indicated a decrease in binding affinity with increasing interacting temperatures for both interactions of gold and silver NPs with HSCOMT, suggesting that the interactions are exothermic (and spontaneous). Thermodynamic analyses for the interactions of HSCOMT with gold and silver NPs signified that both interactions are exothermic (spontaneous) and therefore thermodynamically favourable. This was corroborated with the negative values of the Gibbs' free energy (ΔG) for the interactions. The positive values of the entropy (ΔS) and the negative values of the enthalpy (ΔH) for the interactions of both gold and silver NPs suggested that both interactions are driven by electrostatic interactions.

Fourier transform infrared (FTIR) spectroscopic analyses revealed that the adsorption HSCOMT onto both gold and silver NPs caused vibrational shift of the amide I band, signifying that the HSCOMT absorption onto both gold and silver NPs caused relaxation of ß-sheet structures of the enzyme protein.

Results from the molecular docking simulations disclosed that fourteen and six amino acid residues, respectively, are involved in the interaction of AuNP and AgNP with HSCOMT. The interacting distances of these amino acids with their respective NPs surfaces are less than 3.5 Å, indicating strong interactions between the amino acids and gold/silver NPs. Of the fourteen residues involved in HSCOMT interaction with AuNPs, only two are hydrophobic, while the remaining twelve are hydrophilic. All the residues within HSCOMT involved in the interaction with AgNPs are hydrophilic amino acids. The docking study reveals a positive free energy for the AuNPs-HSCOMT interaction and a negative free energy for AgNPs-HSCOMT interaction, implying non-spontaneous and spontaneous interactions, respectively. The non-spontaneity of AuNPs-HSCOMT interaction is most probably caused by the involvement of the two hydrophobic amino acid residues in the interaction. These variations between experimentally determined (thermodynamic) and computer simulated modelled interaction are due to the presence of stabilisers (citrate and PVP) on the surfaces of gold and silver NPs with respect to the thermodynamic results.

Chapter seven

General discussions and future perspectives

7.1 General discussions

Catechol *O*-methyltransferase (COMT) is a ubiquitous enzyme present in prokaryotes and eukaryotes, plants and animals (Bonifácio *et al.,* 2007). Searches on the National Centre for Biotechnology Information data bases (NCBI Resource Coordinators, 2016) revealed characterized COMT genes of several mammals, including *Bos taurus, Homo sapiens*, *Mus musculus, Rattus norvegicus, Equus caballus* and *Canis lupus familiaris*. The corresponding amino acid sequences encoded by these genes were also present in UniProt (The UniProt Consortium, 2016). Sequence alignment using ClustalW indicated high (>90%) sequence similarity between all of the species in question. As expected, all the reported important amino acid residues for the catalytic activity of COMT are conserved (Figure 2.1). Similarly, analyses of the sequences with MEME-suite revealed very high domain and motif conservations, indicated by the very low E-values among the sequences (Figure 2.2). Furthermore, modelled secondary structure of bovine (*Bos taurus*) soluble COMT (BSCOMT) using Phyre2, showed seven β-sheets squeezed between set of α-helices, a characteristic structural feature of SAM-dependent methyltransferases (Martin and McMillan, 2002). The modelled BSCOMT structure had the same structural arrangement as that of human COMT (HSCOMT) reported by Rutherford *et al.,* (2008b) (Figure 2.3). These observations agree with the reported similarities of mammalian COMT structure, mechanism and function (Bonifácio *et al.,* 2007; Mannisto and Kaakkola, 1999). The high sequence similarity, conservation of catalytically important amino acid residues, domains and motifs and also the similarity of the secondary structure suggest

similar catalytic/inhibition mechanisms between human and bovine SCOMT. Because of availability and accessibility, BSCOMT was initially used as a surrogate to HSCOMT.

The literature reported purification of COMT from mammalian tissues to include multistage extractions, including homogenization, differential centrifugation, ammonium sulfate fractionation, gel filtration and ion-exchange chromatography (Axelrod and Tomchick, 1958; Ball *et al.,* 1971; White and Wu, 1975; Darmenton *et al.,* 1976; Tilgmann and Kalkkinen, 1990; Tilgmann and Kalkkinen, 1991; Piedrafita *et al.,* 1992). These approaches were employed to purify COMT from bovine liver. Increasing specific activity was observed during the purification steps, although the SDS-PAGE gel analyses of the sample of the last purification stage showed protein impurities, indicating that the enzyme was only partially purified. The BSCOMT was partially purified to 7.78 fold, and biochemically characterized. This, to the best of our knowledge, has not previously been reported. With esculetin as the catechol substrate, the enzyme had pH and temperature optima of 8.5 and 40^{o}C, respectively. The BSCOMT pH optimum did not agree with that reported bovine's body physiological pH, while the temperature optimum agreed closely with bovine physiological temperature of 39^{o}C (Fallon, 1962). The kinetic pattern of the partially purified enzyme was hyperbolic, a characteristic of Michaelis-Menten kinetics and K_m, V_{max}, K_{cat} and K_{cat}/K_m were 1.46±0.13 µM, 0.0353 µmol/ml/min, $1.75 \times 10^{-2} \pm 5.0 \times 10^{-4}$ min^{-1} and 1.18×10^{-2} $M^{-1}.min^{-1}$, respectively. Based on the large volume and flexibility of SAM, COMT has been described as a slow enzyme (Vidgren *et al.,* 1994). Importantly, a consistent COMT assay procedure was optimised using the partially purified BSCOMT (initially with commercial porcine COMT as a positive control) and the enzyme characterized for the first time. However, because of our inability to purify BCOMT further, indicated by the impurities observed from the SDS-PAGE (Figure 2.4), which could interfere

with subsequent experiments, the decision was made to express HSCOMT by recombinant DNA technology.

The amino acid sequence of HSCOMT was accessed from the NCBI (accession code: NP_009294.1) and translated back to its corresponding nucleotide sequence (Artimo *et al.,* 2012) and optimized for *E. coli* expression (Puigbò *et al.,* 2007). The optimized gene, housed in pET-22b(+) vector was over-expressed by BL21(DE3) upon induction of the *lac operon* (of the T7 promoter) by the IPTG, and shaking at 150 rpm at 37°C. Under these conditions the C-terminal polyhistidine (6 histidine residues) tagged enzyme was sufficiently expressed in 4 h (Figure 3.3). The western blot analysis of the HSCOMT indicated the presence of the enzyme dimer, possibly as a result of the formation of the intermolecular disulfide bond between cysteine residues 188 and 191 (Cotton *et al.,* 2004). Ehler *et al.,* 2014 and Law *et al.,* 2016 reported domain swap, which involves an exchange between three hinge regions, α2/α3, ß5/ß9 and/or ß6/ß7 between HSCOMT molecules, which may also explain this phenomenon. Both the intermolecular disulfide bond and domain swap occur at high (≥1.2 mg/ml) COMT concentrations (Cotton *et al.,* 2004; Ehler *et al.,* 2014).

The biomass containing the HSCOMT was harvested by centrifugation, lysed by lysozyme and freeze-thaw, and purified to homogeneity by ultracentrifugation, IMAC and desalting (size exclusion chromatography) (Figures 3.4 and 3.5). There was evidence, from the SDS-PAGE and western blot gel images (Figure 3.6) of the formation of both a dimer and higher oligomers of HSCOMT. The his-tagged HSCOMT was purified to 5.62 fold in 22.6% yield and a specific activity of 3.85 U/mg. The purified enzyme had pH and temperature optima of 7.0 and 30°C, which were very close to the broad range of pH (6.5 to 10.5) and temperature (35 to 42°C) reported in the literature, albeit from different sources, different reaction conditions and different

catechol substrates (Ball *et al.,* 1972; Gulliver and Tipton, 1978; Nohta *et al.,* 1984; Dhar and Rosazza, 2000; Alazizi *et al.,* 2011). The purified enzyme exhibited hyperbolic Michaelis-Menten kinetics when incubated (5 min; 30°C) before the addition of SAM to initiate the reaction. Further analysis with Hanes–Woolf kinetics gave K_m, V_{max}, K_{cat} and K_{cat}/K_m values of 1.79 µM, 0.41 µmol/ml/min, 2.08 min^{-1}, and 1.17 M^{-1}. min^{-1}, respectively. While the K_m is comparable to that of BSCOMT, the V_{max}, K_{cat} and K_{cat}/K_m are higher in HSCOMT, possibly due to higher purity of the latter. Nevertheless, both enzymes are regarded as having a low turnover rate, with K_{cat} values of 1.75 x 10^{-2} and 2.08 $min^{-1}$for BSCOMT and HSCOMT, respectively.

The purified enzyme was stable for up to seven days at 4°C and for over three months at -20°C, and therefore suitable for downstream experiments, including measuring its activity in the presence of silver and/or gold nanoparticles.

AuNPs were synthesized by citrate reduction. AgNPs were synthesized by microwave irradiation with ethanol and PVP as reducing and stabilizing agents, respectively. Both gold and silver NPs were spherical, with diameters ≤ 10 nm. The AuNPs gave a plasmon resonance band at 520 nm and were stable in the dark at 4°C for up to 48 h, but storage at this condition for two weeks decreased its plasmonic absorption with a bathochromic red-shift, both caused by aggregation of smaller particles into larger ones. AgNPs had a plasmon resonance peak at 417 nm and were stable in the dark at 23°C with consistent morphology and size distributions for over two weeks. AuNPs were therefore stored in the dark at 4°C and used for interaction studies with HSCOMT within 48 h, while AgNPs were stored in the dark at 23°C and used within two week for interaction studies with HSCOMT.

The present study investigated the effects of AuNPs and AgNPs on HSCOMT. The results showed that the gold and/or silver NPs have concentration-dependent inhibitory effects on HSCOMT after incubation (1 h) before addition of the cofactor, SAM, to initiate the reaction. The incubation time allows for the adsorption of HSCOMT onto the surfaces of gold and/or silver NPs (Rahman *et al.,* 2013). Surprisingly, the kinetic plot of HSCOMT (without the NPs) with the 1 h incubation, of the reaction mixture, at 30°C prior to the addition SAM was sigmoidal (instead of hyperbolic, which occurs after only 5 min incubation) and with a higher V_{max}. Sigmoidal kinetics for COMT have been reported previously (Ball *et al.,* 1972; Dawling *et al.,* 2001). Hyperbolic kinetics were also seen in the presence of 60 μM gold and/or silver NP, indicating that the NPs abolished the sigmoidal effect. To understand the differences between the 5 min and 1 hour incubation conditions and the 1 h incubation in the presence of 60 μM Au/Ag NPs, the HSCOMT samples used for all the kinetic studies were analyzed by SDS-PAGE. Analyses revealed that the enzyme, after 5 min incubation, migrated as a monomer, while after incubation (1 h, 30°C) the enzyme migrated substantially as a dimer, indicating that the extension of the incubation time from 5 min to 1 h allowed for the dimerization of HSCOMT at a concentration lower than its dissociation constant of ≥1.2 mg/ml (Cotton *et al.,* 2004). SDS-PAGE analyses of the HSCOMT used for the kinetic study in the presence of the NPs (with the 1 h incubation) showed the protein as a monomer, indicating that in the presence of gold and/or silver NPs there was no dimerization, and a change in kinetics from sigmoidal to hyperbolic (Figures 5.6 and 5.8). These observations indicate that, upon 1 h incubation at 30°C, HSCOMT exists in both monomer and dimer conformations differing in reactivity, and that the presence of 60 μM gold and/or silver NPs impedes the dimerization and suppresses sigmoidal kinetics. Similarly, the kinetic parameters showed by HSCOMT assays with 5 min incubation (Table 3.2)

are comparable to those obtained with 1 h incubation in the presence of 60 μM gold and/or silver NPs (Table 5.1).

It has been reported that the *O*-methylation of catechols by COMT is regioselective (Masri *et al.*, 1964), with a preference to *meta O*-methylation *in vivo* (Axelrod, 1966) and *para O*-methylation *in vitro* (Kiss and Soares-da-Silva, 2014). Similarly, reports on the regioselectivity of the monomeric and dimeric HSCOMT have indicated that the enzyme monomer favours *para O*-methylation while the dimer prefers *meta O*-methylation (Law *et al.*, 2016). The dimer may possibly be the catalytically relevant form of COMT *in vivo*.

To assess whether the increased catalytic activity exhibited by HSCOMT is caused exclusively by the monomer-dimer structural/activity variation and kinetic hysteresis, or whether it is linked to co-operativity during the catalysis, the kinetic assay procedure, with incubation (1 h, 30°C) prior to the addition of SAM to initiate the reaction, was repeated with a range of SAM (6 to 300 μM) and $MgCl_2$ (1 to 10 mM) concentrations. The analyses of the HSCOMT kinetic data, performed at different concentrations of SAM, indicated a Hill coefficient of greater than 1 ($h>1$), while for the kinetic assay with 6 μM SAM, the Hill coefficient is equivalent to 1 ($h\approx1$) (Figure 5.9 and Table 5.2). The generation of $h>1$ in the kinetic experiments with ≥60 μM SAM concentrations indicates cooperativity during the catalysis at these concentrations. A hyperbolic curve and Hill coefficient of 1 in the experiment with SAM concentration of 6 μM indicates that there is little or no modulatory effect of SAM on HSCOMT activity at this concentration. Again, the $K_{0.5}$ and Hill coefficient increased with increase in SAM concentration, indicating a decrease in the enzyme's affinity towards the substrate binding and an increase in cooperativity with increase in SAM concentration, respectively. The decrease in the affinity with the increase in

SAM concentration indicates co-operative modulation of HSCOMT activity by SAM (Liu *et al.,* 2008).

Conversely, the Hill coefficient does not change with changes in $MgCl_2$ concentration from 1 to 10 mM, suggesting that Mg^{2+} does not have a co-operative modulatory effect on HSCOMT (Table 5.2). Attempts to increase the $MgCl_2$ concentration beyond 10 mM caused precipitation of the reaction mixture.

The concurrent occurrence of dimerization and co-operativity during the kinetic study with incubation (1 h, 30°C) and also in the absence of all of these features when 60 μM gold and/or silver NPs were present suggests that the NPs influence the HSCOMT activity through hindering the enzyme's dimerization.

Subunit interchange as a consequence of domains swap in HSCOMT (Ehler *et al.,* 2014; Law *et al.,* 2016), the presence of allosteric (sigmoidal) kinetics as reported by Ball *et al.,* (1971) and Dawling *et al.,* (2001), and also the currently observed variations in reactivities of the monomer and dimer, are indicative that this enzyme is possibly controlled by a morpheein mechanism. Morpheeins are homo-oligomeric proteins whose function is controlled through reversible transitions between alternate structural assemblies and resultant activities. These proteins can deviate from the classical Michaelis-Menten kinetics and provide a structural basis for allosteric regulations. The oligomer disassembly process distinguishes the morpheein model of allostery from the classic Koshland and Monod-Wyman-Changeux models of allostery (Lawrence and Jaffe, 2008; Jaffe and Lawrence, 2012). Trapping of the alternate conformations by compounds or materials such as gold and/or silver NPs could therefore provide a novel mechanism for the modulation of HSCOMT enzymatic activity.

Although there is no stand alone technique to determine the NPs-protein interactions (Li*et al.,* 2010), analytical strategies such as absorbance, fluorescence and Fourier transform infrared spectroscopy (FTIR) spectroscopy and also *in silico* analysis such as molecular docking studies, provide valuable insight of the interactions.

Incubation of gold and/or silver NP with increasing amounts (0-80 μg/ml) of HSCOMT, afforded visible colour changes of the gold and silver NPs; indicating plasmonic changes, caused by the formation of NPs-HSCOMT corona. The absorbance spectroscopy analyses showed a HSCOMT concentration-dependent red shift and broadening of both gold and silver NPs plasmonic absorption peaks, indicating the direct adsorption of HSCOMT onto the surface of gold and silver NPs, and the formation of both AuNPs-HSCOMT and AgNPs-HSCOMT coronas (Rahman, *et al.,* 2013).

For the fluorescence spectroscopy studies, the HSCOMT (5 μg/ml) was incubated with increasing concentrations (0-60 μM) of gold and/or silver NPs. The fluorescence, with an excitation wavelength at 295 nm selectively excited the tryptophan residues in the HSCOMT (McGuinness *et al.,* 2005), and the observed fluorescence was emitted by tryptophan. HSCOMT has two tryptophan residues, Trp38 and Trp143, with only the latter being at the surface and readily quenched in the folded HSCOMT (Rutherford *et al.,* 2008a). The fluorescence quenching analyses revealed that both gold and silver NPs quenched HSCOMT fluorescence via a static quenching mechanism. This was evident from the decrease in the Stern-Volmer quenching constant (K_{sv}) with the increase in interaction temperatures for both gold and silver NPs with HSCOMT. This suggests the formation of a non-fluorescent NP–fluorophore complex at the ground state (Al-Kady *et al.,* 2011; Adeyemi and Whiteley, 2014). Comparable results were reported in our research group (Adeyemi and Whiteley, 2014) and other researchers (Garabagiu,

2011; Mariam *et al.,* 2011; Dasgupta *et al.,* 2016) for the Stern-Volmer analysis of the interaction between gold and silver NPs with proteins.

The fraction of exposed Trp residues (fluorophore), (θ), and number of binding site(s) (n) were each equivalent to one ($\theta \approx 1$ and $n \approx 1$) for the quenching of HSCOMT by both gold and silver NPs, suggesting NPs had access to a single Trp residue during the quenching, viz Trp143. This Trp residue forms part of the catecholic substrate pocket during catalysis (Bonifácio *et al.,* 2007), and the contact between the NPs and this amino acid residue could therefore affect the catalytic activity of the enzyme. Although without structural assignment (Rutherford *et al.,* 2008b, Ehler *et al.,* 2014), Trp143 is adjacent to Lys144 (Rutherford *et al.,* 2008b) and the latter is part of ß5/ß9 loop which is involved in domain swap, leading to the formation of HSCOMT dimer (Law *et al.,* 2014). Consequently the interaction of gold and/or silver NPs with Trp143 could possibly change the microenvironment of ß5/ß9 hinge, and consequently obstruct the dimerization.

Further fluorimetric analyses indicated a decrease in binding affinity with increasing interacting temperatures for both interactions of gold and silver NPs with HSCOMT, suggesting that the interactions between the NPs and HSCOMT are exothermic. Similarly, thermodynamic analyses for the interactions of HSCOMT with gold and silver NPs signified that both interactions are exothermic, and therefore thermodynamically favourable. This was confirmed by the negative values of the Gibbs free energy (ΔG) for the interactions. The positive values of the entropy (ΔS) and the negative values of the enthalpy (ΔH) for the interactions of both gold and silver NPs suggested that both interactions are driven by electrostatic interactions.

Fourier transform infrared (FTIR) spectroscopic studies indicated that the adsorption of HSCOMT onto both gold and silver NPs surfaces caused a vibrational shift of the amide I band,

signifying that the HSCOMT adsorption onto both gold and silver NPs surfaces caused relaxation of ß-sheet structures of the HSCOMT enzyme protein. Because the domain swap mechanism in HSCOMT involves swapping of ß-sheets structures (ß6/ß7 and ß5/ß9) leading to the formation of dimers (and higher oligomers) (Law *et al.,* 2016), relaxation of HSCOMT ß-sheets caused by the adsorption of the enzyme onto the surfaces of the NPs, again suggests an effect on the enzyme's domain swap mechanism, and hence, the prevention of dimerization.

Our molecular docking study disclosed that fourteen and six amino acid residues, respectively, are involved in the interaction of AuNP and AgNP, with HSCOMT. The binding distances of these amino acids with their respective NPs surfaces are less than 3.5 Å, indicating strong interactions between the amino acids and gold/silver NPs. Two out of the fourteen residues from HSCOMT interaction with AuNPs are hydrophobic, while the remaining twelve are hydrophilic amino acids. All the amino acids from the interaction of HSCOMT with AgNPs are hydrophilic. The docking study reveals a positive free energy for the AuNPs-HSCOMT interaction and a negative free energy for AgNPs-HSCOMT interaction, implying a non-spontaneous and spontaneous interaction, respectively. The non-spontaneity of AuNPs-HSCOMT interaction is, most probably, caused by the involvement of the two hydrophobic amino acid residues in the interaction. The variations between experimentally determined and computer modelled interaction are, most likely, due to the presence of stabilisers (citrate and PVP) on the surfaces of gold and silver NPs with respect to the thermodynamic results (Gnanadhas *et al.,* 2013). These stabilisers were omitted during the computer simulations.

From this study, it was observed that gold and silver NPs had concentration dependent inhibitory effects on the catalytic activity of HSCOMT. The dimerization and co-operativity during the kinetic study and absence of all these features when 60 μM gold and/or silver NPs were present

suggest that the NPs inhibit the HSCOMT activity through obstructing enzyme dimerization, which is indicating the potentials of NPs for controlling HSCOMT activity.

7.2 Future perspectives

Recently, investigations of NP–protein interactions using nuclear magnetic resonance (NMR) spectroscopy (Assfalg *et al.,* 2016) and x-ray crystallography (Kowalski *et al.,* 2016) have been reported. Investigation on the interaction of gold/silver NPs with HSCOMT with NMR spectroscopy would provide information at the NPs-carbon/proton levels. The X-ray crystallographic studies could reveal the exact crystal arrangements of gold/silver NPs-HSCOMT corona (Kowalski *et al.,* 2016).

Because of our technical limitations, the assessment of the effects of gold/silver NPs on the catalytic activity of the HSCOMT monomer and dimer separately, could not be determined. Such assay could provide further insights on the effects of the particles on HSCOMT.

In consideration of the effects of other metallic NPs, such as platinum (Sennuga *et al.,* 2012) on the biological activity of proteins, it would be valuable, for comparison, to investigate the effects of other types of NPs on HSCOMT.

Considering the complexity of living systems, *in vitro* data alone are insufficient to elucidate the effects on live cells/tissues. Consequently an *in vivo* study, using animal models and/or cell lines, on the effects of gold/silver NPs on the catalytic activity of SCOMT is therefore worthwhile once mechanisms are better understood and safety concerns are addressed.

Although the toxicity of metallic NPs has been extensively evaluated, the inconsistent nature of the reports calls for toxicity assessments of metallic NPs prior to any biological applications.

References

Aaij, C. and Bors, P. (1972): The gel electrophoresis of DNA. *Biochimica et Biophysica Acta,* **269:** 197–200.

Adeyemi, O. S. and Whiteley, C. G. (2013): Interaction of nanoparticles with arginine kinase from *Trypanosoma brucei*: Kinetic and mechanistic evaluation. *International Journal of Biological Macromolecules,* **62:** 450–456.

Adeyemi, O. S. and Whiteley, C. G. (2014): Interaction of metal nanoparticles with recombinant arginine kinase from *Trypanosoma brucei*: Thermodynamic and spectrofluorimetric evaluation. *Biochimica et Biophysica Acta,* **1840:** 701–706.

Aggarwal, P., Hall, J. B., McLeland, B. C., Dobrovolskaia, M A. and McNeil, S. E. (2009): Nanoparticle interaction with plasma proteins as it relates to particle biodistribution, biocompatibility and therapeutic efficacy. *Advanced Drug Delivery Reviews,* **61(6):** 428–437.

Ahlberg, S., Antonopulos, A., Diendorf, J., Dringen, R., Epple, M., Flock, R., Goedecke, W., Graf, C., Haberl, N., Helmlinger, J., Herzog, F., Heuer, F., Hirn, S., Johannes, C., Kittler, S., Koller, M., Korn, K., Kreyling, W. G., Krombach, F., Lademann, J., Loza, K., Luther, E. M., Malissek, M., Meinke, M. C., Nordmeyer, D., Pailliart, A., Raabe, J., Rancan, F., Rothen-Rutishauser, B., Ruhl, E., Schleh, C., Seibel, A., Sengstock, C., Treuel, L., Vogt, A., Weber, K. and Zellner, R. (2014): PVP-coated, negatively charged silver nanoparticles: A multi-center study of their physicochemical characteristics, cell culture and in vivo experiments. *Beilstein Journal Nanotechnology,* **5:** 1944–1965.

Akinyemi, R. O. (2012): Epidemiology of Parkinsonism and Parkinson's disease in Sub-Saharan Africa: Nigerian profile. *Journal of Neurosciences in Rural Practice,* **3(3):** 233–4.

Alazizi, A., Liu, M.-Y., Williams, F. E., Kurogi, K., Sakakibara, Y., Suiko, M. and Liu, M.-C. (2011): Identification, characterization, and ontogenic study of a catechol *O*-methyltransferase from Zebrafish. *Aquatic Toxicology,* **102(1-2):** 18–23.

Alexander, J. W. (2009): History of the medical use of silver. *Surgical Infections,* **10(3):** 289–292.

Al-Kady, A. S., Geber, M., Hussein, M. M., and Ebeida, E. M. (2011): Structural and fluorescence quenching characterisation of hematite nanoparticles. *Spectrochimica Acta Part A,* **83:** 398–405.

Annerbrink, K., Westberg, L., Nilsson, S., Rosmond, R., Holm, G. and Eriksson, E. (2008): Catechol *O*-methyltransferase val158-met polymorphism is associated with abdominal obesity and blood pressure in men. *Metabolism Clinical and Experimental,* **57:** 708–711.

Antony, P. M. A., Diederich, N. J., Kruger, R. and Balling, R. (2013): The hallmarks of Parkinson's disease. *FEBS Journal,* **280:** 5981–5993.

Arrondo, J. L. R., Muga, A., Castresana, J. and Goñi, F. M. (1993): Quantitative studies of the structure of proteins in solution by Fourier-Transform Infrared Spectroscopy. *Progress in Biophysics and Molecular Biology*, **59:** 23–56.

Artimo, P., Jonnalagedda, M., Arnold, K., Baratin, D., Csardi, G., de Castro, E., Duvaud, S., Flegel, V., Fortier, A., Gasteiger, E., Grosdidier, A., Hernandez, C., Ioannidis, V., Kuznetsov, D., Liechti, R., Moretti, S., Mostaguir, K., Redaschi, N., Rossier, G., Xenarios, I. and Stockinger, H. (2012): ExPASy: SIB bioinformatics resource portal. *Nucleic Acids Research*, **40:** (Web Server issue) W597–W603.

Ashwini, M., Murugan, S. B., Balamurugan, S. and Sathishkumar, R. (2016): Advances in Molecular Cloning. *Molecular Biology,* **50(1):** 1–6.

Assfalg, M., Ragona, L., Pagano, K., D'Onofrio, M., Zanzoni, S., Tomaselli, S. and Molinar, H. (2016): The study of transient protein–nanoparticle interactions by solution NMR spectroscopy. *Biochimica et Biophysica Acta,* **1864** 102–114.

Axelrod, J. (1966): Methylation reactions in the formation and metabolism of catecholamines and other biogenic amines. *Pharmacological Reviews,* **18 (1):** 95–113.

Axelrod, J. and Tomchick, R. (1958): Enzymatic *O*-methylation of epinephrine and other catechols. *Journal of Biological Chemistry,* **233:** 697–701.

Azimi, O., Emami, Z., Salari, H. and Chamani, J. (2011): Probing the interaction of human serum albumin with norfloxacin in the presence of high-frequency electromagnetic fields: fluorescence spectroscopy and circular dichroism investigations. *Molecules,* **16:** 9792–9818.

Bäckström, R., Honkanen, E., Pippuri, A., Kairisalo, P., Pystynen, J., Heinola, K., Nissinen, E., Linden, I. B., Männistö, P. T. and Kaakkola, S. (1989): Synthesis of some novel potent and selective catechol *O*-methyltransferase inhibitors. *Journal of Medicinal Chemistry,* **32:** 841–846.

Baeshen, N. M., Al-Hejin, A. M., Bora, R. S., Ahmed, M. M. M., Ramadan, H. A. I., Saini, K. S., Baeshen, N. A. and Redwan E. M (2015): Production of Biopharmaceuticals in E. coli: Current Scenario and Future Perspectives. *Journal of Microbiology and Biotechnology,* **25(7):** 953–962.

Bahadar, H., Maqbool, F., Niaz, K. and Abdollahi, M. (2016): Toxicity of nanoparticles and an overview of current experimental models. *Iranian Biomedical Journal,* **20(1):** 1-11.

Bailey, T. L. and Elkan, C. (1994): Fitting a mixture model by expectation maximization to discover motifs in biopolymers. *Proceedings of the Second International Conference on Intelligent Systems for Molecular Biology*, p. 28–36.

Bailey, T. L., Boden, M., Buske, F. A., Frith, M., Grant, C. E., Clementi, L., Ren, J., Li, W. W. and Noble, W. S. (2009): MEME SUITE: tools for motif discovery and searching. *Nucleic Acids Research,* **37:** W202–W208.

Balasubramanian, S. K., Yang, L., Yung, L. L.-Y., Ong, C.-N., Ong, W.-Y. and Yu, L. E. (2010): Characterization, purification, and stability of gold nanoparticles. *Biomaterials,* **31:** 9023–9030.

Ball, P., Knuppen, R. and Breuer, H. (1971): Purification and properties of catechol *O*-methyltransferase of human liver. *European Journal of Biochemistry,* **21:** 517–525.

Ball, P., Knuppen, R., Haupt, M. and Breuer, H. (1972): Kinetic properties of a soluble catechol *O*-methyltransferase of human liver. *European Journal of Biochemistry,* **26:** 560–569.

Ballet, T., Boulange, L., Brechet, Y., Bruckert, F. and Weidenhaupt, M. (2010): Protein conformational changes induced by adsorption onto material surfaces: an important issue for biomedical applications of material science. *Bulletin of the Polish Academy of Sciences,* **58(2):** 303–315.

Banerjee, V. and Das, K. P. (2013): Interaction of silver nanoparticles with proteins: A characteristic protein concentration dependent profile of SPR signal. *Colloids and Surfaces B: Biointerfaces,* **111:** 71–79.

Barker, A. B., Parmarb, M., Kirkeby, A., Bjorklund, A., Thompsonc, L. and Brundin, P. (2016): Are Stem Cell-Based Therapies for Parkinson's Disease Ready for the Clinic in 2016? *Journal of Parkinson's Disease,* **6:** 57–63.

Barré-Sinoussi, F. and Montagutelli, F. (2015): Animal models are essential to biological research: issues and perspectives. *Future Science,* **1(4):** FSO63.

Benabid, A. L. (2003): Deep brain stimulation for Parkinson's disease. *Current Opinion in Neurobiology,* **13:** 696–706.

Benabid, A. L., Chabardes, S., Mitrofanis, J. and Pollak, P. (2009): Deep brain stimulation of the subthalamic nucleus for the treatment of Parkinson's disease. *Lancet Neurology,* **8:** 67–81.

Bennett, M. J., Schlunegger, M. P. and Eisenberg, D. (1995): 3D Domain swapping: A mechanism for oligomer assembly. *Protein Science,* **4:** 2455−2468.

Berg, J. M., Tymoczko, J. L. and Stryer, L. (2002): *The purification of proteins is an essential first step in understanding their function.* Biochemistry 5th edition. New York: W H Freeman.

Berg, J. M., Tymoczko, J. L. and Stryer, L. (2002a): *The Michaelis-Menten Model Accounts for the Kinetic Properties of Many Enzymes* In Biochemistry.5thedition. New York: WH Freeman.

Berg, J. M., Tymoczko, J. L. and Stryer, L. (2002b): *Appendix: V_{max} and K_m can be determined by double-reciprocal plots In Biochemistry.*5thedition. New York: WH Freeman.

Bertocci, B., Miggiano, V., Da Prada, M., Dembic, Z., Lahm, H.- W. and Malherbe, P. (1991): Human catechol *O*-methyltransferase: cloning and expression of the membrane-associated form. *Proceedings of the National Academy of USA,* **88:** 1416–1420.

Betke, A. and Kickelbick, G. (2014): Bottom-up, wet chemical technique for the continuous synthesis of inorganic nanoparticles. *Inorganics,* **2:** 1–15.

Biener, J., Wittstock, A., Baumann, T. F., Weissmüller, J., Bäumer, M. and Hamza, H. (2009): Surface Chemistry in Nanoscale Materials. *Materials,* **2:** 2404–2428.

Birkmayer, W. and Hornykiewicz, O. (1961): The L-3,4-dioxyphenylalanine (DOPA)-effect in Parkinson-akinesia. *Wien Klin Wochenschr,* **73:**787–788.

Bisswanger, H. (2008): *Enzyme Kinetics Principles and Methods*, 2nd ed. Wiley - VCH, Weinheim. p 75–76.

Bisswanger, H. (2014): Enzyme assays. *Perspectives in Science,* **1:** 41–55.

Blanco, S. and Frye, M. (2014): Role of RNA methyltransferases in tissue renewal and pathology. *Current Opinion in Cell Biology,* **31:** 1–7.

Blin, J., Dubois, B., Bonnet, A. M., Vidailhet, M., Brandabur, M. and Agid, Y. (1991): Does ageing aggravate parkinsonian disability? *Journal of Neurology, Neurosurgery, and Psychiatry,* **54:** 780–782.

Block, H., Maertens, B., Spriestersbach, A., Brinker, N., Kubicek, J., Fabis, R., Labahn, J. and Schäfer, F. (2009): Immobilized-Metal Affinity Chromatography (IMAC): A Review. *Methods in Enzymology,* **463:** 439–473.

Blum, K., Badgaiyan, R., Agan, G., Fratantonio, J. and Gold, M. S. (2014): Reward deficiency syndrome (RDS): Is there a solution? *Drug and Alcohol Dependence,* **2:** 5.

Bonifácio, M. J., Palma, P. N., Almeida, L. and Soares-da-Silva, P. (2007): Catechol *O*-methyltransferase and its Inhibitors in Parkinson's Disease. *CNS Drug Reviews,* **13(3):** 352–379.

Bonifácio, M. J., Archer, M., Rodrigues, M. L., Matias, P. M., Learmonth, D. A., Carrondo, M. A. and Soares-da-Silva, P. (2002): Kinetics and crystal structure of catechol *O*-methyltransferase complex with cosubstrate and a novel inhibitor with potential therapeutic application. *Molecular Pharmacology,* **62:** 795–805.

Bonifácio, M. J., Vieira-Coelho, M. A. and Soares-da-Silva, P. (2001): Expression and characterization of rat soluble catechol *O*-methyltransferase fusion protein. *Protein Expression and Purification,* **23:** 106–112.

Borchardt, R. T. and Cheng, C. F. (1978): Purification and characterization of rat heart and brain catechol *O*-methyltransferase. *Biochimica et Biophysica Acta,* **522(1):** 49–62.

Bornhorst, J. A. and Falke, J. J. (2000): purification of proteins using polyhistidine affinity tags. *Methods in Enzymology,* **326:** 245–254.

Bradford, M. M. (1976): A rapid and sensitive method for quantitation of microgram quantities of protein utilizing the principle of protein-dye-binding. *Analytical Biochemistry,* **72:** 248–254.

Brancolini, G., Kokh, D. B., Calzolai, L., Wade, R. C. and Corni, S. (2012): Docking of ubiquitin to gold nanoparticles. *ACS Nano,* **6(11):** 9863–9878.

Canaveras, R. F., Madueno, R., Sevilla, J. M., Blázquez, M. and Pineda, T. (2012): Role of the functionalization of the gold nanoparticle surface on the formation of bioconjugates with human serum albumin. *Journal of Physical Chemistry C,* **116:** 10430–10437.

Cárdenas, M. L. (2015): Understanding mechanisms of enzyme co-operativity: the importance of not being at equilibrium. *Perspectives in Science*, **4:** 10–16.

Caudle, W. M., Guillot, T. S., Lazo, C. R. and Miller, G. W. (2012): Industrial toxicants and Parkinson's disease. *Neurotoxicology*, **33(2):** 178–188.

Chakraborti, S., Joshi, P., Chakravarty, D., Shanker, V., Ansari, Z. A., Singh, S. P. and Chakrabarti, P. (2012): Interaction of polyethyleneimine-functionalized ZnO nanoparticles with Bovine Serum Albumin. *Langmuir,* **28:** 11142−11152.

Charan, R. A. and LaVoie, M. J. (2015): Pathologic and therapeutic implications for the cell biology of Parkin. *Molecular and Cellular Neuroscience*, **66:** 62–71.

Chaudhary, A., Gupta, A., Khan, S. and Nandi, C. K. (2014): Morphological effect of gold nanoparticles on the adsorption of bovine serum albumin. *Physical Chemistry Chemical Physics,* **16:** 20471–20482.

Chen, C. Y., Zhao, B. and Wang, Z. W. (2010): Interaction of thiacloprid with bovine hemoglobin using spectroscopic and molecular modeling methods. *Spectroscopy,* **24:** 559–566.

Chen, R. (2012): Bacterial expression systems for recombinant protein production: *E. coli* and beyond. *Biotechnology Advances,* **30:** 1102–1107.

Cheung, R. C. F., Wong, J. H. and Ng, T. (2012): Immobilized metal ion affinity chromatography: a review on its applications. *Applied Microbiology and Biotechnology,* **96:** 1411–1420.

Chibber, S. and Ahmad, I. (2016): Molecular docking, a tool to determine interaction of CuO and TiO2 nanoparticles with human serum albumin. *Biochemistry and Biophysics Reports,* **6:** 63–67.

Cohen, H., Neumann, L., Glazer, Y., Ebstein, R. P. and Buskila, D. (2009): The relationship between a common catechol *O*-methyltransferase (COMT) polymorphism val158met and fibromyalgia. *Clinical and Experimental Rheumatology,* **27:** S51–S56.

Cookson, M. R. (2012): Parkinsonism due to mutations in PINK1, Parkin, and DJ-1 and oxidative stress and mitochondrial pathways. *Cold Spring Harbor Perspectives in Medicine,* **2:** a009415.

Corti, O., Lesage, S. and Brice, A. (2011): What genetics tells us about the causes and mechanisms of Parkinson's disease. *Physiological Reviews,* **91:** 1161–1218.

Costa, S., Almeida, A., Castro, A. and Domingues, L. (2014): Fusion tags for protein solubility, purification and immunogenicity in: the novel Fh8 system. *Frontiers Microbiology,* **5(63):** 1–20.

Cotton, N. J., Stoddard, B. and Parson, W. W. (2004): Oxidative inhibition of human soluble catechol *O*-methyltransferase. *Journal of Biological Chemistry,* **279 (22):** 23710–23718.

Coward, J. K., Slixz, E. P. and Wu, F. Y. (1973): Kinetic studies on catechol *O*-methyltransferase: Product inhibition and the nature of the catechol binding site. *Biochemistry,* **12:** 2291−2297.

Crout, J .R. (1961): Inhibition of catechol *O*-methyl transferase by pyrogallol in the rat. *Biochemical Pharmacology,* **6:** 47–50.

Cunningham, A. and Bürgi T. (2013): Bottom-up organisation of metallic nanoparticles. *Nano-Optics and Nanophotonics,* **2:** 1–37.

Cutler, P. (2004): *Methods in Molecular Biology, volume 244: Protein Purification Protocols: Second Edition.* Humana Press Inc., Totowa, NJ

Darmenton, P., Cronenberger, L. and Pachéco, H. (1976): Purification and properties of rat kidney catechol *O*-methyltransferase. *Biochimie,* **58(9):** 1031–1045.

Dasgupta, N., Ranjan, S., Patra, D., Srivastava, P., Kumar, A. and Ramalingam, C. (2016): Bovine serum albumin interacts with silver nanoparticles with a “sideon” or “end on” conformation. *Chemico-Biological Interactions*, **253:** 100–111.

Davda, J. and Labhasetwar, V. (2002): Characterization of nanoparticle uptake by endothelial cells. *International Journal of Pharmaceutics,* **233:** 51–59.

Davis, T. L. (1998): Catechol *O*-Methyltransferase Inhibitors in Parkinson’s Disease. *CNS Drugs,* **10(4):** 239–246.

Dawling, S., Noodi, N., Mernaugh, R. L., Wang, X. and Parl, F. F. (2001): Catechol *O*-methyltransferase (COMT)-mediated metabolism of catechol estrogens: comparison of wild-type and variant COMT isoforms. *Cancer Research*, **61:** 6716–672.

Dawson, T. M., Ko, H. S., and Dawson, V. L. (2010): Genetic animal models of Parkinson's disease. *Neuron,* **66:** 646–661.

de Lau L. M. L., and Breteler, M. M. B. (2006). Epidemiology of Parkinson's disease. *Lancet Neurology,* **5:** 525–535.

de Ruiter, A. and Oostenbrink, C. (2011): Free energy calculations of protein–ligand interactions. *Current Opinion in Chemical Biology,* **15:** 547–552.

Debeljak, N., Feldman, L., Davis, K. L., Komel, R. and Sytkowski, A. J. (2006): Variability in the Immunodetection of His-tagged Recombinant Proteins. *Analytical Biochemistry,* **359(2):** 216–223.

Delfino, I. and Cannistraro, S. (2009): Optical investigation of the electron transfer protein azurin–gold nanoparticle system. *Biophysical Chemistry,* **139:** 1–7.

Detrait, E. R., Carr, G. V., Weinberger, D. R. and Lambert, Y. (2016): Brain catechol *O*-methyltransferase (COMT) inhibition by tolcapone counteracts recognition memory deficits in normal and chronic phencyclidine-treated rats and in COMT-Val transgenic mice. *Behavioural Pharmacology,* **27(5):** 415–421.

Dhall, R. and Kreitzman, D. L. (2016): Advances in levodopa therapy for Parkinson disease. *Neurology,* **86:** S13–S24.

Dhar, K. and Rosazza, J. P. N. (2000): Purification and Characterization of *Streptomyces griseus* catechol *O*-Methyltransferase. *Applied and Environmental Microbiology,* **66(11):** 4877–4882.

Dick, F. D., De Palma, G., Ahmadi, A., Scott, N. W., Prescott, G. J., Bennett, J., Semple, S., Dick, S., Counsell, C., Mozzoni, P., Haites, N., Wettinger, S. B., Mutti, A., Otelea, M., Seaton, A., Soderkvist, P. and Felice, A. (2007): Environmental risk factors for Parkinson's disease and parkinsonism: the Geoparkinson study. *Occupational and Environmental Medicine,* **64**: 666–672.

Diederich, N. J., Moore, G. C., Leurgans, S. E., Chmura, T. A. and Goetz, C. G. (2003): Parkinson disease with old-age onset: a comparative study with subjects with middle-age onset. *Archives of neurology,* **60:** 529–533.

Docter, D., Westmeier, D., Markiewicz, M., Stolte, S., Knauer, S. K. and Stauber, R. H. (2015): The nanoparticle biomolecule corona: lessons learned – challenge accepted? *Chemical Society Reviews*, **44:** 6094–6121.

Dodel, R. C., Singer, M., Köhne-Volland, R., Szucs, T., Rathay, B., Scholz, E. and Oertel, W. H. (1998): The economic impact of Parkinson's disease. An estimation based on a 3- month prospective analysis. *Pharmacoeconomics,* **14(3):** 299–312.

Domschke, K., Deckert, J., O'Donovan, M. C. and Glatt, S. J. (2007): Meta analysis of COMT val158met in panic disorder: ethnic heterogeneity and gender specificity. *American Journal of Medical Genetics Part B,* **144:** 667–673.

Donovan, R. S., Robinson, C. W. and Glick, B R. (1996): Review: Optimizing inducer and culture conditions for expression of foreign proteins under the control of the *lac* promoter. *Journal of Industrial Microbiology,* **16:** 145-154.

Drexler, K. E. (2004): Nanotechnology: From Feynman to funding. *Bulletin of Science, Technology & Society,* **24:** 21–27.

Du, X., Li, Y., Xia, Y. L., Ai, S. M., Liang, J., Sang, P., Ji, X. L. and Liu, S. Q. (2016): Insights into Protein–Ligand Interactions: Mechanisms, Models, and Methods. *International Journal of Molecular Science,* **17(2):** 144–177.

Eaton, B. E., Gold, L. and Zichi, D. A. (1995): Let's get specific: the relationship between specificity and affinity. *Chemistry & Biology,* **2:** 633–638.

Edmundson, M. C., Capeness, M. and Horsfall, L. (2014): Exploring the potential of metallic nanoparticles within synthetic biology. *New Biotechnology*, **31(6):** 572–578.

Eftink, M. R. and Ghiron, C. A. (1981): Fluorescence quenching studies with proteins. *Analytical Biochemistry,* **114:** 199–227.

Ehler, A., Benz, J., Schlatter, D. and Rudolph, M. G. (20014): Mapping the conformational space accessible to catechol *O*-methyltransferase. *Acta Crystallographica Section D: Biological Crystallography,* **70:** 2163–2174.

Ehringer, H. and Hornykiewicz, O. (1998): Distribution of noradrenaline and dopamine (3-hydroxytyramine) in human brain: Their behaviour in extrapyramidal system diseases. *Parkinsonism and Related Disorders*, **4:** 53–57.

Eisenberg, J., Mei-Tal, G., Steinberg, A., Tartakovsky, E., Zohar, A., Gritsenko, I., Nemanov, L. and Ebstein, R, P. (1999): Haplotype relative risk study of catechol *O*-methyltransferase (COMT) and attention deficit hyperactivity disorder (ADHD): Association of the high-enzyme activity Val allele with ADHD impulsive-hyperactive phenotype. *American Journal of Medical Genetics*, **88(5):** 497–502.

Eisenhofer, G., Keiser, H., Friberg, P., Mezey, E., Huynh, T.-T., Hiremagalur, B., Ellingson, T., Duddempudi, S., Eijsbouts, A. and Lenders, J. W. M. (1998): Plasma metanephrines are markers of pheochromocytoma produced by catechol *O*-methyltransferase within tumors. *Journal of Clinical Endocrinology and Metabolism,* **83:** 2175–2185.

Ellingson, T., Duddempudi, S., Greenberg, B. D., Hooper, D. and Eisenhofer, G. (1999): Determination of differential activities of soluble and membrane-bound catechol *O*-methyltransferase in tissues and erythrocytes. *Journal of Chromatography B: Biomedical Sciences and Applications,* **729:** 347–353.

El-Sayed, R., Bhattacharya, K., Gu, Z., Yang, Z., Weber, J. K., Li, H., Leifer, K., Zhao, Y., Toprak, M. S. Zhou, R. and Fadeel, B. (2016): Single-walled carbon nanotubes inhibit the cytochrome P450 enzyme, CYP3A4. *Scientific Reports,* **6:** 21316

Erni, R., Rossell, M. D., Kisielowski, C. and Dahmen, U. (2009): Atomic-resolution imaging with a sub-50-pm electron probe. *Physical Review Letters,* **102:** 096101.

Fabian, H. and Mäntele, W. (2002): *Infrared spectroscopy of proteins. In: J.M. Chalmers and P.R. Griffiths, Editors, Handbook of Vibrational Spectroscopy*. John Wiley & Sons, Chichester, p 3399–3426.

Fairbanks, G., Steck, T. L. and Wallach, D. F. H. (1971): Electrophoretic analysis of the major polypeptides of the human erythrocyte membrane. *Biochemistry*, **10(13):** 2606–2617.

Fallon, G. R. (1962): Body temperature and fertilization in the cow. *Journal of Reproduction and Fertility,* **3:** 116–123.

Fatin, F. M. A., Kifah, A. F. A., Ikteffam, A. A., Agelmashotjafar, L. and Ban, A. A. (2013): A simple method for synthesis, purification and concentration stabilized gold nanoparticles. *International Journal of Engineering Research and Applications,* **3(6):** 21–30.

Faure, A., Calmels, C., Desjobert, C., Castroviejo, M., Caumont-Sarcos, A., Tarrago-Litvak, L., Litvak, S. and Parissi, P. (2005): HIV-1 integrase crosslinked oligomers are active *in vitro*. *Nucleic Acids Research,* **33(3):** 977–986.

Fearnley J. M. and Lees, A. J. (1991): Ageing and Parkinson's disease: substantia nigra regional selectivity. *Brain,* **114**:2283–2301.

Fei, L. and Perrett, S. (2009): Effect of nanoparticles on protein folding and fibrillogenesis. *International Journal of Molecular Sciences,* **10:** 646–655.

Femi, O. L., Ibrahim, A., and Aliyu, S. (2012): Clinical profile of parkinsonian disorders in the tropics: Experience at Kano, northwestern Nigeria. *Journal of Neurosciences in Rural Practice,* **3 (3):** 237–241.

Ferreira, L. G., dos Santos, R. N., Oliva, G. and Andricopulo, A. D. (2015): Molecular Docking and Structure-Based Drug Design Strategies. *Molecules,* **20:** 13384–13421.

Ferrell, J. E. (2009): Q & A: Cooperativity. *Journal of Biology,* **8:** 53.

Feynman, R. P. (1961): There's plenty of room at the bottom. In: Gilbert Horace D, editor. Miniaturization. New York: Reinhold; p 282–296.

Fomenko, D. E. and Gladyshev, V. N. (2002): CxxS: fold-independent redox motif revealed by genome-wide searches for thiol/disulfide oxidoreductase function. *Protein Science,* **11(10):** 2285–2296.

Francis, D. M. and Page R. (2010): Strategies to optimize protein expression in E. coli. *Current Protocols in Protein Science,* **24:** 1–29.

Freitas, R. A. (2005): What is nanomedicine? *Nanomedicine,* **1(1):** 2–9.

Fricker, S. P. (1996): Medical Uses of Gold Compounds: Past, Present and Future. *Gold Bulletin,* **29(2):** 53–60.

Friedman, J. H., Beck, J. C., Chou, K. L., Clark, G., Fagundes, C. P., Goetz, C. G., Herlofson, K., Kluger, B., Krupp, L. B., Lang, A. E., Lou, J.-S., Marsh, L., Newbould, A. and Weintraub, D. (2016): Fatigue in Parkinson's disease: report from a mutidisciplinary symposium. *Parkinson's Disease,* **2:** 15025

Frisch, A., Laufer, A., Danziger, Y., Michaelovsky, E., Leor, S., Carel, C., Stein, D., Fenig, S., Mimouni, M., Apter, A. and Weizman, A. (2001): Association of anorexia nervosa with the high activity allele of the COMT gene: A family-based study in Israeli patients. *Molecular Psychiatry,* **6:** 243–245.

Froger, A. and Hall, J. E. (2007): Transformation of plasmid DNA into E. coli using the heat shock method. *Journal of Visualized Experiments,* **6:** 253.

Gagner, J. E., Lopez, M. D., Dordick, J. S. and Siege, R. W. (2011): Effect of gold nanoparticle morphology on adsorbed protein structure and function. *Biomaterials,* **32:** 7241–7252.

Galvão, A. C. S., Krüger, R. C., Campagnolo, P. D. B., Mattevi, V., Vitolo, M. R. and Almeida, S. (2012): Association of MAOA and COMT gene polymorphisms with palatable food intake in children. *Journal of Nutritional Biochemistry,* **23:** 272–277.

Gangula, A., Podila, R., Karanam, L., Janardhana, C. and Rao, A. M. (2011): Catalytic reduction of 4- nitrophenol using biogenic gold and silver nanoparticles derived from *Brevnia rhamnoides. Langmuir,* **27(24):** 15268–15274.

Gao, M. and Skolnick, J. (2012): The distribution of ligand-binding pockets around protein-protein interfaces suggests a general mechanism for pocket formation. *Proceedings of the National Academy of Sciences,* **109(10):** 3784–3789.

Gao, X. and Dluzen, D. E. (2001): The effect of testosterone upon methamphetamine neurotoxicity of the nigrostriatal dopaminergic system. *Brain Research,* **892:** 63–69.

Garabagiu, S. (2011): A spectroscopic study on the interaction between gold nanoparticles and hemoglobin. *Materials Research Bulletin,* **46:** 2474–2477.

Gatoo, M. A., Naseem, S., Arfat, Y. A., Dar, A. M., Qasim, K. and Zubair, S. (2014): Physicochemical Properties of Nanomaterials: Implication in Associated Toxic Manifestations. *BioMed Research International,* **2014:** 498420.

Gillies, G. E., Pienaar, I. S., Vohra, S. and Qamhawi, Z. (2014): Sex differences in Parkinson's disease. *Frontiers in Neuroendocrinology,* **35:** 370–384.

Gnanadhas, D. P., Thomas, M. B., Thomas, R., Raichur, A. M. and Chakravortty, D. (2013): Interaction of silver nanoparticles with serum proteins affects their antimicrobial activity *in vivo*. *Antimicrobial Agents and Chemotherapy,* **57(10):** 4945– 4955.

Goncalves, D., Alves, G., Soares-da-Silva, P. and Falcãoa, A. (2012): Bioanalytical chromatographic methods for the determination of catechol *O*-methyltransferase inhibitors in rodents and human samples: A review. *Analytica Chimica Acta,* **710:** 17–32.

Gonzalez, M. W. and Kann, M. G. (2012): Chapter 4: Protein interactions and disease. *PLoS Computational Biology,* **8:** e1002819.

Grazulis, S., Daskevic, A., Merkys, A., Chateigner, D., Lutterotti, L., Quiros, M., Serebryanaya, N. R., Moeck, P., Downs, R. T. and LeBail, A. (2012): Crystallography Open Database (COD): an open-access collection of crystal structures and platform for world-wide collaboration. *Nucleic Acids Research*, **40:** 420–427.

Gronenborn, A. M. (2009): Protein acrobatics in pairs — dimerization via domain swapping. *Current Opinion in Structural Biology,* **19:** 39–49.

Guiot, E., Carayon, K., Delelis, O., Simon, F., Tauc, P., Zubin, E., Gottikh, M., Mouscadet, J.-F., Brochon, J.-C. and Deprez, E. (2006): Relationship between the oligomeric status of HIV-1 Integrase on DNA and enzymatic activity. *The Journal of Biological Chemistry,* **281(32):** 22707–22719.

Gulliver, P. A. and Tipton, K. F. (1978): The purification and properties of pig-liver catechol *O*-methyl transferase. *European Journal of Biochemistry,* **88:** 439–444.

Gulliver, P. A. and Tipton, K. F. (1978): The purification and properties of pig-liver catechol *O*-methyl transferase. *European Journal of Biochemistry,* **88:** 439–444.

Haasio, K., Koponen, A., Penttila, K. E. and Nissinen, E. (2002): Effects of entacapone and tolcapone on mitochondrial membrane potential. *European Journal of Pharmacology,* **453:** 21–26.

Hamm, P., Lim, M. and Hochstrasser, R. M. (1998): Structure of the amide I band of peptides measured by femto second nonlinear-infrared spectroscopy. *Journal of Physical Chemistry B,* **102:** 6123–6138.

Hanes, C. S. (1932): Studies on plant amylases: The effect of starch concentration upon the velocity of hydrolysis by the amylase of germinated barley. *Biochemical Journal,* **26(5):** 1406–1421.

Hannig, G. and Makrides, S.C. (1998): Strategies for optimizing heterologous protein expression in *Escherichia coli*. *Trends in Biotechnology,* **16:** 54–60.

Haris, P. I. (1999): Characterization of protein structure and stability using Fourier Transform Infrared spectroscopy. *Pharmacy and Pharmacology Communications*, **5:** 15–25.

Hau, H., Khanal, D., Rogers, L., Suchowerska, N., Kumar, R., Sridhar, S., McKenzie, D. and Chrzanowski, W. (2016): Dose enhancement and cytotoxicity of gold nanoparticles in colon cancer cells when irradiated with kilo- and mega-voltage radiation. *Bioengineering & Translational Medicine,* **1:** 94–102.

Heinrich, R., Meléndez-Hevia, E. and Cabezas, H. (2002): Optimization of kinetic parameters of enzymes. *Biochemistry and Molecular Biology Education,* **30:** 184–188.

Henchcliffe, C. and Beal, M. F. (2008): Mitochondrial biology and oxidative stress in Parkinson disease pathogenesis. *Nature Clinical Practice Neurology,* **4:** 600–609.

Hengen, P. (1995): Purification of His-Tag fusion proteins from *Escherichia coli. Trends in Biochemical Sciences,* **20:** 285–286.

Ho, P. W.-L., Tse, Z. H-M., Liu, H-F., Lu, S., Ho, J. W-M., Kung, M. H-W., Ramsden, D. B. and Ho, S-L. (2013): Assessment of cellular estrogenic activity based on estrogen receptor-mediated reduction of soluble-form catechol *O*-methyltransferase (COMT) Expression in an ELISA-Based System. *PLoS ONE,* **8(9):** 1–7.

Ho, Y. T., Poinard, B., Yeoa, E. L. L. and Kah, J. C. Y. (2015): An instantaneous colorimetric protein assay based on spontaneous formation of a protein corona on gold nanoparticles. *Analyst,* **140:** 1026–1036.

Hochuli, E., Bannwarth, W., Do¨beli, H., Gentz, R. and Stuber, D. (1988): Genetic approach to facilitate purification of recombinant proteins with a novel metal chelate adsorbent. *Biotechnology,* **6:** 1321–1325.

Hoda, F., Nicholl, D., Bennett, P., Arranz, M., Aitchison, K. J., AlChalabi, A., Kunugi, H., Vallada, H., Leigh, P. N., Chaudhuri, K. R. and Collier, D. A. (1996): No association between Parkinson's disease and low-activity alleles of catechol *O*-methyltransferase. *Biochemical and Biophysical Research Communications,* **228:**780–784.

Hong, P., Koza, S. and Bouvier, E. S. P. (2012): Size-exclusion chromatography for the analysis of protein biotherapeutics and their aggregates. *Journal of Liquid Chromatography & Related Technologies,* **35:** 2923–2950.

Hornykiewicz, O. (2010): A brief history of levodopa. *Journal of Neurology,* **257:** S249–S252.

Hsu, A., Yao, H.-M., Gupta, S. and Modi, N. B. (2015): Comparison of the pharmacokinetics of an oral extended-release capsule formulation of carbidopa-levodopa (IPX066) with immediate-release carbidopa-levodopa (Sinemet), sustained-release carbidopa-levodopa (Sinemet CR), and carbidopa-levodopa-entacapone (Stalevo). *Journal of Clinical Pharmacology,* **55(9):** 995–1003.

Hsu, S. L. C. and Wu, R. T. (2010): Preparation of silver nanoparticle with different particle sizes for low temperature-sintering. *In: International conference on nanotechnology biosensors.* IACSIT Press, Hong Kong, p 55–58.

Hu, E. L. and Shaw, D. T. (1999): Synthesis and assembly. In: *Nanostructure Science and Technology: A Worldwide Study*. Edited by R. W. Siegel, E. Hu, & M. C. Roco. Washington: National Science and Technology Council, p 15–34.

Huaizhi, Z. and Yuantao, N. (2000): China's Ancient Gold Drugs. *Gold Bulletin*, **34(1):** 24–39.

Huang, C.-S., Chern, H.-D., Chang, K.-J., Cheng, C.-W., Hsu, S.-M. and Shen, C.-Y. (1999): Breast cancer risk associated with genotype polymorphism of the estrogen-metabolizing genes CYP17, CYP1A1, and COMT: A multigenic study on cancer susceptibility. *Cancer Research*, **59:** 4870–4875.

Huang, X. and El-Sayed, A. M. (2010): Gold nanoparticles: optical properties and implementations in cancer diagnosis and photothermal therapy. *Journal of Advanced Research*, **1:** 13–28.

Ibarra-Hurtado, J. M., Virgen-Ortiz, A., Apolinar-Iribe, A. and Luna-Velasco, A. (2014): Control and stabilization of silver nanoparticles size using polyvinylpyrrolidone at room temperature. *Digest Journal of Nanomaterials and Biostructures*, **9(2):** 493–501.

Irvine, G. B. (1997): Size-exclusion high-performance liquid chromatography of peptides: a review. *Analytica Chimica Acta*, **352:** 387–397.

Ivy, N., Miller, M. A. and Cronin-Golomb, A. (2010): Gender differences in Parkinson's disease: Clinical characteristics and cognition. *Movement Disorders*, **25(16):** 2695–2703.

Jabs, A. (2015): Determination of secondary structure in proteins by FTIR spectroscopy, *Jena Library of Biological Macromolecules*, 1–7 (http://jenalib.leibniz-fli.de/ImgLibDoc/ftir/IMAGE_FTIR.html).

Jackson, M. and Mantsch, M. H. (1995): The use and misuse of FTIR spectroscopy in the determination of protein structure. *Critical Reviews in Biochemistry and Molecular Biology*, **30(2):** 95-120.

Jacob, F. and Monod, J. (1961): Genetic Regulatory Mechanisms in the Synthesis of Proteins. *Journal of Molecular Biology*, **3:** 318–356.

Jaffe, E. K. (2010): Morpheeins – A new pathway for allosteric drug discovery. *Open Conference Proceedings Journal*, **2010:** 1–6.

Jaffe, K. E. (2005): Morpheeins – a new structural paradigm for allosteric regulation. *Trends in Biochemical Sciences*, **30(9):** 1–8.

Jaffe, K. E. (2016): The remarkable character of porphobilinogen synthase. *Accounts of Chemical Research*, **49:** 2509−2517.

Jaffe, K. E. and Lawrence, S. H. (2012): The morpheein model of allostery: evaluating proteins as potential morpheeins. *Methods in Molecular Biology*, **796:** 217–231.

Jatana, N., Apoorva, N., Malik, S., Sharma, A. and Latha, N. (2013): Inhibitors of catechol *O*-methyltransferase in the treatment of neurological disorders. *Central Nervous System Agents in Medicinal Chemistry,* **13:** 166–194.

Jiang, J., Ganesh, T., Du, Y., Thepchatri, P., Rojas, A., Lewis, I., Kurtkaya, S., Li, L., Qui, M., Serrano, G., Shaw, R., Sun, A. and Dingledine, R. (2010): Neuroprotection by selective allosteric potentiators of the EP2 prostaglandin receptor. *Proceedings of the National Academy of Sciences USA,* **107:** 2307–2312.

Jiang, J., Oberdorster, G. and Biswas, P. (2009): Characterization of size, surface charge, and agglomeration state of nanoparticle dispersions for toxicological studies. *Journal of Nanoparticle Research,* **11:** 77–89.

Jiao, Q., Li, L., Mu, Q. and Zhang, Q. (2014): Immunomodulation of Nanoparticles in Nanomedicine Applications. *BioMed Research International,* **2014:** 426028.

Jiménez-Jiménez, F. J., Alonso-Navarro, H., García-Martín, E. and Agúndez J. A. G. (2014): *COMT* gene and risk for Parkinson's disease: a systematic review and meta-analysis. *Pharmacogenetics and Genomics,* **24:** 331–39.

Johnston, H. J., Hutchison, G., Christensen, F. M., Peters, S., Hankin, S. and Stone, V. (2010): A review of the in vivo and in vitro toxicity of silver and gold particulates: Particle attributes and biological mechanisms responsible for the observed toxicity. *Critical Reviews in Toxicology,* **40(4):** 328–346.

Jorga, K. M., Fotteler, B., Heizmann, P. and Zürcher, G. (1998): Pharmacokinetics and pharmacodynamics after oral and intravenous administration of tolcapone, a novel adjunct to Parkinson's disease therapy. *European Journal of Clinical Pharmacology,* **54:** 443–447.

Kaakkola, S. (2000): Clinical pharmacology, therapeutic use and potential of COMT Inhibitors in Parkinson's Disease. *Drugs,* **59(6):** 1233–1250.

Kaakkola, S., Mainnisto, P. T. and Nissinen. E. (1987): Striatal membrane-bound and soluble catechol *O*-methyl-transferase after selective neuronal lesions in the rat. *Journal of Neural Transmission,* **69:** 221–228.

Kahana, E., Pinder, J. C., Smith, K. S. and Gratzer, W. B. (1992): Fluorescence quenching of spectrin and other red cell membrane cytoskeletal proteins. *Biochemical Journal,* **282:** 75–80.

Kahn, K., Tollman, S., Thorogood, M., Connor, M., Garenne, M., Collinson, M. and Hundt, G. (2006): *Older adults and the health transition in Agincourt, rural South Africa: new understanding, growing complexity*. In: Cohen B, Menken J, editors. Aging in sub-Saharan Africa: recommendations for furthering research. National Research Council; Washington, District of Columbia. p 166–188.

Karayiorgou, M., Altemus, M., Galke, B. L., Goldman, D., Murphy, D. L., Ott, J. and Gogos, J. A. (1997): Genotype determining low catechol *O*-methyltransferase activity as a risk factor for obsessive-compulsive disorder. *Proceedings of the National Academy of Sciences of the United States of America,* **94:** 4572–4575.

Karling, P., Danielsson, A., Wikgren, M., Soderstrom, I. I., Del-Favero, J., Adolfsson, R. and Norrback, K.-F. (2011): The Relationship between the Val158Met Catechol *O*-Methyltransferase (COMT) Polymorphism and Irritable Bowel Syndrome. *PLoS ONE,* **6(3):** e18035.

Kathiravan, A., Renganathan R. and Anandan, S. (2009): Interaction of colloidal AgTiO2 nanoparticles with bovine serum albumin. *Polyhedron,* **28:** 157–161.

Keeney, P. M., Xie, J., Capaldi, R. A. and Bennett, J. P. (2006): Parkinson's disease brain mitochondrial complex I has oxidatively damaged subunits and is functionally impaired and misassembled. *The Journal of Neuroscience,* **26(19):** 5256 –5264.

Kelley, L. A. and Sternberg, M. J. E. (2009): Protein structure prediction on the web: a case study using the Phyre2 server. *Nature Protocols,* **4:** 363 – 371.

Keränen, T., Gordin, A., Karlsson, M., Korpela, K., Pentikäinen, P. J., Rita, H., Schultz, E., Seppälä, L. and Wikberg, T. (1994): Inhibition of soluble catechol *O*-methyitransferase and single-dose pharmacokinetics after oral and intravenous administration of entacapone. *European Journal of Clinical Pharmacology,* **46:** 151–157.

Keränen, T., Kaakkola, S., Sotaniemi, K., Laulumaa, V., Haapaniemi, T., Jolma, T., Kola, H., Ylikoski, A., Satomaa, O., Kovanen, J., Taimela, E., Haapaniemi, H., Turunen, H. and Takala, A. (2003): Economic burden and quality of life impairment increase with severity of PD. *Parkinsonism and Related Disorders,* **9(3):** 163–168.

Khan, S., Gupta, A., Chaudhary, A. and Nandia, C. K. (2014): Orientational switching of protein conformation as a function of nanoparticle curvature and their geometrical fitting. *The Journal of Chemical Physics,* **141:** 084707-1–084707-8.

Khan, Z., Al-Thabaiti, S. A., Obaid, A. Y. and Al-Youb, A. O. (2011): Preparation and characterization of silver nanoparticles by chemical reduction method. *Colloids and Surfaces B: Biointerfaces,* **82:** 513–517.

Khlebtsov, N. G. and Dykman, L. A. (2010): Optical properties and biomedical applications of plasmonic nanoparticles. *Journal of Quantitative Spectroscopy & Radiative Transfer,* **111:** 1–35.

Kiss, L. E. and Soares-da-Silva, P. (2014**):** Medicinal chemistry of catechol *O*-methyltransferase (COMT) inhibitors and their therapeutic utility. *Journal of Medicinal Chemistry,* **57(21):** 8692–8717.

Klomsiri, C., Karplus, P. A. and Poole, L. B. (2011): Cysteine-Based Redox Switches in Enzymes. *Antioxidants and Redox Signalling,* **14:** 1065–1077.

Kong, J. and Yu, S. (2007): Fourier transform infrared spectroscopic analysis of protein secondary structures. *Acta Biochimica et Biophysica Sinica,* **39(8):** 549–559.

Kowalski, A. E., Huber, T. R., Ni, T. W., Hartje, L. F., Appel, K. L., Yost, J. W., Ackerson, C. J. and Snow, C. D. (2016): Gold nanoparticle capture within protein crystal scaffolds. *Nanoscale,* **8:** 12693–12696.

Krukemeyer, M. G., Krenn, V., Huebner, F., Wagner, W. and Resch, R. (2015): History and possible uses of nanomedicine based on nanoparticles and nanotechnological progress. *Journal of Nanomedicine & Nanotechnology,* **6(6):** 1000336.

Kuhn, B. and Kollman, P. A. (2000): QM-FE and molecular dynamics calculations on catechol *O*-methyltransferase: Free energy of activation in the enzyme and in aqueous solution and regioselectivity of the enzyme-catalyzed reaction. *Journal of the American Chemical Society,* **122(11):** 2586–2596.

Kumar, T. K. S., Prasad, V.V.H. and Pandit, M.W. (1994): Origin of multiple bands of proteins on sodium dodecyl sulphate-polyacrylamide gel electrophoresis - intermolecular disulphide cross-linking due to the presence of oxidizing components in the reducing agent. *Journal of Biochemical and Biophysical Methods,* **28:** 243–247.

Kumar, T. K., Gopalakrishna, K., Prasad, V. V. and Pandit, M. W. (1993): Multiple bands on the sodium dodecyl sulfate-polyacrylamide gel electrophoresis gels of proteins due to intermolecular disulfide cross-linking. *Analytical Biochemistry,* **213:** 226–228.

Kurkela, M., Siiskonen, A., Finel, M., Tammela, P., Taskinen, J. and Vuorela, P. (2004): Microplate screening assay to identify inhibitors of human catechol *O*-methyltransferase. *Analytical Biochemistry,* **331:** 198–200.

Kurogi, K., Alazizi, A., Liu, M.-Y., Sakakibara, Y., Suiko, M., Sugahara, T. and Liu, M.-C. (2012): Concerted actions of the catechol *O*-methyltransferase and the cytosolic sulfotransferase SULT1A3 in the metabolism of catecholic drugs. *Biochemical Pharmacology,* **84(9):** 1186–1195.

Kwakye, G. F., Paoliello, M. B. M., Mukhopadhyay, M., Bowman, A. B. and Aschner, M. (2015): Manganese-induced Parkinsonism and Parkinson's Disease: Shared and distinguishable features. *International Journal of Environmental Research and Public Health,* **12:** 7519–7540.

Lachman, H. M., Morrow, B., Shprintzen, R., Veit, S., Parsia, S. S., Faedda, G., Goldberg, R., Kucherlapati, R. and Papolos, D. F. (1996): Association of codon 108/158 catechol *O*-methyltransferase gene polymorphism with the psychiatric manifestations of velo-cardio-facial syndrome. *American Journal of Medical Genetics,* **67:** 468–472.

Lachman, H. M., Nolan, K. A., Mohr, P., Saito T. and Volavka, J. (1998): Association between catechol *O*-methyltransferase genotype and violence in schizophrenia and schizoaffective disorder. *American Journal of Psychiatry,* **155:** 835–837.

Laemmli, U. K. (1970): Cleavage of Structural Proteins during the Assembly of the Head of Bacteriophage T4. *Nature,* **227(5259):** 680–685.

Lakowicz, J. R. (2006): *Principles of Fluorescence Spectroscopy.* 3rd edition. Berlin: Springer Science and Business Media, p 529–606.

Lancaster, J. Sawyer, P. R., Shepherd, D. M. and Turnbull, M. J. (1973): Effect of chronic *L*-DOPA administration on catecholamine metabolism in the rat. *British Journal of Pharmacology,* **47:** 838–842

Lanone, S., Rogerieux, F., Geys, J., Dupont, A., Maillot-Marechal, E., Boczkowski, J., Lacroix, G. and Hoet, P. (2009): Comparative toxicity of 24 manufactured nanoparticles in human alveolar epithelial and macrophage cell lines. *Particle and Fibre Toxicology,* **6:** 1–12.

Lautala, P., Ulmanen, I. and Taskinen, J. (2001): Molecular mechanisms controlling the rate and specificity of catechol *O*-methylation by Human soluble catechol *O*-Methyltransferase. *Molecular Pharmacology,* **59(2):** 393–402.

Law, B. J. C., Bennett, M. R., Thompson, M. L., Levy, C. Shepherd, S. A., Leys, D. and Micklefield, J. (2016): Effects of active-site modification and quaternary structure on the regioselectivity of catechol *O*-methyltransferase. *Angewandte Chemie International Edition,* **55:** 2683 –2687.

Lawrence, S. H. and Jaffe, E. K. (2008): Expanding the Concepts in Protein Structure-Function Relationships and Enzyme Kinetics: Teaching using Morpheeins. *Biochemistry and Molecular Biology Education,* **36(4):** 274–283.

Lees, A. J. (2002): Drugs for Parkinson's disease. *Journal of Neurology, Neurosurgery, and Psychiatry*, **73:** 607–610.

Lees, A. J., Tolosa, E. and Olanow, C. W. (2015): Four Pioneers of L-dopa Treatment: Arvid Carlsson, Oleh Hornykiewicz, George Cotzias, and Melvin Yahr. *Movement Disorders* **30(1):** 20–36.

Lehrer, S. S. (1971): Solute perturbation of protein fluorescence. The quenching of the tryptophyl fluorescence of model compounds and of lysozyme by iodide ion. *Biochemistry,* **10(17):** 3254–3263.

Lekoubou, A., Echouffo-Tcheugui, J. B. and Kengne, A. P. (2014): Epidemiology of neurodegenerative diseases in sub-Saharan Africa: a systematic review. *BMC Public Health,* **14:** 653.

Lesniak, A., Fenaroli, F., Monopoli, M. P., Aberg, C., Dawson, K. A. and Salvati, A. (2012): Effects of the presence or absence of a protein corona on silica nanoparticle uptake and impact on cells. *ACS NANO,* **6(7):** 5845–5857.

Levy, G., Schupf, N., Tang, M-X., Cote, L. J., Louis, E. D., Mejia, H., Stern, Y. and Marder, K. (2002): Combined effect of age and severity on the risk of dementia in Parkinson's disease. *Annals of Neurology,* **51:** 722–729.

Lewis, C. and Dluzen, D. E. (2008): Testosterone enhances dopamine depletion by methamphetamine in male, but not female, mice. *Neuroscience Letters,* **448:** 130–133.

Li, L., Mu, Q., Zhang, B. and Yan, B. (2010): Analytical strategies for detecting nanoparticle–protein interactions. *Analyst,* **135:** 1519–1530.

Liu, S.-W., Rajagopal, V., Patel, S. S. and Kiledjian, M. (2008): Mechanistic and kinetic analysis of the DcpS scavenger decapping enzyme. *The Journal of Biological Chemistry*, **283(24):** 16427–16436.

Liu, Y. and Eisenberg, D. (2002): 3D domain swapping: As domains continue to swap. *Protein Science,* **11:** 1285–1299.

Liz-Marzán, L. M. (2004): Nanometals: Formation and color. *Materials today,* **7(2):** 26–31.

Loggia, M. L., Jensen, K., Gollub, R. L., Wasan, A. D., Edwards, R. R. and Kong, J. (2011): The catechol *O*-methyltransferase (COMT) val158met polymorphism affects brain responses to repeated painful stimuli. *PLoS ONE,* **6(11):** e27764.

Lotta, T., Vidgren, J., Tilgmann, C., Ulmanen, I., Melen, K., Julkenen, I. and Taskinen, J. (1995): Kinetics of human soluble and membrane-bound catechol *O*-methyltransferase: A revised mechanism and description of the thermolabile variant of the enzyme. *Biochemistry,* **34:** 4202–4210.

Loureiro, A. I., Bonifácio, M. J., Fernandes-Lopes, C., Almeida, L., Wright, L. C. and Soares-Da-Silva, P. (2006): Human metabolism of nebicapone (BIA 3-202), a novel catechol *o*-methyltransferase inhibitor: characterization of *in vitro* glucuronidation. *Drug Metabolism and Disposition,* **34(11):** 1856–1862.

Lücking, C. B., Dürr, A., Bonifati, V., Vaughan, J., De Michele, G., Gasser, T., Harhangi, B. S., Meco, G., Denèfle, P., Wood, N. W., Agid, Y. and Brice, A. for the French Parkinson's Disease Genetics Study Group and European Consortium on Genetic Susceptibility in Parkinson's Disease. (2000): Association between early-onset Parkinson's disease and mutations in the parkin gene. *The New England Journal of Medicine,* **342(21):** 1560–1567.

Lundström, K., Salminen, M., Jalanko, A., Savolainen, R. and lmanen, I. (1991): Cloning and characterization of human placental catechol *O*-methyltransferase cDNA. *DNA and Cell Biology,* **10(3):** 181–189.

Lundström, K., Tenhunen, J., Tilgmann, C., Karhunen, T., Panula, P. and Ulmanen, I. (1995): Cloning, expression and structure of catechol *O*-methyltransferase. *Biochimica et Biophysica Acta,* **1251:** 1–10.

Lundström, K., Tilgmann, C., Peränen, J., Kalkkinen, N. and Ulmanen, I. (1992): Expression of enzymatically active rat liver and human placental catechol *O*-methyltransferase in *Escherichia coli*; purification and partial characterization of the enzyme. *Biochimica et Biophysica Acta*, **1129:** 149–154.

Ma, J., Wang, Z. and Wang, L. W. (2015): Interplay between plasmon and single-particle excitations in a metal nanocluster. *Nature Communication,* **(10107):** 1–11.

Ma, Z., Liu, H. and Wu, B. (2013): Structure-based drug design of catechol *O*-methyltransferase inhibitors for CNS disorders. *British Journal of Clinical Pharmacology,* **77(3):** 410–420.

Makrides, S. C. (1996): Strategies for achieving high-level expression of genes in *Escherichia coli*. *Microbiological Reviews,* **60(3):** 512–538.

Mannisto, P. T. and Kaakkola, S. (1990): Rationale for selective COMT inhibitors as adjuncts in the drug treatment of Parkinson's disease. *Pharmacology and Toxicology,* **66:** 317-323.

Mannisto, P. T. and Kaakkola, S. (1999): Catechol *O*-methyltransferase (COMT): Biochemistry, Molecular Biology, Pharmacology, and Clinical Efficacy of the New Selective COMT Inhibitors. *Pharmacological Reviews,* **51:** 593–628.

Mannisto, P. T., Tuomainen, P. and Tuominen, R. K. (1992): Different in vivo properties of three new inhibitors of catechol *O*-methyltransferase in the rat. *British Journal of Pharmacology,* **105:** 569−574.

Mariam, J., Dongre, P. M. and Kothari, D. C. (2011): Study of interaction of silver nanoparticles with bovine serum albumin using fluorescence spectroscopy. *Journal of Fluorescence,* **21:** 2193–2199.

Martin, J. L. and McMillan, F. M. (2002): SAM (dependent) I AM: the S-adenosylmethionine-dependent methyltransferase fold. *Current Opinion in Structural Biology,* **12:** 783–793.

Masri, M. S., Robbins, D. J., Emerson, O. H. and Deeds, F. (1964): Selective *para-* or *meta-O*-methylation with catechol *O*-methyltransferase from rat liver. *Nature,* **202:** 878 –879.

Massano, J., and Bhatia, K. P. (2012): Clinical approach to Parkinson's disease: features, diagnosis, and principles of management. *Cold Spring Harbor Perspectives in Medicine* **2:** a008870.

McFarland, A. D., Haynes, C. L., Mirkin, C. A., Van Duyne, R. P. and Godwin, H. A. (2004): Color my nanoworld. *Journal of Chemical Education,* **81:** 544A.

McGuinness, C. D., Sagoo, K., McLoskey, D. and Birch, D. J. S. (2005): Selective excitation of tryptophan fluorescence decay in proteins using a subnanosecond 295 nm light-emitting diode and time-correlated single-photon counting. *Applied Physics Letters,* **86(26):** 261911-1–261911-3.

McNamara, K. and Tofail, S. A. M. (2016): Nanoparticles in biomedical applications. *Advances in Physics: X,* **2(1):** 54–88.

McNulty, D. E., Claffee, B. A., Huddleston, M. J. and Kane J. F. (2003): Mistranslational errors associated with the rare arginine codon CGG in *Escherichia coli*. *Protein Expression and Purification,* **27:** 365–374.

MedlinePlus (National Library of Medicine (US)) (2015): Substantia nigra and Parkinson disease, (available online at https://medlineplus.gov/ency/imagepages/19515.htm). Accessed on 12/02/2017.

Mehanna, R. and Lai, E. C. (2013): Deep brain stimulation in Parkinson's disease. *Translational Neurodegeneration,* **2:** 22.

Meng, X. Y., Zhang, H. X., Mezei, M. and Cui, M. (2011): Molecular docking: A powerful approach for structure-based drug discovery. *Computer-Aided Drug Design,* **7:** 146–157.

Meredith, G. E. and Rademacher, D. J. (2011): MPTP Mouse Models of Parkinson's Disease: An Update. *Journal of Parkinson's Disease,* **1(1):** 19–33.

Michaelis, L. and Menten, M. L. (1913): Die Kinetik der Invertinwirkung. *Biochemische Zeitschrift,* **49:** 333–369

Monopoli, M. P., Walczyk, D., Campbell, A., Elia, G., Lynch, I., Baldelli-Bombelli, F. and Dawson, K. A. (2011): Physical–chemical aspects of protein corona: relevance to *in vitro* and *in vivo* biological impacts of nanoparticles.*Journal of the American Chemical Society,* **133:** 2525–2534.

Montagu, K. A. (1957): Catechol compounds in rat tissues and in brains of different animals. *Nature,* **180:** 244-5.

Moon, H. E. and Sun, Paek, H. (2015): Mitochondrial Dysfunction in Parkinson's disease. *Experimental Neurobiology,* **24(2):** 103–116.

Moradi, M., Divsalar, A., Saboury, A. A., Ghalandari, B. and Harifi, A. R. (2015): Inhibitory effects of deferasirox on the structure and function of bovine liver catalase: a spectroscopic and theoretical study. *Journal of Biomolecular Structure and Dynamics,* **33(10):** 2255–2266.

Morello, F. and Partanen, J. (2015): Diversity and development of local inhibitory and excitatory neurons associated with dopaminergic nuclei. *FEBS Letters,* **589:** 3693–3701.

Morris, G. M., Huey, R., Lindstrom, W., Sanner, M. F., Belew, R. K., Goodsell, D. S. and Olson, A. J. (2009): AutoDock4 and AutoDockTools4: Automated docking with selective receptor flexibility. *Journal of Computational Chemistry,* **30:** 2785–279.

Müller-Enoch, D., Seidel, E. and Thomas, H. (1976): 6,7-Dihydroxycoumarin (Aesculetin) as a substrate for catechol *O*-methyltransferase. *Zeitschrift für Naturforschung C*, **31:** 280–284.

Munishkina, L. A. and Fink, A. L. (2007): Fluorescence as a method to reveal structures and membrane-interactions of amyloidogenic proteins. *Biochimica et Biophysica Acta*, **1768:** 1862–1885.

Nadanaciva, S., Rana, P., Beeson, G. C., Chen, D., Ferrick, D. A., Beeson, C. C. and Will, Y. (2012): Assessment of drug-induced mitochondrial dysfunction via altered cellular respiration and acidification measured in a 96-well platform. *Journal of Bioenergetics and Biomembranes,* **44:** 421–437.

Nagahara, N. (2011): Intermolecular disulfide bond to modulate protein function as a redox-sensing switch. *Amino Acids,* **41:** 59–72.

Nair, P. S. (2014): Population aging in sub-Saharan Africa: present and prospects. *Gerontechnology,* **13(1):** 11–15.

NCBI Resource Coordinators (2016): Database resources of the National Center for Biotechnology Information. *Nucleic Acids Research,* **44:** D7–D19.

Netto, C. G. C. M., da Silva, D. G., Toma, S. H., Andrade, L. H., Nakamura, M., Araki, K. and Toma, H. E. (2016): Bovine glutamate dehydrogenase immobilization on magnetic nanoparticles: conformational changes and catalysis. *RSC Advances,* **6:** 12977–12992.

Nishimori, H., Kondoh, M., Isoda, K., Tsunoda, S., Tsutsumi, Y. and Yagi, K. (2009): Silica nanoparticles as hepatotoxicants. *European Journal of Pharmaceutics and Biopharmaceutics,* **72:** 496–501.

Nissinen, E., Kaheinen, P., Penttila, K. E., Kaivola, J. and Linden, I.-B. (2007): Entacapone, a novel catechol *O*-methyltransferase inhibitor for Parkinson's disease, does not impair mitochondrial energy production. *European Journal of Pharmacology,* **340:** 287–294.

Nissinen, E., Tuominen, R. K., Perhoniemi, V. and Kaakkola, S. (1988): Catechol *O*-methyltransferase activity in human and rat small intestine. *Life Sciences*, **42:** 2609–2614.

Nohta, H., Noma, S. and Ohkura, Y. (1984): Assay for catechol *O*-methyltransferase in erythrocytes using a new fluorogenic substrate, 2-(3,4-dihydroxyphenyl) naphtho[1,2-*d*] thiazole. *Journal of Chromatography,* **308:** 93–100.

Novgorodovo, M. I., Gorshkov, A. I. and Mokhov, A. V. (1979): Native silver and its new structural modifications. *Zapiski Vsesoyuznogo Mineralogicheskogo Obshchestva*, **108:** 552–563.

Nutt, J. G. (2008): Pharmacokinetics and Pharmacodynamics of Levodopa. *Movement Disorders,* **23(3):** S580–S584.

Nuytemans, K., Theuns, J., Cruts, M. and Van Broeckhoven, C. (2010): Genetic etiology of Parkinson disease associated with mutations in the *SNCA, PARK2, PINK1, PARK7*, and *LRRK2* genes: a mutation update. *Human Mutatation,* **31:** 763–780.

Nyholm, D., Odin, P., Johansson, A., Chatamra, K., Locke, C., Dutta, S. and Othman, A. A. (2012): Pharmacokinetics of Levodopa, Carbidopa, and 3 *O*-Methyldopa Following 16-hour Jejunal Infusion of Levodopa-Carbidopa Intestinal Gel in Advanced Parkinson's Disease Patients. *The American Association of Pharmaceutical Scientists,* **15(2):** 316–323.

Olanow, C. W. and Brundin, P. (2013): Parkinson's Disease and Alpha Synuclein: Is Parkinson's Disease a Prion-Like Disorder? *Movement Disorders,* **28(1):** 31–40.

Oliver, C. N. and Stadtman,E. R. (1983): A proteolytic artifact associated with the lysis of bacteria by egg white lysozyme. *Proceedings of the National Academy of Sciences, USA,* **80:** 2156–2160.

Osuntokun, B. O. (1971): The Pattern of Neurological Illness in Tropical Africa: Experience at Ibadan, Nigeria. *Journal of the Neurological Sciences,* **12:**417–42.

Ozin, G. A., Hou, K., Lotsch, B. V., Cademartiri, L., Puzzo, D. P., Scotognella, F., Ghadimi, A. and Thomson, J. (2009): Nanofabrication by self-assembly. *Materials Today,* **12:** 12–23.

Padayachee, E. R. and Whiteley, C. G. (2011): Spectrofluorimetric analysis of amyloid peptides with neuronal nitric oxide synthase: Implications in Alzheimer's disease. *Biochimica et Biophysica Acta,* **1810:** 1136–1140.

Padayachee, E. R. and Whiteley, C. G. (2013a): Etiology of Alzheimer's disease: Kinetic, thermodynamic and fluorimetric analyses of interactions of pseudo Aß-peptides with neuronal nitric oxide synthase. *Neuropeptides,* **47:** 321–327.

Padayachee, E. R. and Whiteley, C. G. (2013b): Interaction of glycine zipper fragments of Aß-peptides with neuronal nitric oxide synthase: Kinetic, thermodynamic and spectrofluorimetric analysis. *Neuropeptides,* **47:** 171–178.

Pal, A., Shah, S. and Devi, S. (2008): Microwave-assisted synthesis of silver nanoparticles using ethanol as a reducing agent. *Materials Chemistry and Physics,* **114:** 530–532.

Palma, P. N., Rodrigues, M. L., Archer, M., Bonifacio, M. J., Loureiro, A. I., Learmonth, D. A., Carrondo, M. A. and Soares-da-Silva, P. (2006): Comparative Study of *ortho*- and *meta*-nitrated inhibitors of catechol *O*-methyltransferase: Interactions with the active site and regioselectivity of *O*-methylation. *Molecular Pharmacology,* **70(1):** 143–153.

Park, C. and Raines, R. T. (2000): Dimer formation by a "monomeric" protein. *Protein Science,* **9:** 2026–2033.

Park, C. K., Joshi, H. K., Agrawal, A., Ghare, M. I., Little, E. J., Dunten, P. W., Bitinaite, J. and Horton, N. C. (2010): Domain swapping in allosteric modulation of DNA specificity. *PLoS Biology,* **8(12):** e1000554.

Park, D. H. (1986): *Monoamine methyltransferases phenylethanolamine N-methyltransferase and catechol O-methyltransferase* In: Boulton, A. A., Baker, G. B. Yu, P. H., editors. neuromethods 5 neurotransmitter enzymes. Clifton, NJ: Humana Press. p. 117–145.

Parkinson J. (1817): *An essay on the shaking palsy.* Reprint of monograph published by Sherwood, Neely, and Jones, London.

Passarinha, L. A., Bonifácio, M. J. and Queiroz J. A. (2009): Application of a Fed-Batch Bioprocess for the Heterologous Production of hSCOMT in *Escherichia coli. Journal of Microbiology and Biotechnology,* **19:** 972–81.

Passarinha, L. A., Bonifácio, M. J., Soares-da-Silva, P. and Queiroz, J. A. (2008): A new approach on the purification of recombinant human soluble catechol *O*-methyltransferase from an *Escherichia coli* extracts using hydrophobic interaction chromatography. *Journal of Chromatography A,* **1177:** 287–296.

Passarinha, L. A., Bonifácio, M. J. and Queiroz J. A. (2006): The effect of temperature on the analysis of metanephrine for catechol *O*-methyltransferase activity assay by HPLC with electrochemical detection. *Biomedical Chromatography,* **20:** 937–944.

Patil, R. S., Kokate, M. R., Salvi, P. P. and Kolekar, S. S. (2011): A novel one step synthesis of silver nanoparticles using room temperature ionic liquid and their biocidal activity. *Comptes rendus – Chimie,* **14(12):** 1122–1127.

Paulsen, C. E. and Carroll, K. S. (2013): Cysteine-Mediated Redox Signaling: Chemistry, Biology, and Tools for Discovery. *Chemical Reviews,* **113:** 4633−4679.

Pedro, Q. A., Bonifácio, M. J., Queiroz, J. A, Maiaa, C. J and Passarinha, L. A (2011): A novel prokaryotic expression system for biosynthesis of recombinant human membrane-bound catechol *O*-methyltransferase. *Journal of Biotechnology,* **156:** 141–146.

Pedro, Q. A., Martins, L. M., Dias, J. M. L., Bonifácio, M. J., Queiroz J. A. and Passarinha, L. A. (2015): An artificial neural network for membrane-bound catechol *O*-methyltransferase biosynthesis with *Pichia pastoris* methanol-induced cultures. *Microbial Cell Factories,* **14(113):** 1–14.

Piedrafita, F. J., Fernandez-Alvarez, E., Nieto, O. and Tipton, K. F. (1992): Kinetic and inhibition studies on catechol *O*-methyltransferase by N-(3,4-dihydrohydroxyphenyl) maleimide. *Biochemical Journal,* **286:** 951–958.

Podila, R., Chen, R., Ke, P. C., Brown, J. M. and Rao, A. M. (2012): Effects of surface functional groups on the formation of nanoparticle-protein corona. *Applied Physics Letters,* **101:** 263701–263704.

Pope, B. and Kent, H. M. (1996): High efficiency 5 min transformation of *Escherichia coli. Nucleic Acids Research,* **24(3):** 536–537.

Powers, K. W., Brown, S. C., Krishna, V. B., Wasdo, S. C., Moudgil, B. M. and Roberts, S. M. (2006): Research Strategies for Safety Evaluation of Nanomaterials. Part VI. Characterization of Nanoscale Particles for Toxicological Evaluation. *Toxicological Sciences,* **90(2):** 296–303.

Pramanik, S., Banerjee, P., Sarkar, A. and Bhattacharya, S. C. (2013): Size-dependent interaction of gold nanoparticles with transport protein: A spectroscopic study. *Journal of Luminescence,* **128:** 1969–1974.

Priyadarshi, A., Khuder, S. A., Schaub, E. A. and Priyadarsh, S. S. (2001): Environmental Risk Factors and Parkinson's Disease: A Metaanalysis. *Environmental Research Section A,* **86:** 122–127.

Przedborski, S., Vila, M. and Jackson-Lewis, V. (2003): Neurodegeneration: What is it and where are we? *Journal of Clinical Investigation,* **111:** 3–10.

Puigbò, P., Guzmán, E., Romeu, A. and Garcia-Vallvé, S. (2007): OPTIMIZER: A web server for optimizing the codon usage of DNA sequences. *Nucleic Acids Research*, **35:** Web Server issue W126–W131.

Rahman, M., Laurent, S., Tawil, N., Yahia, L. and Mahmoudi, M. (2013*): Nanoparticle and protein corona.* In: Martinac B, editor. Protein-nanoparticle interactions Springer, 21–44.

Rai, M. and Padh, H. (2001): Expression systems for production of heterologous proteins. *Current Science*, **80(9):** 1121–1128.

Ramachandran, G. N., Ramakrishnan, C. and Sasisekharan, V. (1963): Stereochemistry of Polypeptide Chain Configurations. *Journal of Molecular Biology,* **7:** 95–99.

Rawat, A., Mahavar, H. K., Tanwar, A. and Singh, P. J. (2014): Study of electrical properties of polyvinylpyrrolidone/polyacrylamide blend thin films. *Bulletin of Materials Science,* **37(2):** 273–279.

Recasens, A. and Dehay, B. (2014): Alpha-synuclein spreading in Parkinson's disease. *Frontiers in Neuroanatomy,* **8:** 159.

Reymond, J. L. and Sicard, R. (2006): *Enzyme assays: High–throughput screening, genetic selection and fingerprinting*. Wiley-VCH Verlag GmbH & Co. KGaA.,Weinheim, p 4426–4427.

Richards, D. G., McMillin, D. L., Mein, E. A. and Nelson, C. D. (2002): Gold and its relationship to neurological/glandular conditions. *International Journal of Neuroscience,* **112:** 31–53.

Ritchie, R. J. and Prvan, T. (1996): Current statistical methods for estimating the K_m and V_{max} of Michaelis-Menten kinetics. *Biochemical Education,* **24(4):** 196–206.

Ross, P. D. and Subramanian, S. (1981): Thermodynamics of protein association reactions: forces contributing to stability. *Biochemistry,* **20**: 3096–3102.

Rost, B. (2001): Review: protein secondary structure prediction continues to rise. *Journal of Structural Biology,* **134:** 204–218.

Rutherford, K., Alphandéry, E., McMillan, A., Daggett, V. and Parson, W. W. (2008a): The V108M mutation decreases the structural stability of Catechol *O*-methyltransferase. *Biochimica et Biophysica Acta,* **1784:** 1098–1105.

Rutherford, K., Le Trong, I., Stenkamp, R. E. and Parson, W. W. (2008b): Crystal structures of human 108V and 108M catechol *O*-methyltransferase. *Journal of Molecular Biology,* **380:** 120–130.

Saini, R., Saini, S. and Sharma, S. (2010): Nanotechnology: The Future Medicine. *Journal of Cutaneous and Aesthetic Surgery,* **3(1):** 32–33.

Salata, D. and Tolosa, E. (2013): Levodopa in the Treatment of Parkinson's Disease: Current Status and New Developments. *Journal of Parkinson's Disease,* **3:** 255–269

Salminen, M., Lundström, K., Tilgmann, C., Savolainen, R., Kalkkinen, N. and Ulmanen, I. (1990): Molecular cloning and characterization of rat liver catechol *O*-methyltransferase. *Gene,* **93:** 241–247.

Samii, A., Nutt, J. G. and Ransom, B. R. (2004): Parkinson's disease. *Lancet,* **363:** 1783–1793.

Samworth, C. M., Degli-Esposti, M. and Lenaz, G. (1988): Quenching of the intrinsic tryptophan fluorescence of mitochondrial ubiquinol - cytochrome-c reductase by the binding of ubiquinone. *European Journal of Biochemistry,* **171:** 81–86.

Santo, G. M. E., Pedro, Q. A., Oppolzer, D., Bonifácio, M. J., Queiroz, J. A., Silva, F. andPassarinha, L A. (2014): Development of fed-batch profiles for efficient biosynthesis of catechol *O*-methyltransferase. *Biotechnology Reports,* **3:** 34–41.

Santos, F. M., Pedro, A. Q., Soares, R. F., Martins, R., Bonifacio, M. J., Queiroz, J. A. and Passarinha, L. A. (2013): Performance of hydrophobic interaction ligands for human membrane-bound catechol *O*-methyltransferase purification. *Journal of Separation Science,* **36(11):** 1693–1702.

Saptarshi, S. R., Duschl, A. and Lopata, A. L. (2013): Interaction of nanoparticles with proteins: relation to bio-reactivity of the nanoparticle. *Journal of Nanobiotechnology,* **11(26):** 1–12.

Sarkar, S., Raymick, J. and Imam, S. (2016): Neuroprotective and therapeutic strategies against Parkinson's Disease: Recent perspectives. *International Journal of Molecular Sciences,* **17:** 904.

Sawan, C. and Herceg, Z. (2010): Histone modifications and cancer. *Advances in Genetics,* **70:** 57–85.

Schluckebier, G., O'Gara, M., Saenger, W. and Cheng, X. (1995): Universal Catalytic Domain Structure of AdoMet-dependent Methyltransferases. *Journal of Molecular Biology,* **247:** 16–20.

Schrag, A., Hovris, A., Morley, D., Quinn, N. and Jahanshahi, M. (2006): Caregiver-burden in Parkinson's disease is closely associated with psychiatric symptoms, falls, and disability. *Parkinsonism and Related Disorders,* **12:** 35–41.

Schultz, E., Tarpila, S., Backstrom, A.-C., Gordin, A., Nissinen, E. and Pohto, P. (1991): Inhibition of human erythrocyte and gastroduodenal catechol *O*-methyltransferase activity by nitecapone. *European Journal of Clinical Pharmacology,* **40:** 577–580.

Sennuga, A., van Marwijk, J. and Whiteley, C. G. (2012): Ferroxidase activity of apoferritin is increased in the presence of platinum nanoparticles. *Nanotechnology,* **23:** 035102.

Sezonov, G., Joseleau-Petit, D. and D'Ari R. (2007): *Escherichia coli* physiology in Luria-Bertani broth. *Journal of Bacteriology,* **189:** 8746–8749.

Shapiro, A. L., Viuinela, E. and Maizel, J. V. (1967): Molecular weight estimation of polypeptide chains by electrophoresis in SDS-polyacrylamide gels. *Biochemical and Biophysical Research Communications,* **28:** 815–820.

Shield, A. J., Thomae, B. A., Eckloff, B. W., Wieben, E. D. and Weinshilboum, R. M. (2004): Human catechol *O*-methyltransferase genetic variation: Gene resequencing and functional characterization of variant allozymes. *Molecular Psychiatry,* **9:** 151–160.

Shifman, S., Bronstein, M., Sternfeld, M., Pisante, A., Weizman, A., Reznik, I., Spivak, B., Grisaru, N., Karp, L., Schiffer, R., Kotler, M., Strous, R. D., Swartz-Vanetik, M., Knobler, H. Y., Shinar, E., Yakir, B., Zak, N. B. and Darvasi, A. (2004): COMT: A common susceptibility gene in bipolar disorder and schizophrenia. *American Journal of Medical Genetics Part B,* **128(1):** 61–4.

Shiga, K. and Shiga, T. (1971): The Functional difference between the monomer and the dimer of *D*-Amino Acid Oxidase. *Archives of Biochemistry and Biophysics,* **145:** 701−702.

Shing, C.-Y., Whiteley, C. G. and Lee, D.-J. (2014): HIV protease: Multiple fold inhibition by silver nanoparticles— Spectrofluorimetric, thermodynamic and kinetic analysis. *Journal of the Taiwan Institute of Chemical Engineers,* **45:** 1140–1148.

Siddiqi, S. H., Abraham, N. K., Geiger, C. L., Karimi, M., Perlmutter, J. S. and Black, K. J. (2016): The Human Experience with Intravenous Levodopa. *Frontiers in Pharmacology,* **6:** 307.

Siedlecki, P. and Zielenkiewicz, P. (2006): Mammalian DNA methyltransferases. *Acta Biochimica Polonica*, **53:** 245–256.

Šileikaitė, A., Puišo, J., Prosyčevas, I. and Tamulevičius, S. (2009): Investigation of Silver Nanoparticles Formation Kinetics During Reduction of Silver Nitrate with Sodium Citrate. *Materials Science (Medžiagotyra),* **(15)1:** 21–27.

Składanowski, M., Golinska, P., Rudnicka, K., Dahm, H. and Rai, M. (2016): Evaluation of cytotoxicity, immune compatibility and antibacterial activity of biogenic silver nanoparticles. *Medical Microbiology and Immunology,* **205:** 603–613.

Smith, D. J. (2007): Characterisation of nanomaterials using transmission electron microscopy, In: *Nanocharacterisation,* A.I. Kirkland & J.L. Hutchison (Eds), RSC Publishing, Cambridge, p 1–27.

Stefanis, L. (2012): α-Synuclein in Parkinson's Disease. *Cold Spring Harbor Perspectives in Medicine,* **4:** a009399.

Stern, O. and Volmer, M. (1919): Über die Abklingzeit der Fluoreszenz. *Physikalische Zeitschrift,* **20:** 183–188.

Structural Genomics Consortium, Architecture et Fonction des MacromoléculesBiologiques, Berkeley Structural Genomics Center, China Structural Genomics Consortium, Integrated Center for Structure and Function Innovation, Israel Structural Proteomics Center, Joint Center for Structural Genomics, Midwest Center for Structural Genomics, New York Structural GenomiX, Research Center for Structural Genomics, Northeast Structural Genomics Consortium, Oxford Protein Production Facility, Protein Sample Production Facility, Max Delbrück Center for Molecular Medicine, RIKEN Structural Genomics/Proteomics Initiative and SPINE2-Complexes (2008): Protein production and purification. *Nature Methods,* **5(2):** 135–146.

Studier, F. W. (1991): Use of bacteriophage T7 lysozyme to improve an inducible T7 expression system. *Journal of Molecular Biology,* **219:** 37–44.

Studier, F. W. (2005): Protein Production by Auto-Induction in High Density Shaking Cultures. *Protein Expression Purification,* **41(1):** 207–34.

Studier, F. W. (2014): *Stable expression clones and auto-induction for protein production in E. coli.* In Chen YW (ed) Methods in Molucular Biology, vol 1091. Humana Press, 17–32.

Subramaniam, S. R. and Chesselet, M.-F. (2013): Mitochondrial dysfunction and oxidative stress in Parkinson's disease. *Progress in Neurobiology,* **0:** 17–32.

Sugiura, L., Toyota, T., Matsuba-Kurita, H., Iwayama, Y., Mazuka, R., Yoshikawa, T. and Hagiwara, H. (2016): Age-dependent effects of catechol *O*-methyltransferase (COMT) gene Val^{158}Met polymorphism on language function in developing children. *Cerebral Cortex,* **216:** 1–13.

Suh, I.-K., Ohta, H. and Waseda, Y. (1988): High-temperature thermal expansion of six metallic elements measured by dilatation method and X-ray diffraction. *Journal of Materials Science,* **23:** 757–760.

Sulzer, D. (2007): Multiple hit hypotheses for dopamine neuron loss in Parkinson's disease. *TRENDS in Neurosciences,* **30(5):** 244–250.

Šutković, J. and Jašarević, A. (2016): A review on nanoparticle and protein interaction in biomedical applications. *Periodicals of Engineering and Natural Sciences,* **4(2):** 34–40.

Tahan, C. (2007): Identifying Nanotechnology in Society. *Advances in Computers,* **71:** 251–271.

Taskinen, J., Ethell, B. T., Pihlavisto, P., Hood, A. M., Burchell, B. And Coughtrie, M. W. H. (2003): Conjugation of catechols by recombinant human sulfotransferases, UDP-glucuronosyltransferases, and soluble catechol *O*-methyltransferase: structure-conjugation relationships and predictive models. *Drug Metabolism and Disposition,* **31(9):** 1187–1197.

Tenhunen, J. and Ulmanen, I. (1993): Production of rat soluble and membrane-bound catechol *O*-methyltransferase forms from bifunctional mRNAs. *Biochemical Journal,* **296:** 595–400.

Tenhunen, J., Salminen, M., Lundström, K., Kiviluoto, T., Savolainen, R. and Ulmanen, I. (1994): Genomic organization of the human catechol *O*-methyltransferase gene and its expression from two distinct promoters. *European Journal of Biochemistry,* **223:** 1049–1059.

Thakkar, K. N., Snehit, S., Mhatre, M. S., Rasesh, Y. and Parikh, M. S. (2010): Biological synthesis of metallic nanoparticles. *Nanomedicine: Nanotechnology, Biology, and Medicine,* **6:** 257–262.

The UniProt Consortium, (2016): UniProt: the universal protein knowledgebase. *Nucleic Acids Research,* **45:** D158–D169.

Thompson, J. D., Higgins, G. D. and Gibson, T. J. (1994): "CLUSTALW: Improving the sensitivity of progressive multiple sequence alignment through sequence weighting, position specific gap penalties and weight matrix choice. *Nucleic Acids Research,* **22:** 4673–4680.

Tiihonen, J., Hallikainen, T., Lachman, H., Saito, T., Volovka, J., Kauhanen, J., Salonen, J. T., Ryynanen, O.-P., Koulu, M., Karvonen, M. K., Pohjalainen, T., Syvalahti, E. and Hietala, J. (1999): Association between the functional variant of the catechol *O*-methyltransferase (COMT) gene and type 1 alcoholism. *Molecular Psychiatry,* **4:** 286–290.

Tilgmann, C. and Kalkkinen, N. (1990): Purification and partial characterization of rat liver soluble catechol *O*-methyltransferase. *FEBS Letters,* **264:** 95–99.

Tilgmann, C. and Kalkkinen, N. (1991): Purification and partial sequence analysis of the soluble catechol *O*-methyltransferase from human placenta: comparison to the rat liver enzyme. *Biochemical and Biophysical Research Communications,* **174(2):** 995–1002.

Tilgmann, C., Melen, K., Lundstrom, K., Jalanko, A., Julkunen, I., Kalkkinen, N. and Ulmanen, I. (1992): Expression of recombinant human soluble- and membrane bound catechol *O*-methyltransferase in eukaryotic cells and identification of the respective enzymes in rat brain. *European Journal of Biochemistry,* **207:** 813–821.

Tom, R. T., Samal, A. K., Sreeprasad, T. S. and Pradeep, T. (2007): Hemoprotein bioconjugates of gold and silver nanoparticles and gold nanorods: structure-function correlations. *Langmuir,* **23:** 1320–1325.

Toma, H. E., Zamarion, V. M., Toma S. H. and Araki, K. (2010): The coordination chemistry at gold nanoparticles. *Journal of the Brazilian Chemical Society,* **21(7):** 1158–1176.

Tong, E. K. and Harry Duckworth, W. (1975): The Quaternary Structure of Citrate Synthase from *Escherichia coli K* $I2^{+}$. *Biochemistry,* **14(2):** 235–241.

Toshima, N. and Yonezawa, T. (1998): Bimetallic nanoparticles – novel materials for chemical and physical applications. *New Journal of Chemistry,* **22:** 1179–1201.

Towbin, H., Staehelin, T. and Gordon, J. (1979): Electrophoretic transfer of proteins from polyacrylamide gels to nitrocellulose sheets: procedure and some application. *Proceedings of the National Academy of Sciences of the USA,* **76(9):** 4350–4354.

Treuel, L., Eslahian, K. A., Docter, D., Lang, T., Zellner, R., Nienhaus, K., Nienhaus, G. U., Stauberc, R. H. and Maskos, M. (2014): Physicochemical characterization of nanoparticles and their behavior in the biological environment. *Physical Chemistry Chemical Physics*, **16:** 15053–15067.

Treuel, L., Malissek, M., Gebauer, S. J. and Zellner, R. (2010): The Influence of surface composition of nanoparticles on their interactions with serum albumin. *ChemPhysChem*, **11:** 3093–3099.

Tsao, D., Diatchenko, L. and Dokholyan, N. V. (2011): Structural mechanism of S-adenosyl methionine binding to catechol *O*-methyltransferase. *PLoS ONE*, **6:** e24287.

Tsuji, E., Okazaki, K. and Takeda, K. (2009): Crystal structures of rat catechol *O*-methyltransferase complexed with coumarine-based inhibitor. *Biochemical and Biophysical Research Communications,* **378:** 494–497.

Tu, Z., He, G., Li, K. X., Chen, M. J., Chang, J., Chen, L., Yao, Q., Liu, P. D., Ye, H., Shi, J. and Wu, X. (2005): An improved system for competent cell preparation and high efficiency

plasmid transformation using different *Escherichia coli* strains. *Electronic Journal of Biotechnology,* **8(1):** 144–120.

Tunbridge, E. M., Harrison, P. J. and Weinberger, D. R. (2006): Catechol *O*-methyltransferase, cognition, and psychosis: Val^{158}Met and beyond. *Biological Psychiatry,* **60:**141–151.

Ulmanen, I. and Lundström, K. (1991): Cell-free synthesis of rat and human catechol *O*-methyltransferase insertion of the membrane-bound form into microsomal membranes *in vitro. European Journal of Biochemistry,* **202:** 1013–1020.

Ulusu, N. N. (2015): Evolution of enzyme kinetic mechanisms. *Journal of Molecular Evolution,* **80:** 251–257.

Umer, A., Naveed, S. and Ramzan, N. (2012): Selection of a suitable method for the synthesis of copper nanoparticles. *NANO: Brief Reports and Reviews,* **7(5):** 1–18.

van der Merwe, C., Haylett, W., Harvey, J., Lombard, D., Bardien, S. and Carr, J. (2012): Factors influencing the development of early-or-late-onset Parkinson's disease in a cohort of South African patients. *South African Medical Journal,* **102(11):** 848–854.

Vandenbergh, D. J., Rodriguez, L. A., Miller, I. T., Uhl, G. R. and Lachman, H. M. (1997): High-activity catechol *O*-methyltransferase allele is more prevalent in polysubstance abusers. *American Journal of Medical Genetics,* **74:** 439–442.

Venkatachalam, C. M. (1968): Stereochemical criteria for polypeptides and proteins. V. conformation of a system of three linked peptide units. *Biopolymers,* **6:** 1425–1436.

Veser, J. (987): Kinetics and Inhibition Studies of Catechol *O*-Methyltransferase from the yeast *Candida tropicalis. Journal of Bacteriology,* **169(8):** 3696–3700.

Vidgren, J., Svensson, L. A. and Liljas, A. (1994): Crystal structure of catechol *O*-methyltransferase. *Nature,* **368:** 354–358.

Wakabayashi, K., Tanji, K., Mori, F. and Takahashi, H. (2007): The Lewy body in Parkinson's disease: Molecules implicated in the formation and degradation of α-synuclein aggregates. *Neuropathology,* **27:** 494–506.

Wakabayashi, K., Tanji, K., Odagiri, S., Miki, Y., Mori, F. and Takahashi, H. (2013): The Lewy Body in Parkinson's Disease and related neurodegenerative disorders. *Molecular Neurobiology,* **47:** 495–508.

Wanga, Y. and Ni, Y. (2014): New insight into protein–nanomaterial interactions with UV-visible spectroscopy and chemometrics: human serum albumin and silver nanoparticles. *Analyst,* **139:** 416–424.

Waters, C. (2000): Catechol *O*-Methyltransferase (COMT) Inhibitors in Parkinson's Disease. *Journal of the American Geriatrics Society,* **48:** 692–698.

Weber, R. E. and Campbell, K. L. (2011): Temperature dependence of haemoglobin–oxygen affinity in heterothermic vertebrates: mechanisms and biological significance. *Acta Physiologica,* **202:** 549–562.

Weinshilboum, R. M. and Raymond, F. A. (1977): Inheritance of low erythrocyte catechol *O*-methyltransferase activity in man. *American Journal of Human Genetics,* **29:** 125–135.

Westbrook, J., Feng, Z., Chen, L., Yang, H. and Berman, H. M. (2003): The Protein Data Bank and structural genomics. *Nucleic Acids Research,* **31:** 489–491.

White, H. L. and Wu, J. C. (1975): Properties of catechol *O*-methyltransferases from brain and liver of rat and human. *Biochemical Journal,* **145:** 135–143.

Whiteley, C. G., Shing, C.-Y., Kuo, C.-C. and Lee, D.-J. (2016): Docking of HIV protease to silver nanoparticles. *Journal of the Taiwan Institute of Chemical Engineers,* **60:**83–91.

Winklhofer, K. F. and Haass, C. (2010): Mitochondrial dysfunction in Parkinson's disease. *Biochimica et Biophysica Acta,* **1802:** 29–44.

Woo, J.-M., Yoon, K.-S. and Yu, B.-H. (2002): Catechol *O*-methyltransferase genetic polymorphism in Panic Disorder. *American Journal of Psychiatry,* **159:** 1785–1787.

Woo, J.-M., Yoon, K.-S., Choi, Y.-H., Oh, K.-S., Lee, Y.-S. and Yu, B.-H. (2004): The association between panic disorder and the L/L genotype of catechol *O*-methyltransferase. *Journal of Psychiatric Research,* **38:** 365–370.

Wu, M.-X. and Wedding, R. T. (1985): Diurnal regulation of phosphoenolpyruvate carboxylase from *Crassula*. *Plant Physiology*, **77:** 667−675.

Xiao, Q., Huang, S., Qi, Z. D., Zhou, B., He, Z. K. and Liu, Y. (2008): Conformation, thermodynamics and stoichiometry of HSA adsorbed to colloidal CdSe/ZnS quantum dots. *Biochimica et Biophysica Acta,* **1784:** 1020–1027.

Yang, S. T., Liu, Y., Wang, Y. W. and Cao, A. N. (2013): Biosafety and bioapplication of nanomaterials by designing protein-nanoparticle interactions. *Small*, **9:** 1635−1653.

Yao, J., van Marwijk, J., Wilhelmi, B. and Whiteley, C. G. (2015): Isolation, characterization, interaction of a thiazolekinase (Plasmodium falciparum) with silver nanoparticles. *International Journal of Biological Macromolecules,* **79:** 644–653.

Yehia, H. N., Drapern, R. K., Mikoryak, C., Walker, E. K., Bajaj, P., Musselman, I. H., Daigrepont, M. C., Dieckmann, G. R. and Pantano, P. (2007): Single-walled carbon nanotube interactions with HeLa cells. *Journal of Nanobiotechnology,* **5(8):** 1–17.

Yen, H.-J., Hsu, S.-H. and Tsai, C.-L. (2009): Cytotoxicity and immunological response of gold and silver nanoparticles of different sizes. *Small,* **5(13):** 1553–1561.

Yeragani V. K., Tancer, M., Chokka, P. and Baker, G. B. (2010): Arvid Carlsson, and the story of dopamine. *Indian Journal of Psychiatry,* **52(1):** 87–88.

Yildirimer, L., Thanh, T. K. N., Loizidoua, M. and Seifaliana, A. M. (2011): Toxicological considerations of clinically applicable nanoparticles. *Nano Today,* **6:** 585—607.

Yoritaka, A., Hattori, N., Yoshino, H. and Mizuno, Y. (1997): Catechol *O*-methyltransferase genotype and susceptibility to Parkinson's disease in Japan. *Journal of Neural Transmission,* **104:** 1313–1317.

Zhang, J., Hao, G., Yao, C., Yu, J., Wang, J., Yang, W., Hu, C. and Zhang, B. (2016): Albumin-mediated biomineralization of paramagnetic NIR Ag2S QDs for tiny tumor bimodal targeted imaging *in vivo. ACS Applied Materials & Interfaces,* **8:** 16612–16621.

Zhang, S., Zhou, H., Yu, F., Bai, C., Zhao, Q., He, J. and Liu, C. (2016): Structural insight into the cooperation of chloroplast chaperonin subunits. *BMC Biology,* **14(29):** 1–14.

Zheng, Y.-J., and Bruice, T. C. (1997): A theoretical examination of the factors controlling the catalytic efficiency of a transmethylation enzyme: catechol *O*-methyltransferase. *Journal of the American Chemical Society,* **119:** 8137–8145.

Zhu, B. T., Ezell, L. E. and Liehr, J. G. (1994): Catechol *O*-methyltransferase catalyzed rapid *O*-methylation of mutagenic flavonoids. *Journal of Biological Chemistry,* **269(1):** 292–299.

Zhu, B. T., Patel, U. K., Cai, M. X. and Conney, A. H. (2000): *O*-Methylation of tea polyphenols catalyzed by human placental cytosolic catechol *O*-methyltransferase. *Drug Metabolism and Disposition,* **28:** 1024-1030.

Zubieta, J.-K., Heitzeg, M. M., Smith, Y. R., Bueller, J. A., Xu, K., Xu, Y., Koeppe, R. A., Stohler, C. S. and Goldman, D. (2003): COMT val^{158}met genotype affects μ-opioid neurotransmitter responses to a pain stressor. *Science,* **299:** 1240–1243.

Appendices

Appendix I: Chemicals and reagents

Tris (hydroxymethyl) aminomethane (Tris), DEAE-cellulose (H^+ medium mesh no. D8382), Sephadex G-100, dithiothreitol (DTT), ß–mercaptoethanol, bovine serum albumin (BSA), esculetin, scopoletin, *S*-(5'-adenosyl)-*L*-methionine (SAM), 30% acrylamide mix, Bradford reagent, glucose, Polyvinylpyrrolidone (PVP), Ethylenediaminetetraacetic acid, sodium dodecyl sulfate (SDS), tetramethylethylenediamine (TEMED), (EDTA), imidazole, Isopropyl β-D-1-thiogalactopyranoside (IPTG), silver nitrate ($AgNO_3$) *L*-cyteine, gold (III) chloride hydrate (tetrachloroauric acid), Bradford reagent and commercial COMT (porcine) were purchased from Sigma-Aldrich, South Africa. Potassium chloride (KCl), glacial acetic acid, sodium dihydrogen orthophosphate, disodium hydrogen orthophosphate, hydrochloric acid (HCl), glycerol, ammonium sulfate, tryptone, peptone, yeast extract, potassium dihydrogen orthophosphate, dipotassium hydrogen orthophosphate, dimethyl sulfoxide (DMSO), Coomassie Brilliant Blue R-250, Congo red, magnesium chloride ($MgCl_2$), ethidium bromide, acetic acid (glacial), glycine, ethanol, isopropanol and trisodium citrate were purchased from Merk (Pty), South Africa. Agarose, DNA Ladder Mix™, protein Ladder Mix™, restriction enzymes (*Nde*I, and *Xho*I), and *E. coli* cells (BL21(DE3) and JM109) were purchased from Thermo Scientific™ South Africa. Ampicillin and lysozyme were purchased from Roche, South Africa, while ammonium persulfate was purchased RADCHEM (Pty) South Africa. In all the experiments, Milli-Q water dispensed by Milli-Q Elix (Merk) in our laboratory was used.

Appendix II: Media, buffers and solutions

Luria Broth (LB)	10 g/l tryptone 5 g/l yeast extract 10 g/l NaCl	Autoclave
Luria Agar (LA)	10 g/l tryptone 5 g/l yeast extract 10 g/l NaCl 15 g/l agar	Autoclave
TAE	0.04 M Tris-HCl 1 mM EDTA pH 8.0 0.021 mM glacial acetic acid	
SOB	20 g/l tryptone 5 g/l yeast extract 0.584 g/l NaCl 0.186 g/l KCl 2.034 g/l $MgCl_2$ 2.464 g/l $MgSO_4$	Autoclave
SOC	20 g/l tryptone 5 g/l yeast extract 0.584 g/l NaCl 0.186 g/l KCl 2.034 g/l $MgCl_2$.464 g/l $MgSO_4$	Add 20 ml/l sterile glucose after autoclave
TB buffer	2.6 g/l HEPES pH6.72.203 g/l $CaCl_2$ 18.638 g/l KCl 10.886 g/l $MnCl_2$	Mix all the components except $MnCl_2$, adjust pH to 6.7 with KOH/HCl, then add MnCl2, and filter sterilize (0.22 μm)
Binding buffer	0.2 M NaCl, 5 mM ß–mercaptoethanol, 20 mM imidazole 20 mM Tris-HCl	Adjust pH to 7.4, degas and filter
Elution buffer	0.2 M NaCl, ß–mercaptoethanol, 0.4 M imidazole 20 mM Tris-HCl	Adjust pH to 7.4, degas and filter

SDS-PAGE TD solution	1 ml 10 % SDS 50 µl ß-mercaptoethanol	
SDS-PAGE TS solution	13.3 ml 3 M Tris-HCl, pH 8.8 2 ml 0.5 M EDTA 40 ml Glycerol	Prepared and stored at 4°C
SDS-PAGE loading dye TD + TS	200 µl TS solution + 50 µl of TD solution	Prepared fresh all the time
12% Resolving gel	1.6 ml H_2O 2.0 ml 30 %/0.8 % Acrylamide/Bis-Acrylamide 1.25 ml 3 M Tris-HCl, pH 8.8 50 µl 10 % SDS 50 µl 10 % APS 5 µl tetramethylethylenediamine	APS and TEMED added just prior to pouring of the gel
4% Stacking gel	1.2 ml H_2O 0.27 ml 30 %/0.8 % Acrylamide/Bis-Acrylamide 0.5 ml 1.5 M Tris-HCl, pH 6.8 20 µl 10 % SDS 20 µl 10 % APS 2 µl tetramethylethylenediamine	APS and TEMED added last. After pouring 10 wells comb was inserted into the gel and left to set for 1 h
SDS-PAGE running buffer	25 mM Tris powder 192 mM glycine 0.1% SDS	

Fairbanks solution A	0.05% Coomassie Brilliant Blue R-250 25% isopropanol 10% acetic acid	
Fairbanks solution B	0.005% Coomassie Brilliant Blue R-250 10% isopropanol 10% acetic acid	
Fairbanks solution C	0.002% Coomassie Brilliant Blue R-250 10% acetic acid	
Fairbanks solution D	10% acetic acid	

Components of the cocktail buffer covering a pH range of 3-10.

Buffer salt	**pH range covered**
Sodium acetate	3 – 5.5
2(N-morpholino)ethane sulfonic acid (MES)	5.5 – 7
Tris	7–9
2(cyclohexylamino)ethane sulfonic acid (CHES)	8.6–10

Appendix III: Supplementary figures

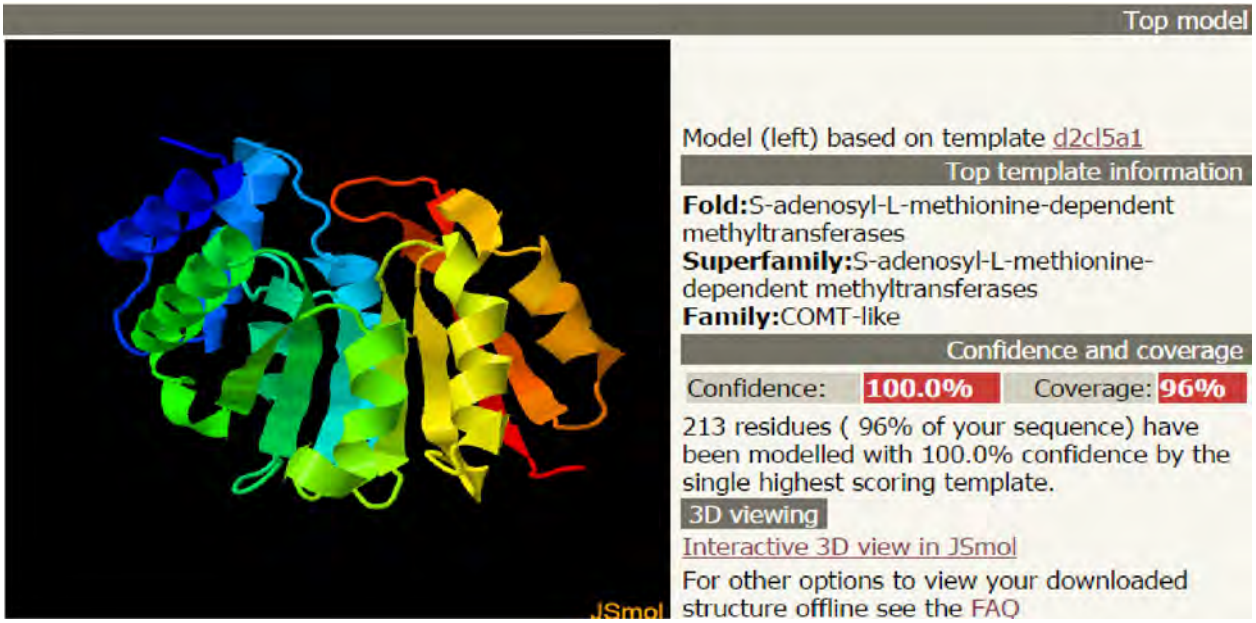

Figure S1: Modeled structure of BSCOMT using Phyre2 with the modeling information before extracting the structures. The BSCOMT amino acid sequence submitted and the program used profile-to-profile matching algorithms and the three-dimensional structure automatically predicted based on similar proteins (rat SCOMT) of known function and structure. The picture was visualized using JSmol.

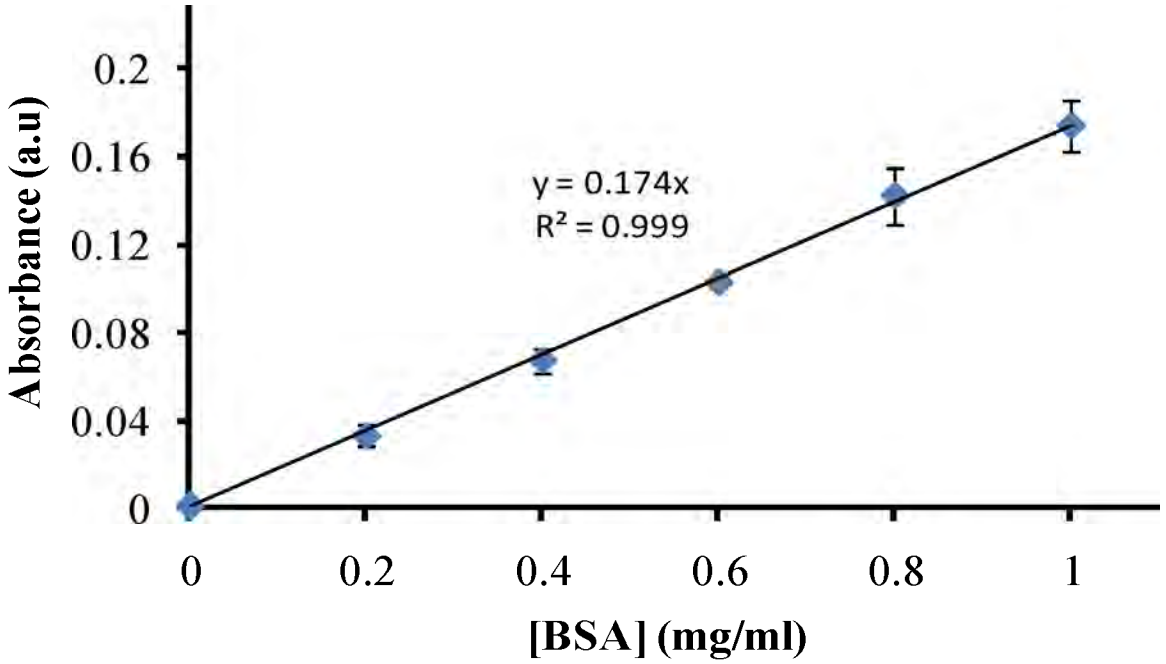

Figure S2: A representative standard curves for the determination of protein concentration using Bradford assay. Protein (5 µl) was added to a well, followed by Bradford reagent (245 µl). The mixture was incubated at 22°C for 10 min and absorbance of the solution measured at 595 nm. The protein concentration was routinely assayed using bovine serum albumin as standard. Values represent the mean (n = 3, ± SD).

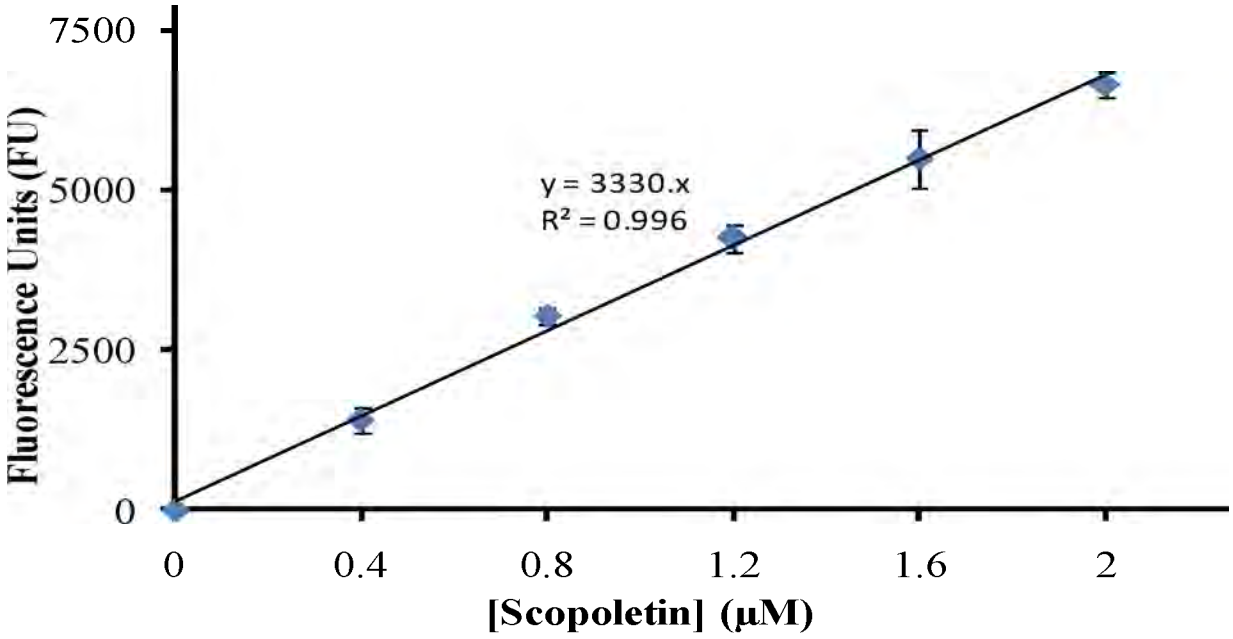

Figure S3: A representative of scopoletin standard curves. Scopoletin was initially dissolved in DMSO and diluted with the activity assay buffer (100 mM phosphate, 5 mM $MgCl_2$, 20 mM *L*-cysteine, pH 7.0) to a DMSO concentration of 2% and a range (0 to 2 µM) of scopoletin concentrations. Fluorescence of 200 µl of each of the scopoletin concentrations was recorded at the excitation and emission wavelengths of 355 nm and 460 nm, respectively. The standard curve was routinely prepared for each COMT assays and used for the extrapolation of the amount of scopletin produced during the assay. Values represent the mean (n = 3, ± SD).

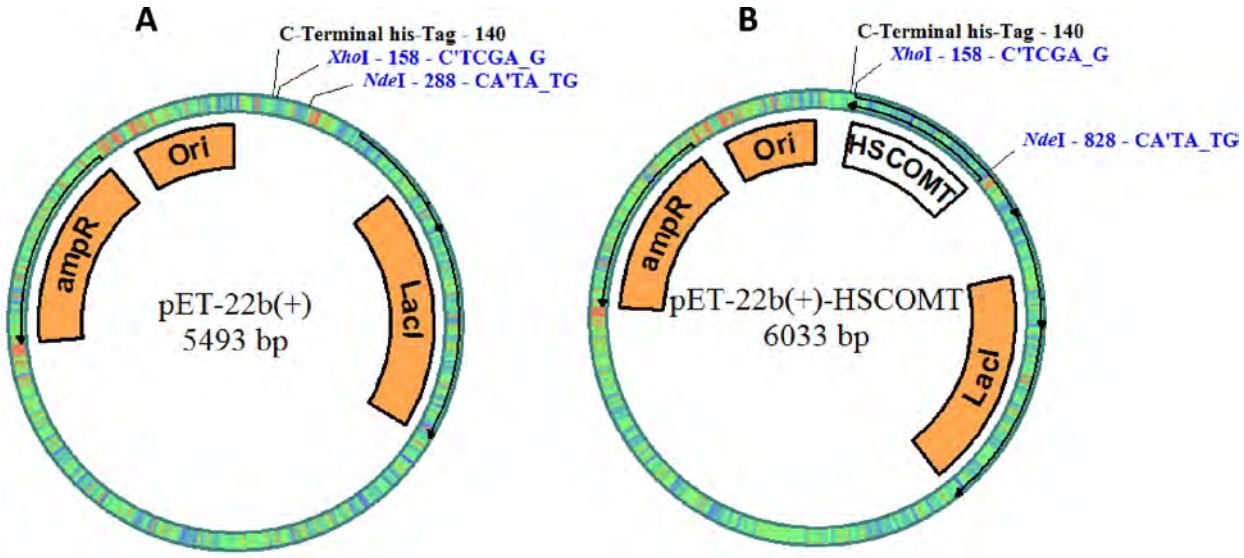

Figure S4: (A) Map of pET-22b(+) vector indicating *lac1*, ampicillin resistance gene, replication origin, C-terminal His-tag and the cloning sites of interest. (B) Map of pET-22b(+) vector system showing HSCOMT inserted into the vector. *Xho*I and *Nde*I restriction sites were chosen as their sequences were not found in optimized HSCOMT gene (virtual cloning prepared using pDraw32 revision 1.1.130).

Appendix IV: Line equations of the fluorescence spectroscopic studies

- AuNP-HSCOMT interactions
  - Straight line equations (equation 6.1) for Stern-Volmer analyses, with the slope equals to the of Stern-Volmer constant quenching constant (K_{sv}) at four different temperatures in Kelvin (K).

    298K $y = 0.072x + 1.006,\ R^2 = 0.958$

    303K $y = 0.056x + 0.993,\ R^2 = 0.980$

    308K $y = 0.050x + 0.977,\ R^2 = 0.984$

    313K $y = 0.035x + 1.001,\ R^2 = 0.956$
  - Line equations for equation 6.2. Plots of $F_o/\Delta F$ versus 1/ [AuNPs] yielded straight lines of slopes $1/\theta K_a$ and intercepts of $1/\theta$ (θ is the fraction of fluorophore accessible to quencher and K_a is the association constant of the interaction) at four temperatures in Kelvin (K).

    298K $y = 6.77x + 1.661,\ R^2 = 0.955$

    303K $y = 13.05x + 1.634,\ R^2 = 0.980$

    308K $y = 18.19x + 1.309,\ R^2 = 0.998$

    313K $y = 20.63x + 1.264,\ R^2 = 0.955$
  - Line equations for equation 6.3. Plots of F_o-F/F versus log1/ [AuNPs] yielded straight lines of slopes equivalent to n (number of binding site(s)) of AuNPs to HSCOMT at four different temperatures in Kelvin (K).

    298K $y = 0.693x - 1.625,\ R^2 = 0.989$

303K $y = 1.015x - 2.300,\ R^2 = 0.980$

308K $y = 1.100x - 2.509,\ R^2 = 0.990$

313K $y = 1.091x - 2.471,\ R^2 = 0.969$

- The linear equation of Van't Hoff plot (equation 6.5) of lnK_{sv} versus 1/T (T is temperature in Kelvin) with slope equivalent to -ΔH/R and intercept equivalent to ΔS/R.

  $y = 4354x - 17.23x,\ R^2 = 0.960$

- AgNP-HSCOMT interactions
  - Straight line equations (equation 6.1) for Stern-Volmer analyses, with the slope equals to the of Stern-Volmer constant quenching constant (K_{sv}) at four temperatures in Kelvin (K).

    298K $y = 0.062x + 1.064,\ R^2 = 0.923$

    303K $y = 0.045x + 1.028,\ R^2 = 0.970$

    308K $y = 0.033x + 1.008,\ R^2 = 0.958$

    313K $y = 0.030x + 0.968,\ R^2 = 0.920$

  - Line equations for equation 6.2. Plots of $F_o/\Delta F$ versus 1/ [AuNPs] yielded straight lines of slopes $1/\theta K_a$ and intercepts of $1/\theta$ (θ is the fraction of fluorophore accessible to quencher and K_a is the association constant of the interaction) at four different temperatures in Kelvin (K).

    298K $y = 4.092x + 1.782,\ R^2 = 0.929$

    303K $y = 10.84x + 1.715,\ R^2 = 0.956$

    308K $y = 14.61x + 1.1.681,\ R^2 = 0.926$

313K $y = 85.45x + 1.664,\ R^2 = 0.960$

- Line equations for equation 6.3. Plots of F_o-F/F versus log1/ [AuNPs] yielded straight lines of slopes equivalent to *n* (number of binding site(s)) of AuNPs to HSCOMT at four different temperatures.

  298K $y = 0.514x - 1.287,\ R^2 = 0.951$

  303K $y = 0.669x - 1.745,\ R^2 = 0.986$

  308K $y = 0.9103x - 2.322,\ R^2 = 0.981$

  313K $y = 1.414x - 3.386,\ R^2 = 0.973$

- The linear equation of Van't Hoff plot (equation 6.5) of lnK_{sv} versus 1/T (T is temperature in Kelvin) with slope equivalent to -ΔH/R and intercept equivalent to ΔS/R.

  $y = 4526x - 18.01x,\ R^2 = 0.957$